DOT/FAA/TC-21/17

Federal Aviation Administration
William J. Hughes Technical Center
Aviation Research Division
Atlantic City International Airport
New Jersey 08405

Bonded Repairs to Composite Wing Panel Structure: Phase 2, Baseline Study

July 2021

Final report

U.S. Department of Transportation
Federal Aviation Administration

NOTICE

This report is available at the Federal Aviation Administration William J. Hughes Technical Center's Full-Text Technical Reports page: actlibrary.tc.faa.gov in Adobe Acrobat portable document format (PDF).

Technical Report Documentation Page

Form DOT F 1700.7 (8-72) Reproduction of completed page authorized

1. Report No.	2. Government Accession No.	3. Recipient's Catalog No.
DOT/FAA/TC-21/17		

4. Title and Subtitle	5. Report Date
Bonded Repairs to Composite Wing Panel Structure: Phase 2, Baseline Study	December 2020 6. Performing Organization Code

7. Author(s)	8. Performing Organization Report No.
Ryan J. Neel[1], Reewanshu Chadha[2], John G. Bakuckas, Jr.[3], Michael Fleming[4], John Z. Lin[4], Erick Espinar-Mick[5] [1]Federal Aviation Administration (FAA-Drexel Fellow) [2]Federal Aviation Administration (Diakon Solutions, LLC) [3]Federal Aviation Administration [4]Boeing Research & Technology [5]Boeing Commercial Airplane	

9. Performing Organization Name and Address	10. Work Unit No. (TRAIS)
William J. Hughes Technical Center Aviation Research Division Structures and Materials Section Atlantic City International Airport, NJ 08405	11. Contract or Grant No.

12. Sponsoring Agency Name and Address	13. Type of Report and Period Covered
U.S. Department of Transportation Federal Aviation Administration Transport Standards Branch Airframe & Cabin Safety Section, AIR-675 2200 South 216th Street Des Moines, Washington 98198	Final Report 14. Sponsoring Agency Code

15. Supplementary Notes

The FAA William J. Hughes Technical Center Aviation Research Division COR was John G. Bakuckas, Jr.

16. Abstract

In a collaborative effort, the Federal Aviation Administration (FAA) and the Boeing Company are assessing bonded repair technologies of composite panels representative of transport airplane wing structures through test and analysis using the FAA's Aircraft Beam Structural Test (ABST) fixture. Emphasis has been placed on investigating methods and tools used to conduct analysis and predict structural performance of bonded repairs and those used to monitor and evaluate repair quality over the life of the part. This project is undertaken in a phased approach, where phase 1 was fixture development and verification. In this current second phase, baseline testing was undertaken on carbon fiber reinforced polymer (CFRP) panels in the unnotched pristine and open-hole configurations to characterize the material response, to verify analysis models and to provide an initial reference point for inspection and monitoring system. Panels were 24-inches wide and 40-inches long consisting of an 18-ply quasi-isotropic layout attached as top-side components (e.g., skins) of a cantilevered wingbox structure subjected to constant-moment loading. Fatigue loading conditions were applied that produce typical operational strain levels for transport-category wing panels for three design service objectives (~165,000 cycles). Results from this second phase effort verified the test-fixture loading, validated analysis models, and provided an initial baseline for Nondestructive inspection (NDI) and other monitoring systems to detect damage. For the unnotched panel, structural integrity was maintained through testing with no signs of damage in the test section. Measured strains in the test section were relatively constant and remained unchanged during fatigue. For the open-hole panel strain surveys revealed excellent correlation between test and analysis. Strain concentrations measured using strain gages and a digital image correlation (DIC) system matched finite element analysis results.

Future, phase 3 efforts will be focused on Bonded Repair Size Limit (BRSL) study, where the goal is to develop data to support BRSL assessment methods for solid laminate panels. The test results of phase 3 panels will be provided in forthcoming technical notes.

17. Key Words	18. Distribution Statement
Bonded repair size limit, Carbon fiber reinforced polymer, Nondestructive inspection, Test, Analysis, Digital image correlation, Thermography	This document is available to the U.S. public through the National Technical Information Service (NTIS), Springfield, Virginia 22161. This document is also available from the Federal Aviation Administration William J. Hughes Technical Center at actlibrary.tc.faa.gov.

19. Security Classif. (of this report)	20. Security Classif. (of this page)	21. No. of Pages	22. Price
Unclassified	Unclassified	177	

Contents

Figures

Tables

Acronyms

Acronym	Definition
AE	Acoustic Emission
ABST	Aircraft Beam Structural Test
BRSL	Bonded Repair Size Limits
CFRP	Carbon Fiber Reinforced Polymer
DIC	Digital Image Correlation
DSO	Design Service Objectives
FAA	Federal Aviation Administration
NDI	Non-Destructive Inspection
PCL	Predicted Critical Load
SHM	Structural Health Monitoring
SL	Service Load

Executive summary

In a collaborative effort, the Federal Aviation Administration (FAA) and the Boeing Company are assessing bonded repair technologies of composite panels representative of transport airplane wing structures through test and analysis using the FAA's Aircraft Beam Structural Test (ABST) fixture. Emphasis has been placed on investigating the methods and tools used to conduct analysis and predict structural performance of bonded repairs, and those used to monitor and evaluate repair quality over the life of the part. This project is being undertaken in a phased approach, where phase 1 was fixture development and verification. In this current second phase, baseline testing was undertaken on carbon fiber reinforced polymer (CFRP) panels in the unnotched pristine and open-hole configurations to characterize the material response, to verify analysis models, and to provide an initial reference point for inspection and monitoring systems. Panels were 24-inches wide and 40-inches long consisting of an 18-ply quasi-isotropic layout attached as top-side components (e.g., skins) of a cantilevered wingbox structure subjected to constant-moment loading. Fatigue loading conditions were applied that produce typical operational strain levels for transport-category wing panels for three design service objectives (~165,000 cycles). Results from this second phase effort verified the test-fixture loading, validated analysis models, and provided an initial baseline for non-destructive inspection (NDI) and other monitoring systems to detect damage. For the unnotched panel, structural integrity was maintained through testing with no signs of damage in the test section. Measured strains in the test section were relatively constant and remained unchanged during fatigue. For the open-hole panel strain surveys revealed excellent correlation between test and analysis. Strain concentrations measured using strain gages and a digital image correlation (DIC) system matched finite element analysis results.

Future, phase 3 efforts will be focused on Bonded Repair Size Limit (BRSL) study, where the goal is to develop data to support BRSL assessment methods for solid laminate panels. The test results of phase 3 panels will be provided in forthcoming technical reports.

1 Introduction

Although the effectiveness of adhesive bonded repair patches has been demonstrated to maintain aging military fleets worldwide (Baker, Rose, & Jones, 2003), challenges remain with respect to commercial aircraft applications. One such challenge pertains to the integrity of the bond between the repair patch and the damaged structure, which depends on numerous installation parameters. Errors during installation, including exposure of the repair patch to a humid environment, improper surface preparation, contamination of the bond line, insufficient control of the curing temperature, and loss of vacuum pressure, can lead to a reduction in bond-line strength. Furthermore, bond integrity, especially weak bonds, cannot be detected by existing non-destructive inspection (NDI) techniques. Consequently, the Federal Aviation Administration (FAA) issued a policy statement regarding bonded repair size limits (BRSL) to primary structure (Federal Aviation Administration, 2014). According to this BRSL policy statement: "All critical structures must have a repair size limit no larger than a size that maintains limit load residual strength capability with the repair completely failed or failed within arresting design structures." To expand the size limits of a given bonded repair patch, repair designs must have structural substantiation based on tests or analysis supported by tests. Additional data sets are required to qualify bonded material and process compatibilities, to demonstrate proof of structure, and to establish reliable inspection procedures.

In a multi-year, multi-phased research program, the FAA and the Boeing Company are working in partnership to gain better insight into the fatigue and damage tolerance performance of adhesive bonded repairs and to help address issues cited in the FAA policy statement above. Current efforts are focused on testing and analyzing bonded repairs to representative composite wing panels using the Aircraft Beam Structural Test (ABST) fixture (Chadha, Bakuckas Jr., Fleming, Lin, & Korkosz, 2019), a new structural test capability at the FAA William J. Hughes Technical Center. The program objectives are to characterize the fatigue and damage tolerance performance of bonded repairs subjected to a simulated service load and to evaluate the limit load capability of a typical composite wing panel of transport category aircraft with a failed repair. In addition, methods and tools used for the analysis of performance and for evaluating and monitoring repair integrity are being assessed.

This program was undertaken in a phased approach, where phase 1 was the development of the ABST fixture, the details of which are provided in (Chadha, Bakuckas Jr., Fleming, Lin, & Korkosz, 2019). In this document, the results of phase 2 (initial baseline testing) are provided. This initial baseline testing characterized the material response of composite panels in unnotched pristine and open-hole configurations under constant moment loading. This baseline information

provided verification of the test fixture loading, validation of analysis models, and an initial reference point for NDI and structural health monitoring (SHM) systems. In general, the baseline panels were subjected to fatigue loading conditions that produce typical operational strain levels for transport-category wing panels for three design service objectives (~165,000 cycles). For the unnotched panel (panel 1), structural integrity was maintained through testing with no signs of damage in the test section. Measured strains in the test section were relatively constant and remained unchanged during fatigue. For the open-hole panel (panel 2), strain surveys revealed excellent correlation between test and analysis. Strain concentrations measured using strain gages and a digital image correlation (DIC) system matched finite element analysis results.

Future phase 3 efforts of this program more directly support the FAA BRSL policy, where several scarf configurations on solid laminate panels were tested. This testing was used to validate such analysis methods to determine allowable repair sizes within the requirements of BRSL policy. Results of phase 3 will be disclosed in a separate report.

2 Experimental procedures

A description of the experimental procedures used in this program, including the test fixture, panels, applied loads, and the inspection and monitoring methods, are outlined in this section.

2.1 Test fixture description

Testing was conducted by the FAA using the ABST fixture located at the FAA William J. Hughes Technical Center, as described in (Chadha, Bakuckas Jr., Fleming, Lin, & Korkosz, 2019). In general, this new structural test capability was developed in collaboration with the Boeing Company as part of this program, and is capable of applying major modes of loading to panels representative of a typical wing or stabilizer components (see Figure 1).

The ABST fixture is self-reacting and integrates mechanical, hydraulic, control, and data-acquisition systems. The mechanical system consists of a load module, wingbox assembly, and reaction structure. The wingbox assembly consists of the test panel (24-inches wide and 40-inches long), two pultruded fiberglass channels, and a lower steel plate, all mounted on one end to the load module and on the other to the reaction structure. The fiberglass channels allow for efficient load transfer to the test panels. Loads are applied via the loading module using four hydraulic actuators (50 Kips capacity and 12-inch stroke) powered by a 60 gallons/minute hydraulic power unit (HPU), controlled by an MTS FlexTest™ 100 system. Two central vertical actuators (A1 and A2) and two end actuators (A3 and A4) mounted at a 45˚ angle provide a multitude of individual loading modes, including constant moment, torsion, cantilever shear, and

horizontal bending, which can be combined to yield complex loading configurations. In the current test program, only constant moment loading is applied to the panels. An MTS FlexDAC™ 20 data acquisition system provides 64 channels to collect strain gages and displacement sensors data. A detailed, component-by-component description of the ABST fixture and supporting systems within the FAA's Structures and Materials Laboratory is provided in (Chadha, Bakuckas Jr., Fleming, Lin, & Korkosz, 2019).

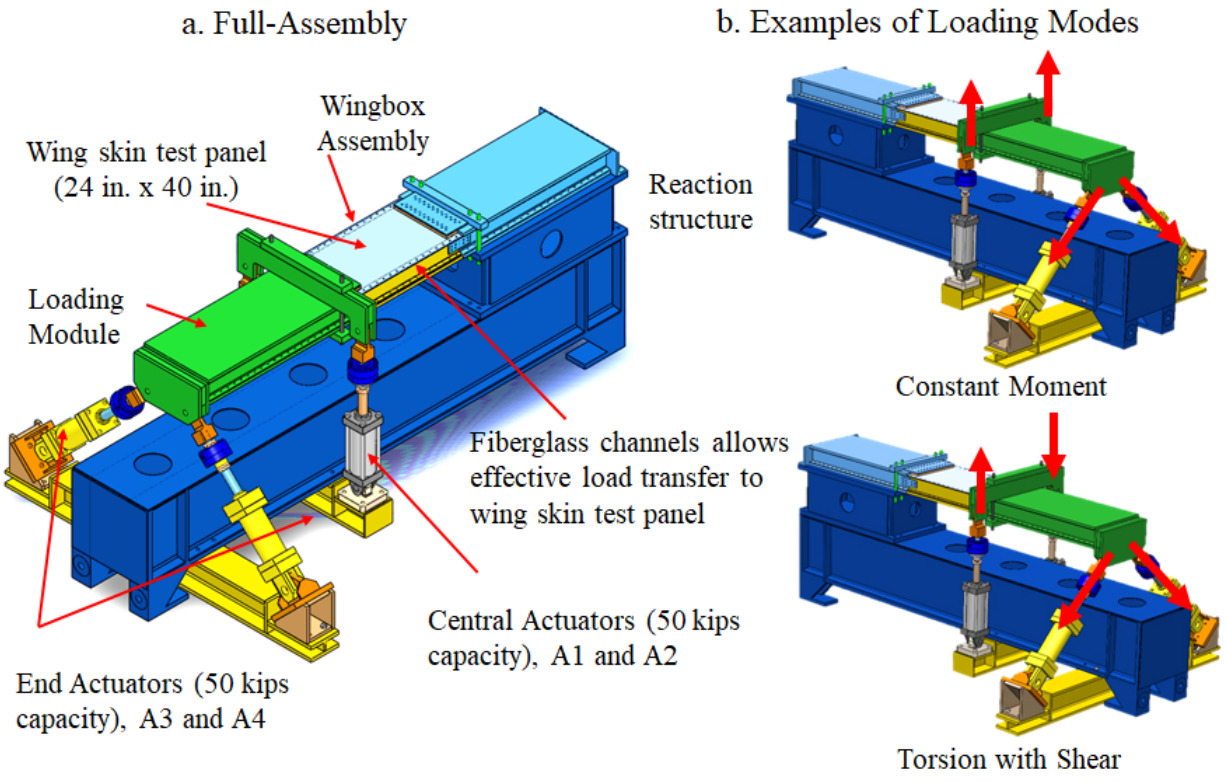

Figure 1. (a) ABST fixture and sub-components; (b) examples of fixture loading modes

2.2 Test specimens description

The test articles fabricated by Boeing were flat composite solid laminate panels (24-in wide, 40-in long, and 0.135-in-thick) representing typical carbon fiber reinforced polymer (CFRP) skin in outboard wing panels approaching wing tips. An 18-ply panel was considered having a quasi-isotropic lay-up, [±45°fabric/-45°/90°/45°/0°/-45°/90°/45°/0°]s. Panels were fabricated with a high modulus carbon/epoxy prepreg material, a typical material used by Boeing for the composite primary structure of commercial applications. These panels had holes machined to match the fixture attachment points. The 24-in long ends of the panel were reinforced with doublers (end tabs) for load introduction into the test article. These end tabs were made from the

same material and lay-up as the test panel, and included a taper region with ratios ranging from 10:1 to 30:1.

During the testing of the pristine panel (panel 1), it was noticed that delaminations and strain concentrations were initiating along the tapered regions of the panel (near the end tabs). To mitigate this issue in subsequent tests, the design of the panel was updated from a 10:1 ratio to a 30:1 ratio. Further discussion of this change, and the results that spurred it, are provided in the results section of this report. Images displaying this change in tab end dimensions are provided in Figure 2, where the initial tab is for the pristine panel, and the updated for the open-hole panel. Detailed engineering drawings of the panels are provided in appendix A.

a) Panel 1 - Pristine panel

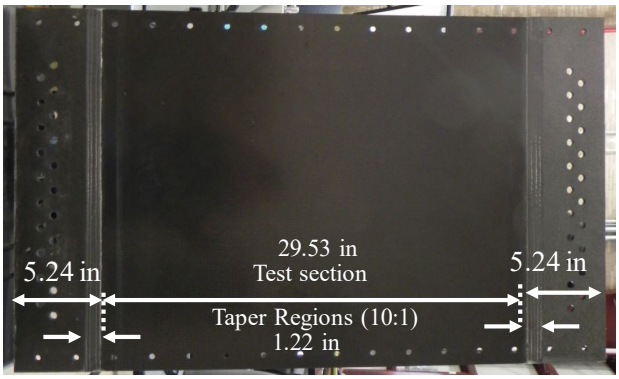

b) Panel 2 - Open-hole panel

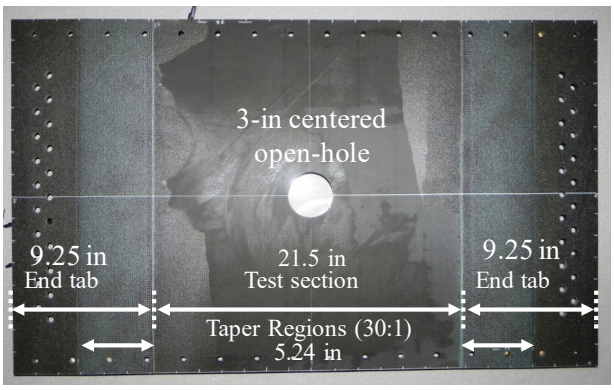

Figure 2. (a) Panel 1 - pristine panel; (b) Panel 2 - open-hole panel

2.3 Applied load and test matrix

The applied test loads used in this study represent the strains experienced by a composite wing panel of a typical transport-category aircraft, which usually includes compression, tension, and shear. In general, the following three loading types were considered:

1) Strain survey loads applied quasi-statically to a percentage of the service load (SL) conditions (typically 75% – 100% of the SL conditions) to ensure proper load introduction into the panel;
2) Fatigue loads simulating SL conditions conservatively estimated to be 37% of the ultimate load conditions and elevated fatigue loads to induce damage growth (40% – 60% of the ultimate load conditions);
3) Ultimate loads applied quasi-statically based on notched allowable coupons or barely visible impact damage load conditions.

A summary of these load configurations and the corresponding strain values is provided in Table 1. The tests covered in this paper were for tensile loading conditions only.

The applied maximum loads used in each test phase are shown in Table 2. The actuator loads were first predetermined from finite element analysis to provide constant target strains under a tensile bending moment. Slight adjustments in the actuator loads were made during the test until the target strains were obtained. Fatigue loading was conducted at R=0.1 and a frequency of 0.5 Hz. All testing was done under lab ambient conditions. For the open-hole panel, three increments of fatigue testing were conducted, each to one design service objectives (DSO) under 110%, 136% and 163% of the SL condition to promote the development of damage.

Table 1. Strain levels used in program

Test Description	**Load Type**	**Tensile Strain (με)**
Strain survey – 82% - 110% of the simulated service loads (SL) strain conditions	Static	1,800 – 2,400
Fatigue – simulated SL conditions (37% of ultimate strains)	Cyclic (R = 0.1)	2,200
Fatigue – elevated loads to induce damage growth (40 - 60% of ultimate strain)	Cyclic (R = 0.1)	2,400 – 3,600
Residual strength (ultimate strains) – typical design ultimate loads of notched allowables	Static	6,000

Table 2. Summary of applied loads

Panel	Load Type	Moment (lb_f-ft)	Actuator 1 & 2 (lb_f)	Actuator 3 & 4 (lb_f)	Target Strain (με)
1 – Pristine	Strain survey at 0.81SL	32,077	-3,811	5,391	1,800
	Strain survey at 1.10SL	42,764	-5,081	7,185	2,400
	Fatigue (3 DSOs, 0-165,000 cycles) at 1.10SL	42,764	-5,081	7,185	2,400
2 – Open-Hole	Strain survey at 0.81SL	30,196	-3,588	5,074	1,800
	Strain survey at 1.10SL	40,271	-4,784	6,767	2,400
	Fatigue (1st interval, 0-55,000 cycles) at 1.10SL	40,271	-4,784	6,767	2,400
	Fatigue (2nd interval, 55,000-110,000 cycles) at 1.36SL	53,363	-6,340	8,965	3,000
	Fatigue (3rd interval, 110,000-165,000 cycles) at 1.63SL	65,850	-7,823	11,065	3,600
	Predicted critical loads	104,498	-12,416	17,558	6,000
	Measured failure loads	116,992	-13,900	19,349	6,014

2.4 Deformation monitoring methods

Several methods were used to monitor the deformation of the specimens throughout the duration of the tests. Displacement sensors installed on the load application assembly were used to monitor the horizontal and vertical deflections of the cantilevered wingbox. Strain gages installed in the internal and external surfaces of the panel, and DIC systems situated above the wingbox, were used to monitor strains and displacements. Detailed descriptions of these instruments are provided in the subsequent sections.

2.4.1 String potentiometer-type displacement transducers

Four string potentiometer-type displacement transducers manufactured by TE Connectivity Measurement Specialties (P/N SP2-12) were installed on the load application assembly of the ABST fixture to monitor the horizontal and vertical deflection of the cantilevered specimens throughout testing. Two displacement transducers were installed at the far end of the structure to monitor vertical and horizontal deflection, while two displacement transducers installed near the central location of the fixture (i.e., where the load application assembly meets the wingbox, 6 inches away from the vertical actuators attachment points) were used to monitor vertical deflection alone. Each displacement transducer having a linear range of 0 to 12.5 inches, an

operating temperature of -0.4°F to 159.8°F, was connected via an analog voltage output to the MTS FlexDAC™ 20 or VTI EX1629 data acquisition system. Images depicting the locations of these devices are provided in Figure 3.

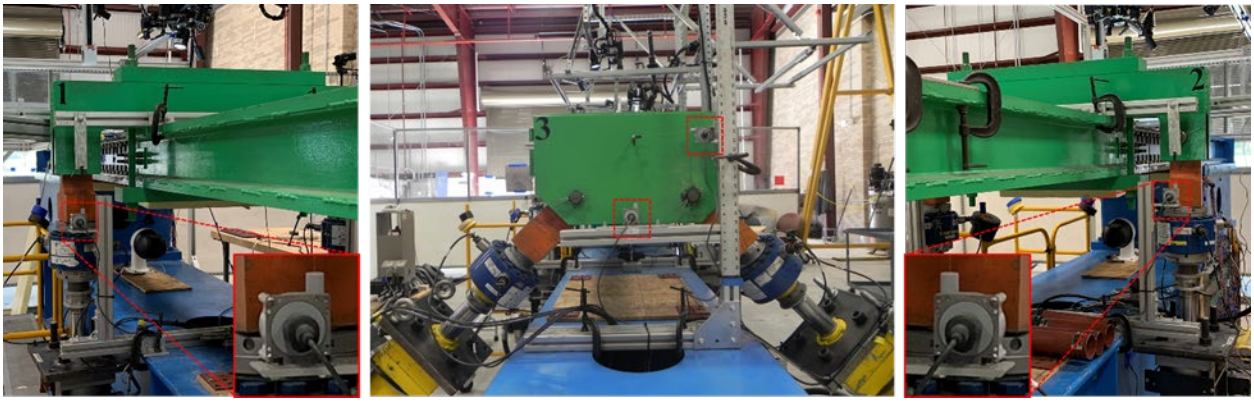

Figure 3. Displacement sensors used to monitor deflection of the load head near the actuators

2.4.2 Strain gages

CFRP test panels and the fiberglass side channels of the wingbox structure were instrumented with approximately 23 uniaxial and rosette strain gages. During initial phases of the test, strain gages were directly connected to the VTI strain gage measurement unit. During residual strength test of the open-hole panel and all subsequent tests in this program, strain gages were connected to a breakout board, which were connected to the FlexDAC system. Adhesives used to bond the strain gages included M-Bond AE-10 adhesive and M-Bond 200 adhesive. Schematics depicting strain gage positions during each panel test are provided in Figure 4.

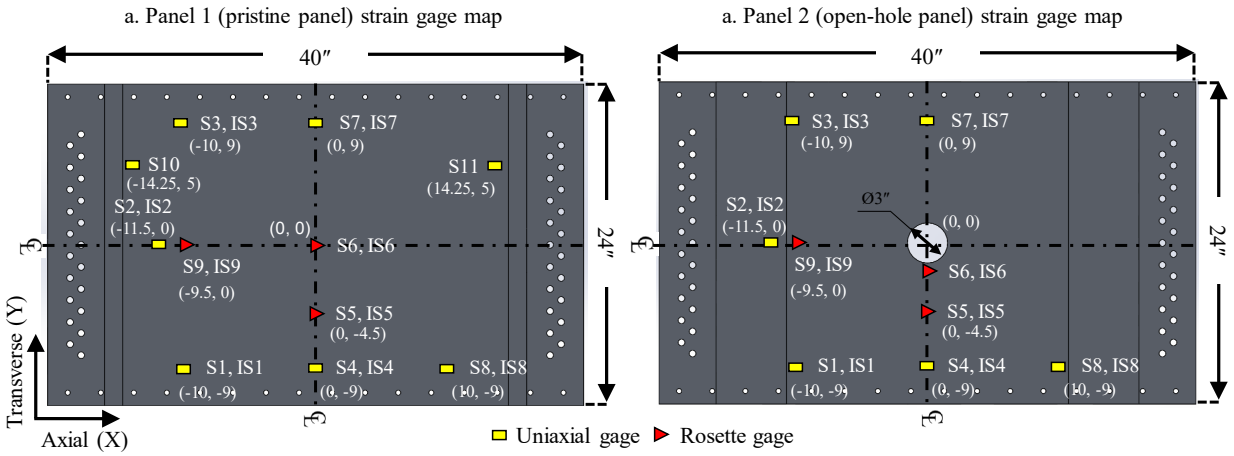

Figure 4. Strain gages layout for panels 1 and 2 during testing

2.4.3 Digital image correlation (DIC)

For each test, 5M ARAMIS 3D DIC systems were used to monitor strains and displacement exhibited by the CFRP specimens during quasi-static strain surveys. Each DIC system consisted of a sensor unit, a sensor controller unit, a high-performance PC system, two 5-megapixel cameras with 12-mm and 50-mm focal length lenses, and ARAMIS software. The cameras for each system were mounted on a custom-built structure above the external surface of the CFRP specimens, as shown in Figure 5a. The external surfaces of the panels were coated with a stochastic pattern by spraying speckles of flat black paint over a consistent layer of flat white paint, as shown in Figure 5b. The DIC system was interfaced with the MTS controller to provide load levels used to trigger and synchronize data acquisition during strain surveys and residual strength tests. During residual strength loadings, DIC data was acquired at a frequency of 1 Hz.

2.5 Damage monitoring methods

Throughout the duration of the test, several methods were utilized to monitor the initiation and growth of damage within the CFRP specimens. For visual detection, several camera systems, with varying specifications, were used to monitor the specimen from a multitude of zooms and angles. For detection of non-visual damage, flash thermography, phased array ultrasonic, pulse-echo ultrasonic methods were used. For real-time detection, an acoustic emission system was used. Additionally, a structural health monitoring system was used intermittently.

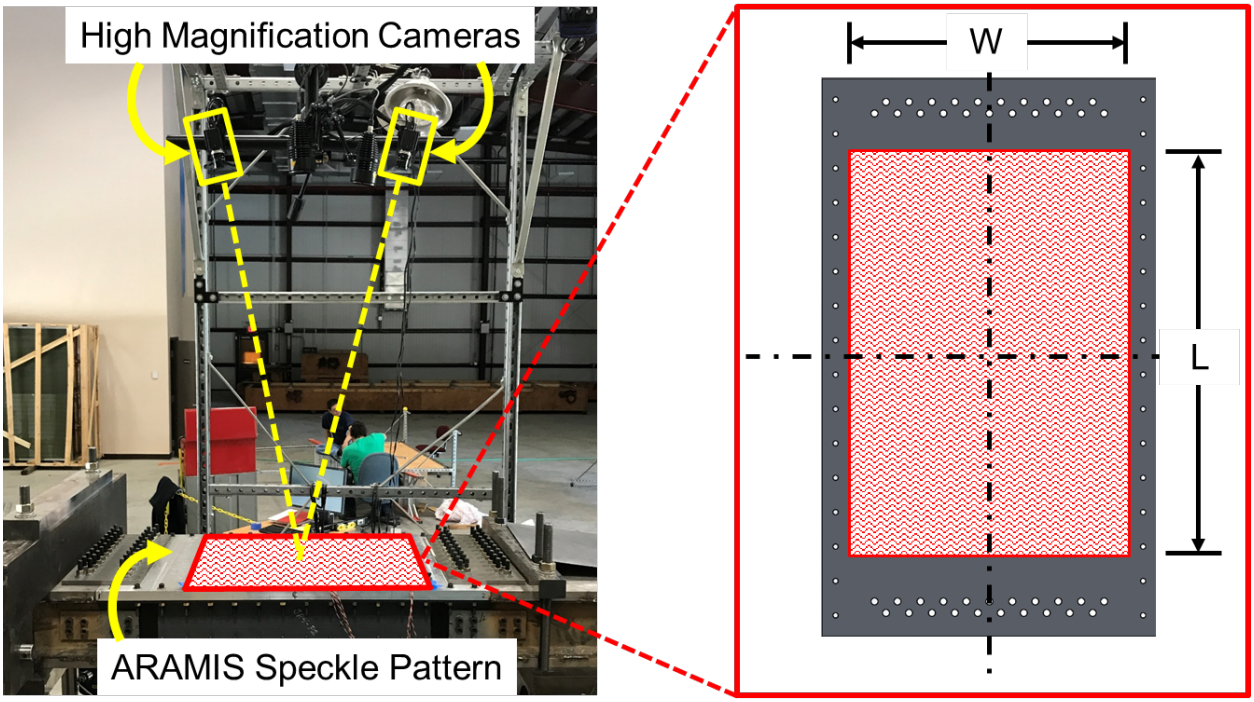

Figure 5. Images displaying typical setup of a DIC system during the tests

2.5.1 Visual

Eight high definition camera systems featuring a variety of specifications were used to monitor the specimens from a variety of vantage points. Camera systems included two LOREX 4K ultra high definition IP bullet security cameras, two LOREX 4MP HD IR bullet IP camera NTSC, a Canon VIXIA HF R80 camcorder, two GigE color zoom cameras manufactured by Imaging Source, and a Sony compact full-HD camcorder. In general, the quantity and positioning of the cameras varied throughout the test and changed depending upon the test requirements. Each camera was connected to a monitor located in the laboratory control area to continuously monitor and record during test. Examples of the camera positioning are provided in Figure 6.

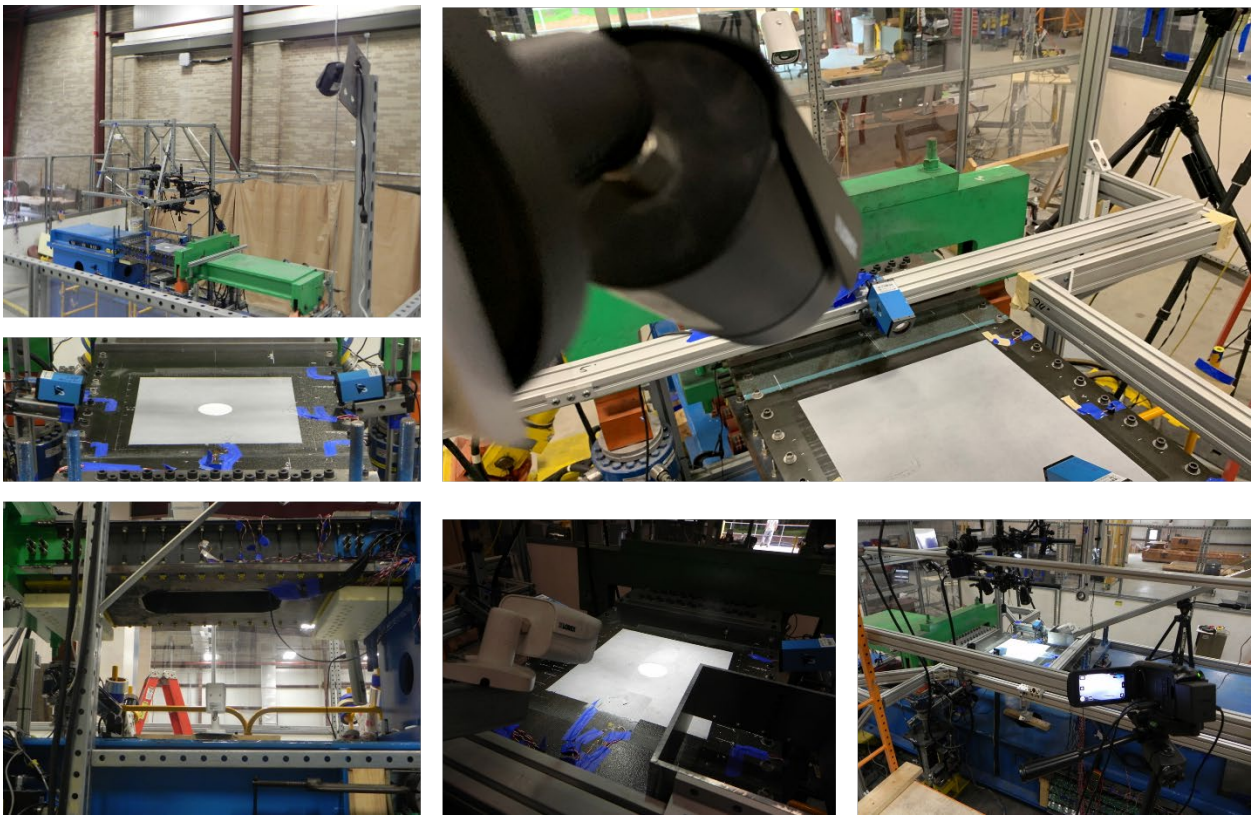

Figure 6. Images displaying camera systems used to monitor panels 1 and 2

2.5.2 Flash thermography

Flash thermography is an NDI method that utilizes measured changes in the surface temperature of a specimen subjected to a spatially uniform flash of light, captured via sequential infrared images, to detect subsurface irregularities (e.g., interlaminar and intralaminar delaminations). A Thermal Wave Imaging (TWI) Thermoscope® II system was used to monitor the formation and growth of damage in the central test sections of each panel. The Thermoscope® II system consists of: (1) A portable high-performance PC system pre-equipped with MOSAIQ® analysis software, shown in Figure 7a, and; (2) an integrated illumination head with two xenon flash lamps, an infrared camera, and an LCD monitor, shown in Figure 7b. For each inspection, properties were as detailed in Table 3.

Table 3. Properties of flash thermography system throughout panel 2 test

Property	**Value**	**Property**	**Value**
Acquisition length (s)	30.3	Flash frame	21
Capture rate (frames/s)	29.97	PFD (ms)	4.1
TSR skip frames	2	FTO (ms)	0.2
Trigger mode	Internal	-	-

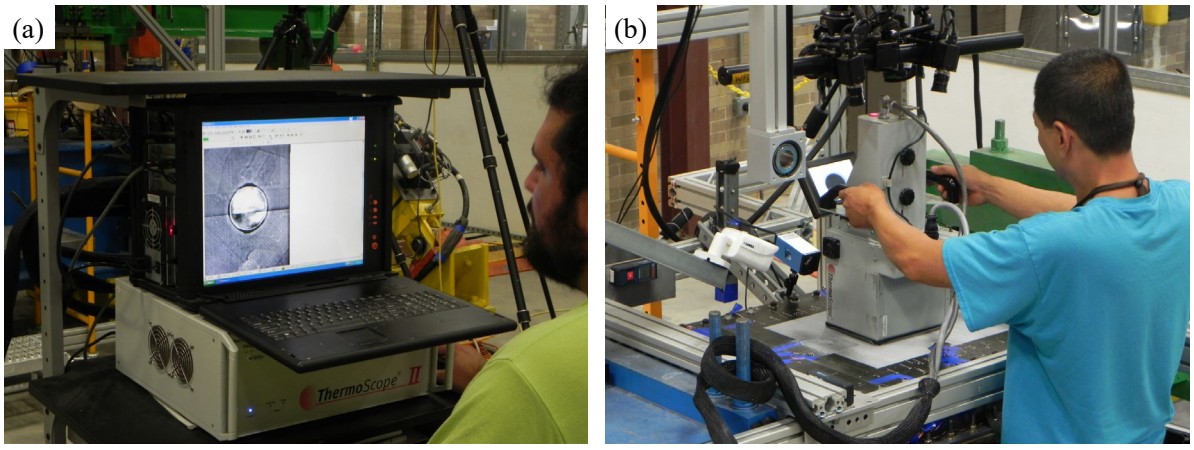

Figure 7. Flash thermography system

2.5.3 Phased array ultrasound

Phased array ultrasound is an NDI method that utilizes measured changes in ultrasonic waveforms, generated by an array of piezoelectric crystals, in a specimen to detect subsurface irregularities (e.g., interlaminar and intralaminar delaminations). An Olympus MX ultrasonic flaw detector was used in conjunction with several supporting components, such as an Olympus 3.5L64-NW1 probe, an Olympus 3.5L64-NW1 wedge, and a versaMOUSE scanner, and with water supplied via a small pump acting as a couplant, to monitor the formation and growth of damage in the central test sections of each panel. Images of the equipment being used during inspection are provided in Figure 8. For each inspection, properties were as detailed in Table 4.

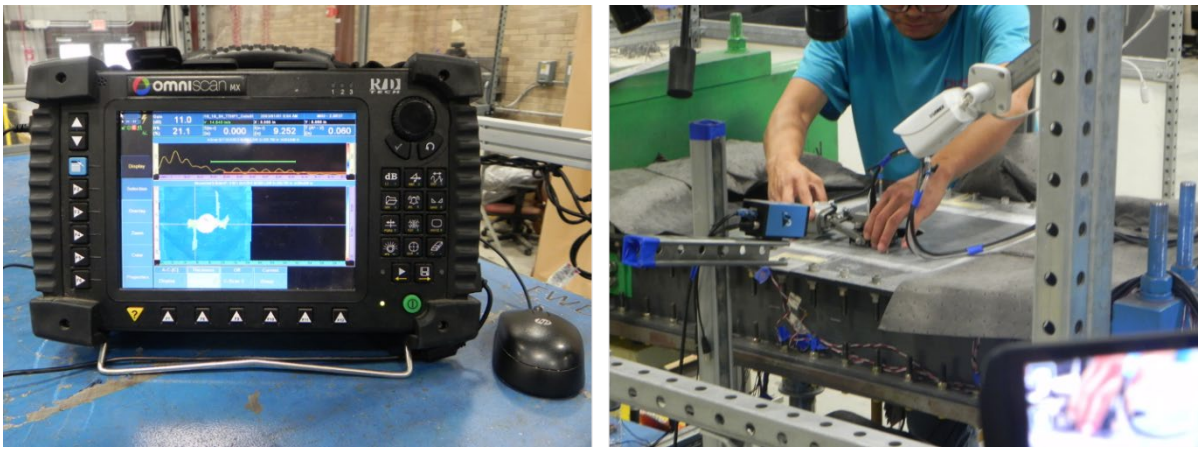

Figure 8. Phased array ultrasonic system used throughout testing

Table 4. Properties of phased array ultrasound system throughout panel 2 test

Property	**Value**	**Property**	**Value**
Wave type	Longitudinal	Pulser mode	Pulse-echo
Sound velocity (in/μs)	0.075, 0.090	Pulser voltage (V)	80 (High)
Gain (dB)	11.00	Receiver filter	4 MHz
Range (in)	0.120, 0.144	Pre-trigger (μs)	0.00
Band-pass filter (MHz)	3.1-7.5	Gate threshold	30%, 40%
Beam delay (μs)	0	Gate start (in)	0.508, 0.040
Pulse width (ns)	142.50	Gate width (in)	0.254, 0.065
Skew (deg)	90.0		

2.5.4 Pulse-echo ultrasound

Pulse-echo ultrasound is an NDI method that utilizes measured changes in ultrasonic waveforms, generated by a piezoelectric crystal, in a specimen to detect subsurface irregularities (e.g., interlaminar and intralaminar delaminations). An Olympus EPOCH 650 ultrasonic flaw detector was used in conjunction with an AeroFab NDT ARD-525 probe and Sonotech Ultragel II to monitor the formation and growth of damage in the central test sections of each panel. Images of the equipment being used during inspection are provided in Figure 9. For each inspection, properties were as detailed in Table 5.

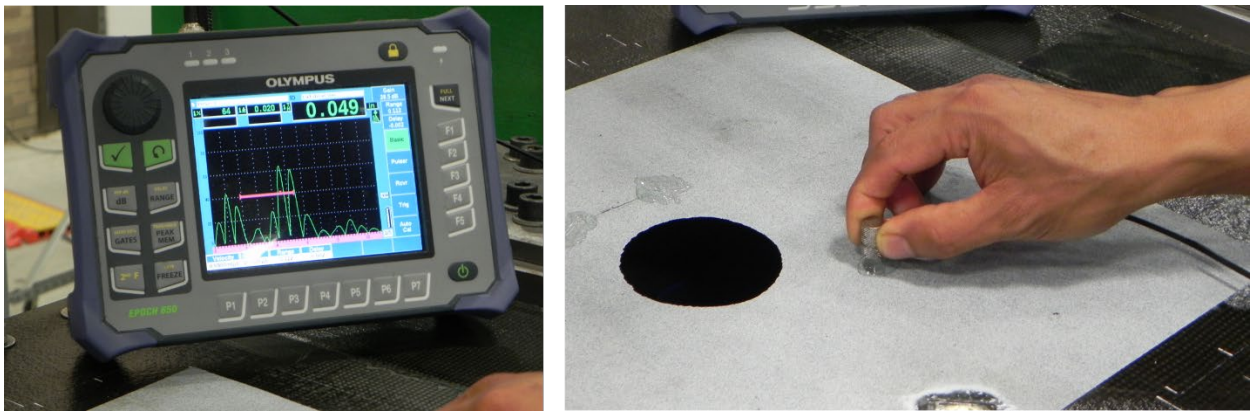

Figure 9. Pulse-echo ultrasound system used throughout testing

Table 5. Properties of pulse-echo ultrasound system throughout panel 2 test

Property	**Value**
Sound velocity (in/μs)	0.090
Pulser energy (V)	400
Pulser damp (Ohm)	50
Pulser mode	Pulse-echo
Pulser frequency	5 MHz
Receiver filter	0.5 - 4 MHz

2.5.5 Acoustic emission (AE)

AE is a passive, receptive, NDI technique that is capable of detecting, in real-time, stress waves generated within a structure during the initiation and growth of damage. A MISTRAS AE was used to monitor and record acoustic activity within the open-hole panel during each sequence of quasi-static loading/unloading and constant amplitude fatigue loading. The AE system consists of a SAMOS 32 system with two eight-channel (PCI-8) data acquisition boards, a parametric board, and data acquisition software (AEWin) installed and operated on a Windows XP operating system. The AE system was interfaced with the MTS controller to synchronize data with the applied loads. Images of the equipment used during test is provided in Figure 10. Two six-sensor-sets (one with R15I sensors and one with WDI sensors), installed concentric to the central hole and equally spaced at a diameter of 16 inches, were used to monitor AE. A schematic depicting the location of the AE sensors with respect to the panel is provided in Figure 11. AE data analysis methodology and results for panel 2 were reported in (Neel, Awerbuch, Tan, & Ozevin) for fatigue test and (Neel, Awerbuch, Tan, & Ozevin) for the residual strength

test. In general, results revealed a good correlation between AE activity and location of damage as well as the occurrence of imminent fracture using four-prong approach.

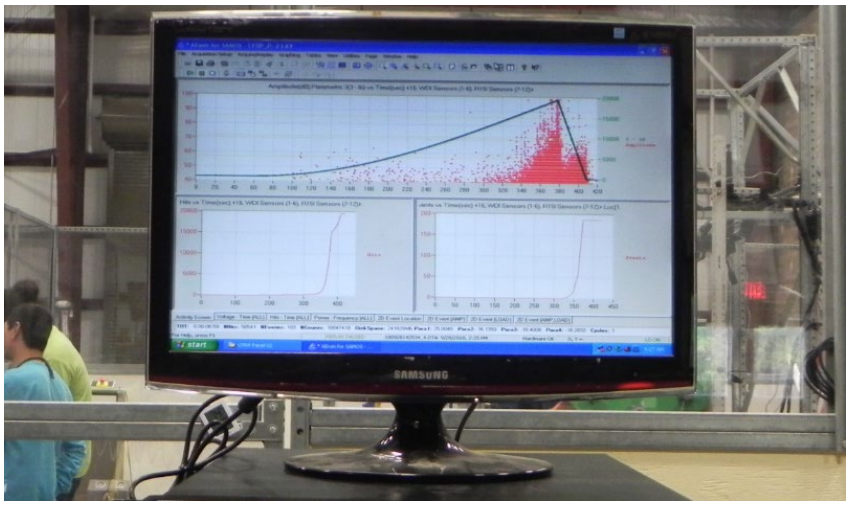

Figure 10. Acoustic emission system used throughout testing

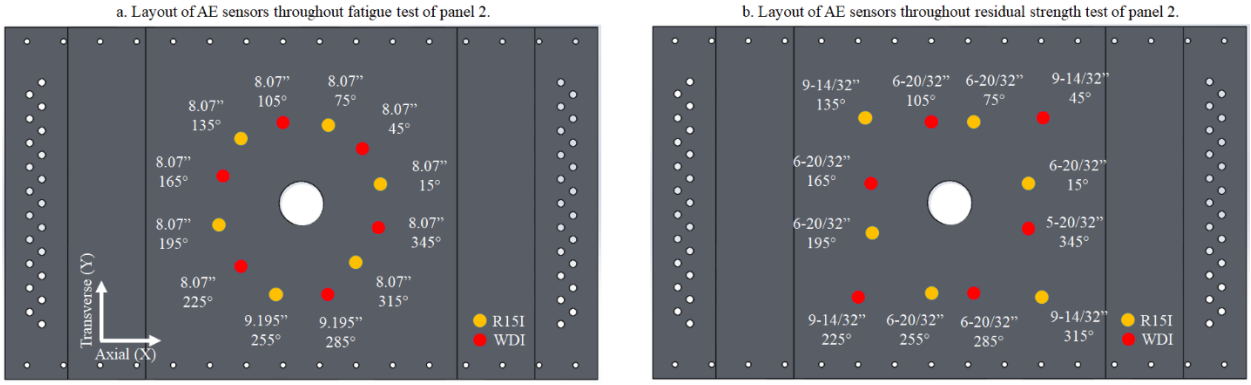

Figure 11. Layout of AE sensors throughout fatigue testing of panel 2

2.5.6 Structural health monitoring (SHM)

A Piezoelectric-based SHM system utilizes measured changes in the characteristics of ultrasonic waveforms induced in a specimen to detect damage. An Acellent system was used in a pitch-catch approach to monitor the initiation and growth of damage in the specimens described herein. Equipment included a high-performance PC system equipped with a data processing, visualization and analysis software (ACESS/SmartComposite), a ScanGenie III data acquisition system, Acellent SMART layer transducers (P/N SML-SP1-1/4-20), and Acellent temperature sensors (P/N SML-TEMP-2). Images of the equipment used during test are provided in Figure

12, and the layout of the sensors placed on the pristine panel and open-hole panel are shown in Figure 13. The collected SHM data is currently being processed and is not reported in this document.

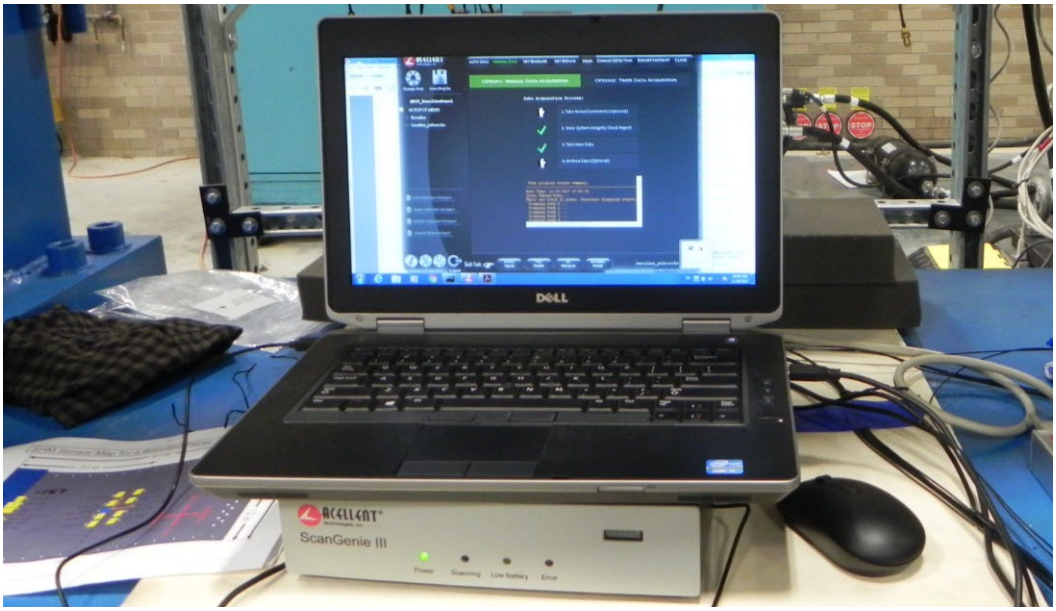

Figure 12. SHM system used throughout testing

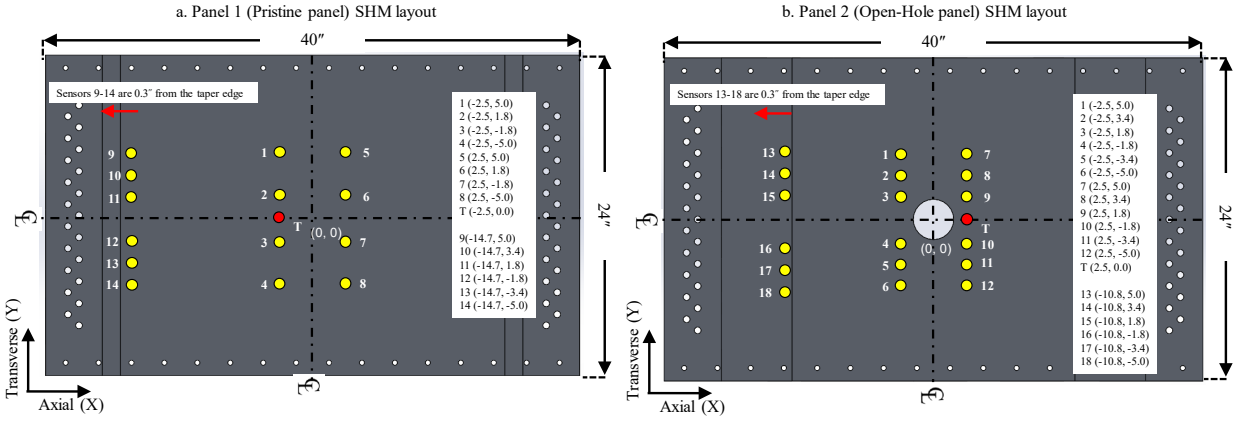

Figure 13. Layout of SHM sensors used throughout testing

2.5.7 Climate monitoring

A Rotronic environmental sensor was used to monitor the temperature and humidity in the laboratory during testing. An image of the sensor as it was positioned during testing is provided in Figure 14a. As shown, the sensor was consistently positioned on the base structure of the ABST fixture, directly under the wingbox structure. In addition, Figure 14b shows the actual temperature and humidity data in the vicinity of the test panel collected during panel 2 fatigue test.

(a) Temperature and humidity sensor

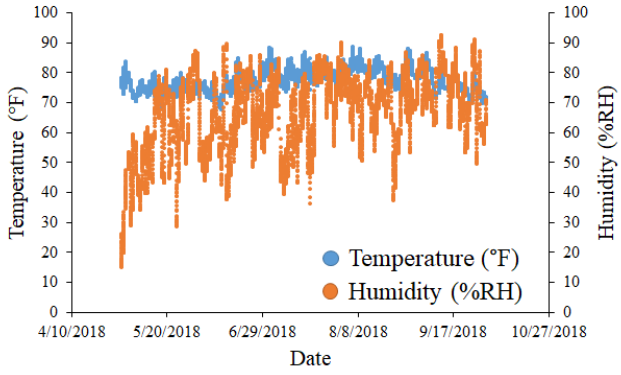

(b) Temperature and humidity data collected during panel 2 fatigue test

Figure 14. Temperature and humidity sensor and sample data collected during panel 2 test

3 Analytical procedures

Boeing conducted analysis procedures in support of this program, as outlined below.

3.1 Finite element analysis

Finite element models (FEM) of the test fixture and test panels, shown for example in Figure 15, were created to simulate the loading of the panel prior to actual testing and provided predictions of: (1) Actuator loads that the ABST fixture should apply to provide appropriate target strains; (2) stress and strain fields; (3) damage initiation and growth in the composite panel, and; (4) ultimate load and residual strength.

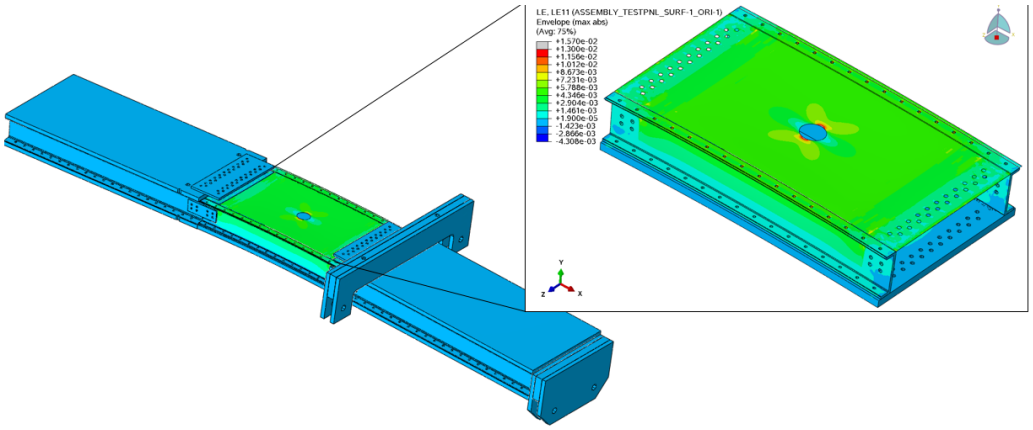

Figure 15. FEM used in test setup and pre-test prediction

Figure 16 shows FEM predicted axial strain field under 75% of the fatigue load for the open-hole panel, as well as strain distribution along the critical section from the edge of the hole. DIC results along multiple sections are also included for comparison.

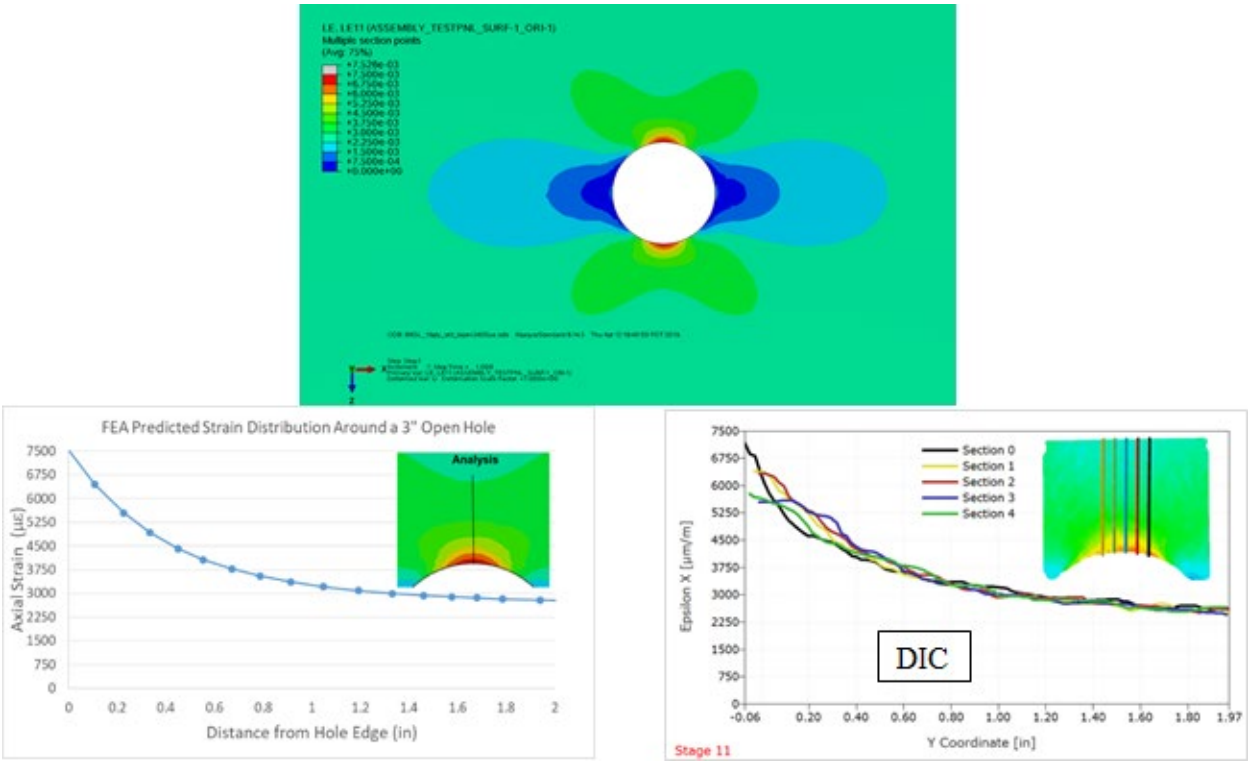

Figure 16. Strain concentration around the open hole showing good correlation with DIC

Figure 17 shows test-analysis correlation results for all strain gages on the open-hole panel. These results demonstrate that FEM predictions are within 10% of the test results.

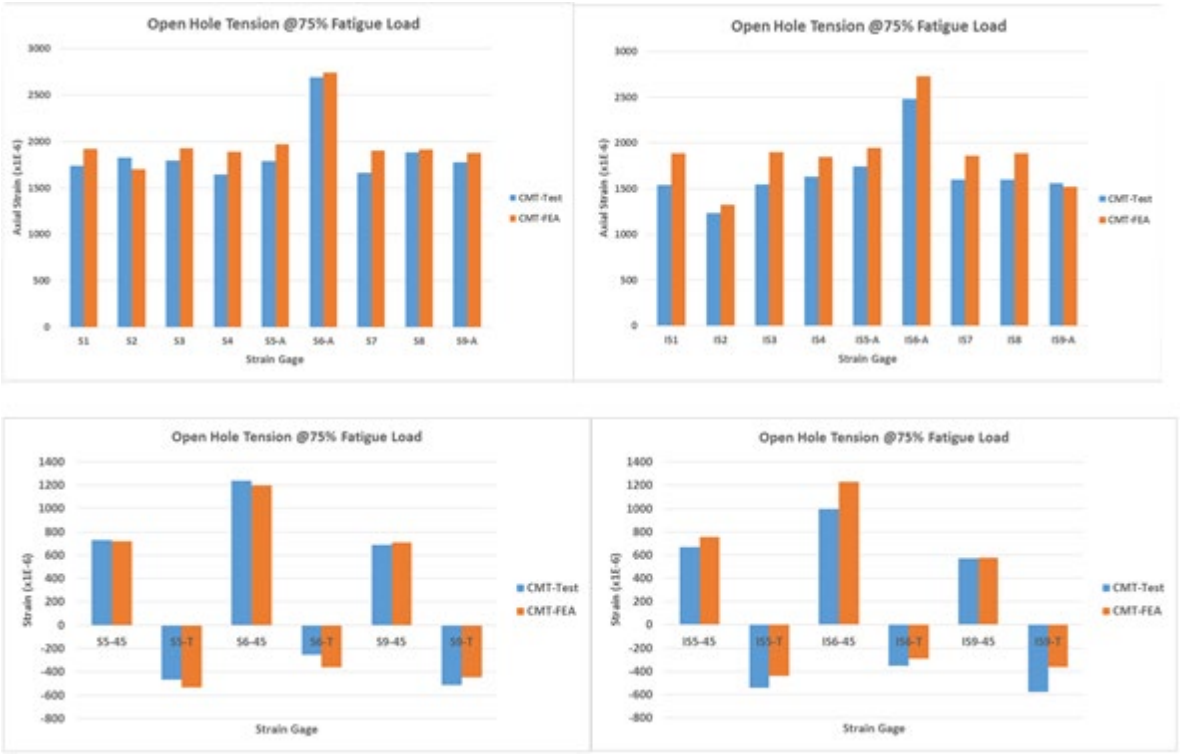

Figure 17. Open-hole panel strain gage predictions (FEA) vs measurements (test)

An advanced progressive failure analysis (PFA) approach was used to predict the ultimate load levels for various damaged panels in this test program. The current approach implements the Hashin in-plane failure criteria, and the PFA input properties were derived from analysis and tests for the specific materials, processes, and design practices. Figure 18 shows fiber tensile failure index contour (a) at ultimate load for the open-hole panel (only the damaged regions were shown) and (b) the axial strain contour. The predicted final failure moment was 104,498 lb_f-ft, within 15% of the test result. It should be noted that only the center of the panel was assigned damage initiation and evolution properties, as shown in Figure 18(a).

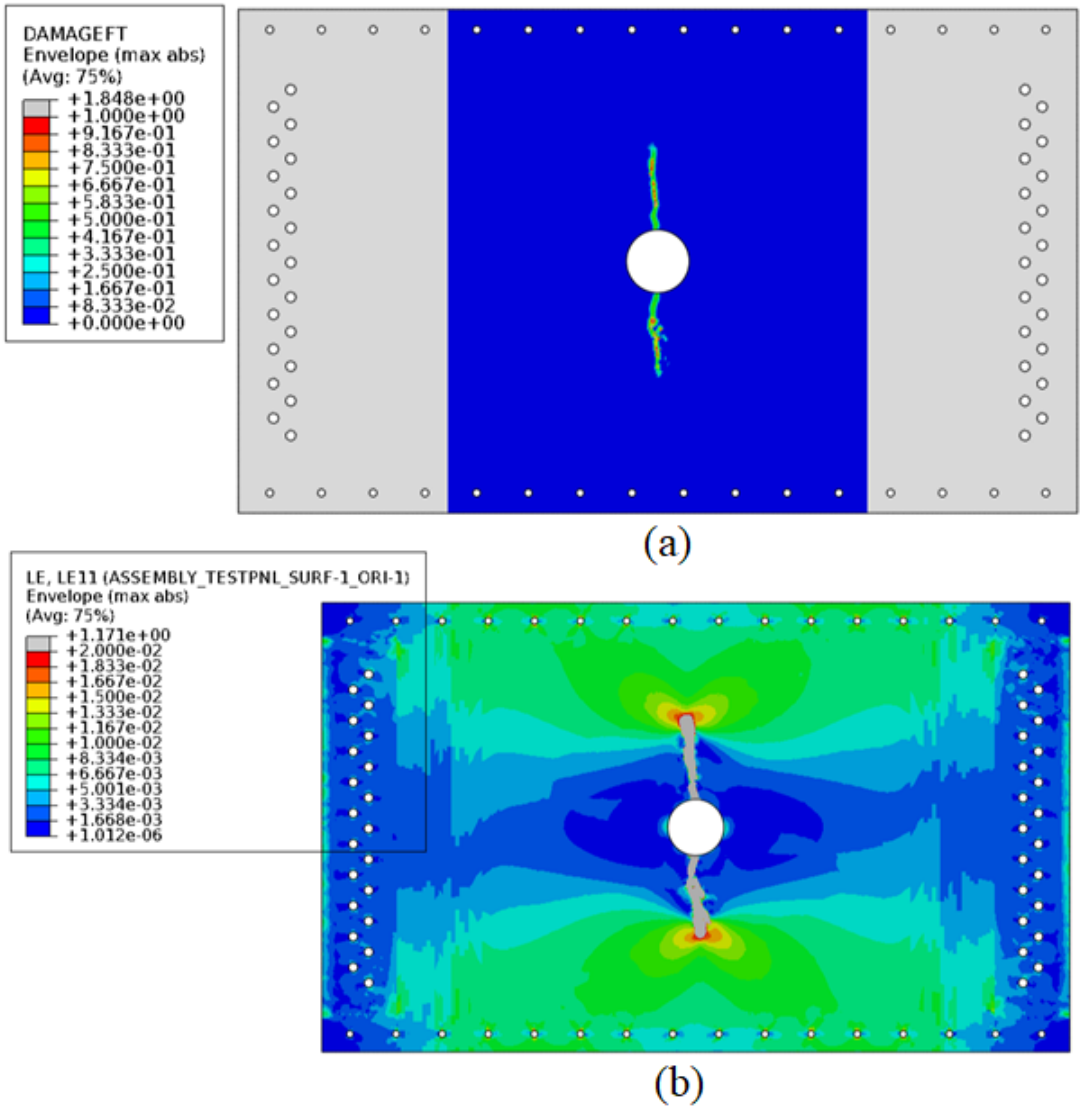

Figure 18. PFA prediction of fiber tension failure and axial strain at final failure

3.2 BRSL semi-analytical method development and verification

The development and verification of a rapid-executing BRSL analysis method is being undertaken to predict the limit load residual strength for a failed scarf repair in solid composite laminates and honeycomb panels. It is based on the classic strain concentration factor K_{d0} approach modified by a geometry factor K_{sr}, as shown in Figure 19, under tensile loading. Testing will be used to support improved analysis methods to better represent the actual damage within the requirements of BRSL policy. The initial focus of this phase has been the limit-load characterization for partial and full-depth scarf configurations for solid laminates under tension

produced by constant moment. From the open-hole panel testing, the characteristic length parameter d_0 was found to be 0.05" based on equation (4) in Figure 19.

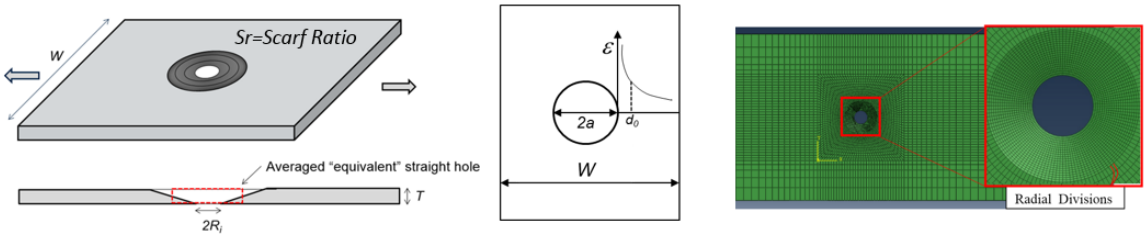

(1)Strain Concentration Factor (SCF)	$K_t = K_{d0}(K_{Sr})$
(2) Scarf Factor	$K_{Sr} = 1 + function(\frac{T}{Ri}, \frac{Ri}{W}, Sr)$
(3) Predicted failure strain	$\varepsilon_{scarf} = {}^{\varepsilon_{unt}}/_{K_t}$
(4) Strain Concentration Factor for straight Hole (d_0: Characteristic Length)	$K_{d0} = \frac{1}{2}C_w\left\{2 + \left(\frac{a}{a+d_0}\right)^2 + 3\left(\frac{a}{a+d_0}\right)^4 - (K_T^\infty - 3)\left[5\left(\frac{a}{a+d_0}\right)^6 - 7\left(\frac{a}{a+d_0}\right)^8\right]\right\}$
(5) Edge Factor	$C_w = \left\{\frac{3(1-2\,a/W)}{2+(1-2\,a/W)^3} + \frac{1}{2}\left(\frac{2a}{W}M\right)^6 (K_T^\infty - 3)\left[1 - \left(\frac{2a}{W}M\right)^2\right]\right\}^{-1}$
(6)Edge Factor Term M	$M^2 = \frac{\sqrt{1 - 8\left[\frac{3(1-2\,a/W)}{2+(1-2\,a/W)^3} - 1\right]} - 1}{2(2a/W)^2}$
(7) SCF for an infinitely large orthotropic plate	$K_T^\infty = 1 + \sqrt{2\left(\sqrt{\frac{E_x}{E_y}} - \nu_{xy}\right) + \frac{E_x}{G_{xy}}}$

Figure 19. Engineering approach based on K_t to predict residual strength

4 Results and discussion

Throughout each test, several strain measurement techniques and NDI methods were used to monitor and assess distributions of strain as well as evidence of damage. Representative results obtained using these methods is provided in the subsequent sections for panels 1 and 2.

4.1 Panel 1 (pristine)

Figure 20 summarizes initial results from the baseline testing for panel 1, an unnotched pristine panel. For this test, the loads applied by the four actuators produced a moment resulting in a constant far-field target strain of 2400 με within the test section of the panel, as determined from DIC and strain-gage measurements. This strain level represents 40% of notch ultimate allowable strains and simulates conservative operational strain levels for transport-category wing panels.

In the end tab sections, strain levels were higher than in the test section, resulting in local delaminations of the taper region. End tabs were redesigned with a high taper ratio (from 10:1 to 30:1) to reduce peel stresses in subsequent panels. Excellent correlation in strains was obtained

and was measured using DIC and strain gages. In addition, strains on the external and internal surfaces of the panel were monitored during fatigue up to 165,000 cycles (i.e., 3 DSOs). Throughout fatigue, the strains remained unchanged, as shown in Figure 21. The detailed strain gage and displacement sensors are provided in appendix B, and the DIC results are provided in appendix D.

The structural integrity of panel 1 was maintained through fatigue testing with no signs of damage in the test section. However, NDI inspections indicated the development and slow growth of disbonds between the panel and the end tabs during fatigue. Figure 22 shows the flash thermography and phased array ultrasonic results of the pristine panel, captured prior to the panel installation, and results of the end tabs captured after approximately 64,272 fatigue cycles. As shown, multiple disbonds developed less than halfway through 165,000 cycles in multiple sections of the end tab-main panel transition region. Overall, these disbonds had no effect on the load transfer to the test section.

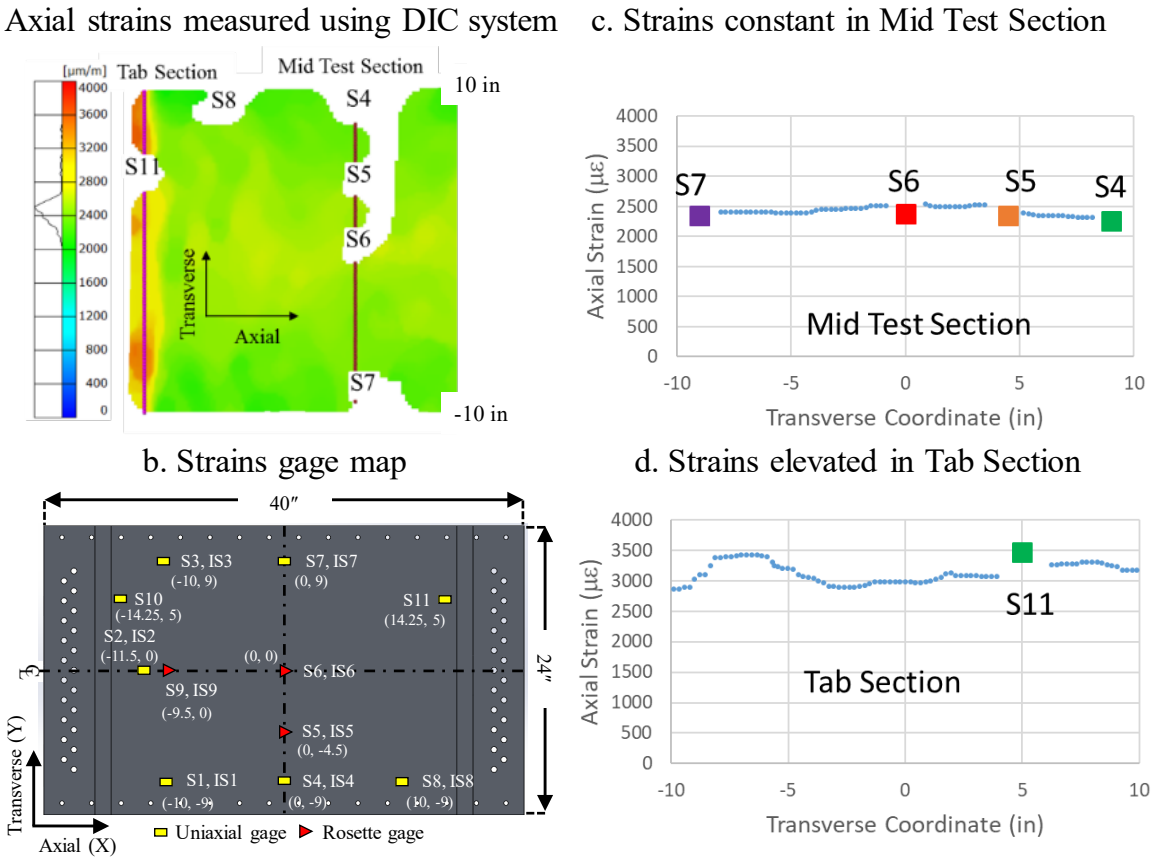

Figure 20. Strain distribution in the center and tab sections of the pristine panel

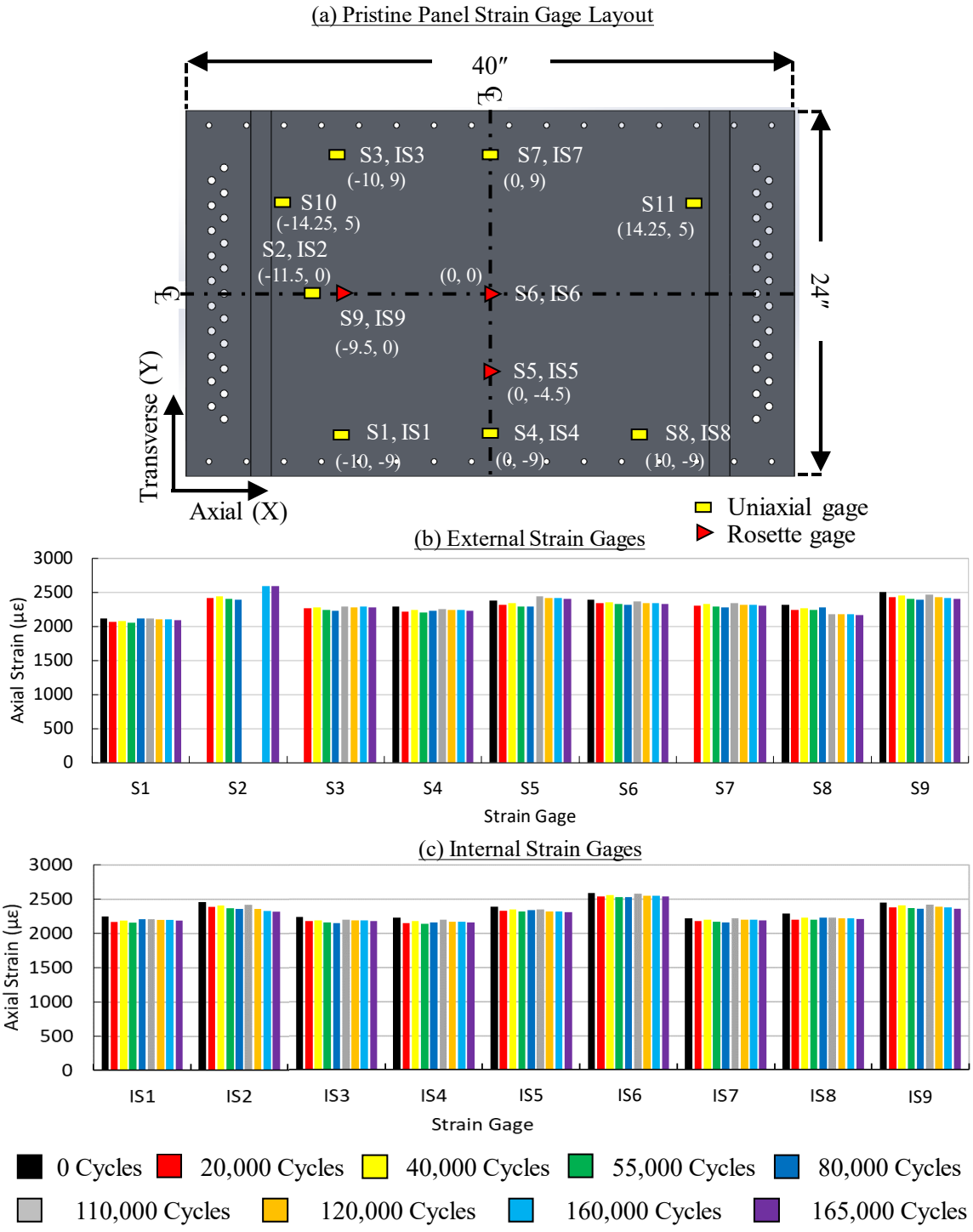

Figure 21. Strain gage results for panel 1 during fatigue

(a) Flash Thermography Result Showing Delaminations in Tab Region

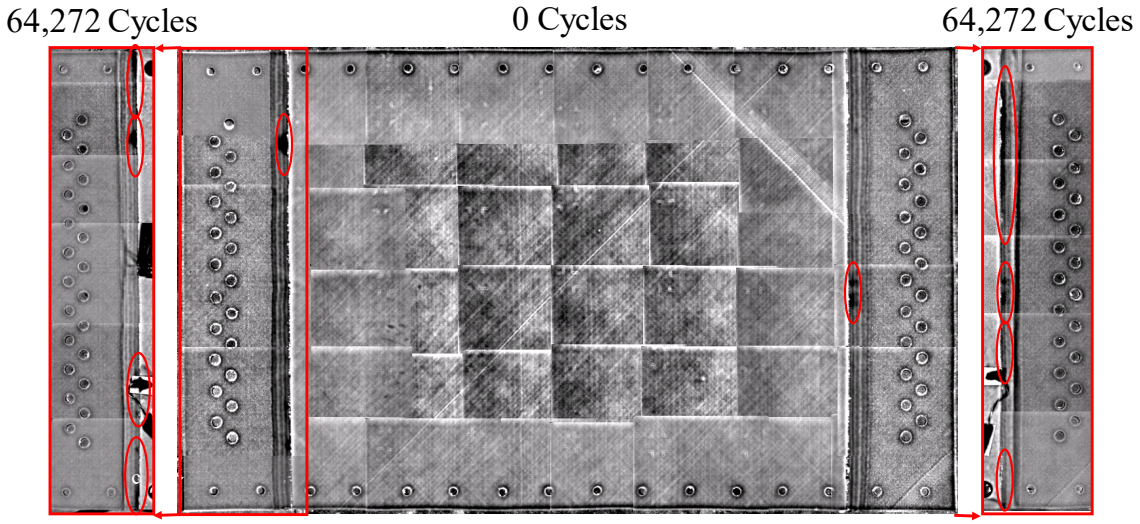

(b) Phased Array Result Showing Delaminations in Tab Region

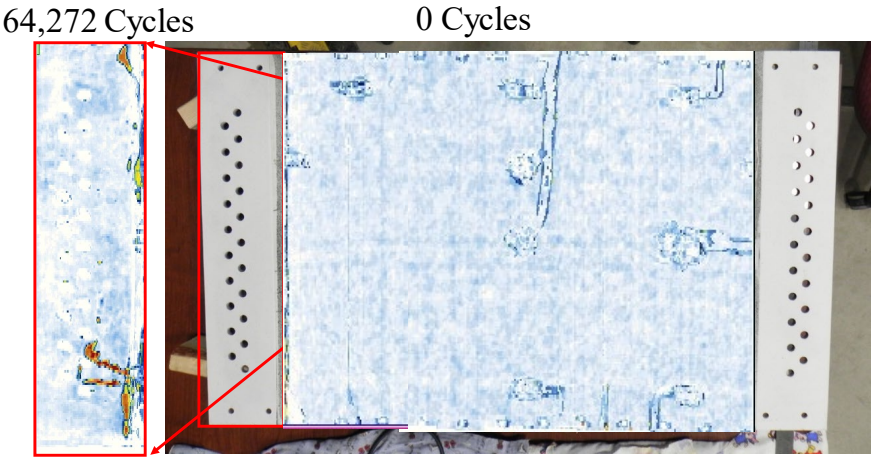

Figure 22. Flash thermography and phased array results in the tab regions of panel 1

4.2 Panel 2 (Open-hole)

The open-hole panel was subjected to 3 steps of testing as follows:

1) Baseline strain surveys to compare the test results with analysis predictions.
2) Fatigue loading (40% - 60%) of the ultimate load during which the panel was fatigued tested to 3 DSOs, i.e., 165,000 cycles in 55,000-cycle intervals at three different target strain levels of 2,400, 3,000 and 3,600 με.
3) Post-fatigue residual strength loading was applied in five increments, each with increased level up to failure.

Representative results from the first step of testing are provided in Figure 23, showing axial strain results recorded by strain gages installed on the external surface of the panel and axial strain results recorded by DIC, both gathered at maximum load level of the strain surveys. As shown, good correlations were observed between results by strain gages and DIC and those predicted by finite element analysis.

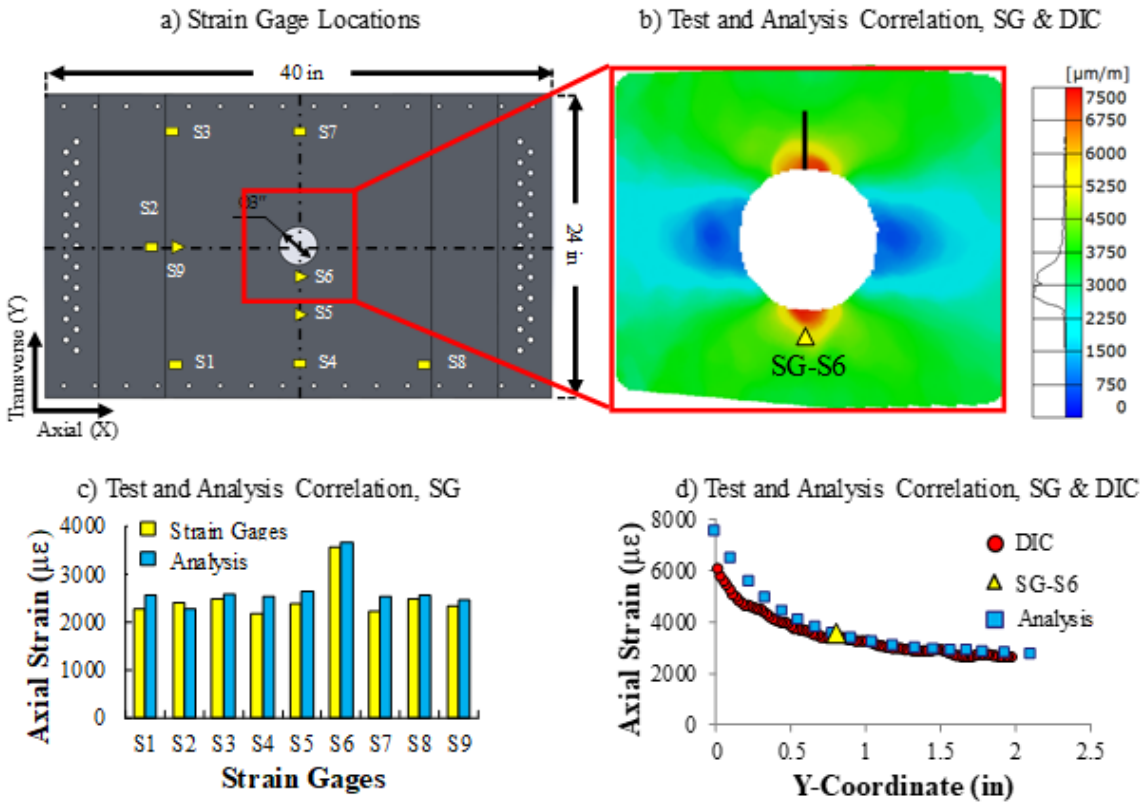

Figure 23. Correlation between strain gage, DIC and analysis results during strain survey

In step two, panel 2 was fatigued tested to 165,000 cycles in 55,000-cycle intervals (each 1 DSO) at three different target strain levels of 2400, 3000, and 3600με. The increase in load levels was to promote the development of damage. Localized hole-edge delaminations were initially detected visually during the 3000με target strain fatigue test and were subsequently monitored using NDI. At the end of fatigue testing, delaminations approximately 0.5-in wide, located near the surface at 15%–20% of the panel depth along the hole boundary at the 6 and 12 o'clock positions were measured. Indications of visual damage are provided in Figure 24, while those captured by flash thermography, phased array ultrasonic, and by pulse-echo ultrasonic are provided in Figure 25. The detailed thermography, phased array, and pulse-echo results are

provided in appendices F, G, and H, respectively. Detailed visual results are provided in appendix E.

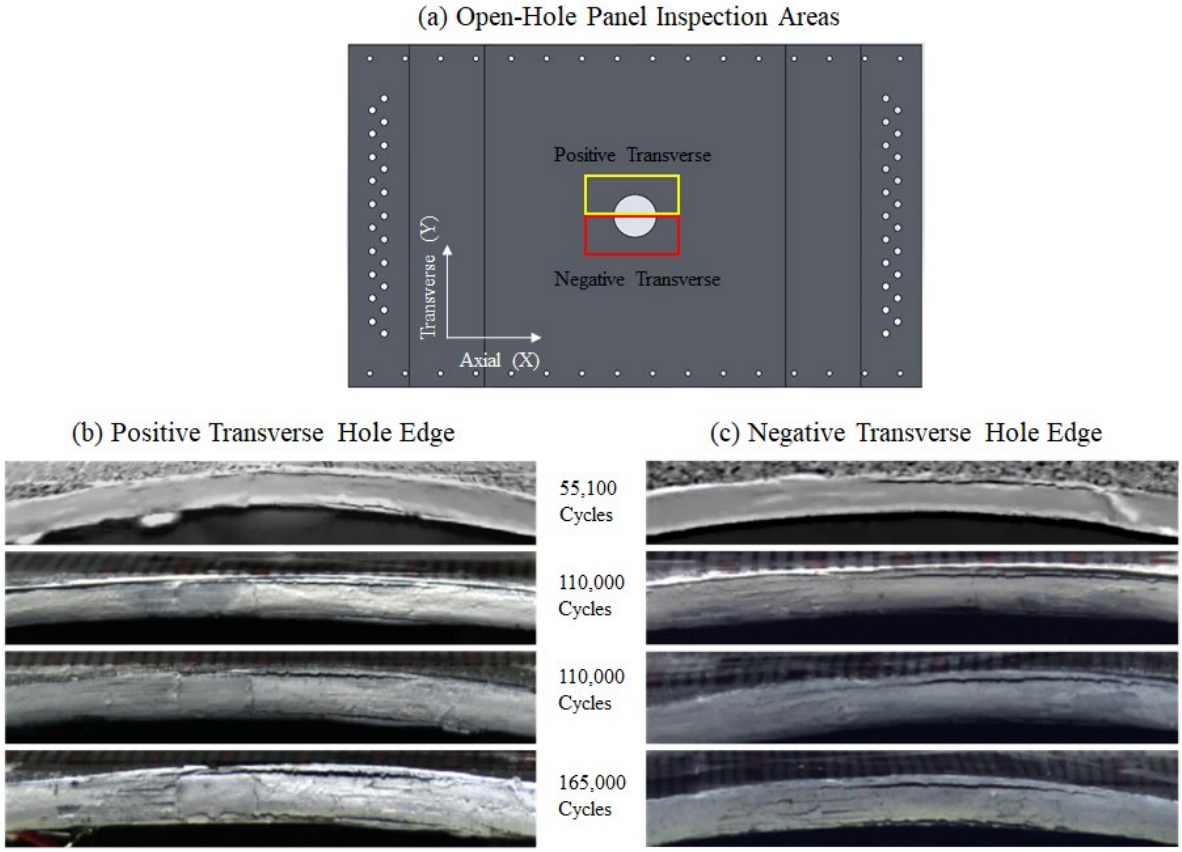

Figure 24. Visual results for the open-hole panel throughout fatigue

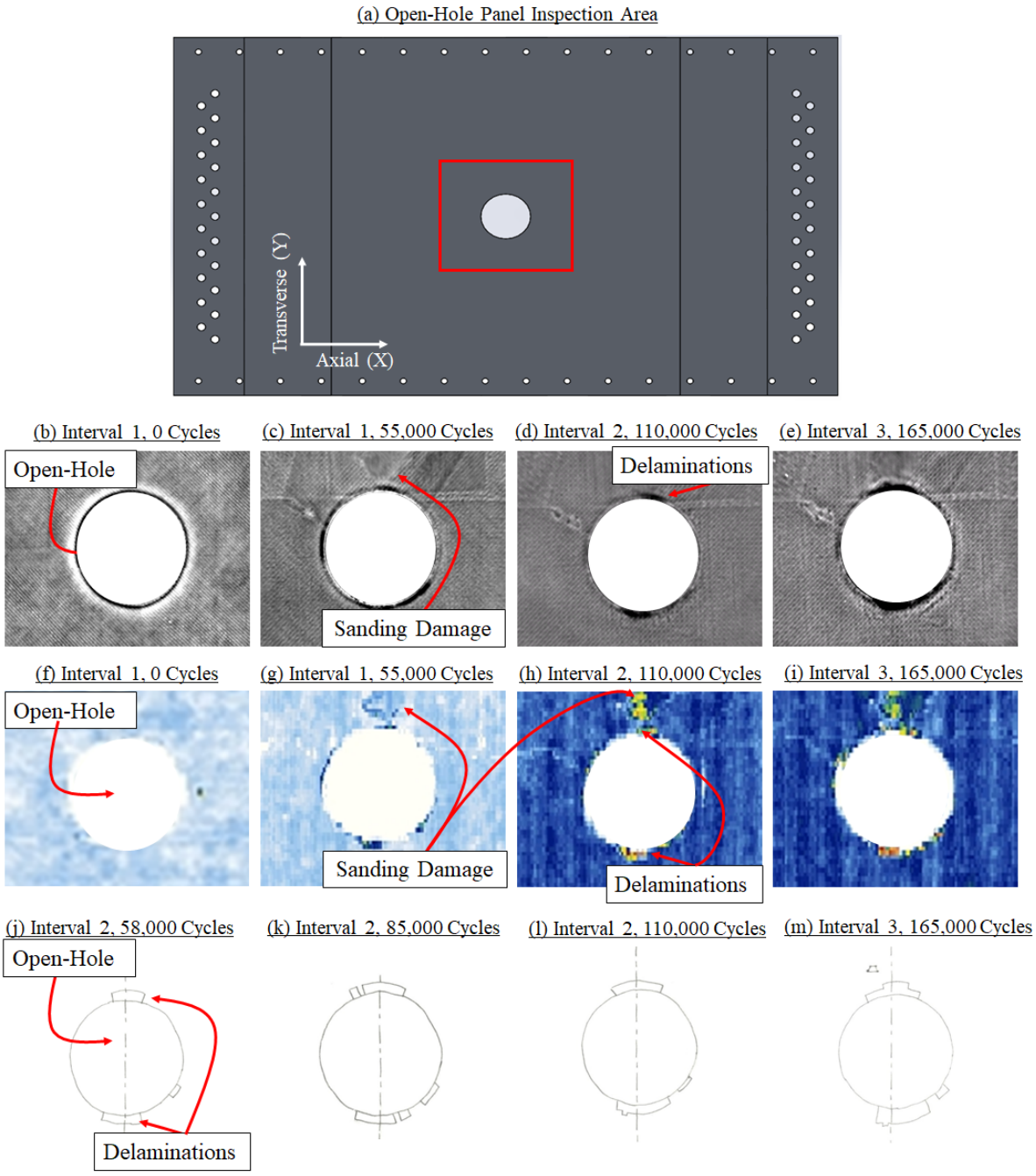

Figure 25. Flash thermography results for the open-hole panel throughout fatigue

Strains measured during strain surveys for each fatigue interval are provided in Figure 26 for panel 2. As shown, strain values were consistent in-phase for all strain gages across the board, indicating the local delaminations, present along the hole edges, did not impact the far-field strain distributions. Some exceptions, fluctuations in values, can be attributed to relocation of strain gages, which happened after strain gages failed.

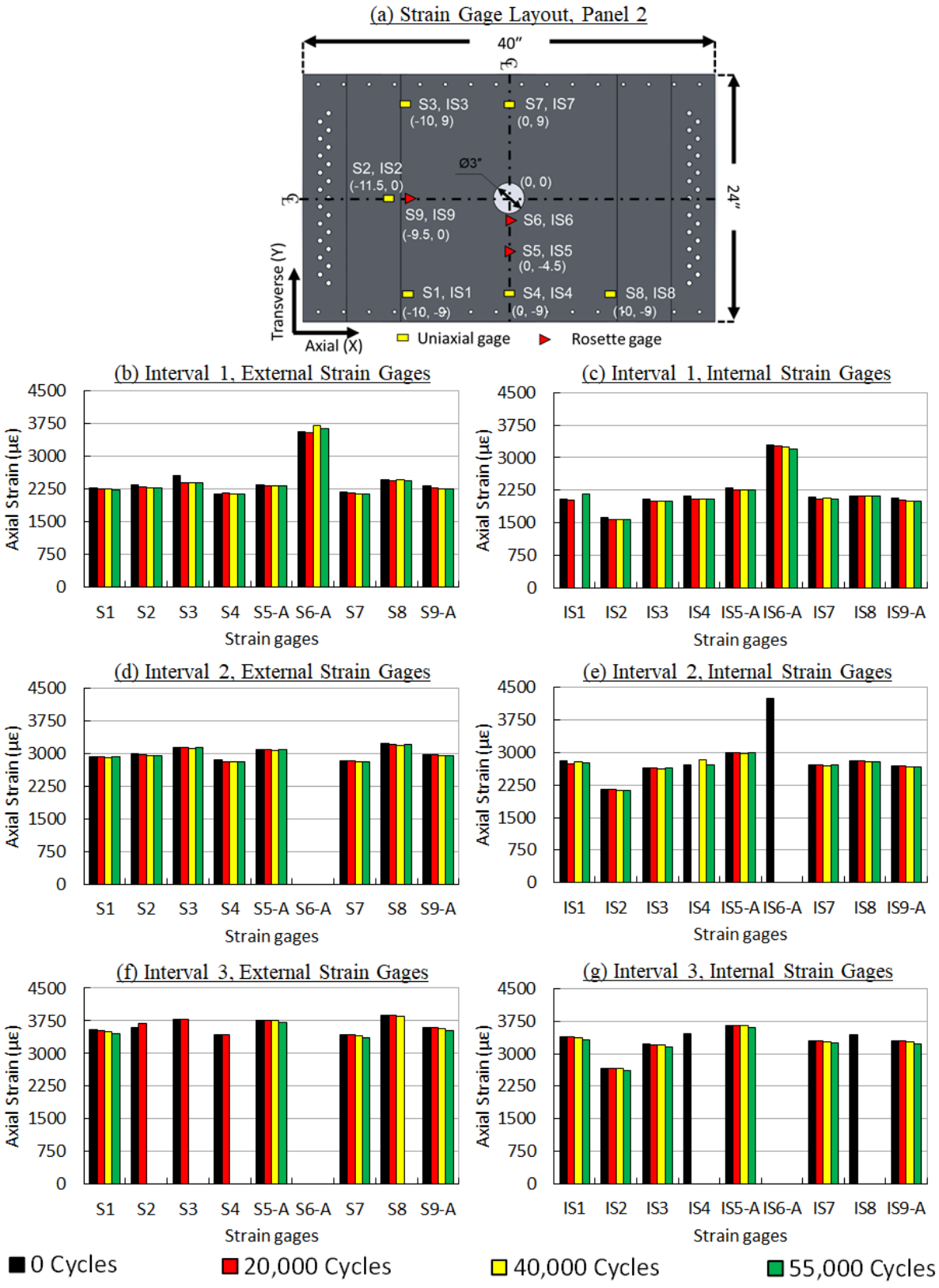

Figure 26. Strain gage results captured throughout panel 2 fatigue test

Following the completion of 165,000 fatigue cycles, panel 2 was subjected to residual strength loading per the schematics provided in Figure 27. In general, the panel was subjected to five successive quasi-static loading increments, each with increased load level up to failure. These load increments were defined based on the predicted critical load (PCL) level, which was considered as 100% load level. The load increments were 70%, 80%, 90%, 100% of the PCL level and final failure. After each load increment, during unloading, the test was paused at 20% load level to collect SHM data and NDI inspections were conducted at unloaded (0%) state. The final loading increment went beyond 100% PCL level. The axial strains captured by strain gages and DIC at the peak load for each load increment from 70% to 100% are shown in Figure 28 and Figure 29, respectively. As shown, strain values increased steadily as the loads increased, at an approximately linear rate, indicating no strain redistribution up to 100% load level. In addition, all the NDI inspections showed no progression in damage from 70% to 100% load increments. Flash thermography and phased array images after these load increments are shown in Figure 30.

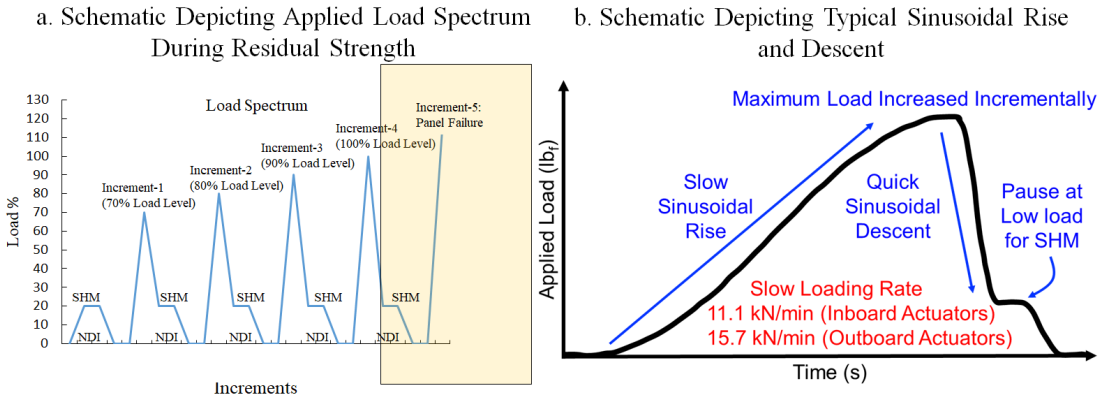

Figure 27. Residual strength test load increments for panel 2

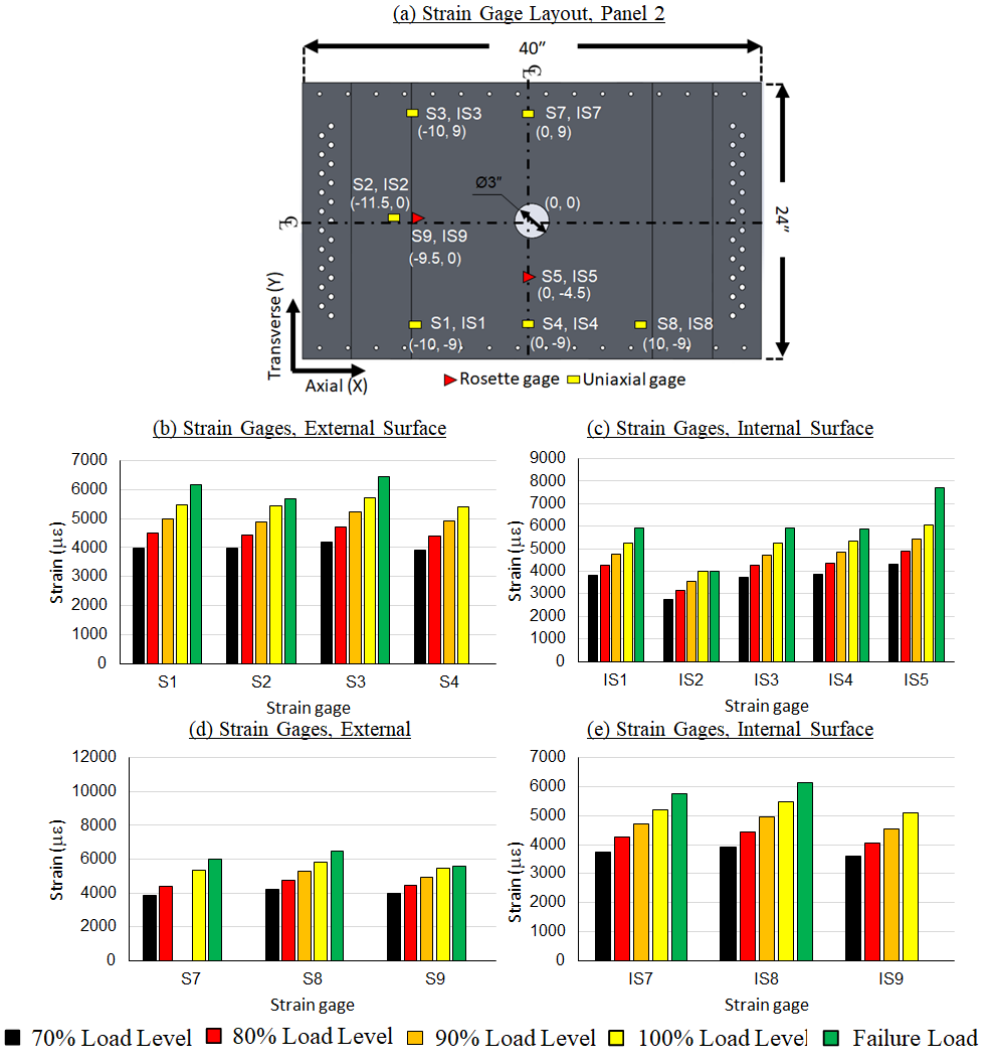

Figure 28. Strain measured during residual strength test

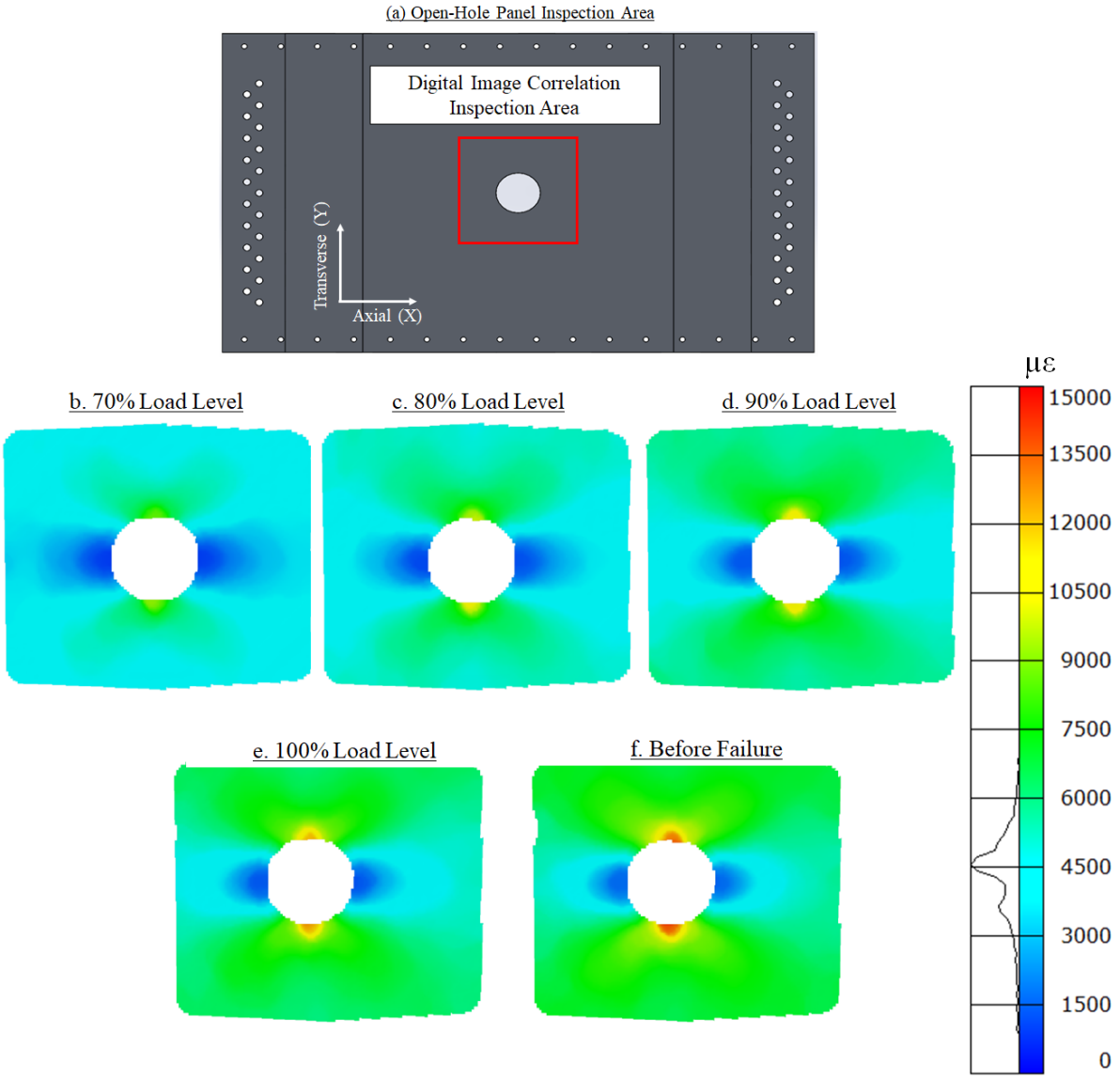

Figure 29. Full-field axial strains measured using DIC during panel 2 residual strength test

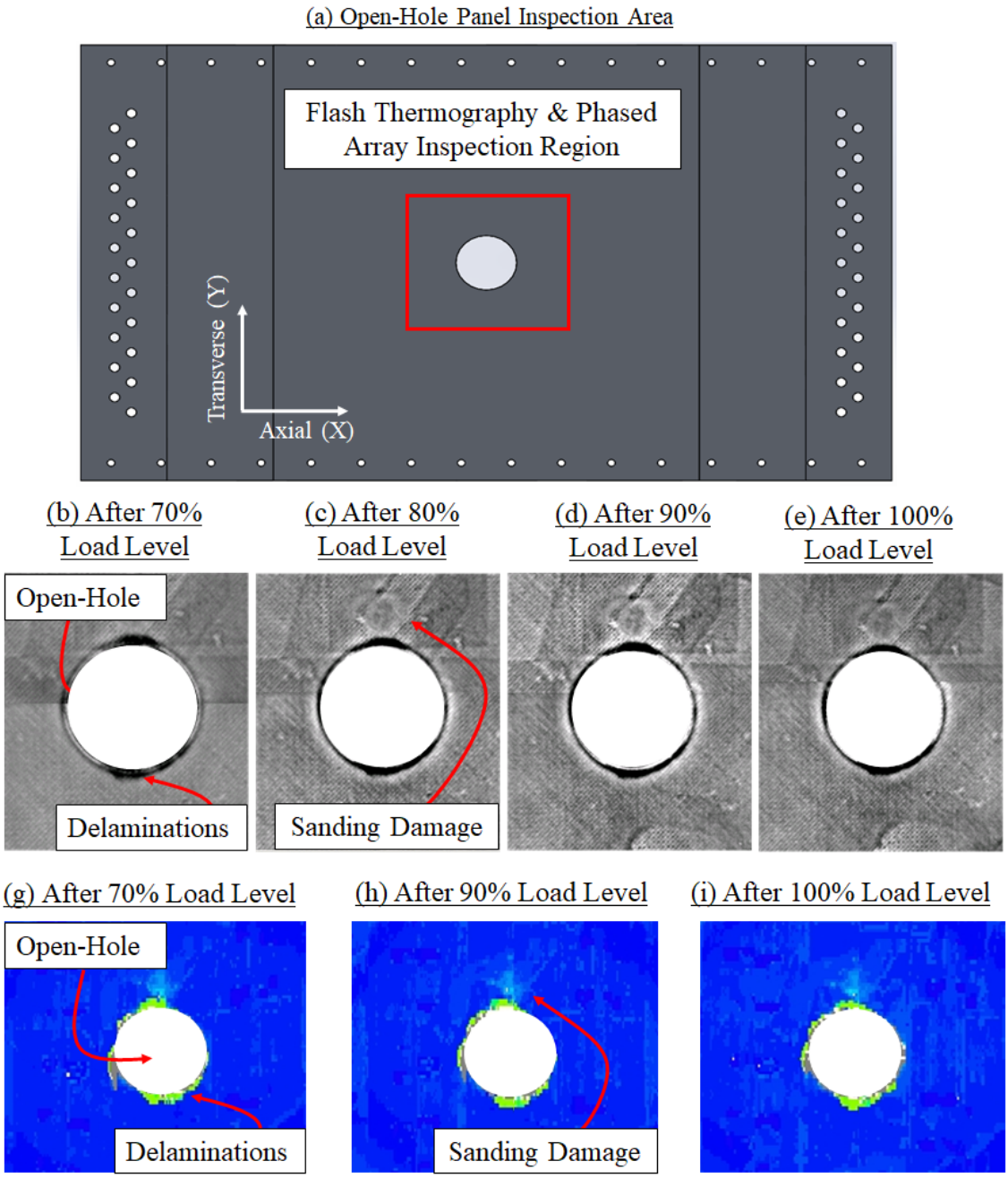

Figure 30. Inspection results during panel 2 residual strength test

In the final load increment, the panel was quasi-statically loaded to failure. The panel failed through the net section at an applied moment of 116,535 lbf-ft, comparing well to the prediction of 104,734 lbf-ft (as obtained by K_t-based analysis). The damage growth from the hole in the transverse direction was quite rapid and the strain redistribution was evident from DIC results, as shown in Figure 31. This figure also shows the visual image and the NDI results captured by flash thermography and phased array after failure, which were all able to capture the breaking of

the fibers in the net section. The phased array inspection along with the fiber breakage in the net section also showed one of the internal 0° ply delamination. The residual strength test was terminated after the significant failure emanated from the hole edges to conserve the panel for future NDI or fractography studies. The detailed load, strains, and displacement information for each load step is provided in appendix C.

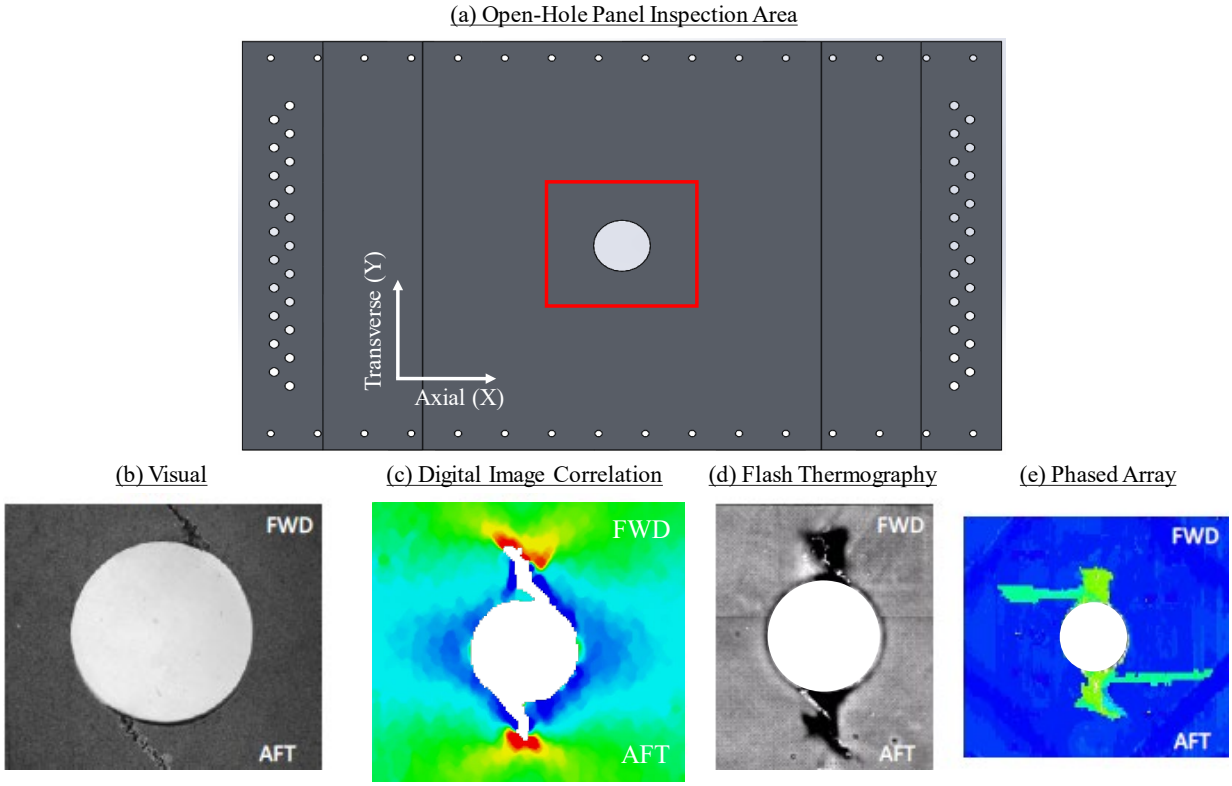

Figure 31. Visual, flash thermography and phased array results after failure of panel 2

5 Summary and conclusions

In a joint effort, The Federal Aviation Administration and The Boeing Company are addressing safety and structural integrity issues of bonded repair technology. Recent efforts have focused on bonded repairs to composite panels representative of typical transport aircraft wing structure. The program objectives are to characterize the fatigue and damage tolerance performance of bonded repairs subjected to simulated service load and to evaluate the limit-load capability of typical composite wing panels with a failed repair. Emphasis has been placed on investigating the methods and tools used for predicting structural performance of repairs and as those used to evaluate and monitor repair integrity over the life of the part.

A phased approach is being undertaken in the multiyear effort. The initial baseline testing of this program characterized the material response of composite panels in the unnotched pristine and open-hole configurations under constant moment loading. This verified the test-fixture loading, validated analysis models, and provided an initial reference point for NDI and SHM systems. In general, the baseline panels were subjected to fatigue loading conditions that produce typical operational strain levels for transport-category wing panels for three design service objectives (~165,000 cycles). In the test section of the unnotched panel, measured strains were relatively constant. For the center-hole panel, strain concentrations measured using DIC and strain gages matched finite element analysis results. In addition, the K_t based analysis was successfully able to predict the failure loads for the center-hole panel. The next phase of the testing focuses directly on the BRSL, and these results will be published in the accompanying technical notes.

6 References

Baker, A. A., Rose, L., & Jones, R. (2003). *Advances in the Bonded Composite Repair of Metallic Aircraft Structure.* Elsevier.

Chadha, R., Bakuckas Jr., J. G., Fleming, M., Lin, J., & Korkosz, G. (2019). *Airframe Beam Structural Test (ABST) Fixture - Capabilities Description and User Manual.* DOT/FAA/TC-TN19/7.

Federal Aviation Administration. (2014). Bonded Repair Size Limits. *FAA Policy Statement, Policy No. PS-AIR-14-130-001*. U.S. Department of Transportation.

Neel, R. J., Awerbuch, J., Tan, T.-M., & Ozevin, D. (2019). Damage Detection Through Acoustic Emission During Post-Fatigue Residual Strength Test of CFRP Skin of a Cantilevered Wingbox Under Constant-Moment Loading. *2019 International Conference on Acoustic Emission.* Chicago, Illinois.

Neel, R. J., Awerbuch, J., Tan, T.-M., & Ozevin, D. (2019). Damage Detection Through Fretting Emission in Center-Hole CFRP Skin of Cantilever Wingbox Under Constant-Moment Fatigue Loading. *2019 International Conference on Acoustic Emission.* Chicago, Illinois.

A Specimen engineering drawings

This appendix provides detailed drawings of the pristine and open-hole panels. A detailed drawing of the pristine panel is provided in Figure 32, while a detailed drawing of the open-hole panel is provided in Figure 33.

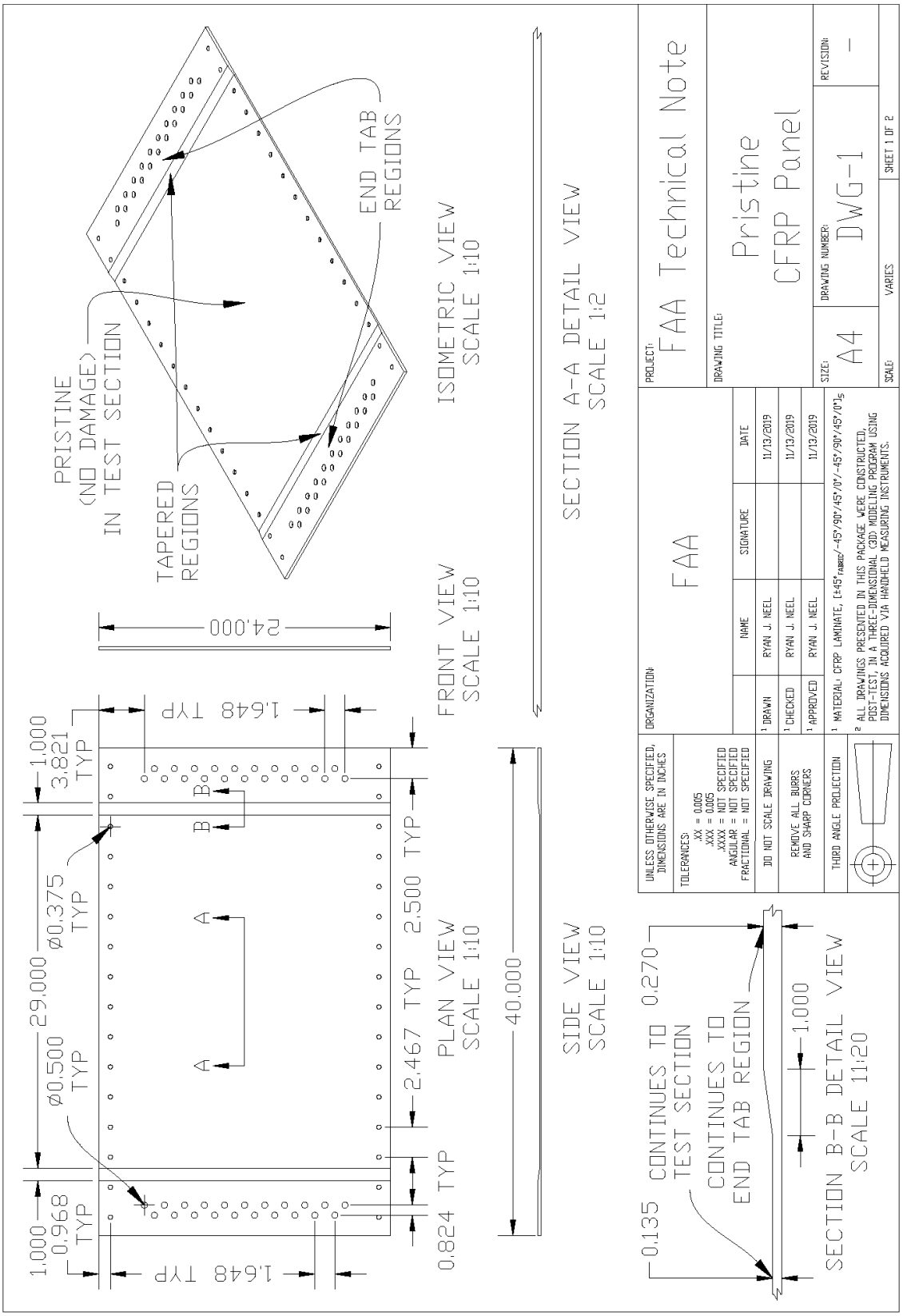

Figure 32. Drawing of panel 1 (pristine panel)

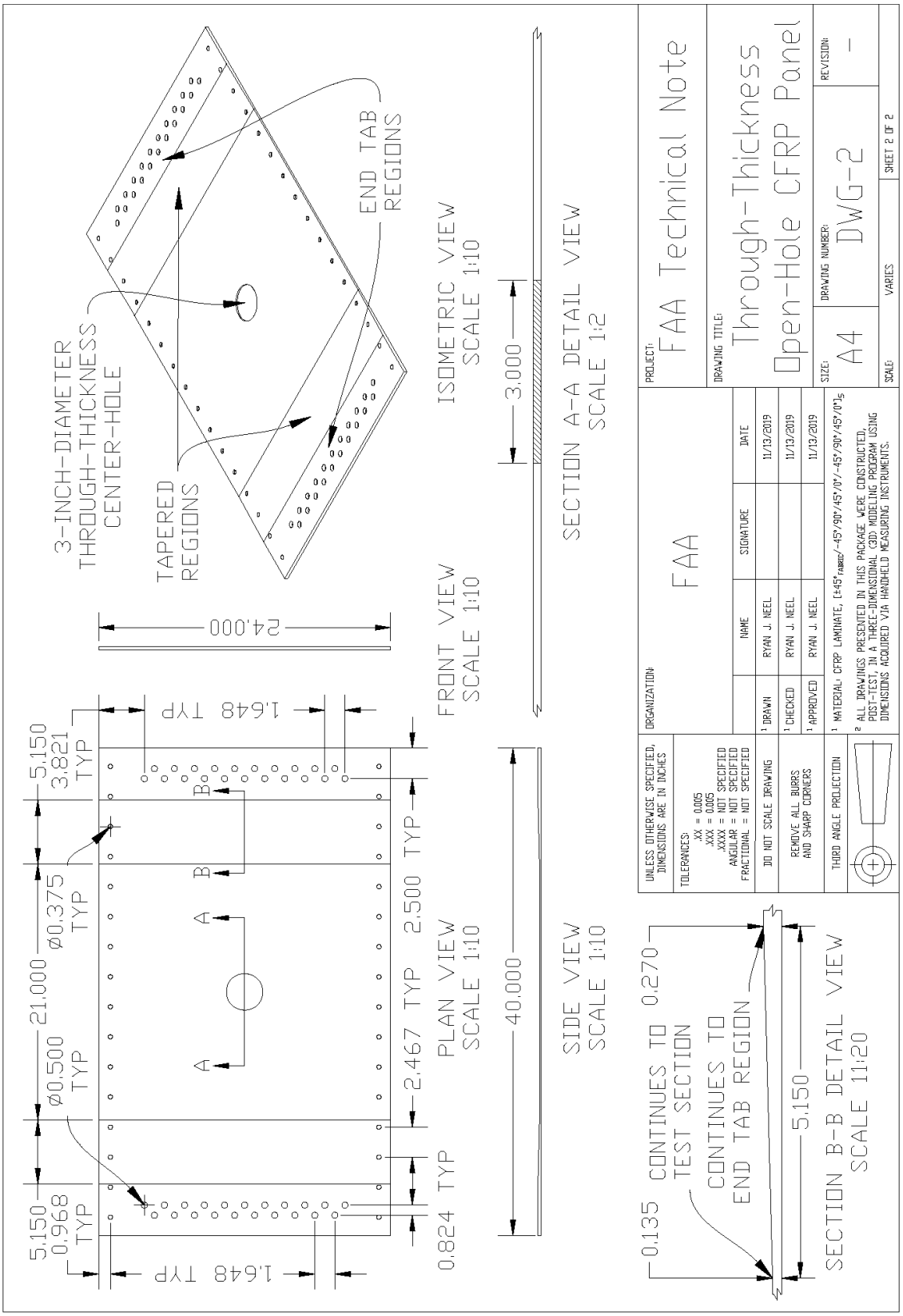

Figure 33. Drawing of panel 2 (open-hole panel)

B Strain and displacement during strain surveys

This appendix provides strain gages results captured during quasi-static loading of the pristine and open-hole panel specimens. The location and nomenclature for displacement sensors and strain gages for both the panels are shown in Figure 34 and Figure 35, respectively. As shown in Figure 34, string-pot displacement sensors D1 and D2 were placed near the central location of the fixture (i.e., where the load application assembly meets the wingbox, 6 inches away from the vertical actuators attachment points) to measure the vertical displacement; sensors D3V and D3H were placed at the end of the load application assembly to measure the vertical and horizontal displacement near the end actuators. For panel 1, all the strain and displacement measurements were regularly collected up to 165,000 cycles, and they are shown in Figure 36 – Figure 57 for panel 1. Similarly, the strain survey results for panel 2 from 0 –165,000 cycles are shown in Figure 58 – Figure 95.

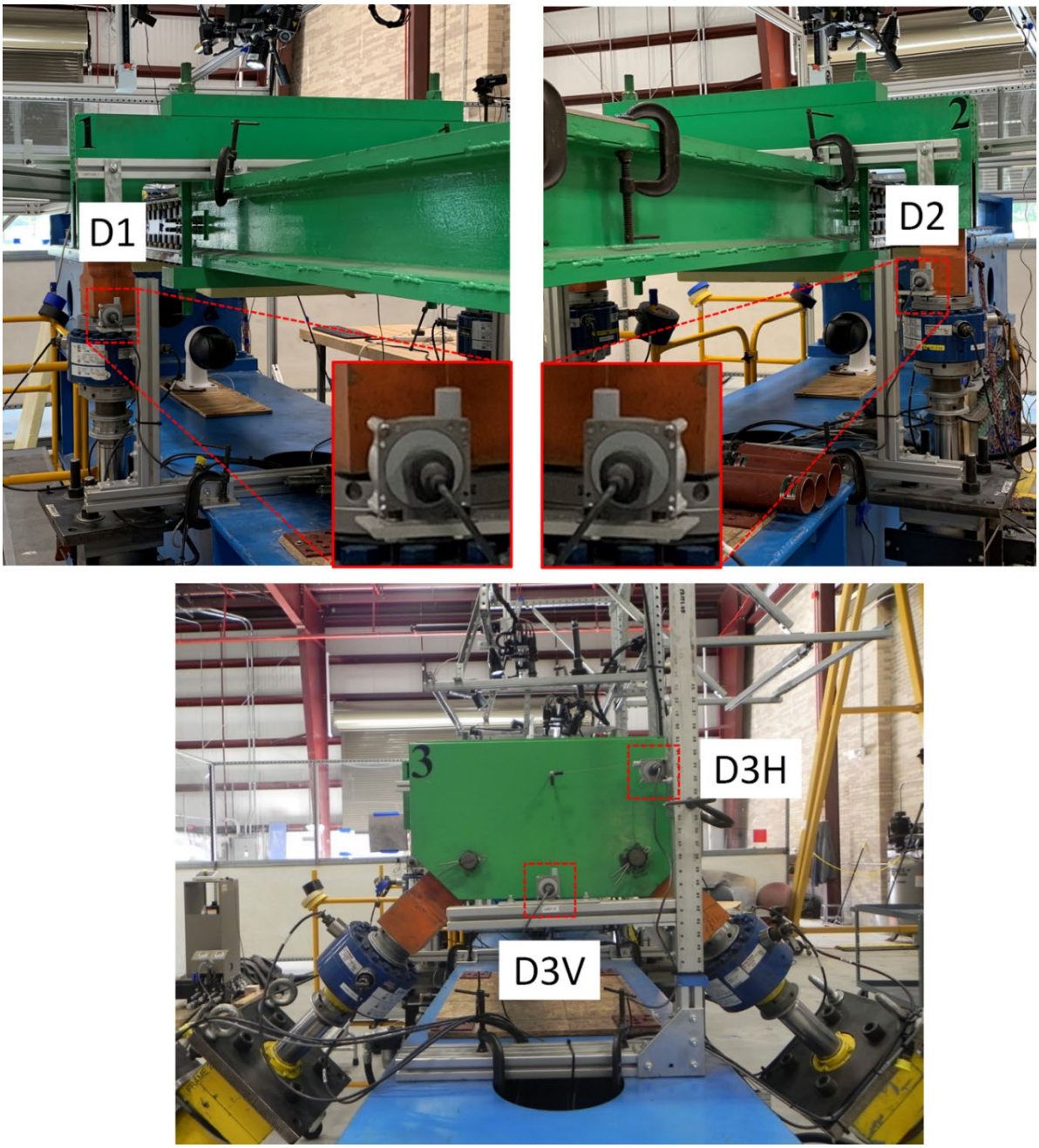

Figure 34. Images displaying the displacement transducer positions

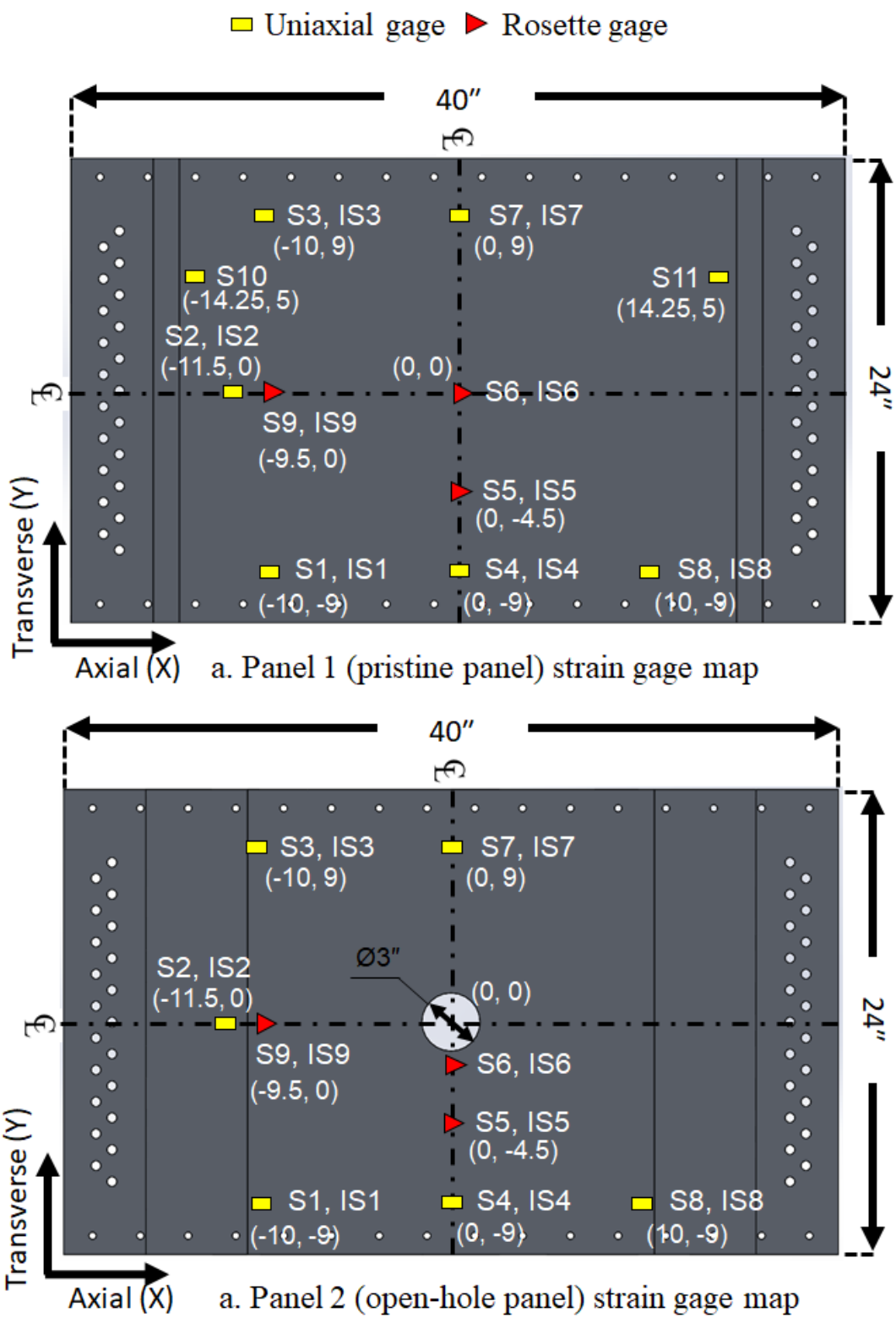

Figure 35. Strain gages layout for panels 1 and 2

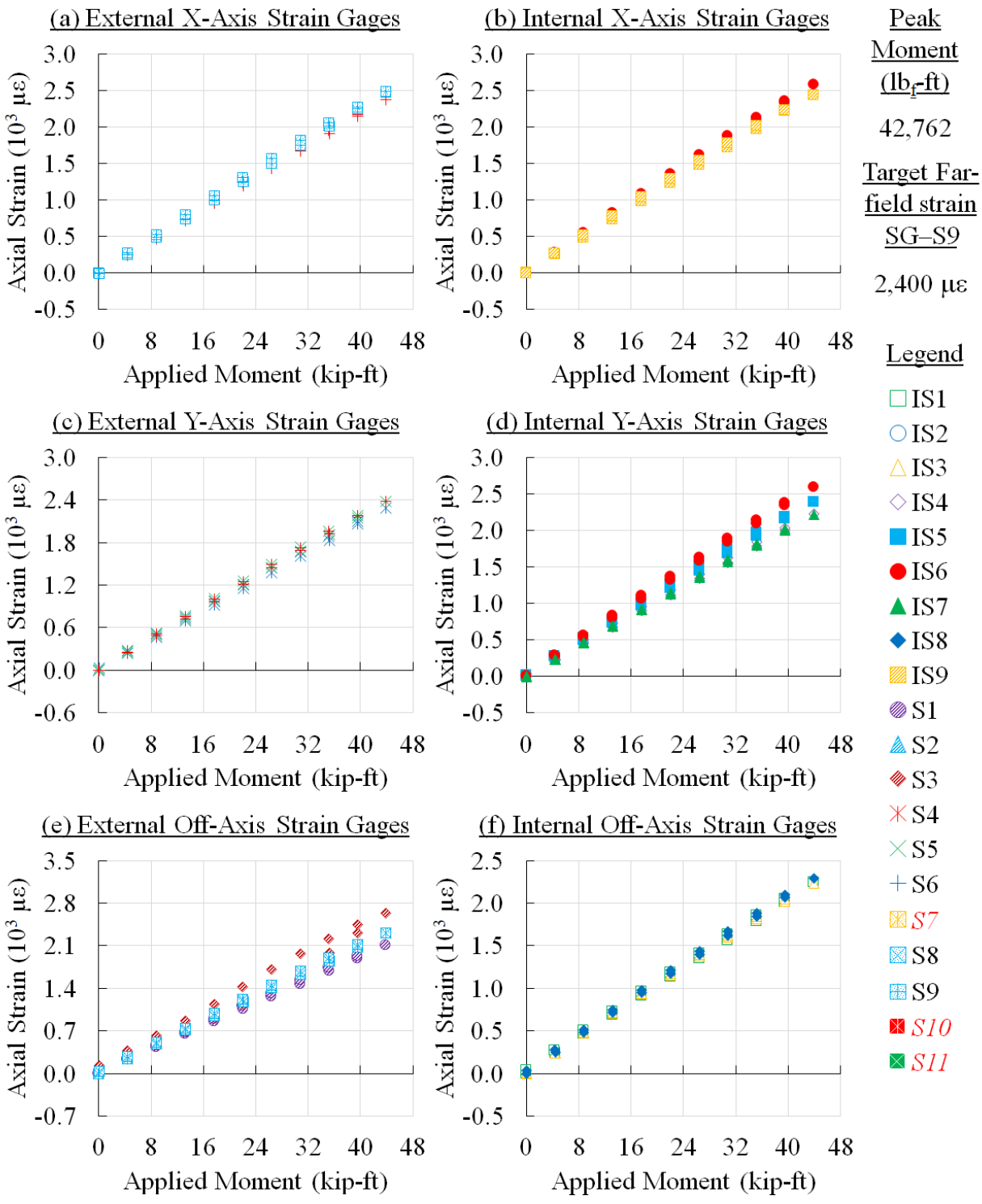

Figure 36. Panel 1 strain survey results at 0 cycles

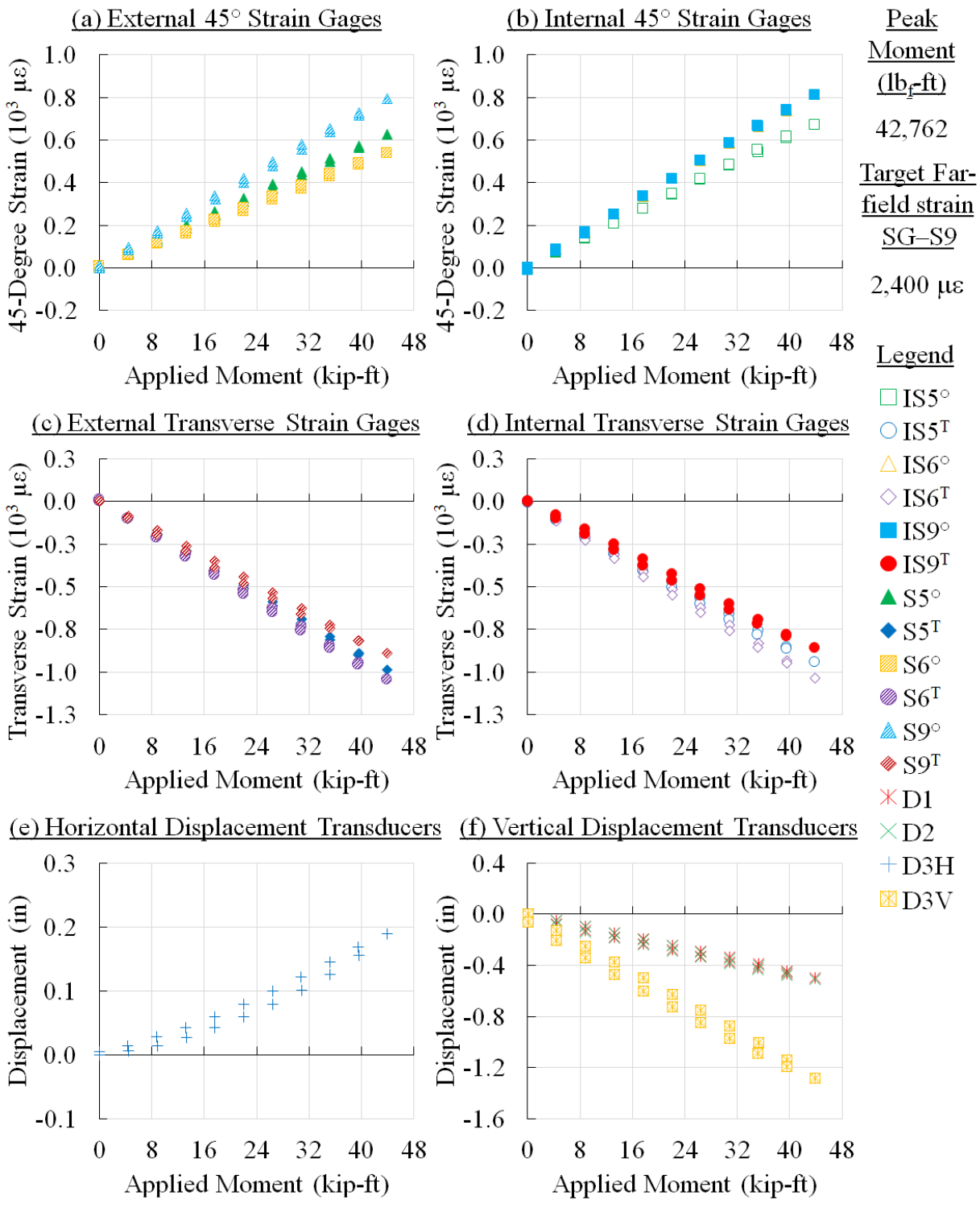

Figure 37. Panel 1 strain survey results at 0 cycles

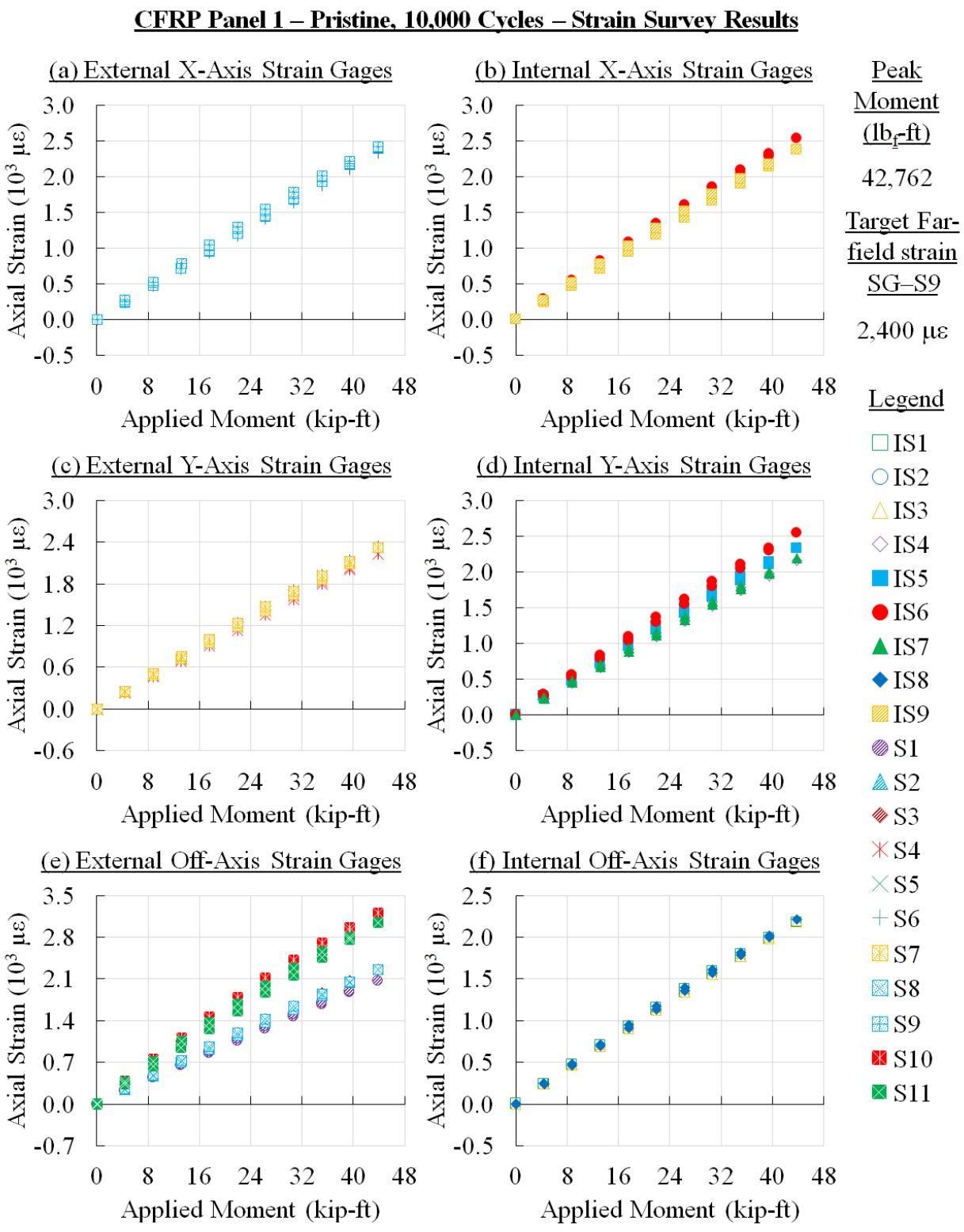

Figure 38. Panel 1 strain survey results at 10,000 cycles

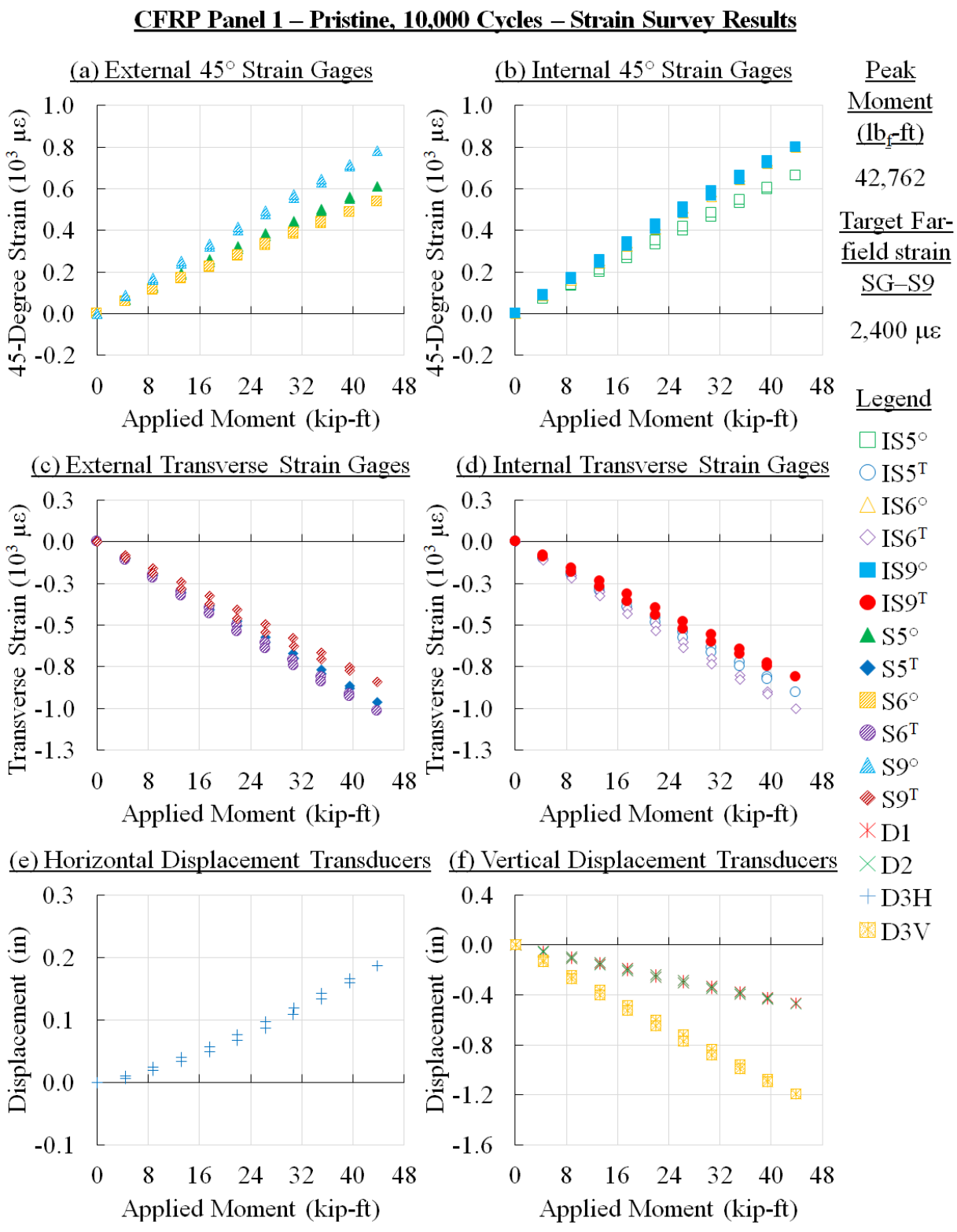

Figure 39. Panel 1 strain survey results at 10,000 cycles

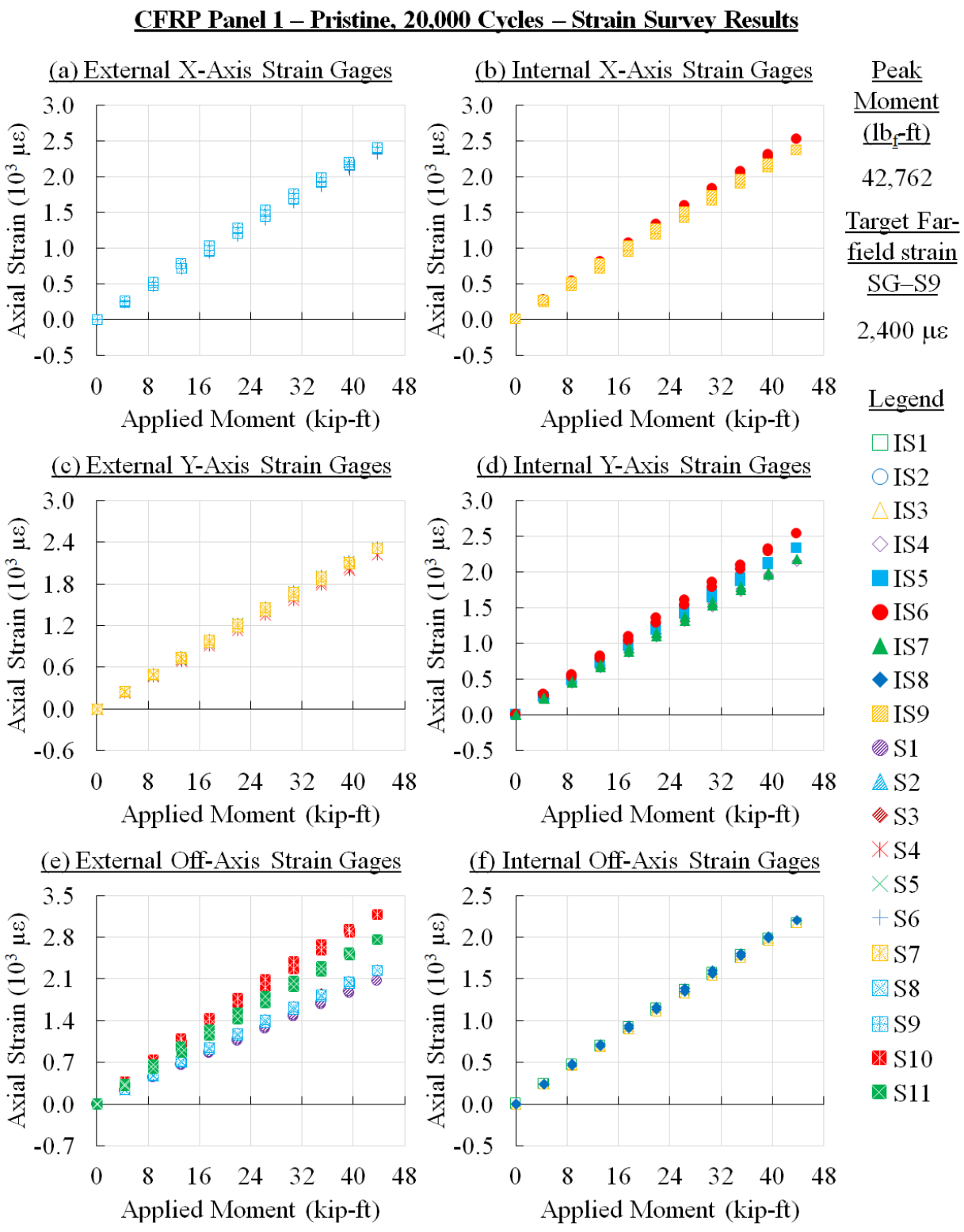

Figure 40. Panel 1 strain survey results at 20,000 cycles

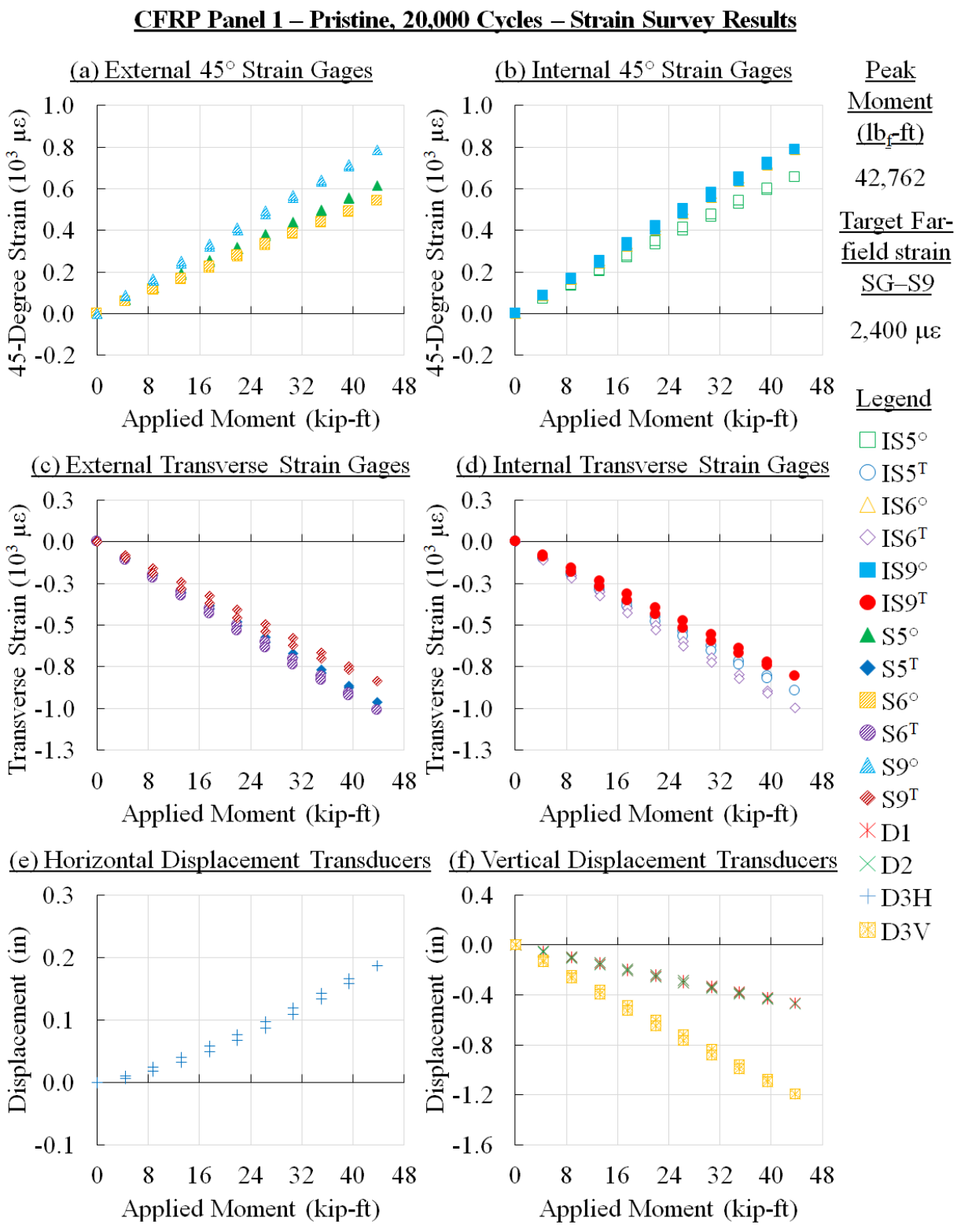

Figure 41. Panel 1 strain survey results at 20,000 cycles

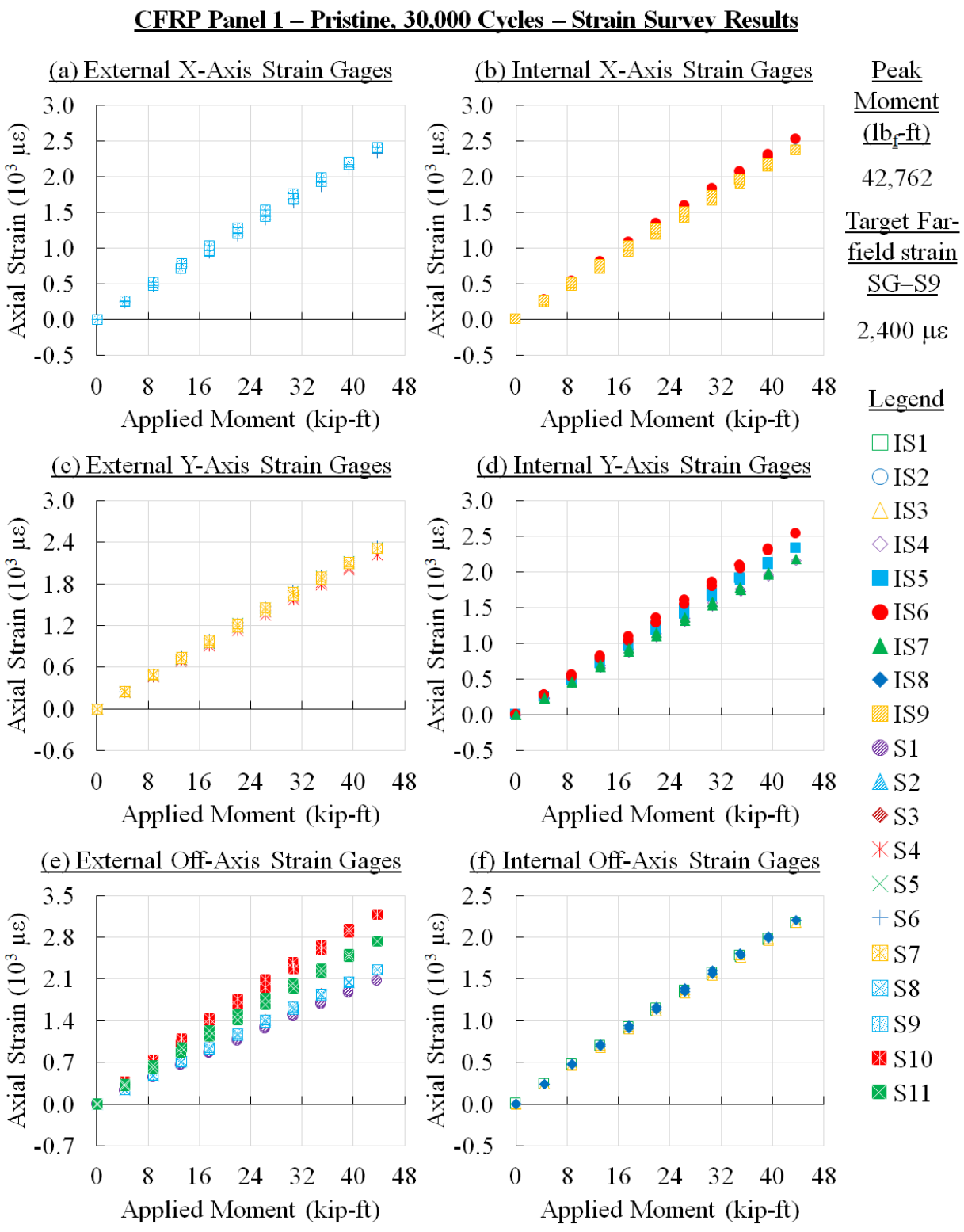

Figure 42. Panel 1 strain survey results at 30,000 cycles

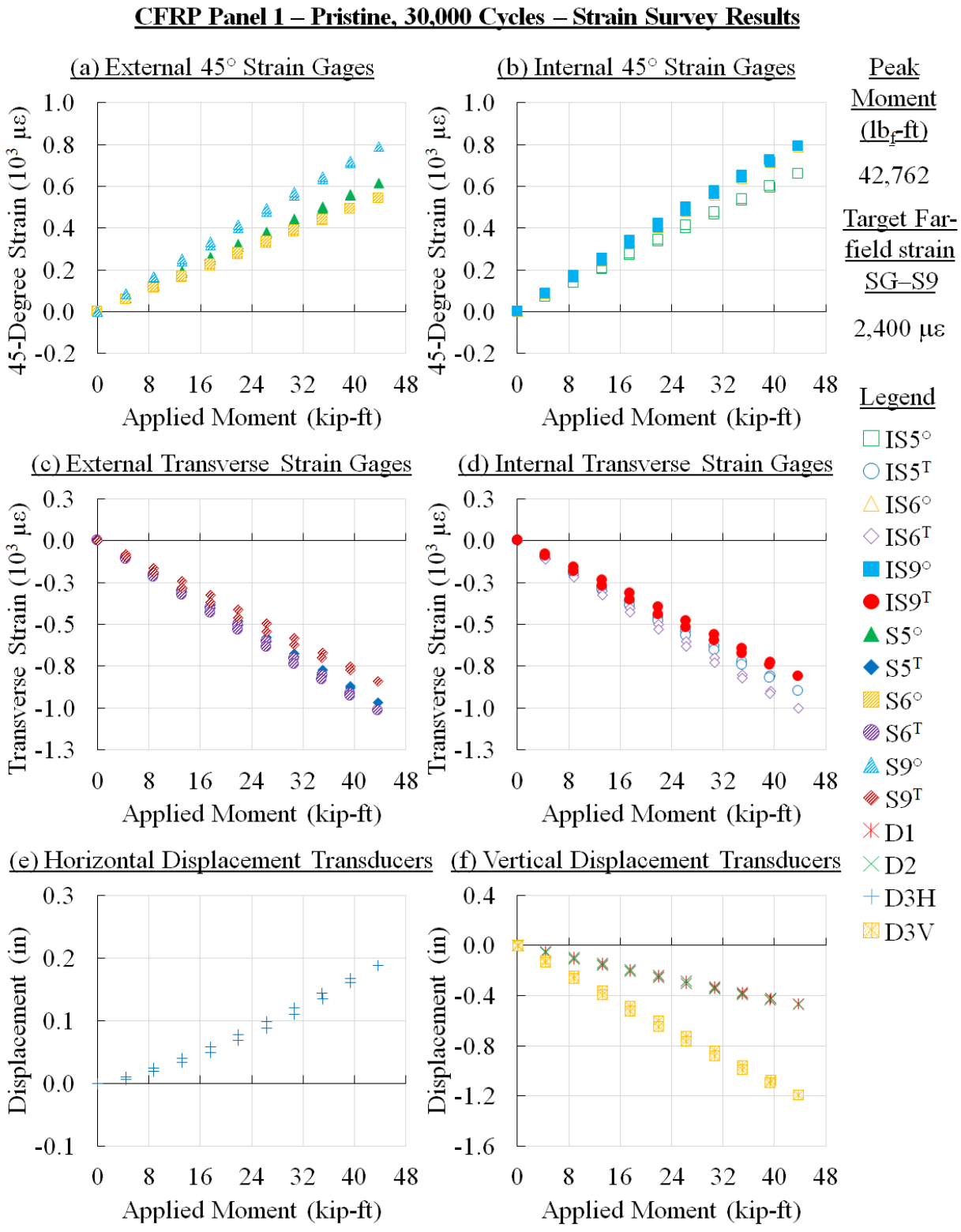

Figure 43. Panel 1 strain survey results at 30,000 cycles

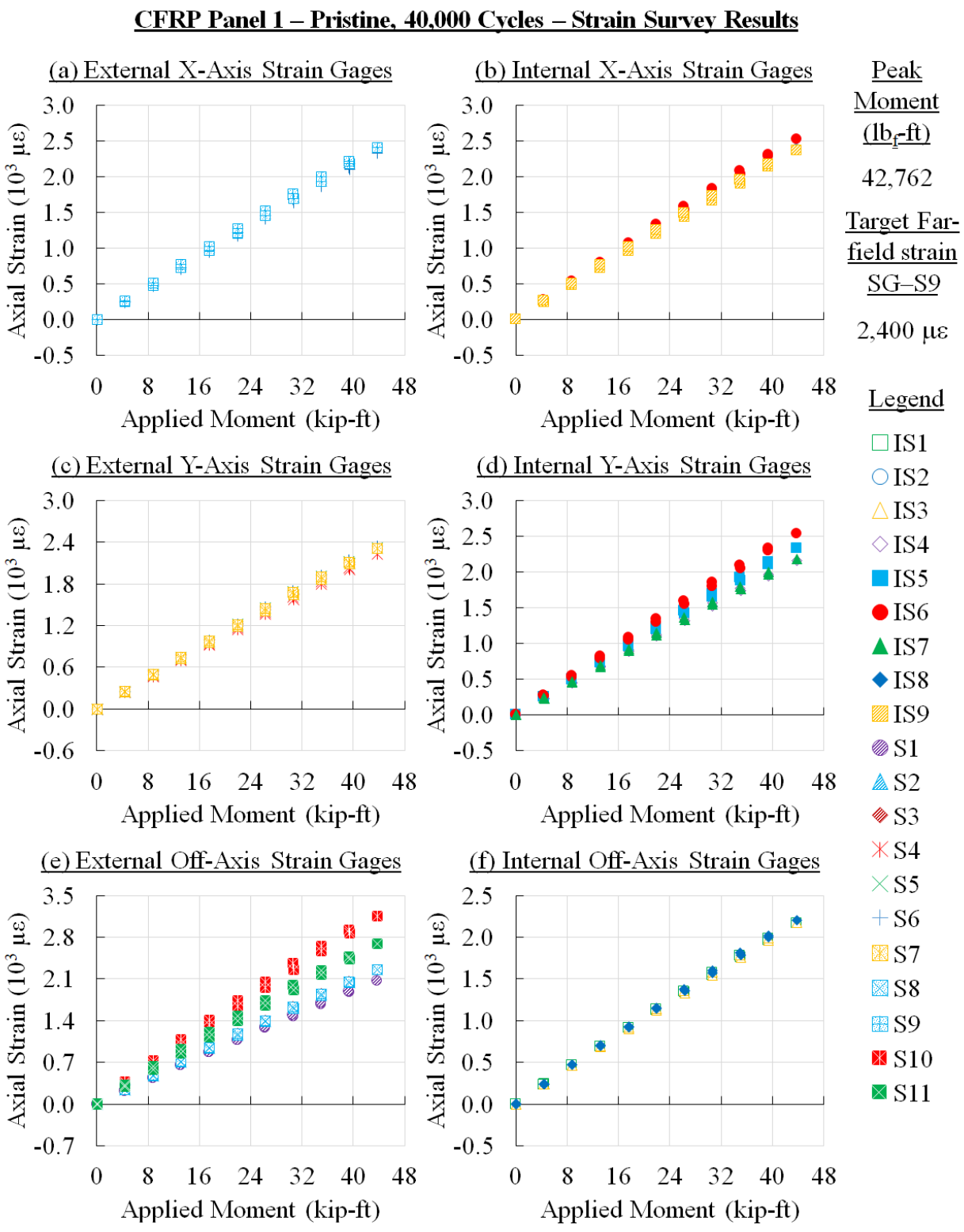

Figure 44. Panel 1 strain survey results at 40,000 cycles

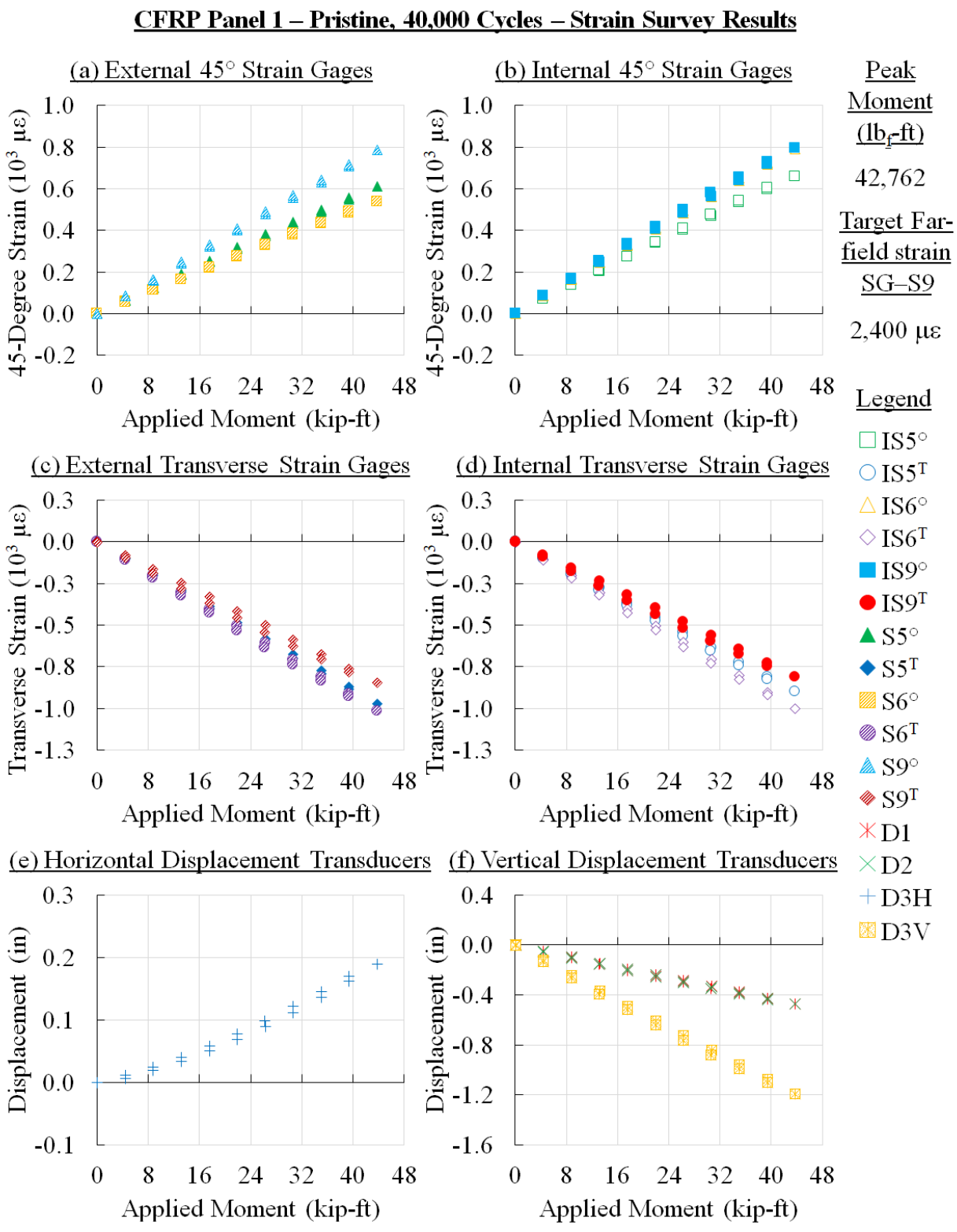

Figure 45. Panel 1 strain survey results at 40,000 cycles

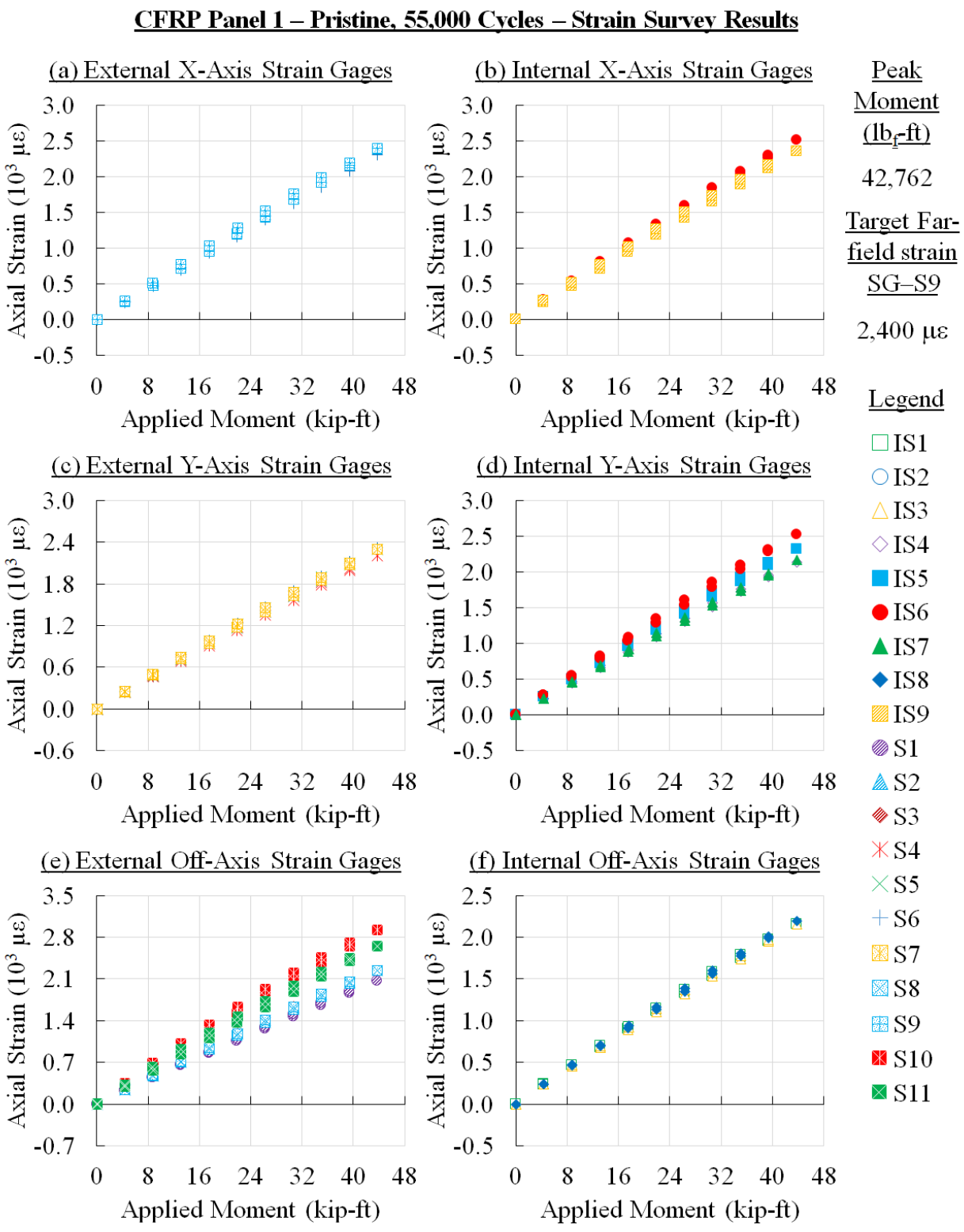

Figure 46. Panel 1 strain survey results at 55,000 cycles

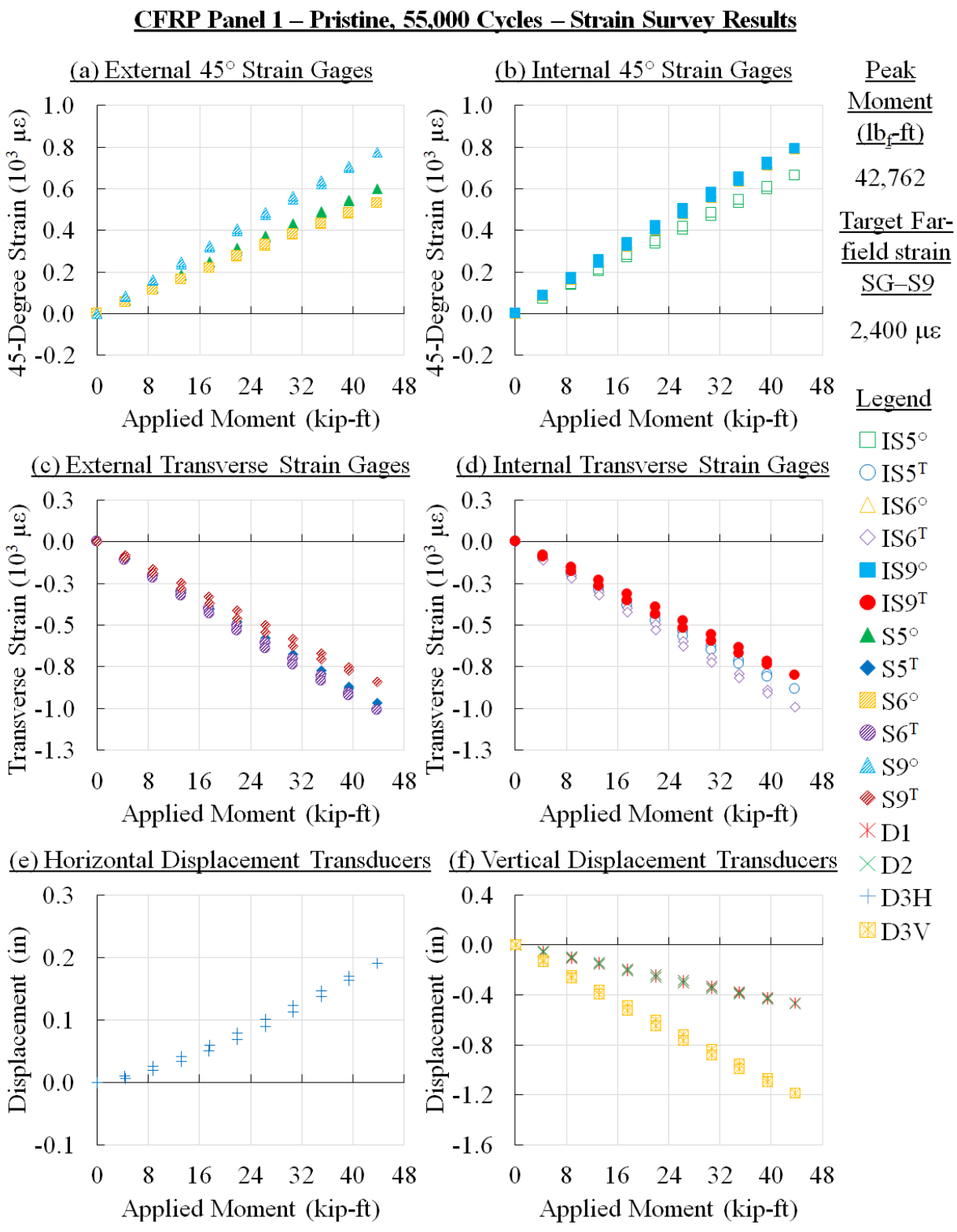

Figure 47. Panel 1 strain survey results at 55,000 cycles

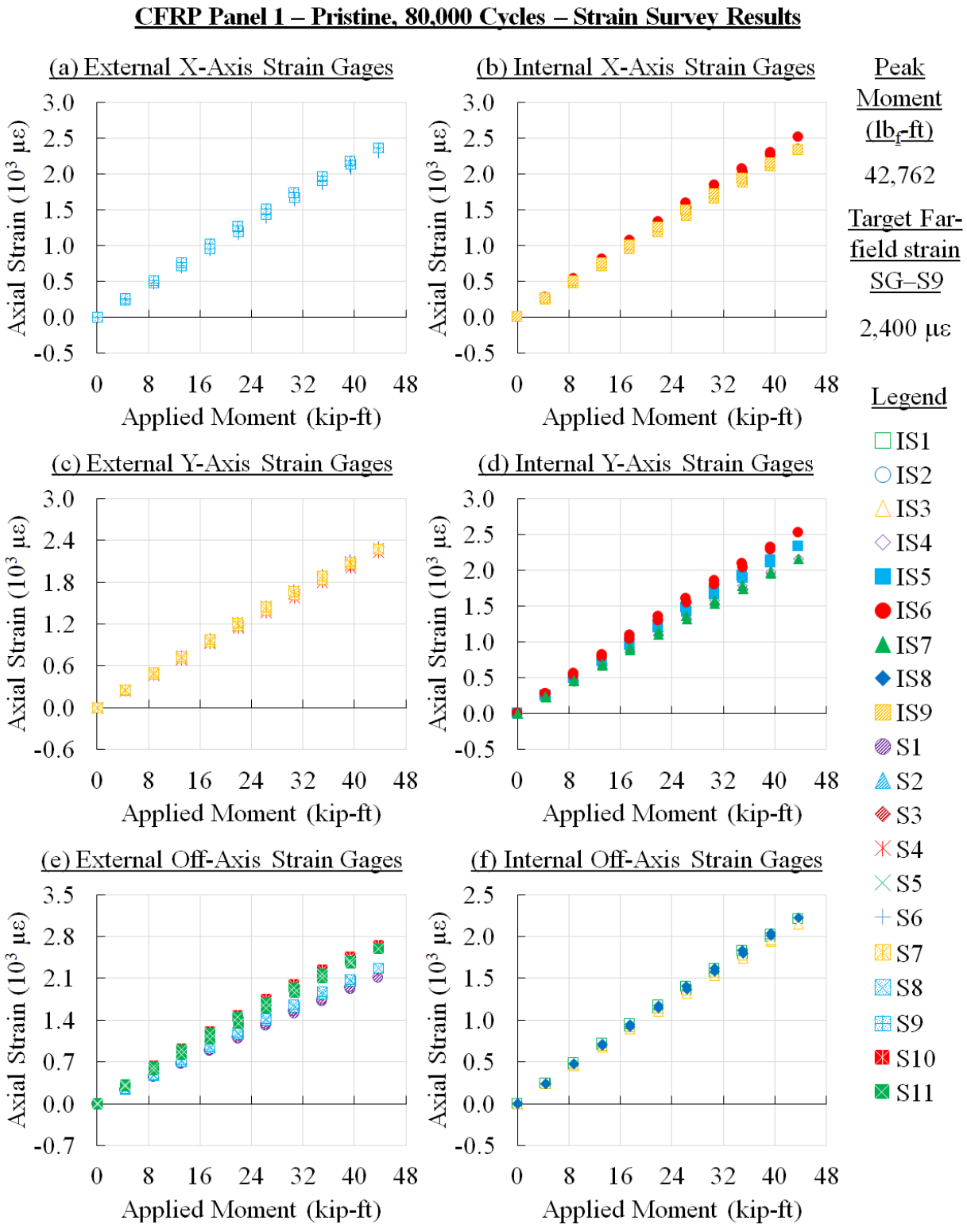

Figure 48. Panel 1 strain survey results at 80,000 cycles

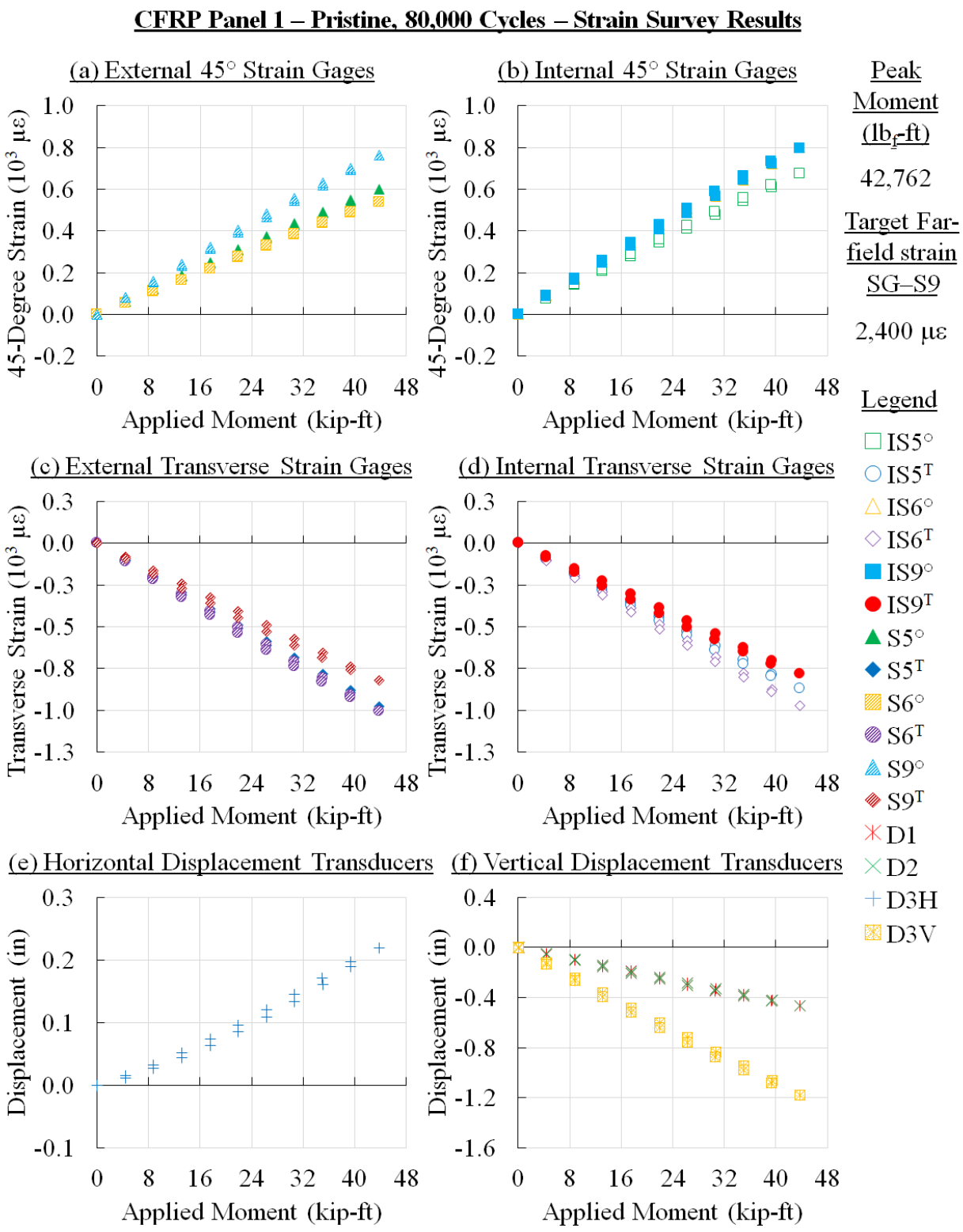

Figure 49. Panel 1 strain survey results at 80,000 cycles

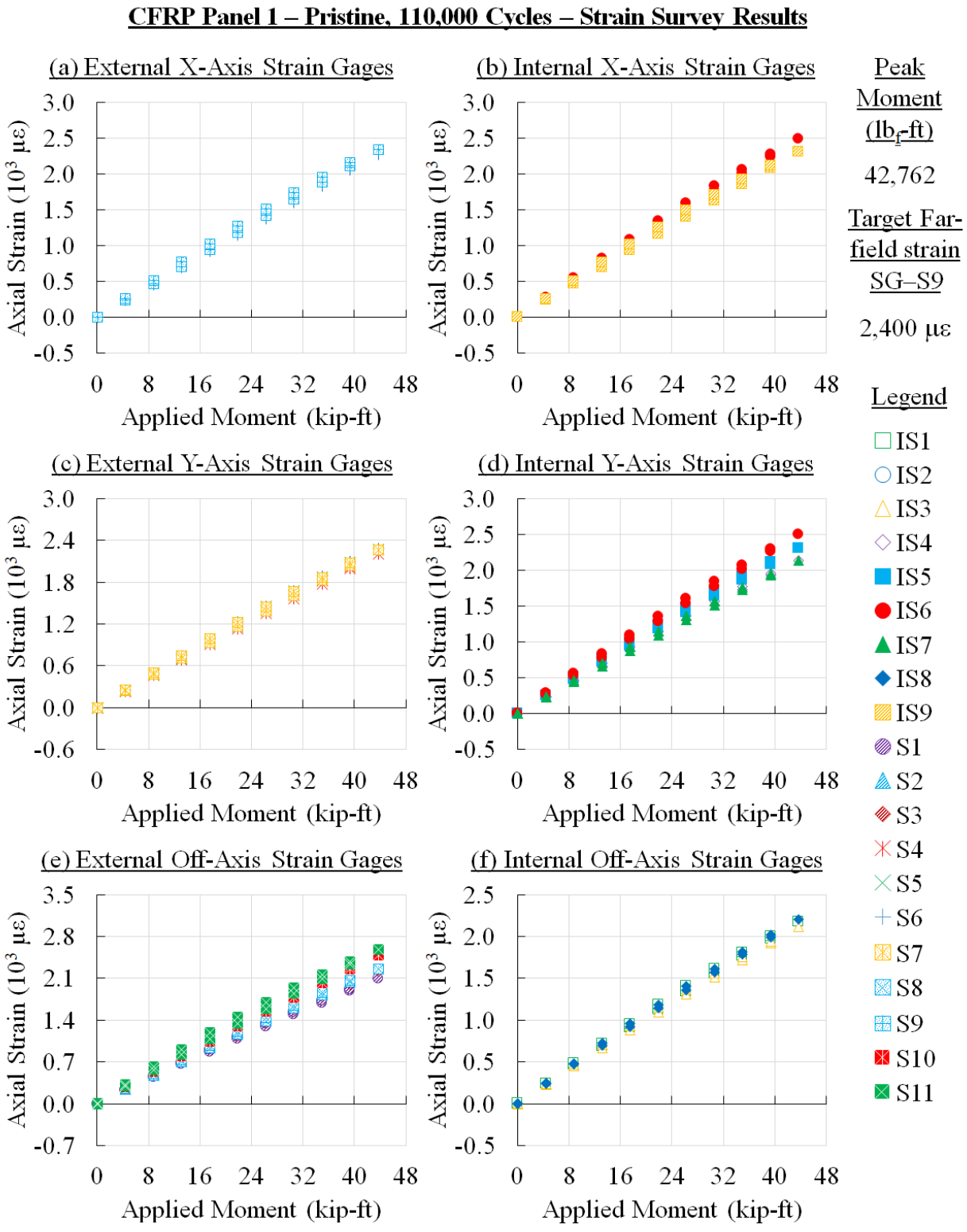

Figure 50. Panel 1 strain survey results at 110,000 cycles

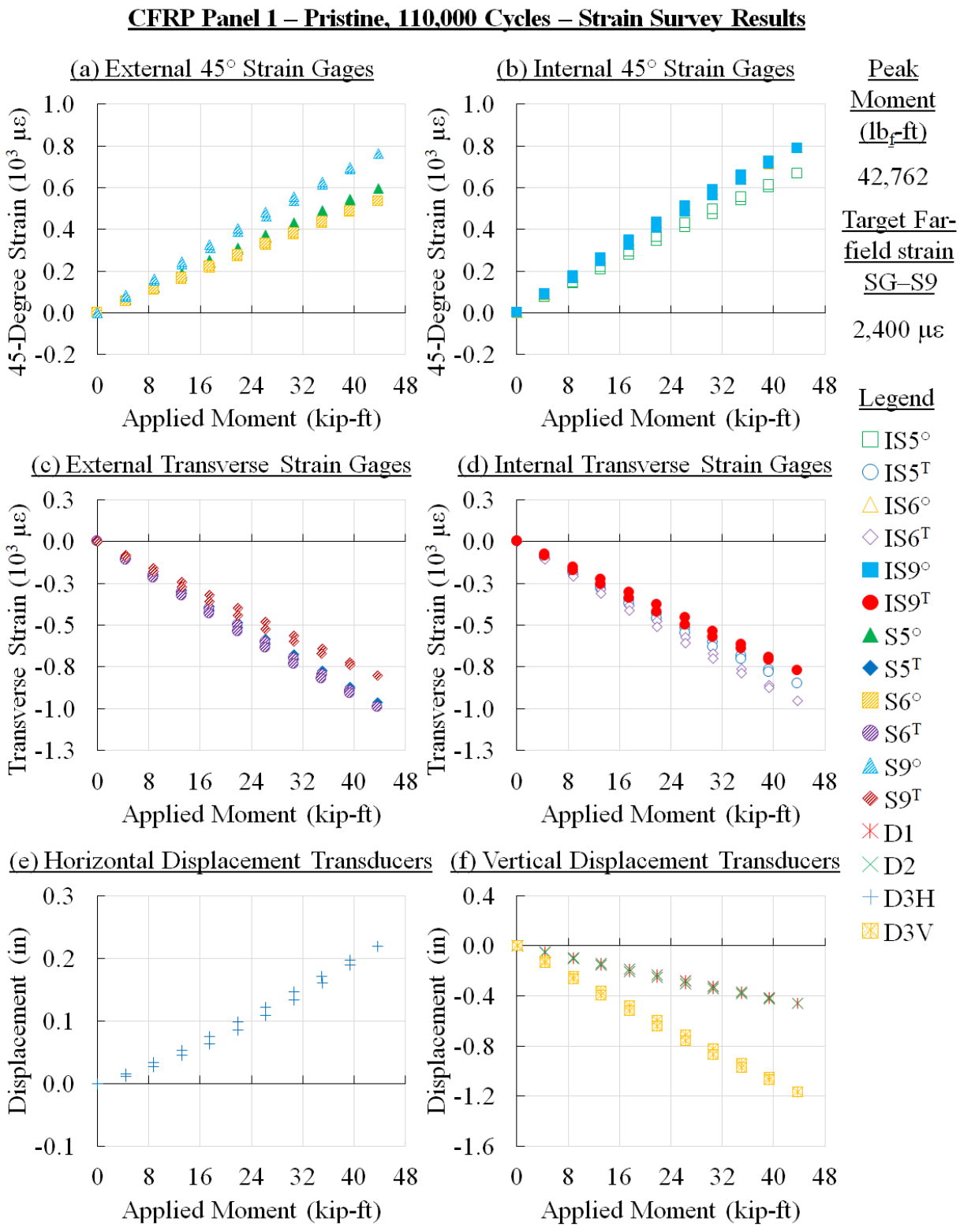

Figure 51. Panel 1 strain survey results at 110,000 cycles

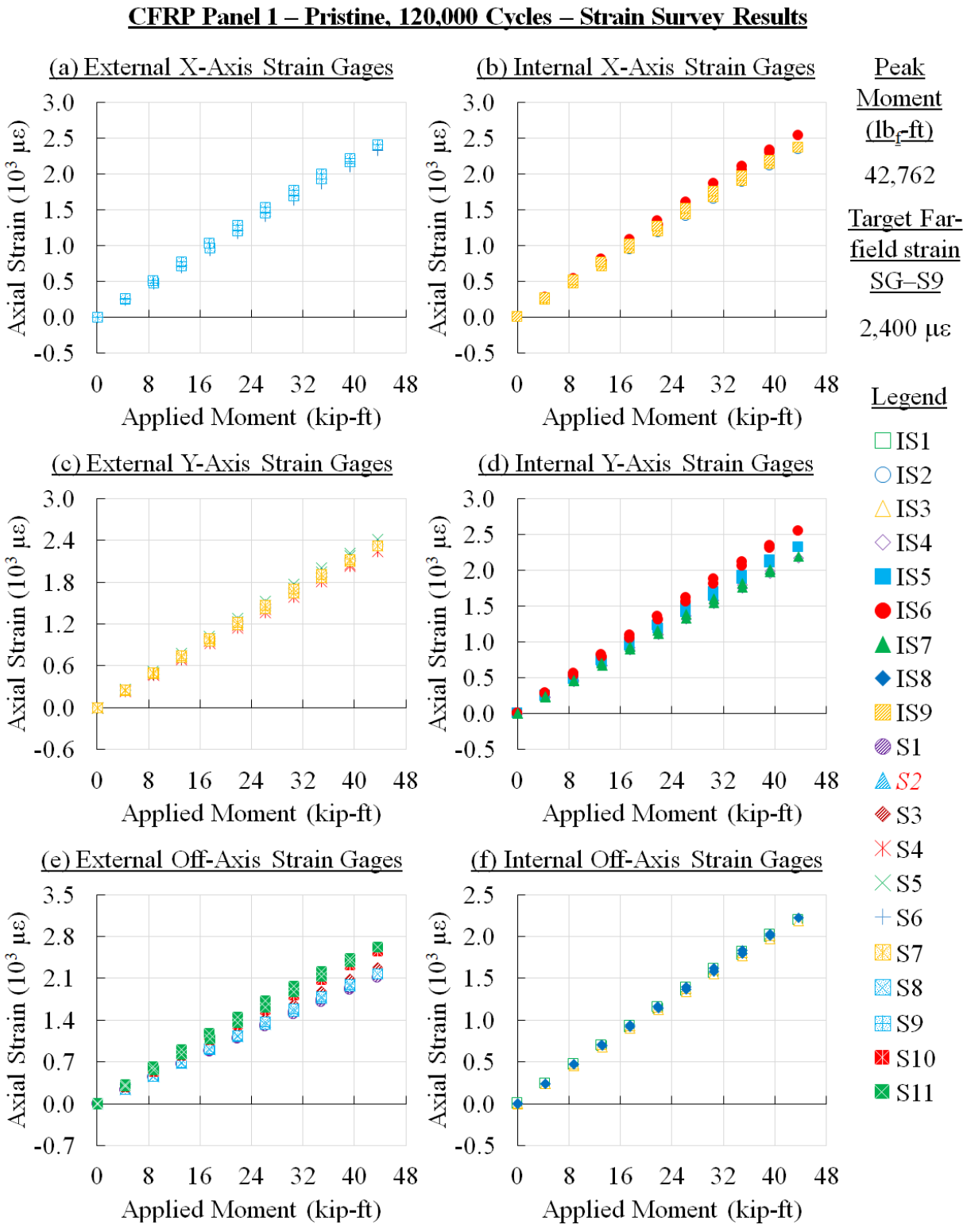

Figure 52. Panel 1 strain survey results at 120,000 cycles

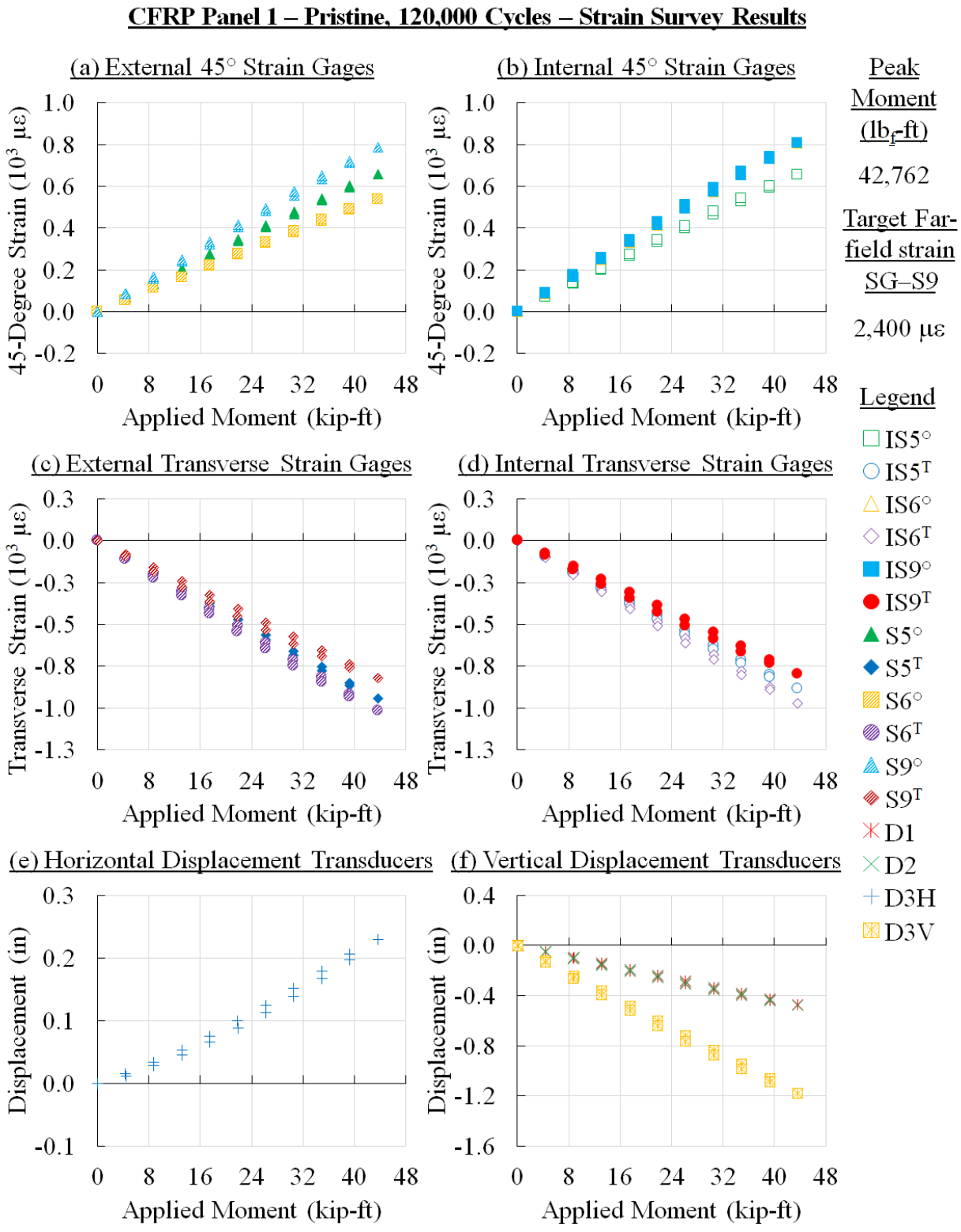

Figure 53. Panel 1 strain survey results at 120,000 cycles

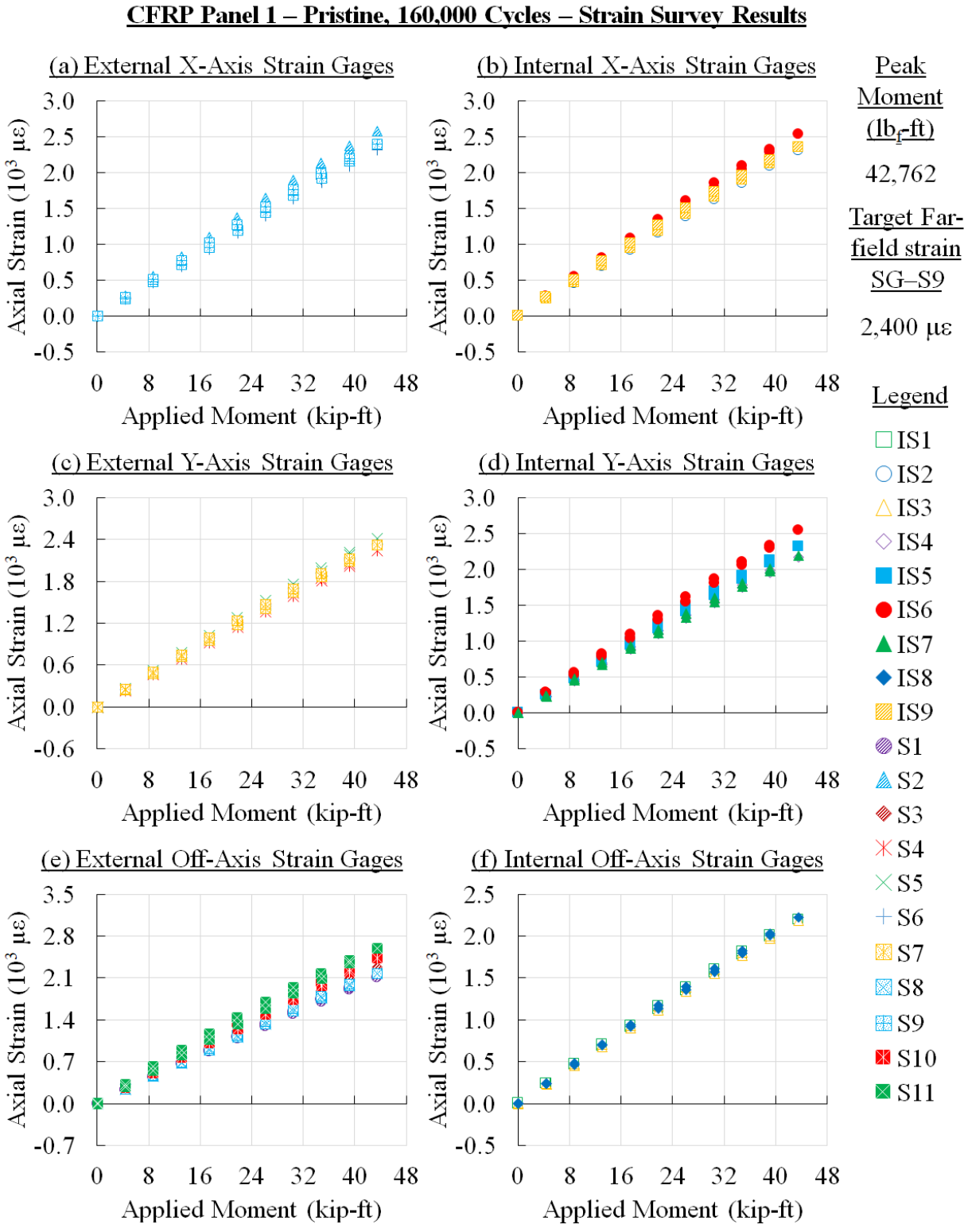

Figure 54. Panel 1 strain survey results at 160,000 cycles

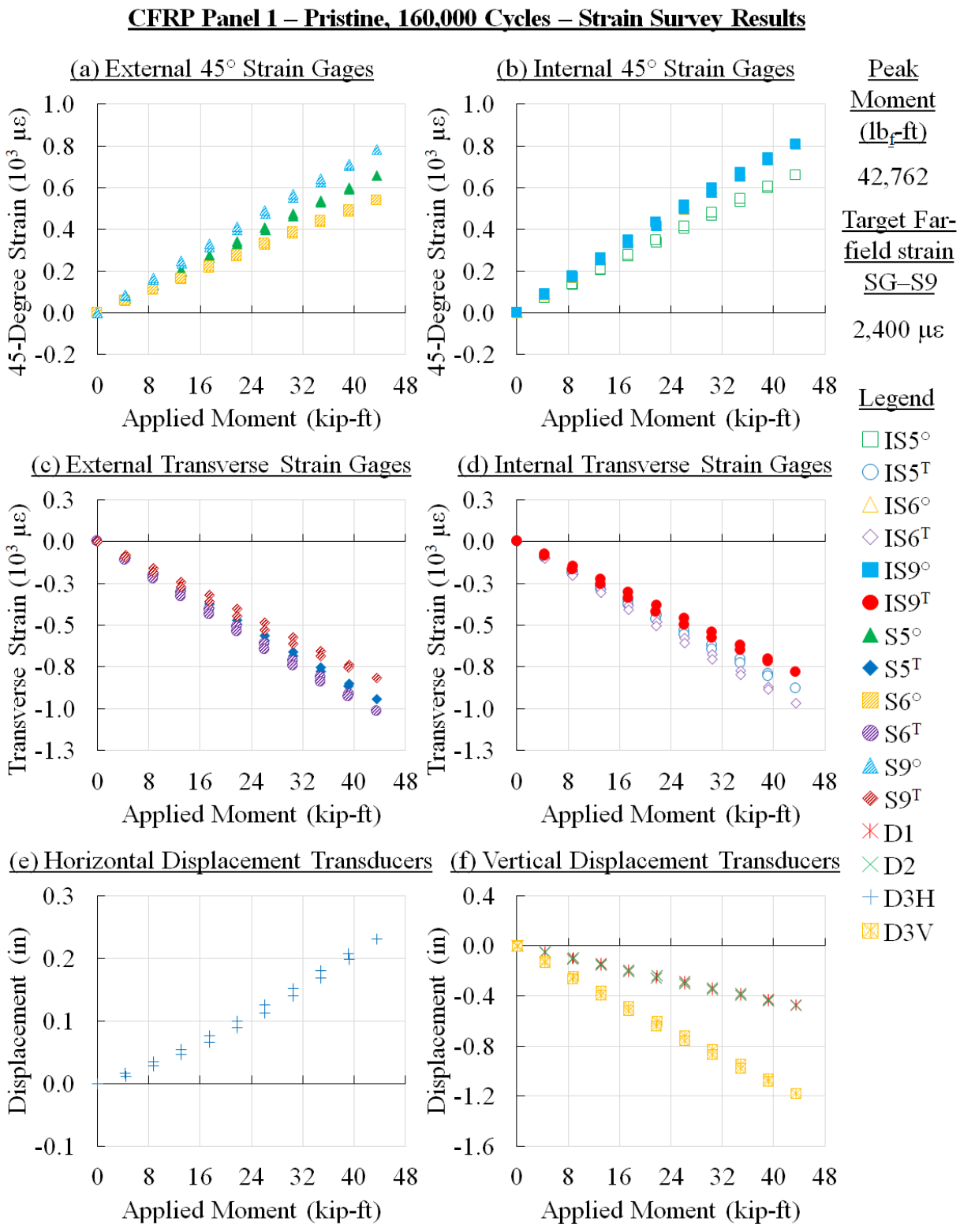

Figure 55. Panel 1 strain survey results at 160,000 cycles

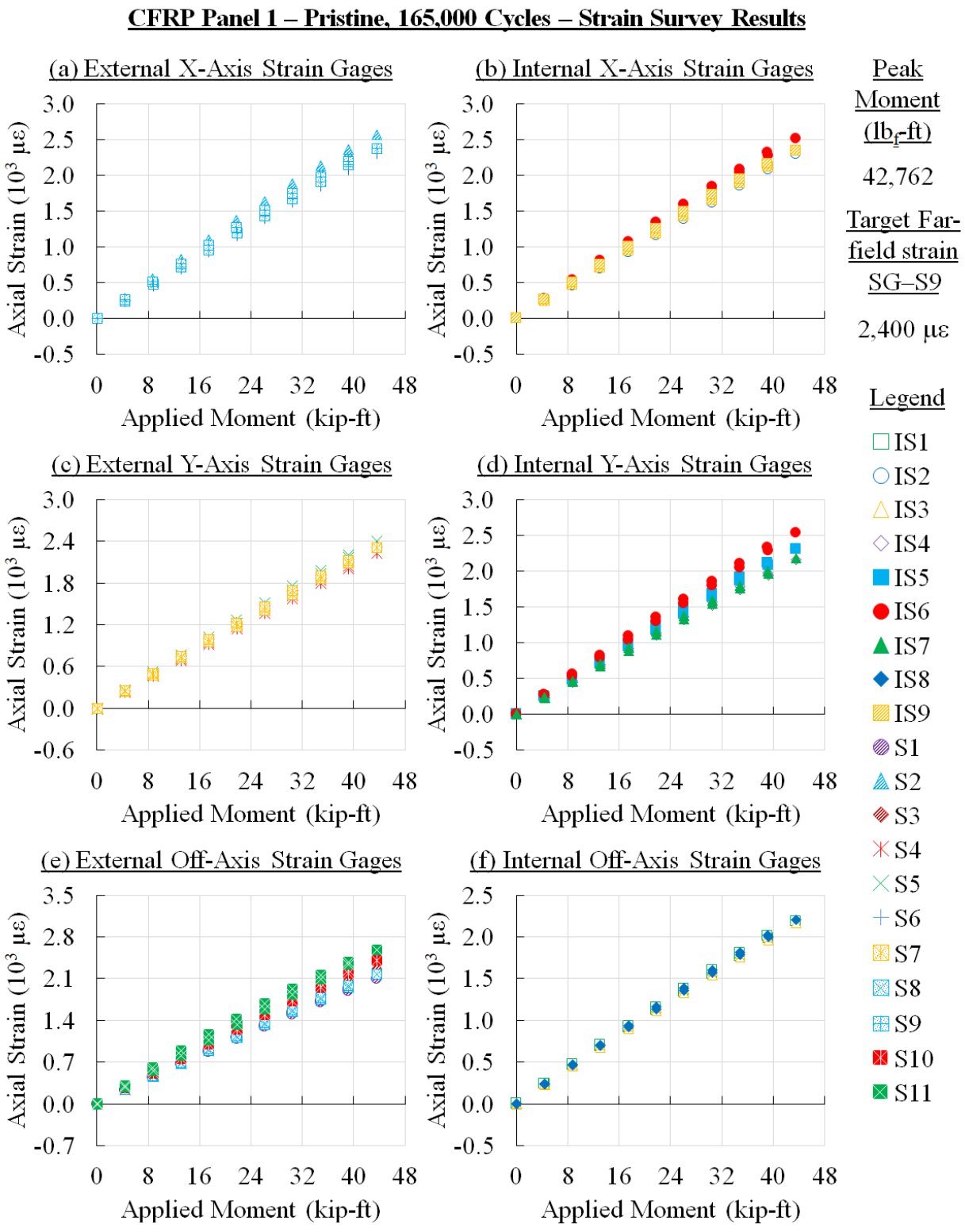

Figure 56. Panel 1 strain survey results at 165,000 cycles

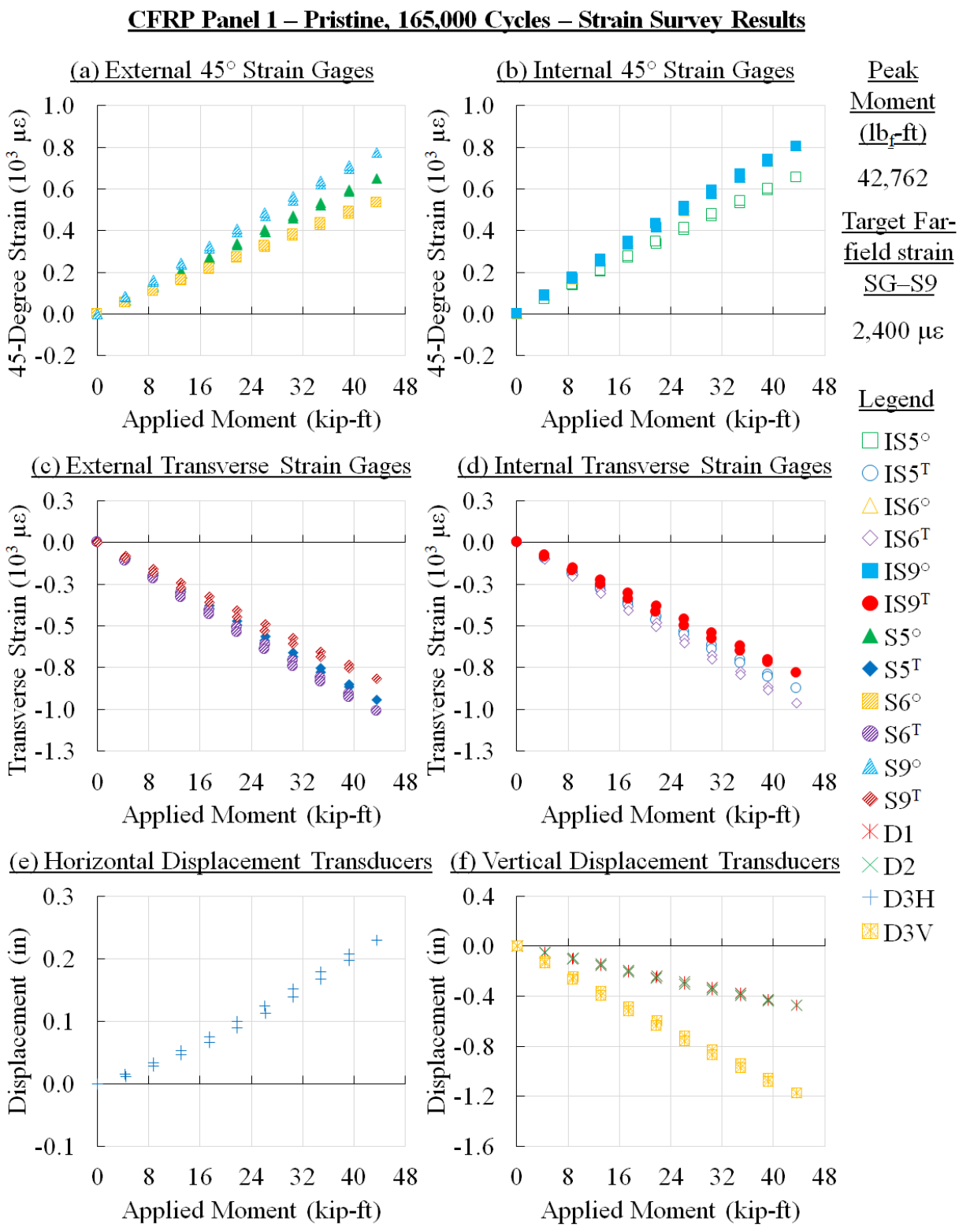

Figure 57. Panel 1 strain survey results at 165,000 cycles

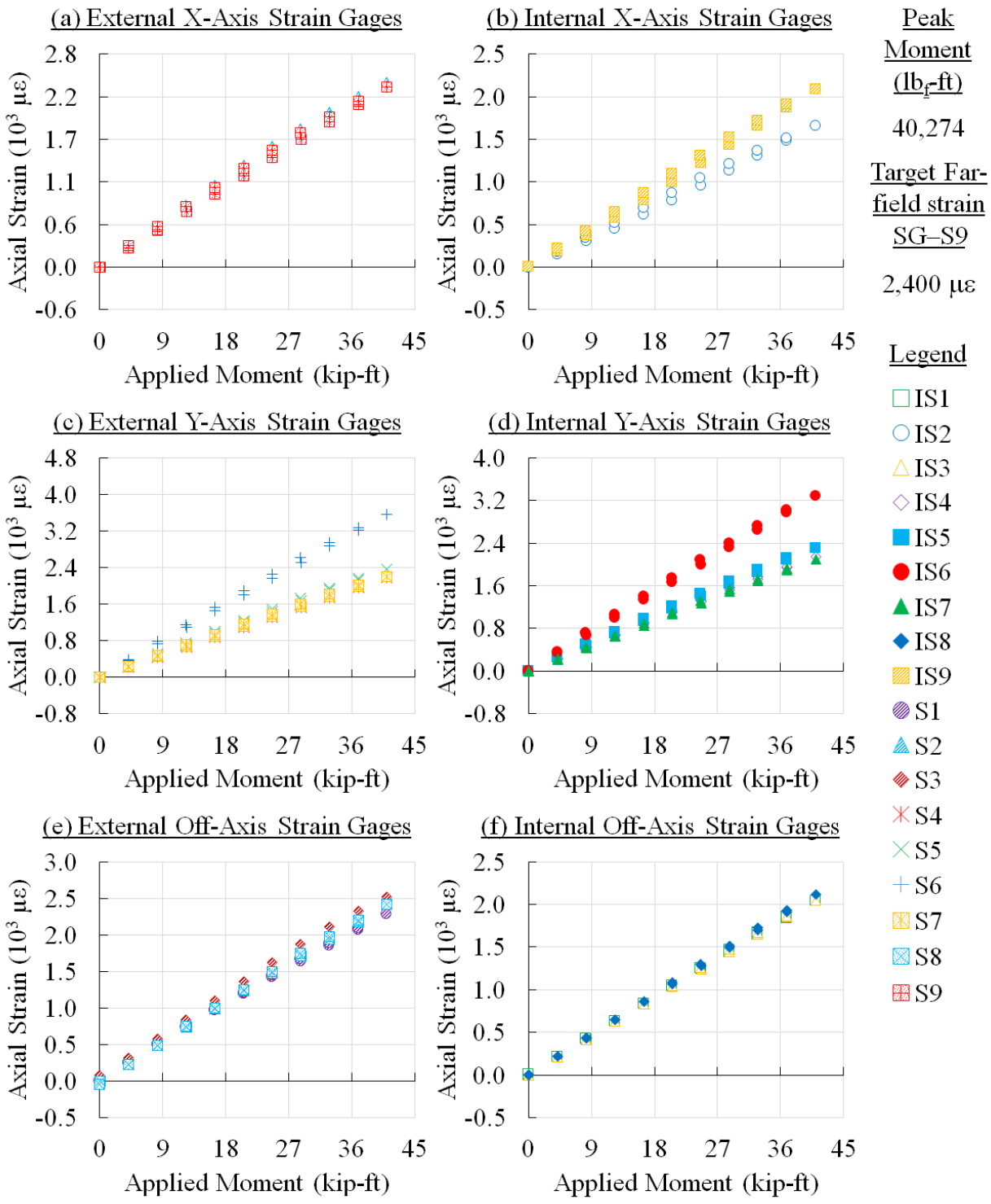

Figure 58. Panel 2 strain survey results at 0 cycles (interval 1)

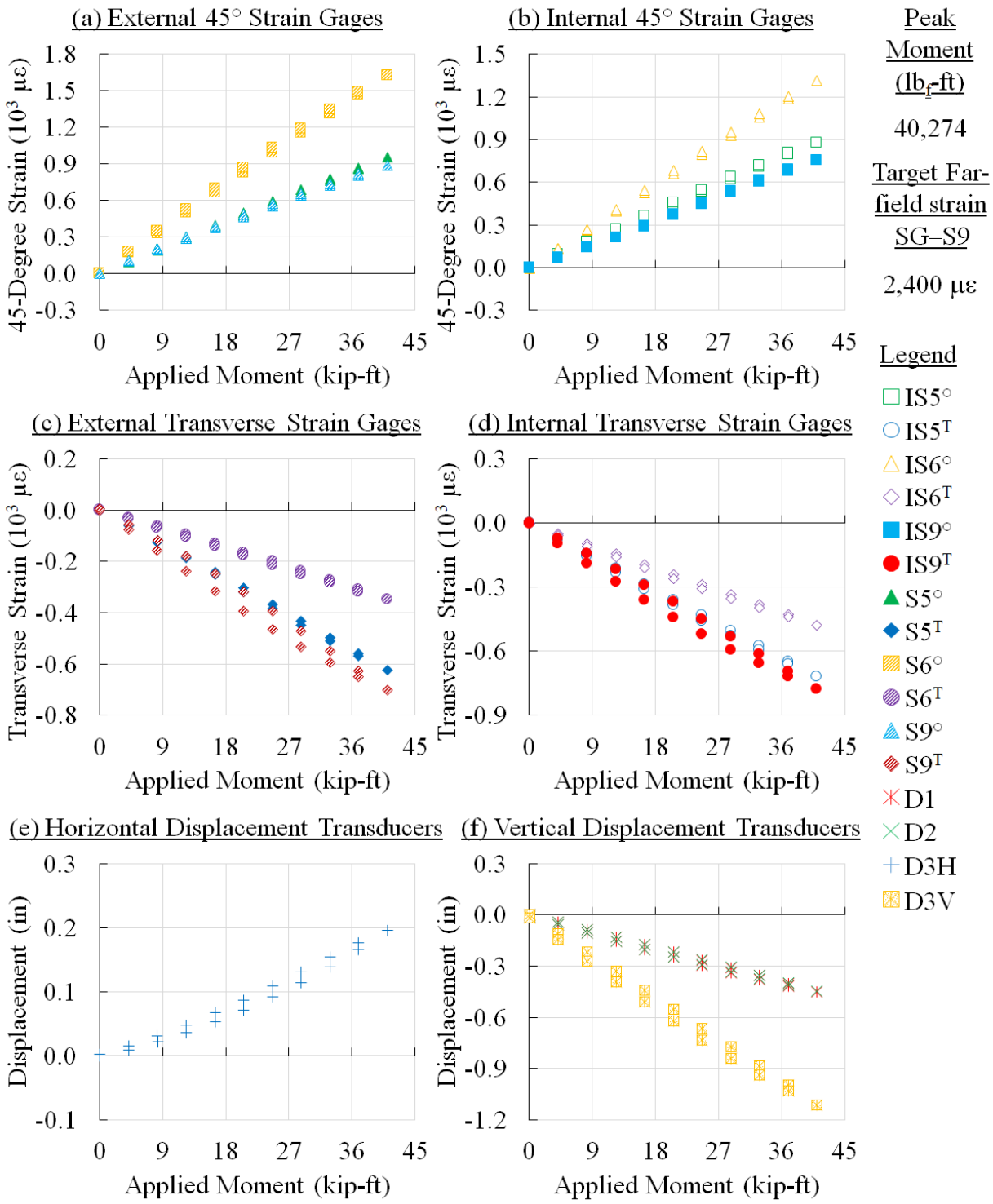

Figure 59. Panel 2 strain survey results at 0 cycles (interval 1)

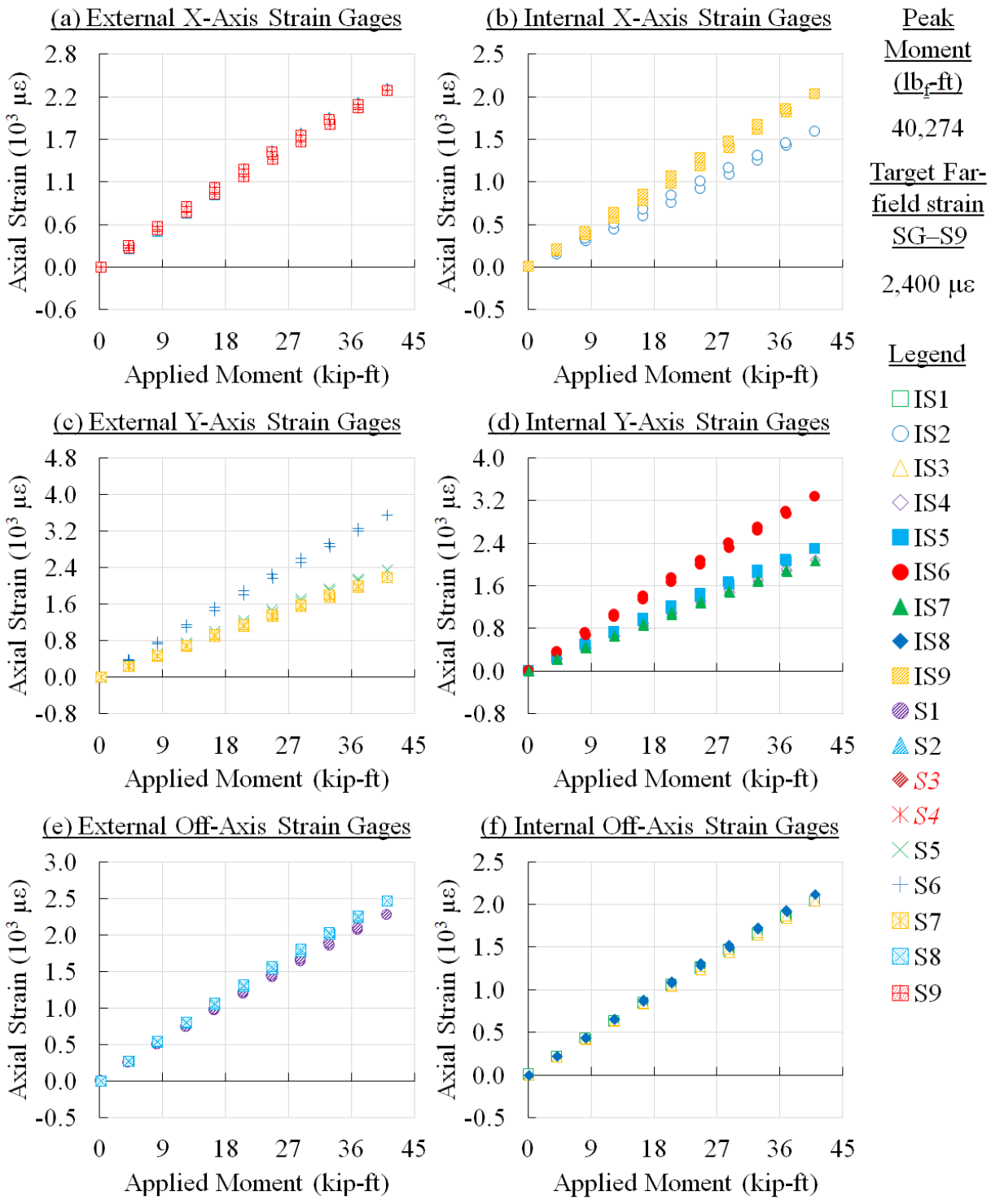

Figure 60. Panel 2 strain survey results at 5,000 cycles (interval 1)

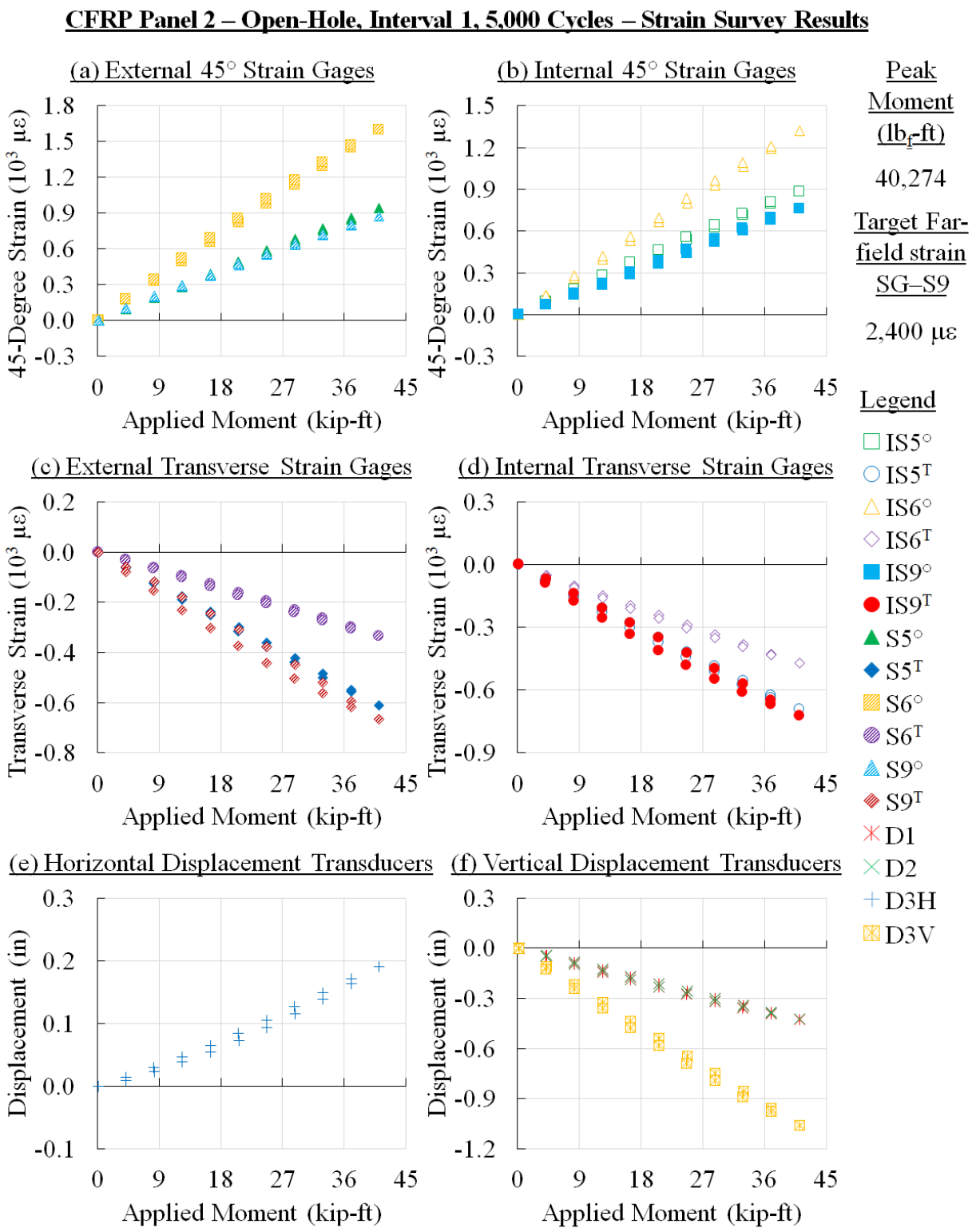

Figure 61. Panel 2 strain survey results at 5,000 cycles (interval 1)

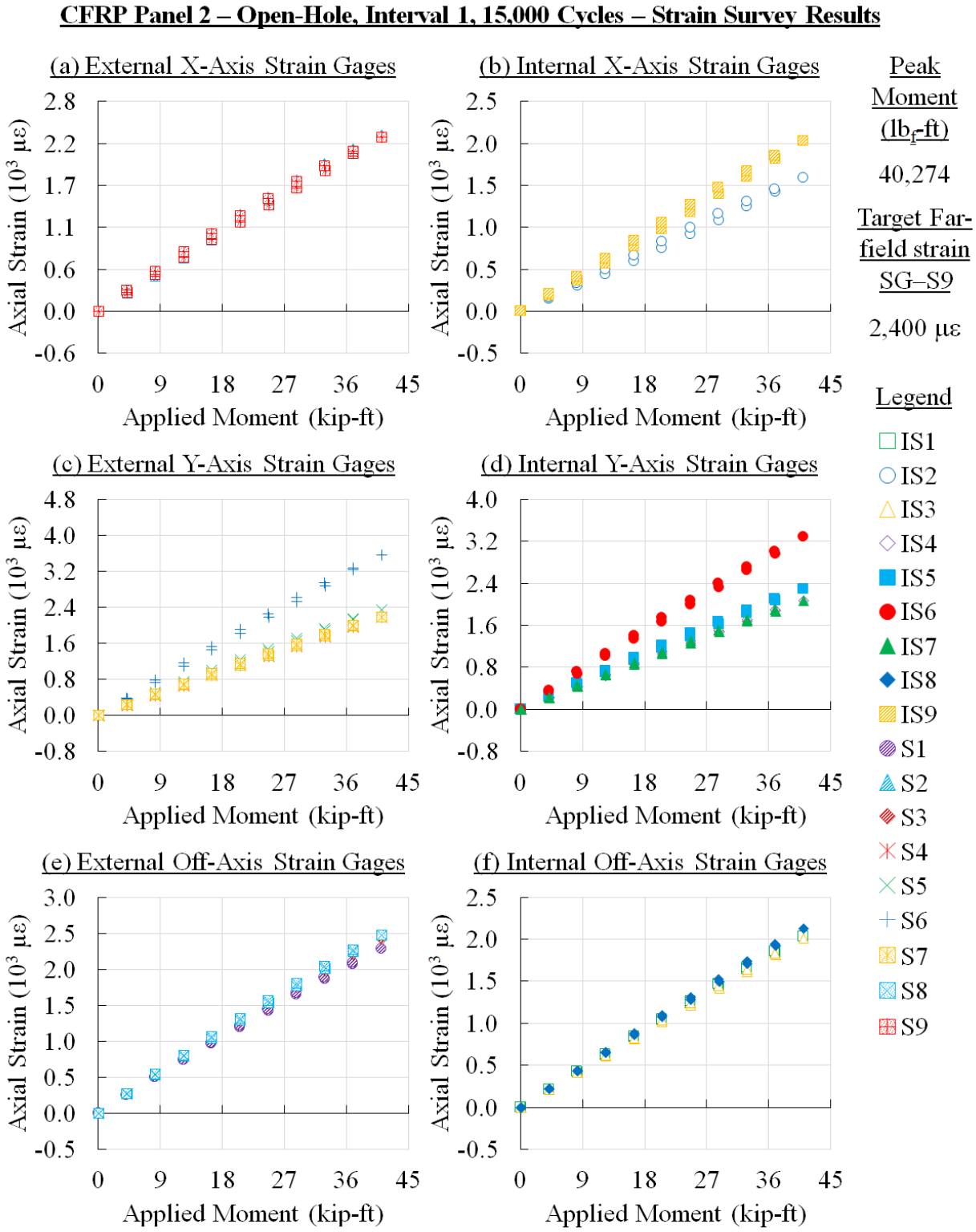

Figure 62. Panel 2 strain survey results at 15,000 cycles (interval 1)

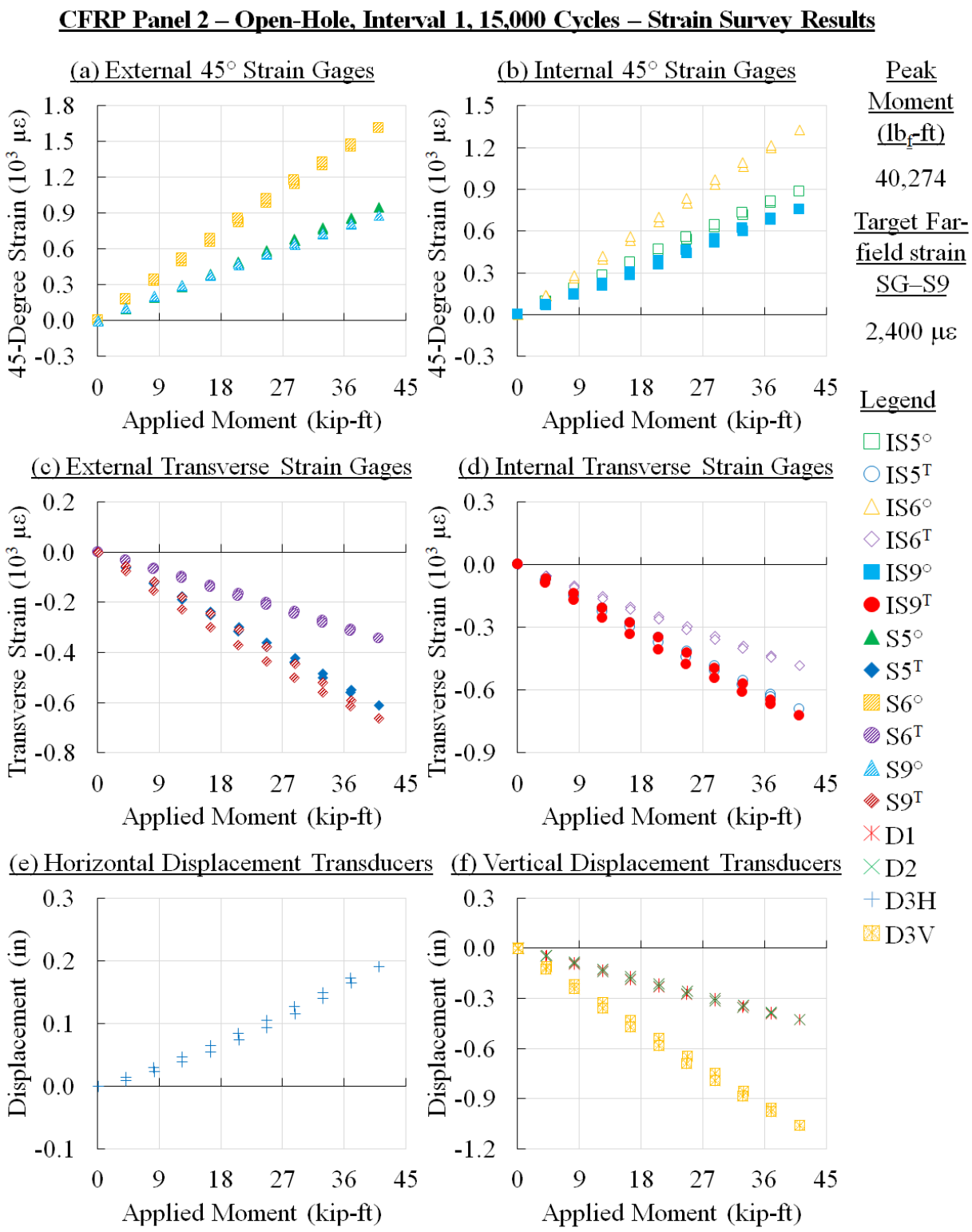

Figure 63. Panel 2 strain survey results at 15,000 cycles (interval 1)

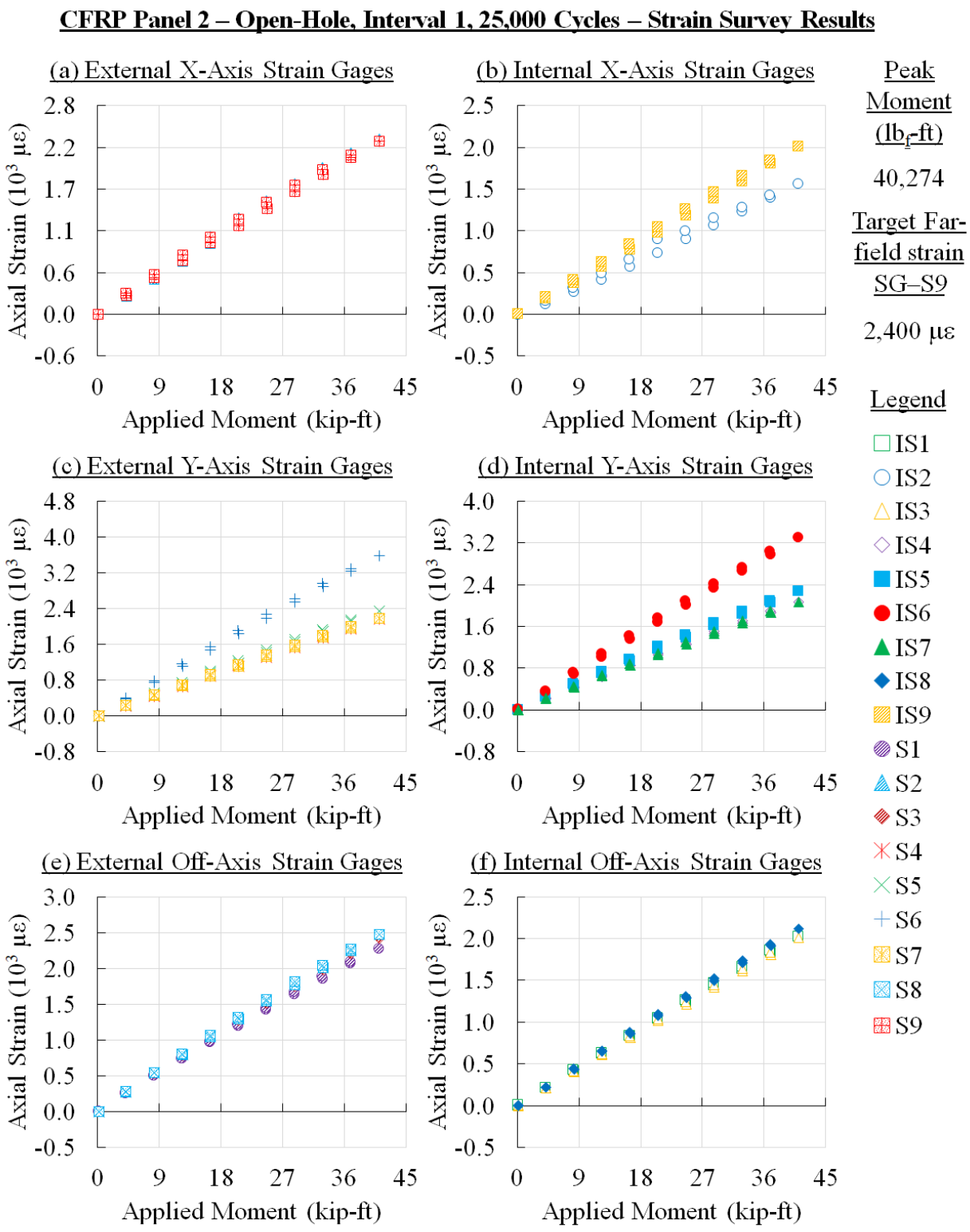

Figure 64. Panel 2 strain survey results at 25,000 cycles (interval 1)

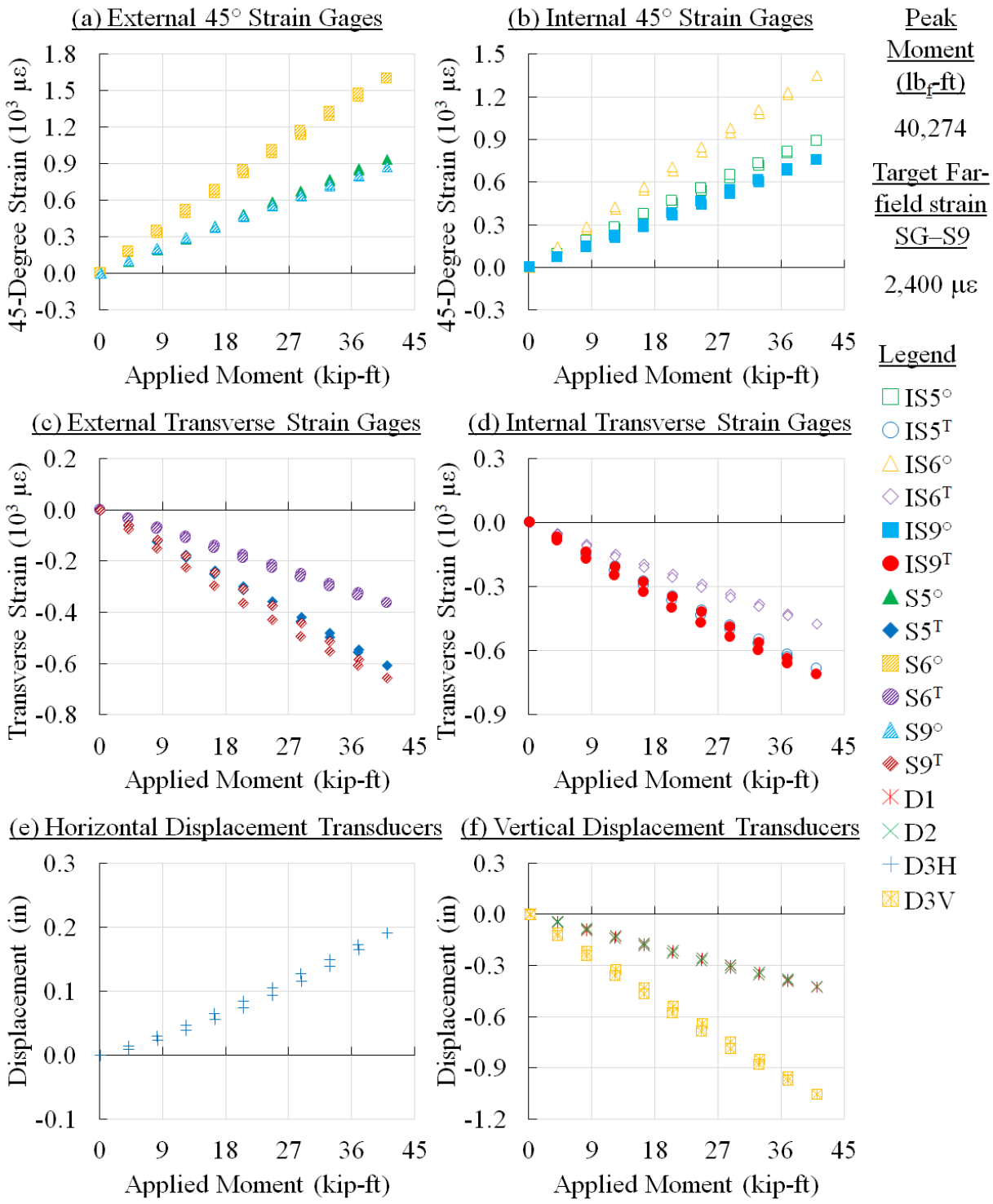

Figure 65. Panel 2 strain survey results at 25,000 cycles (interval 1)

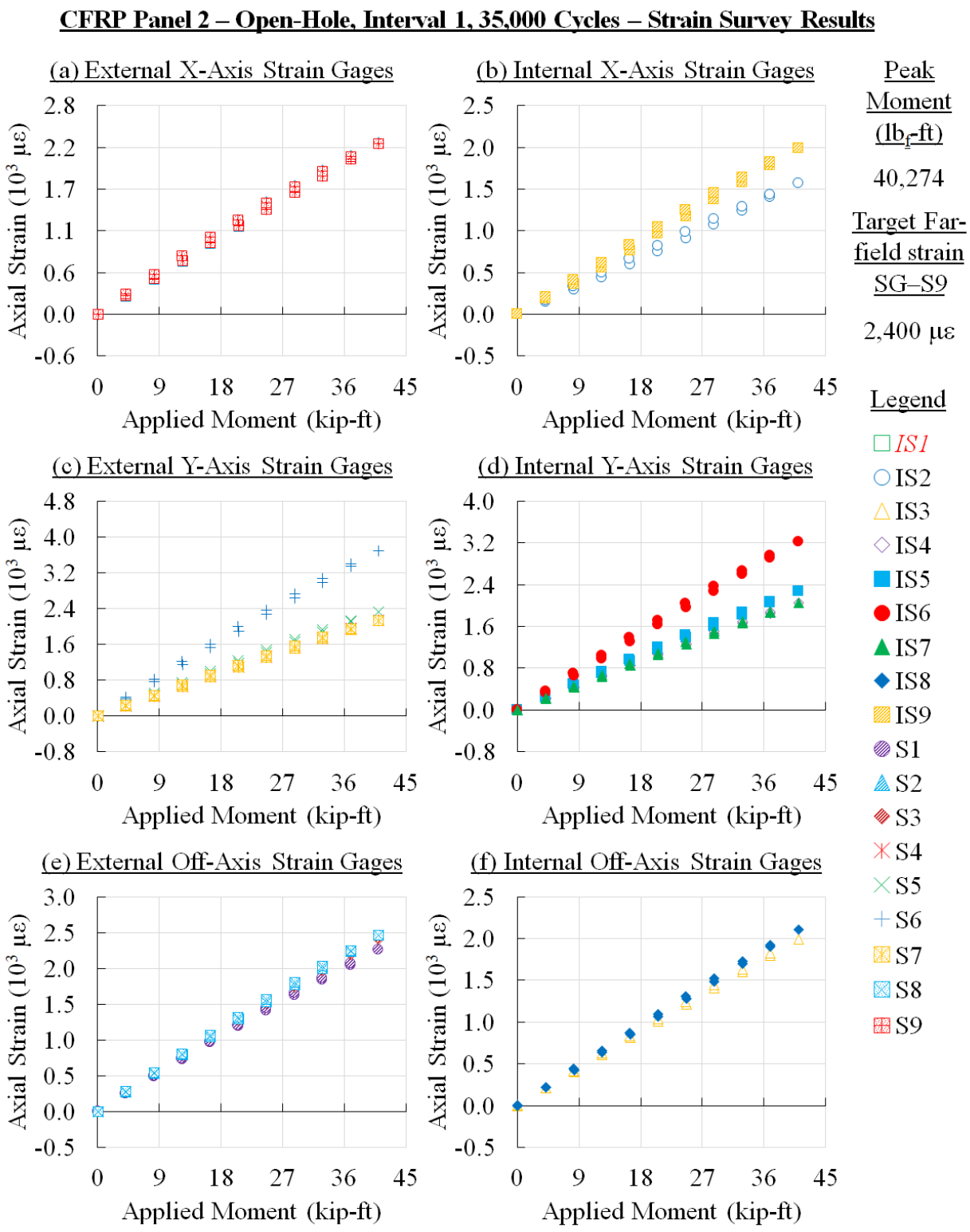

Figure 66. Panel 2 strain survey results at 35,000 cycles (interval 1)

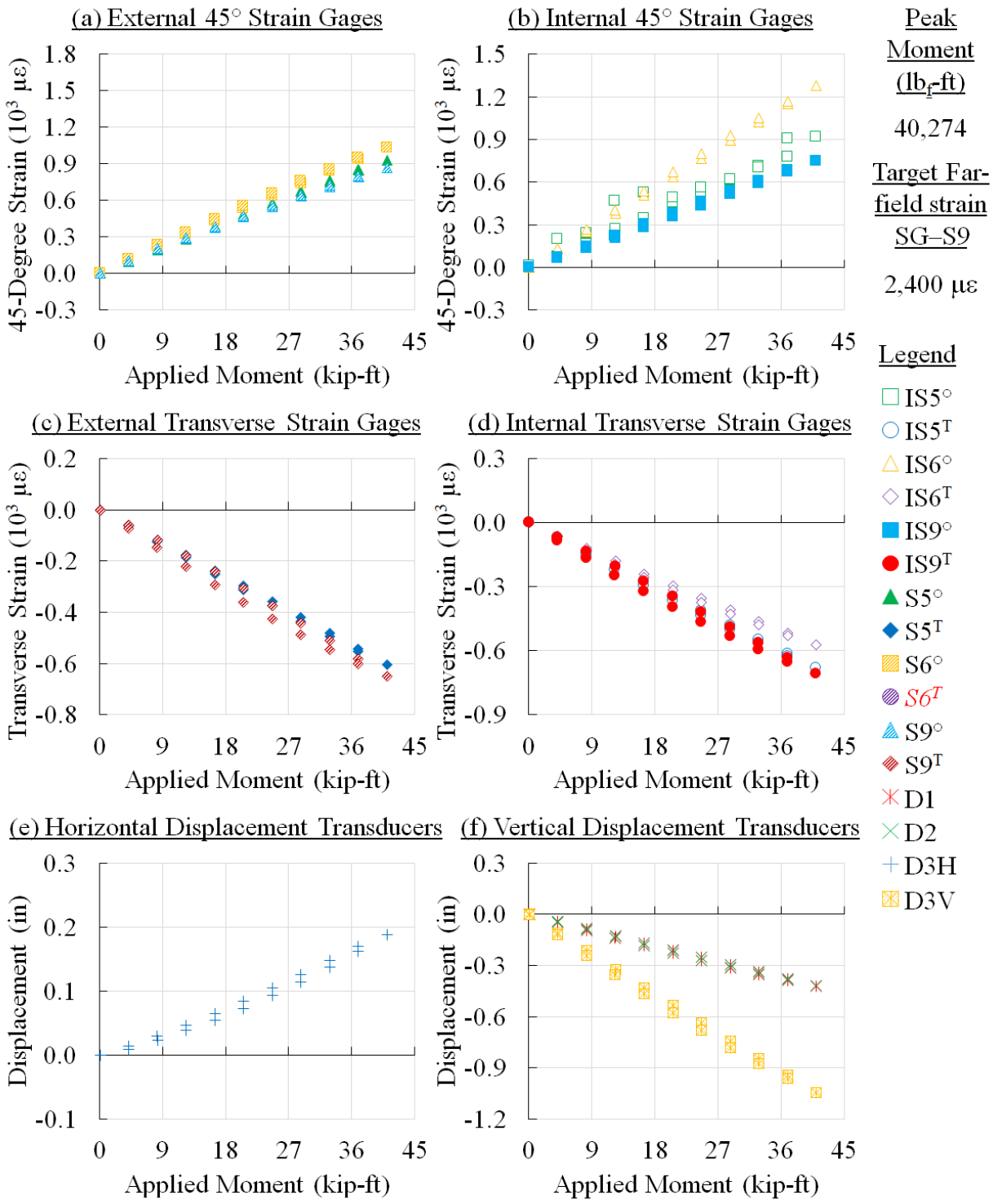

Figure 67. Panel 2 strain survey results at 35,000 cycles (interval 1)

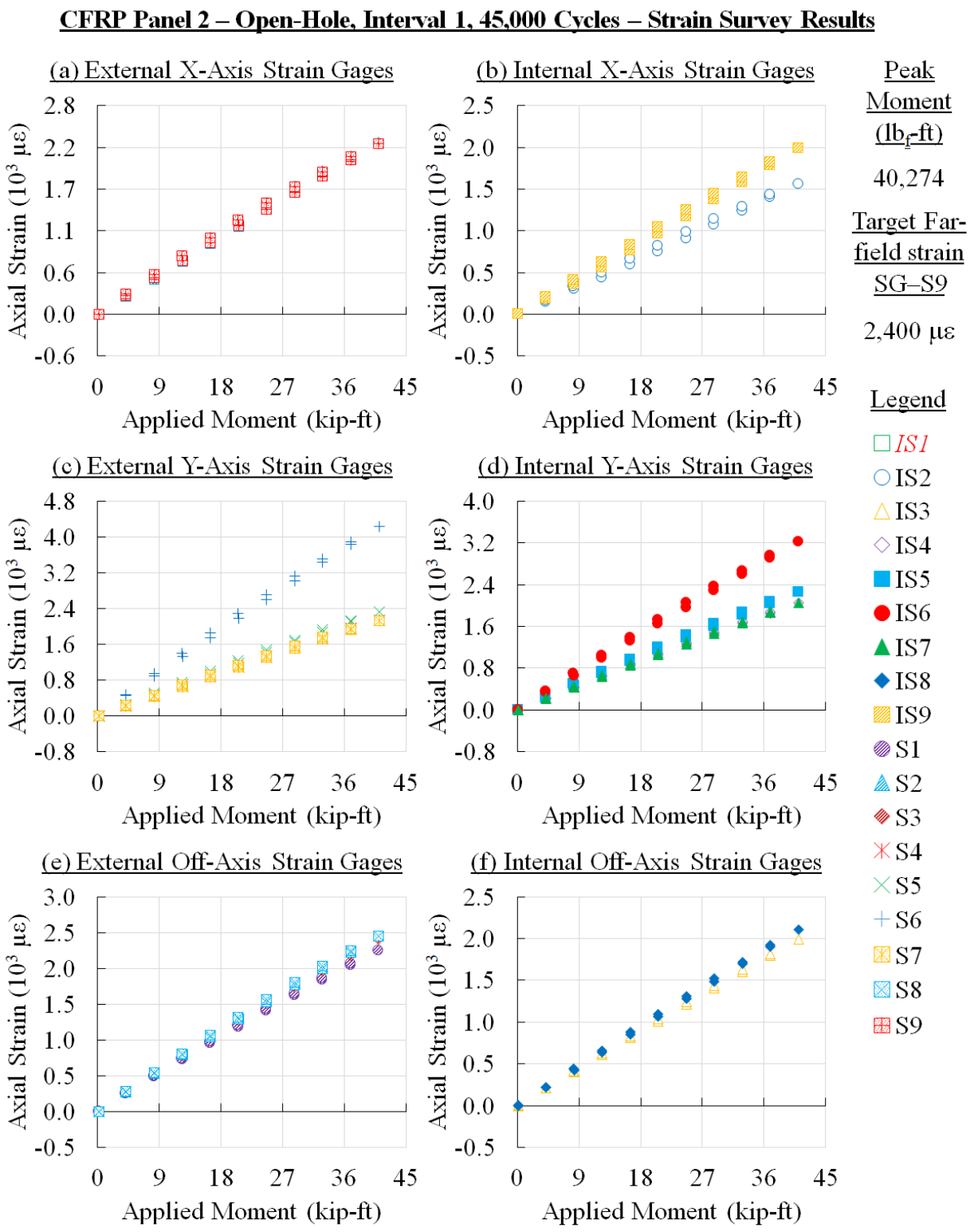

Figure 68. Panel 2 strain survey results at 45,000 cycles (interval 1)

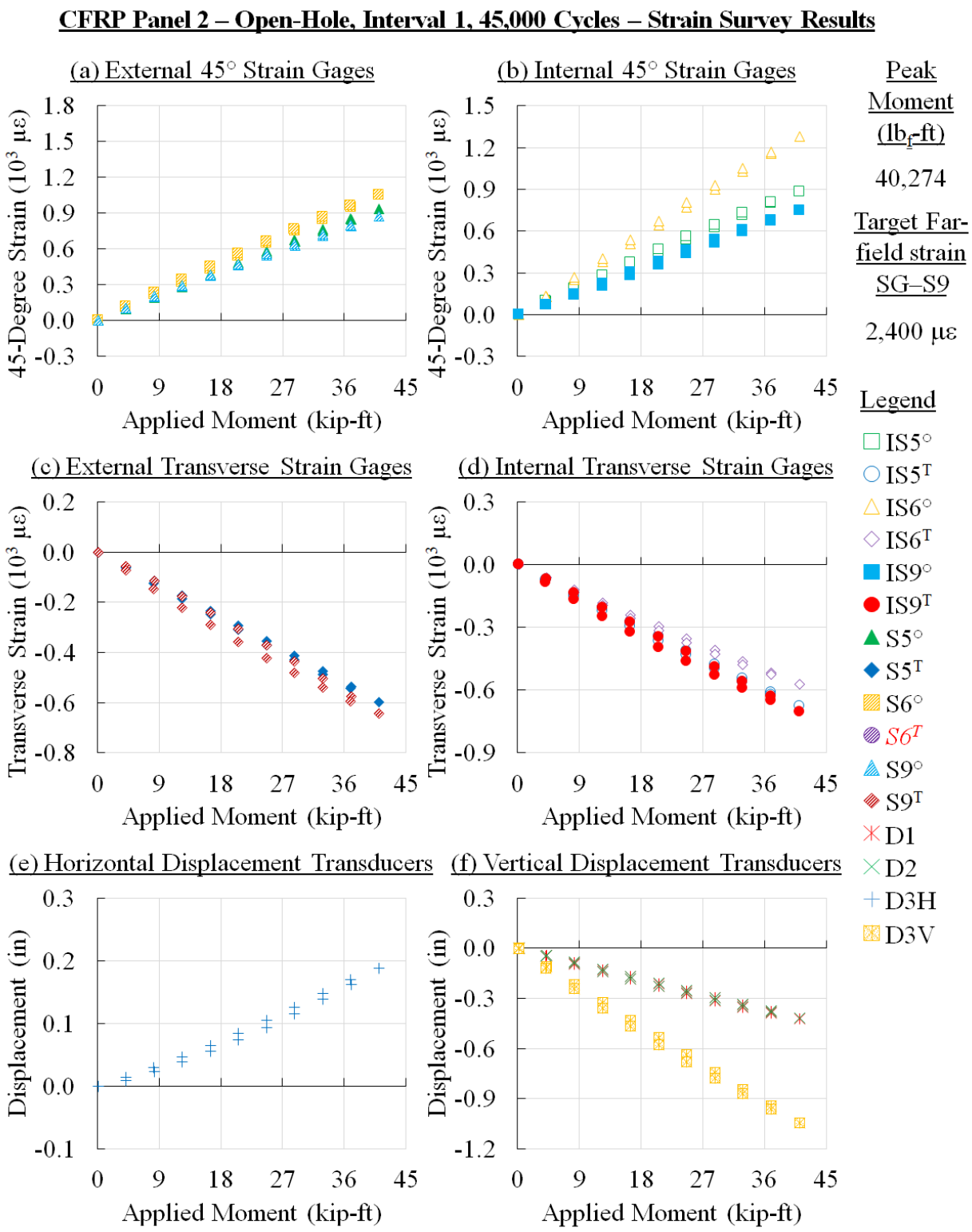

Figure 69. Panel 2 strain survey results at 45,000 cycles (interval 1)

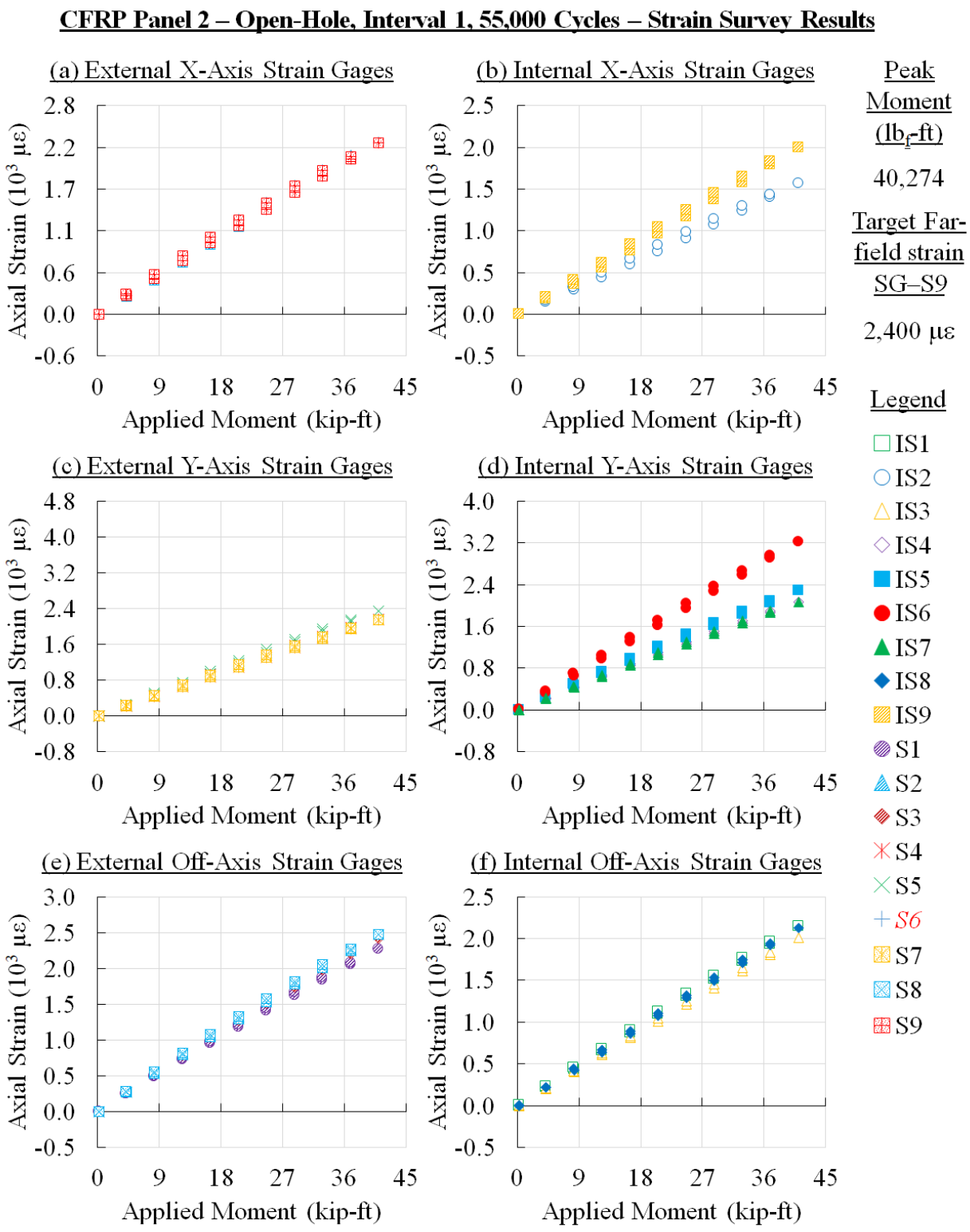

Figure 70. Panel 2 strain survey results at 55,000 cycles (interval 1)

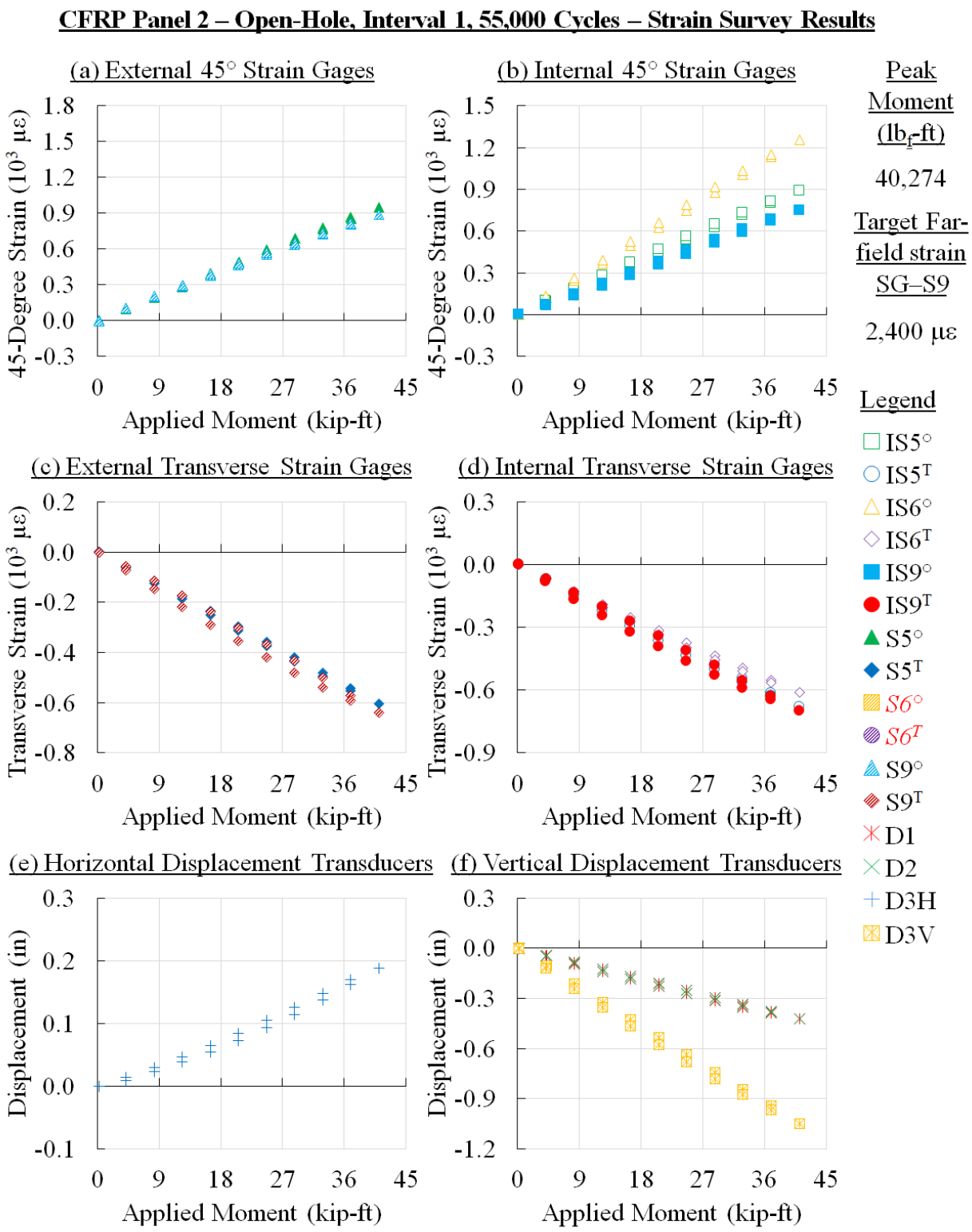

Figure 71. Panel 2 strain survey results at 55,000 cycles (interval 1)

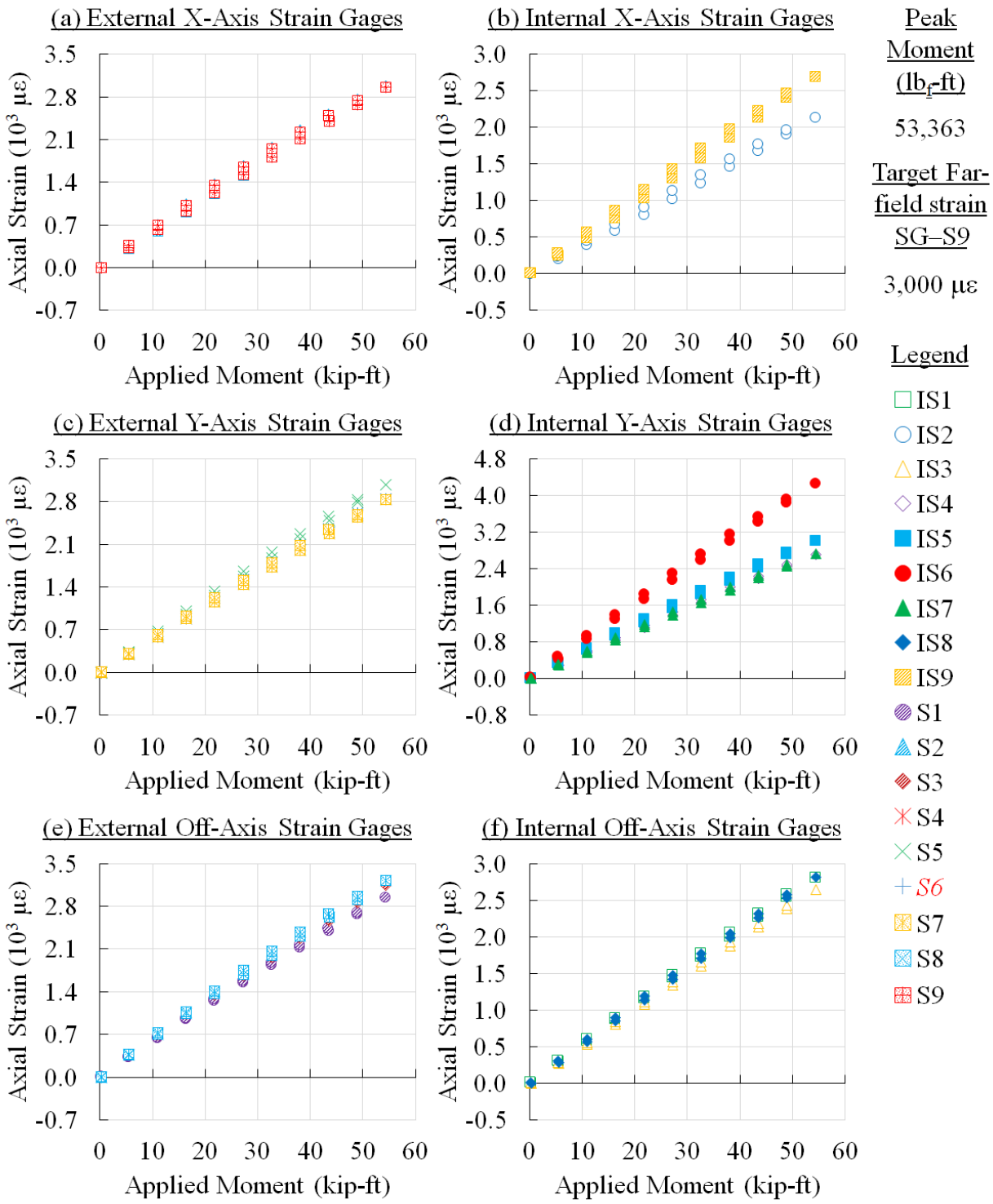

Figure 72. Panel 2 strain survey results at 55,000 cycles (interval 2)

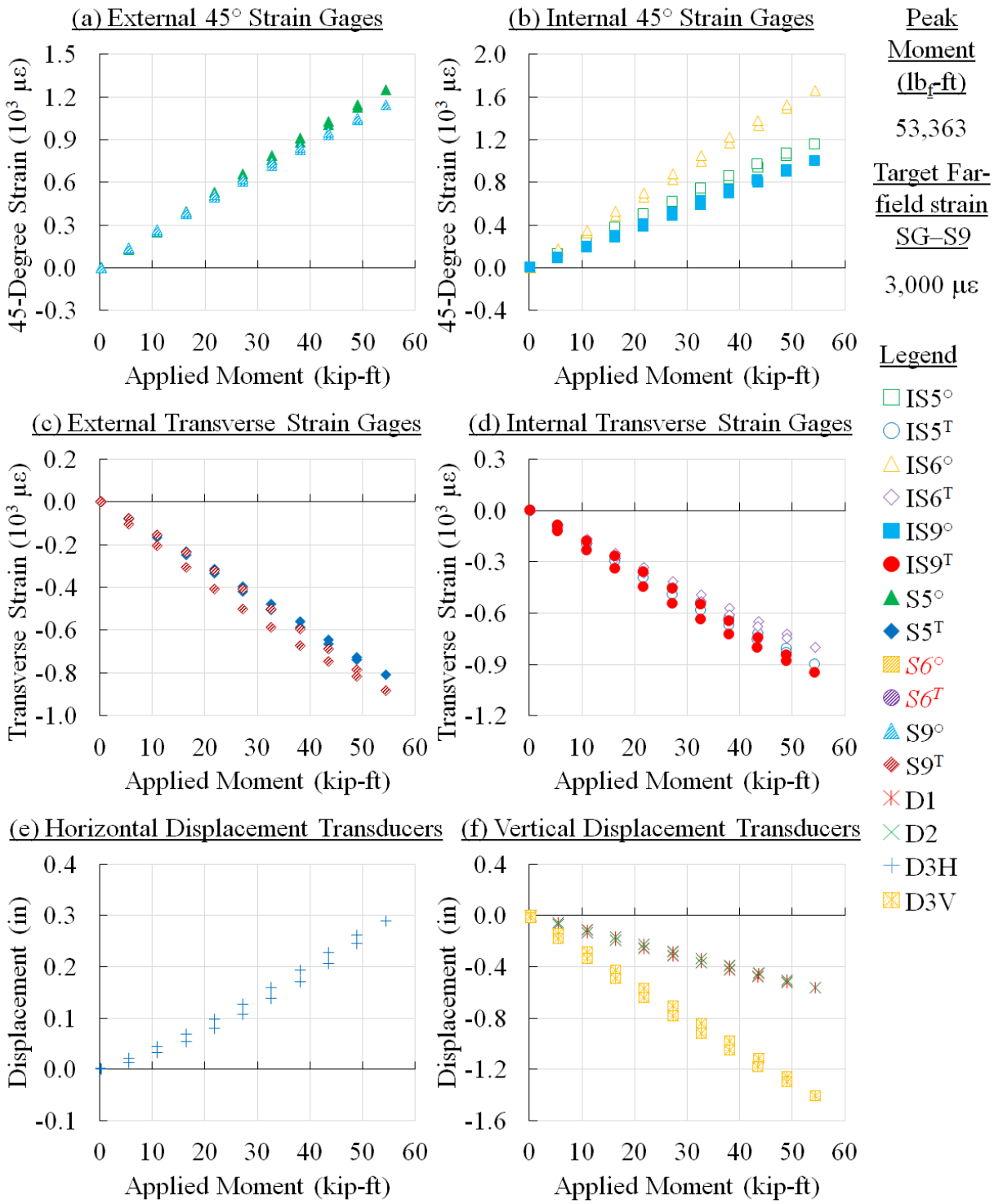

Figure 73. Panel 2 strain survey results at 55,000 cycles (interval 2)

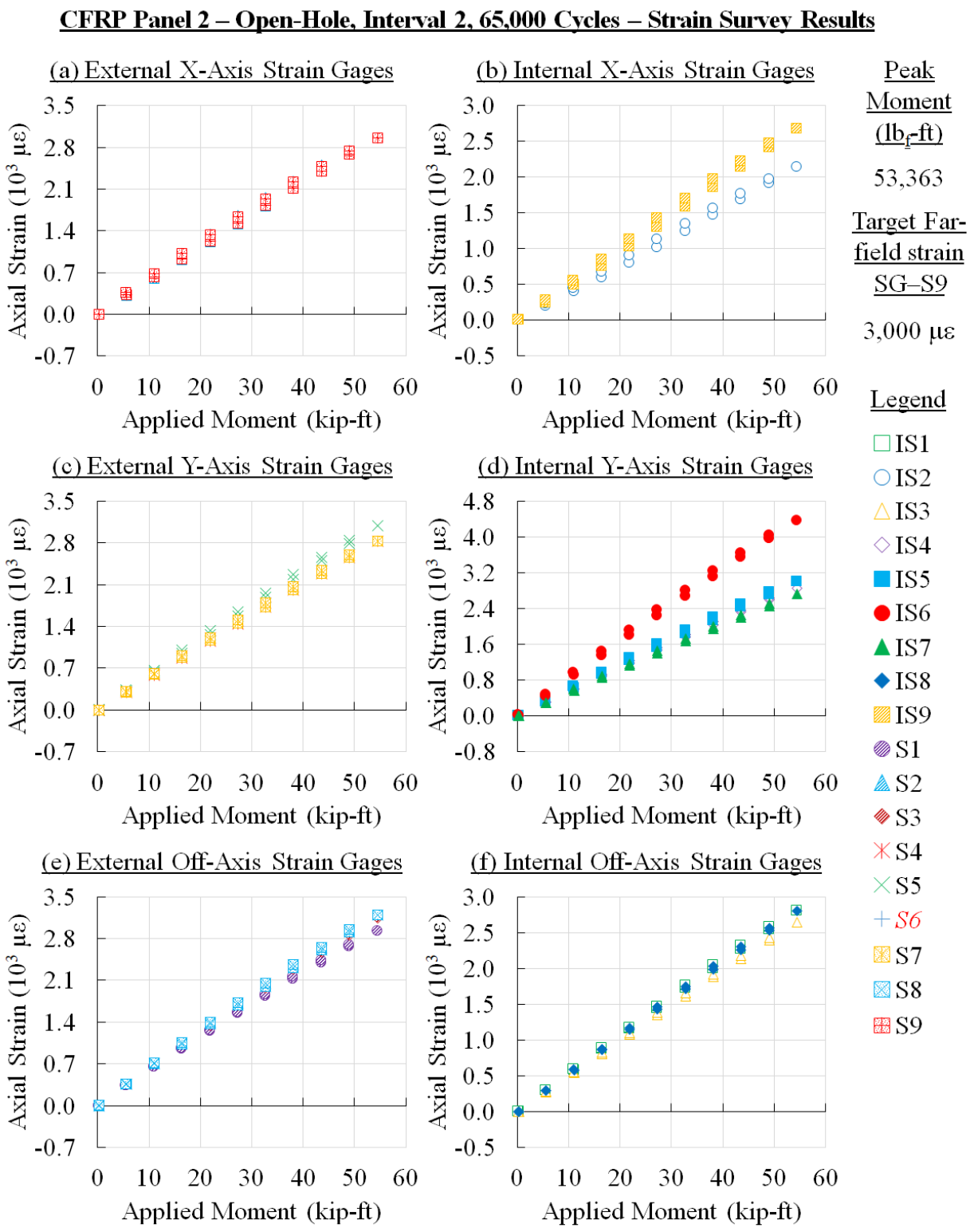

Figure 74. Panel 2 strain survey results at 65,000 cycles (interval 2)

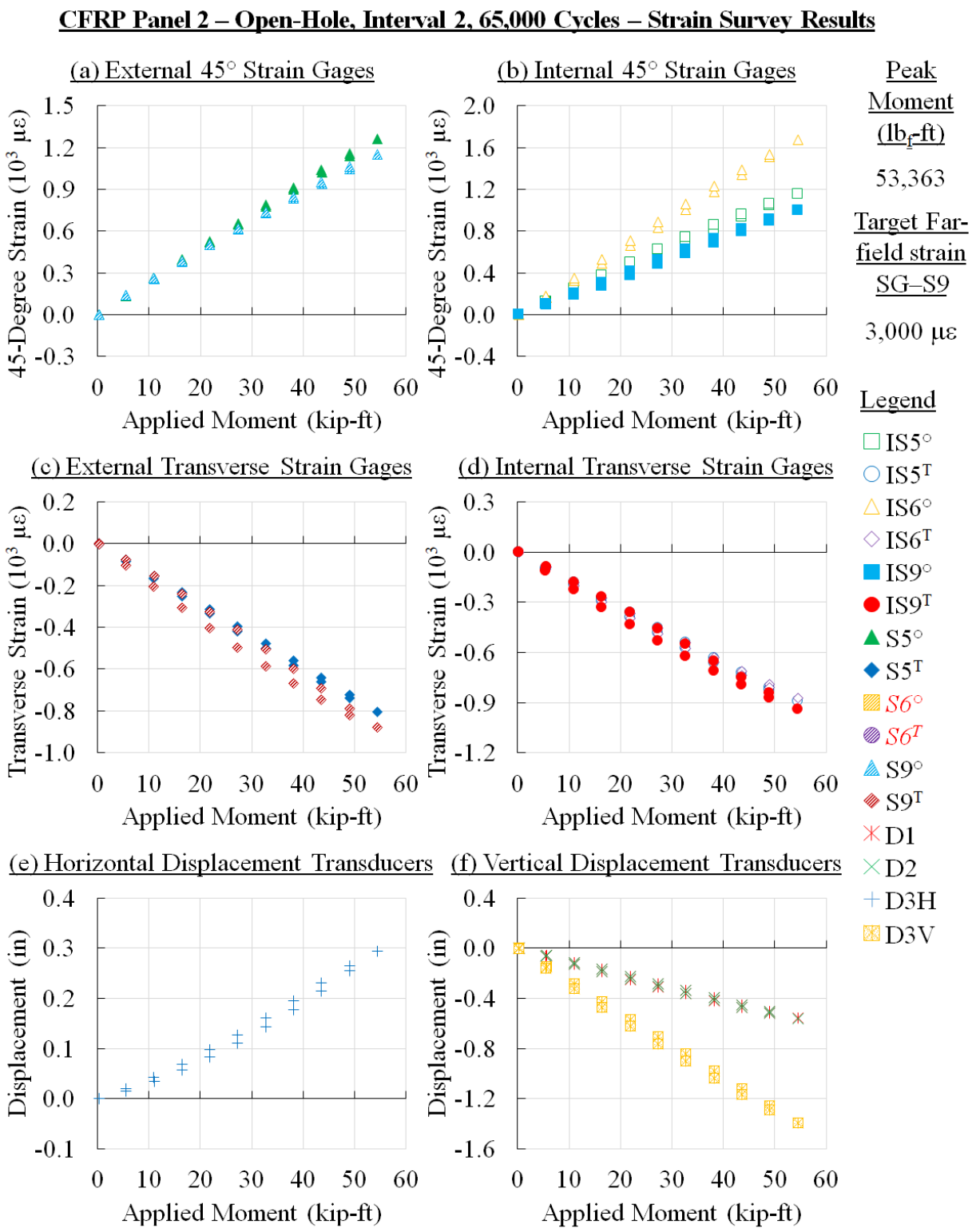

Figure 75. Panel 2 strain survey results at 65,000 cycles (interval 2)

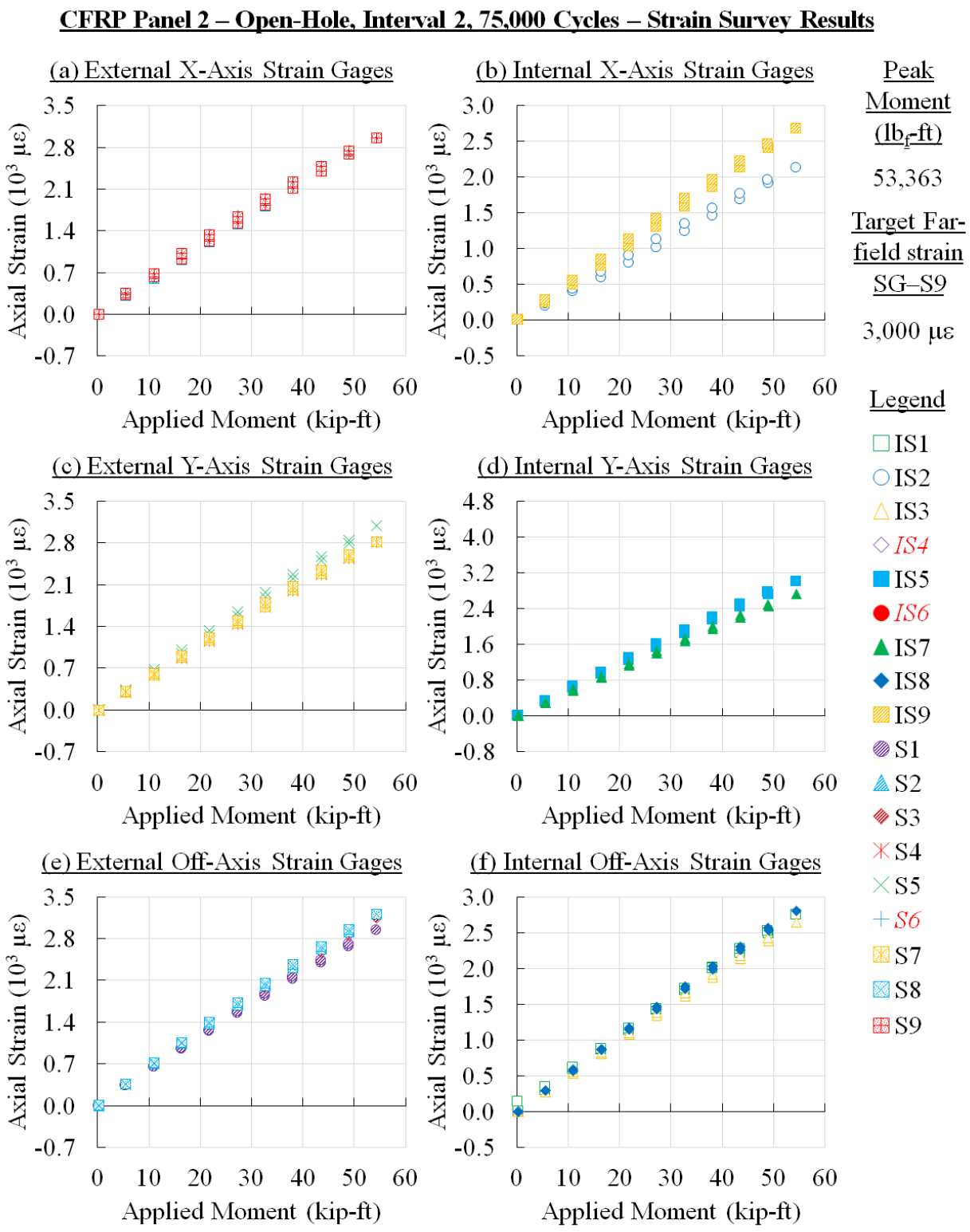

Figure 76. Panel 2 strain survey results at 75,000 cycles (interval 2)

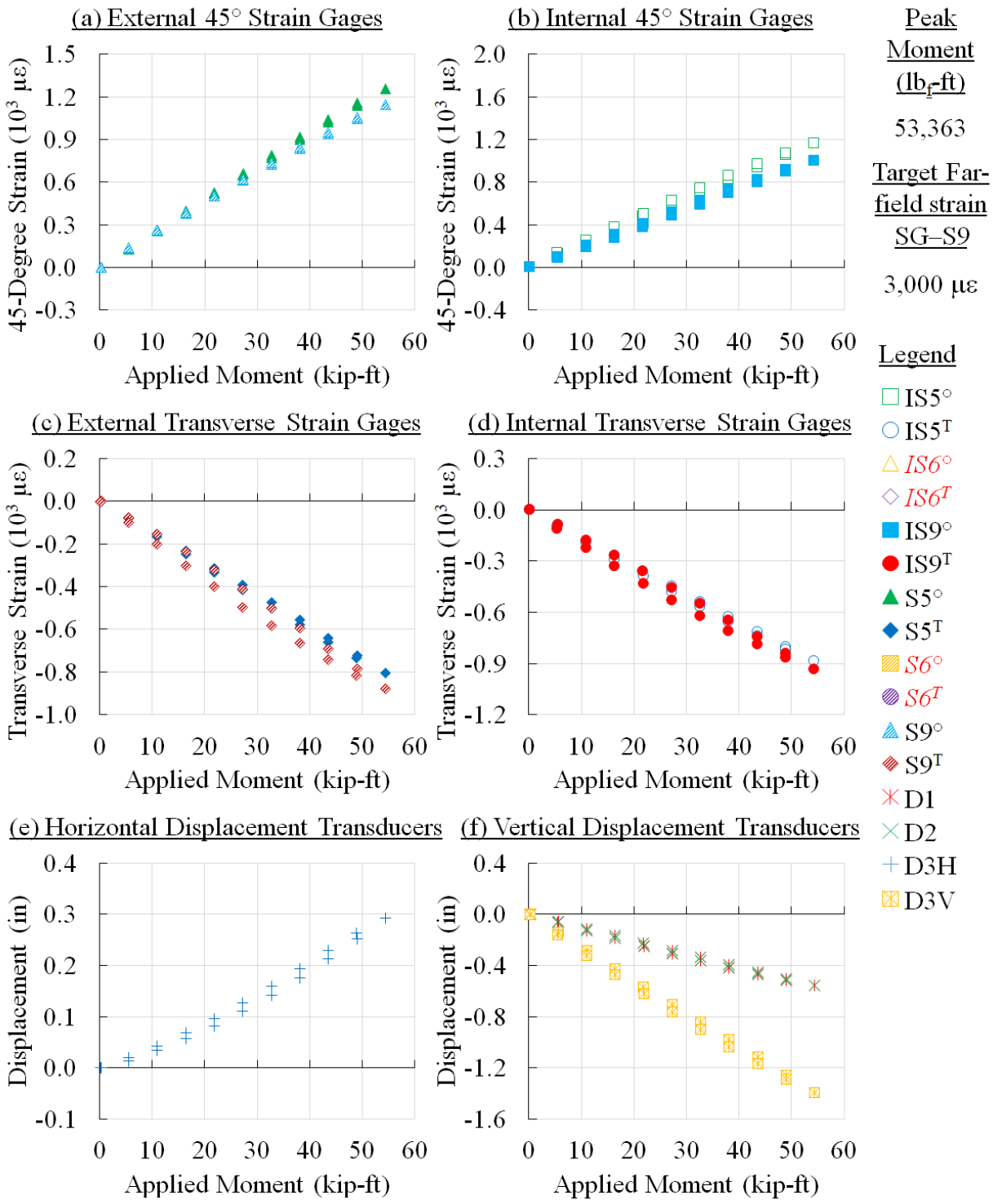

Figure 77. Panel 2 strain survey results at 75,000 cycles (interval 2)

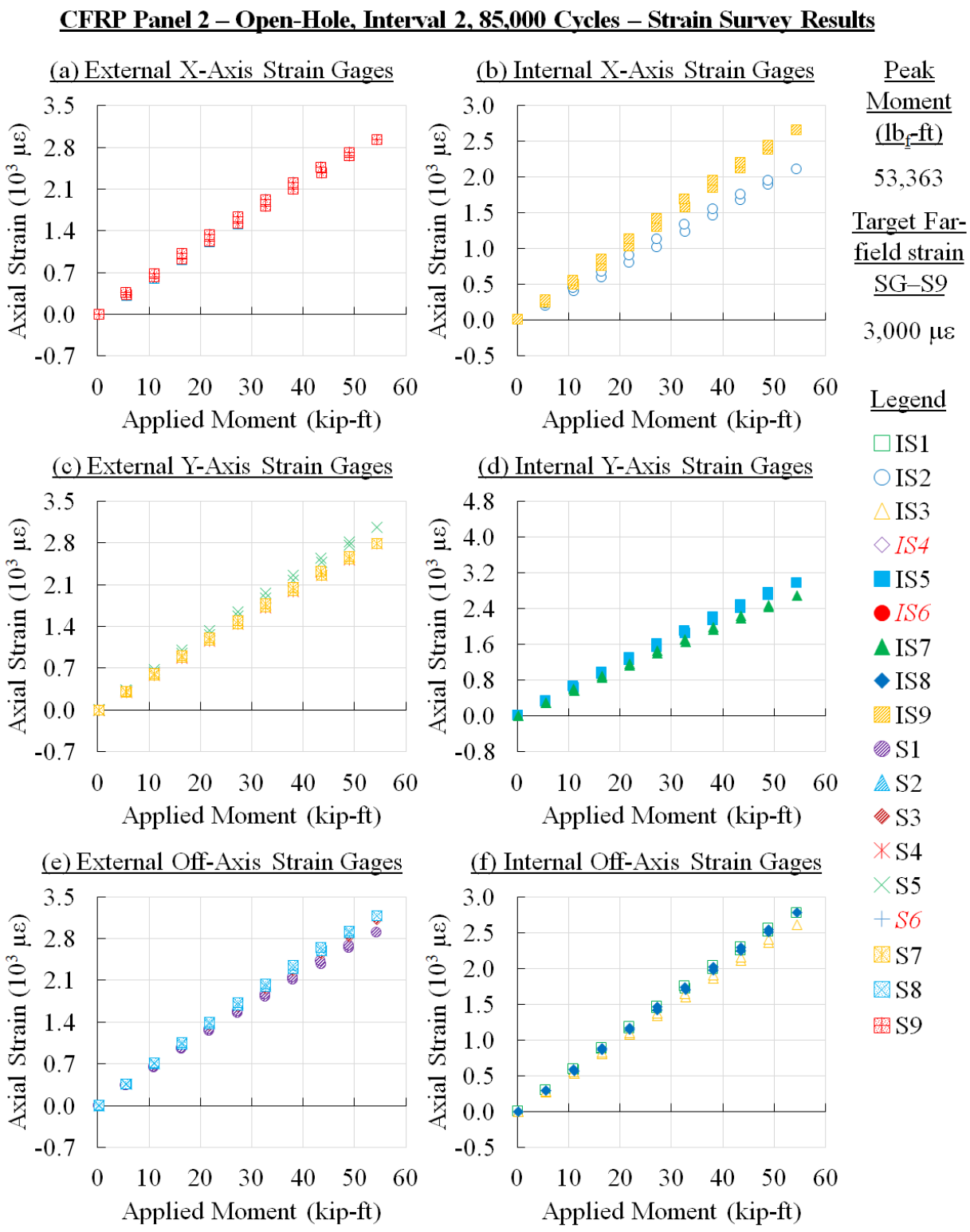

Figure 78. Panel 2 strain survey results at 85,000 cycles (interval 2)

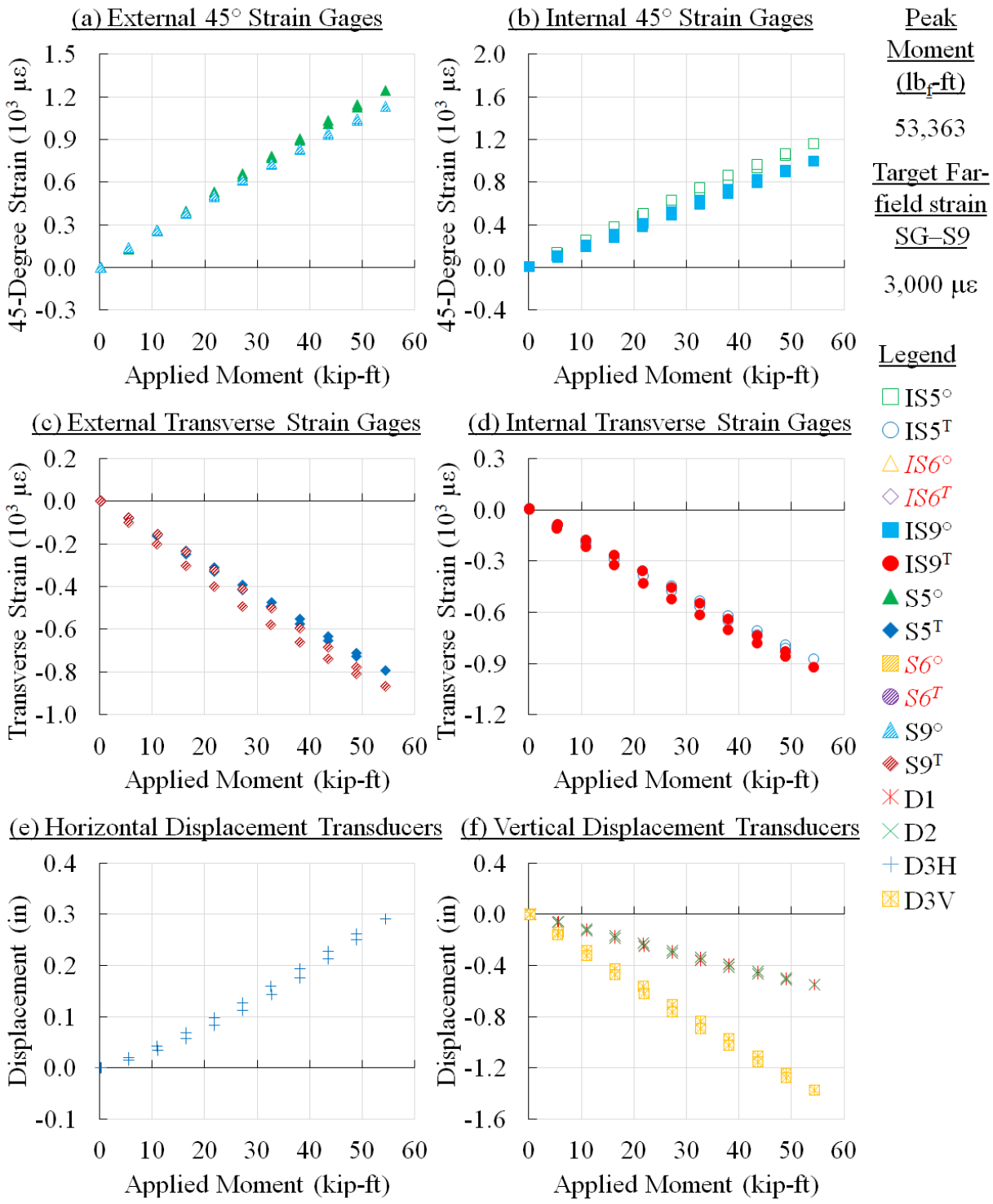

Figure 79. Panel 2 strain survey results at 85,000 cycles (interval 2)

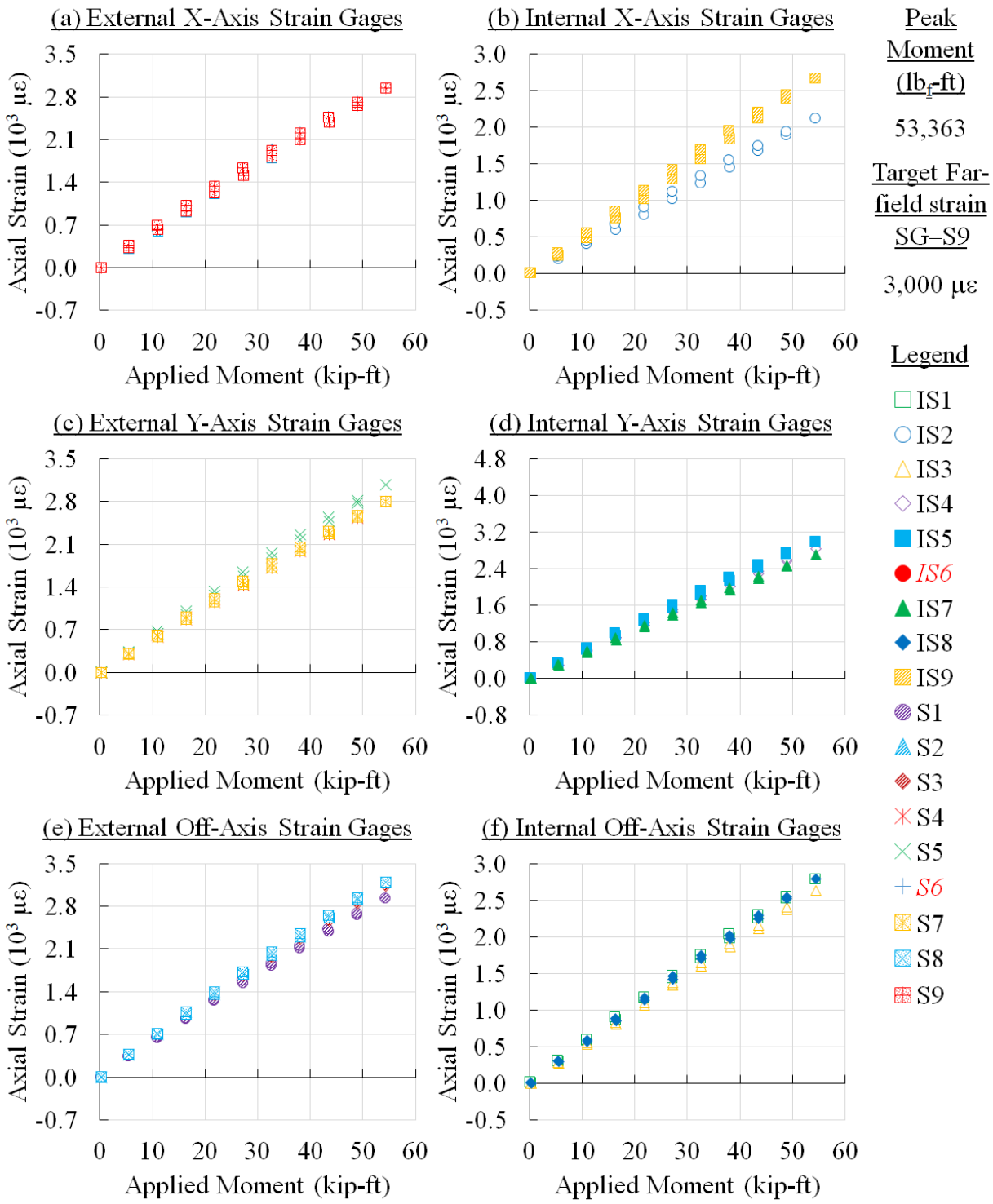

Figure 80. Panel 2 strain survey results at 95,000 cycles (interval 2)

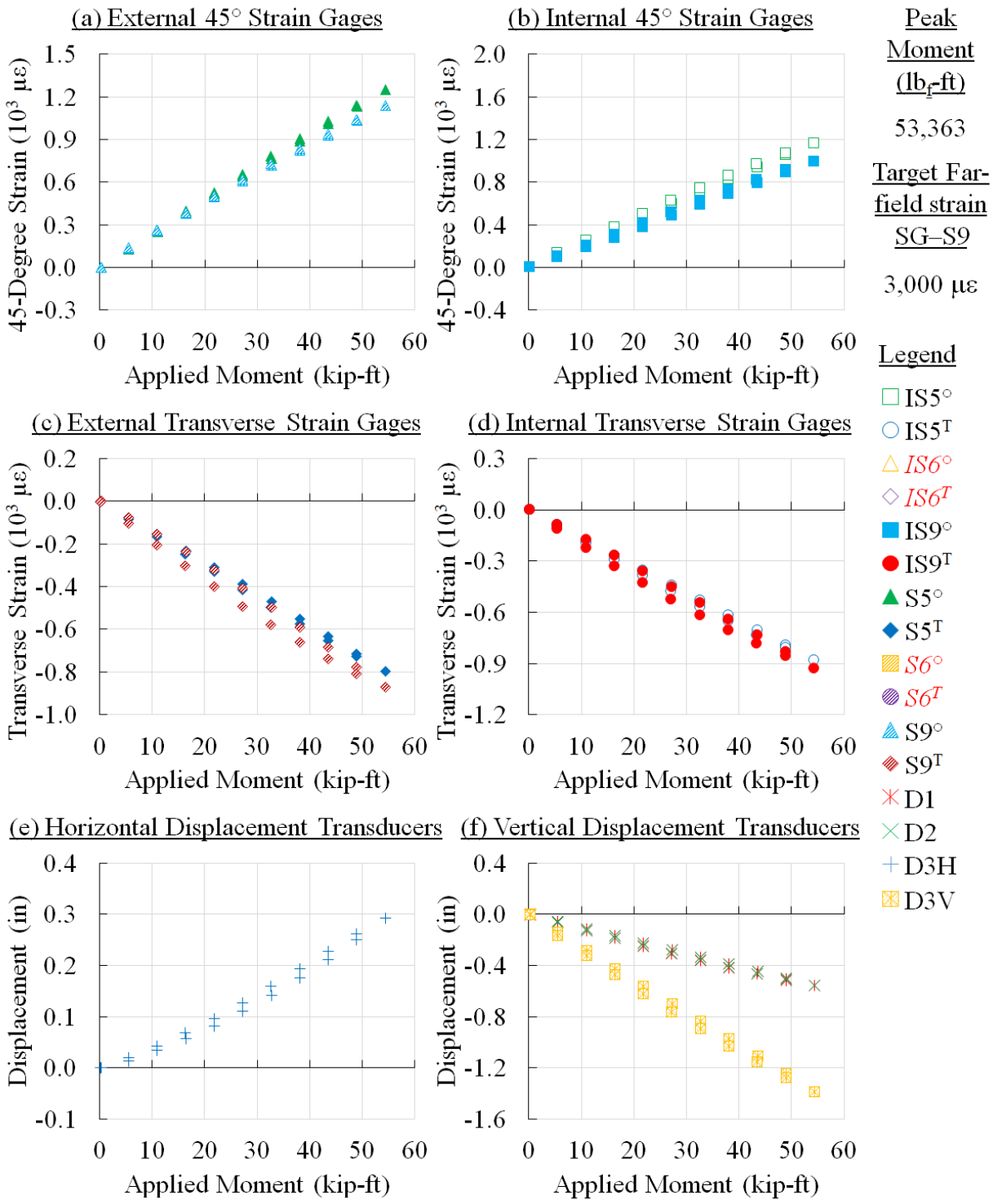

Figure 81. Panel 2 strain survey results at 95,000 cycles (interval 2)

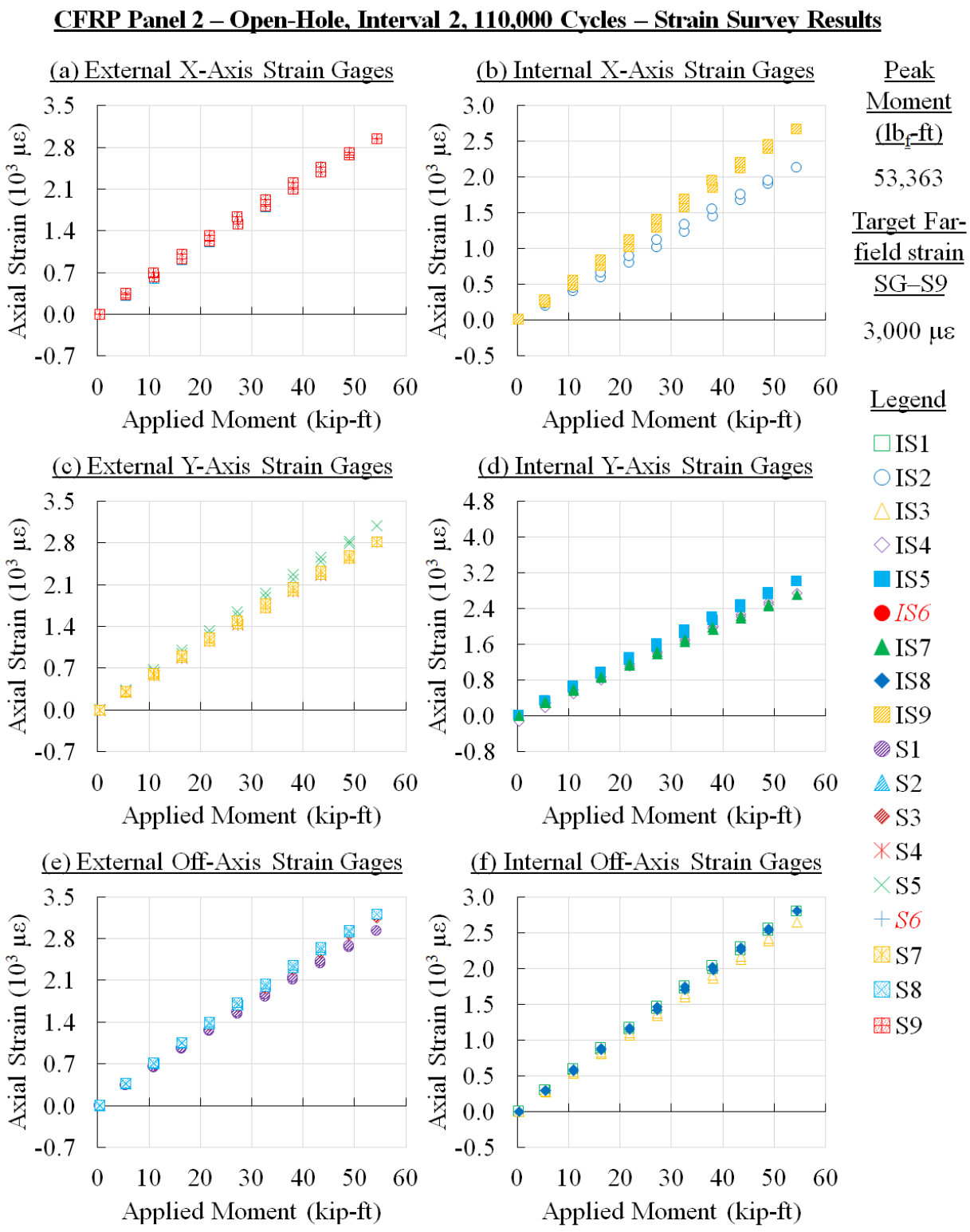

Figure 82. Panel 2 strain survey results at 110,000 cycles (interval 2)

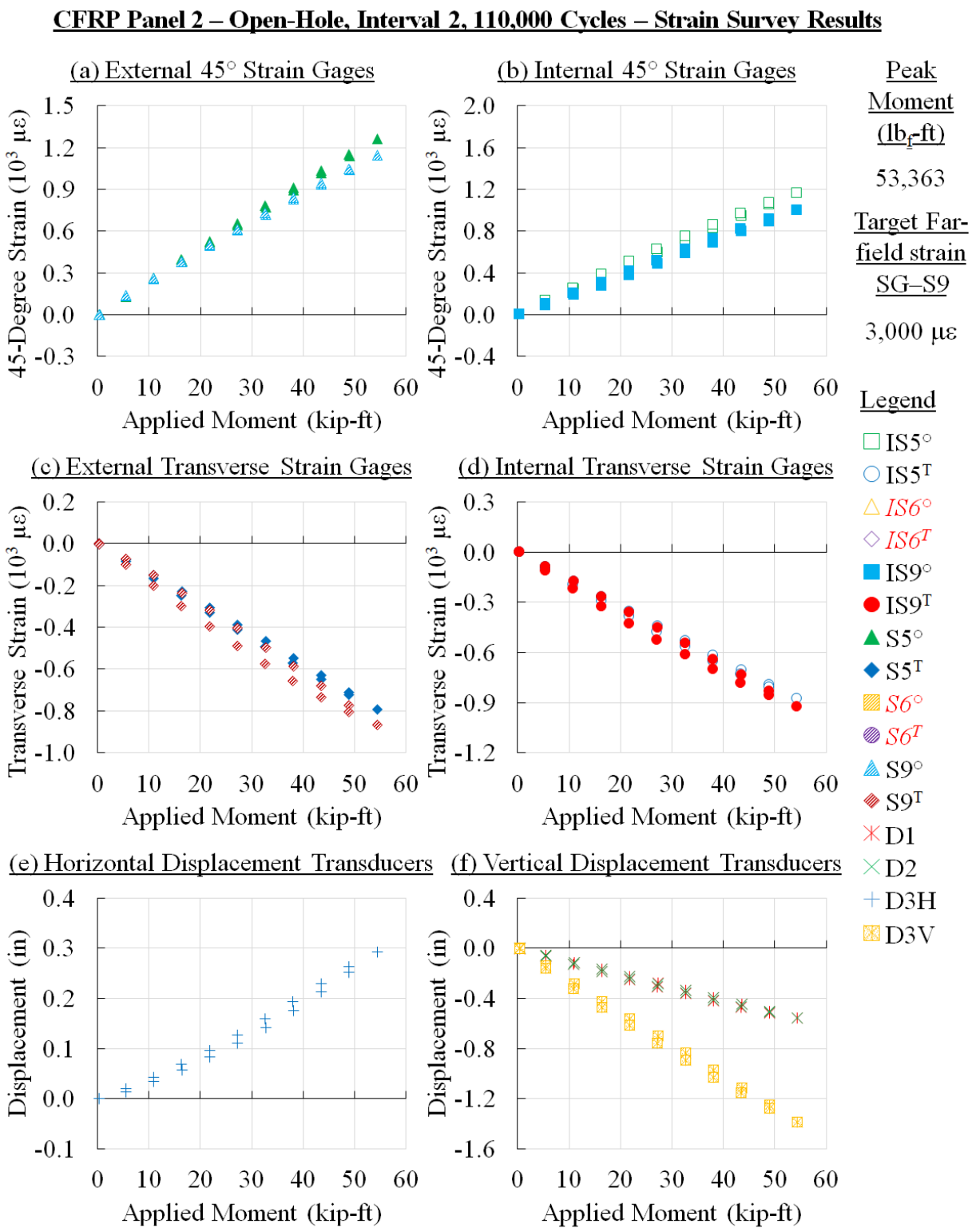

Figure 83. Panel 2 strain survey results at 110,000 cycles (interval 2)

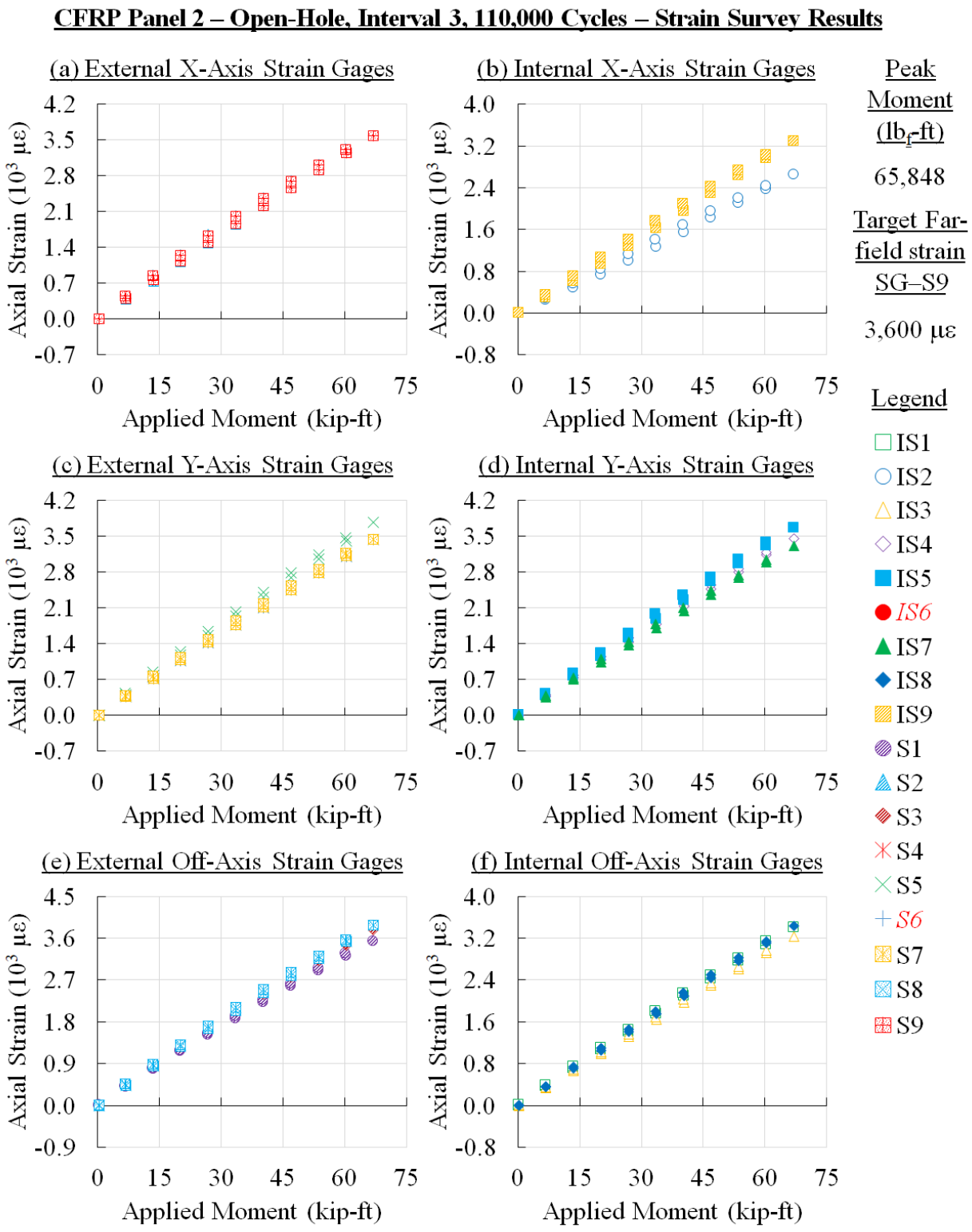

Figure 84. Panel 2 strain survey results at 110,000 cycles (interval 3)

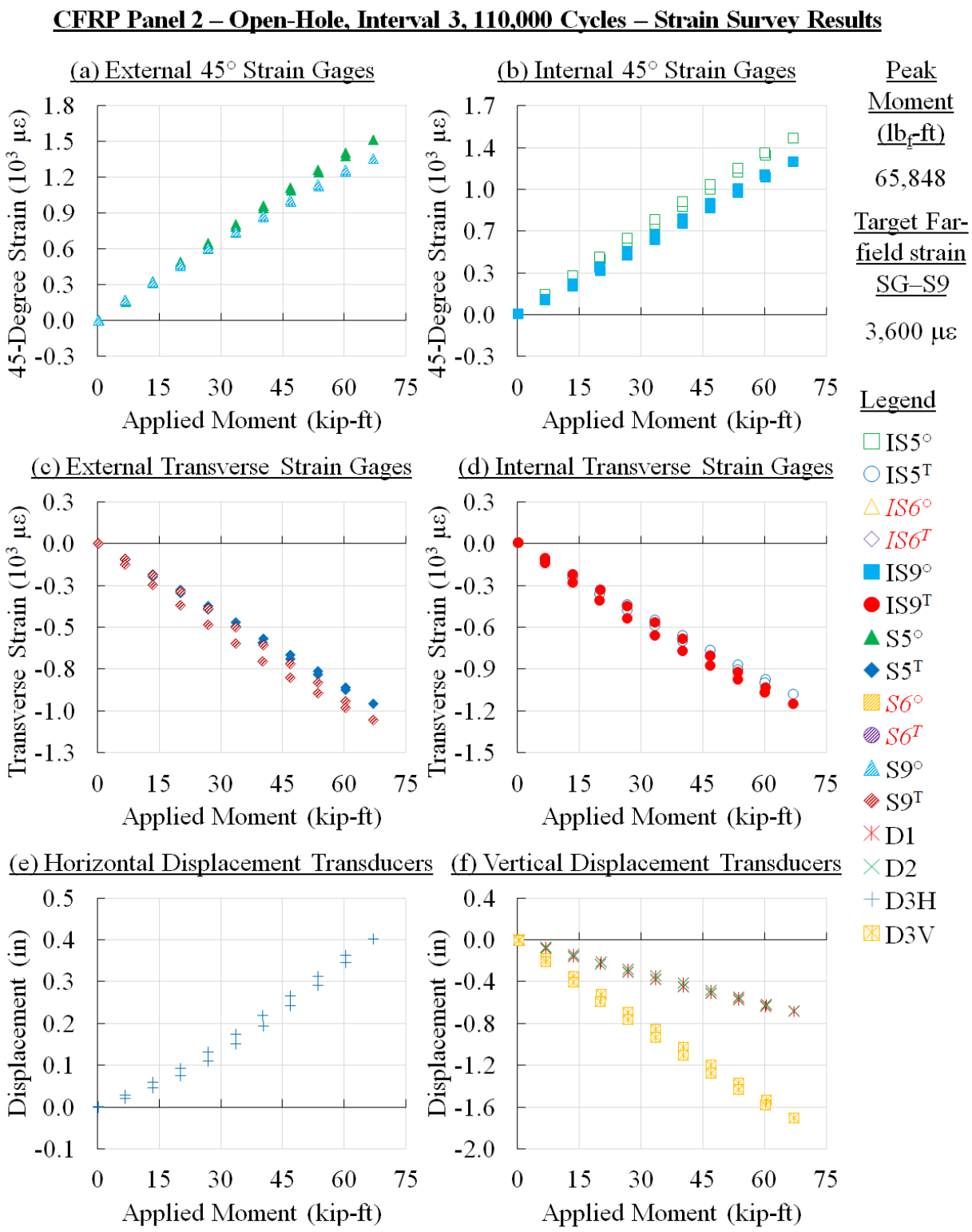

Figure 85. Panel 2 strain survey results at 110,000 cycles (interval 3)

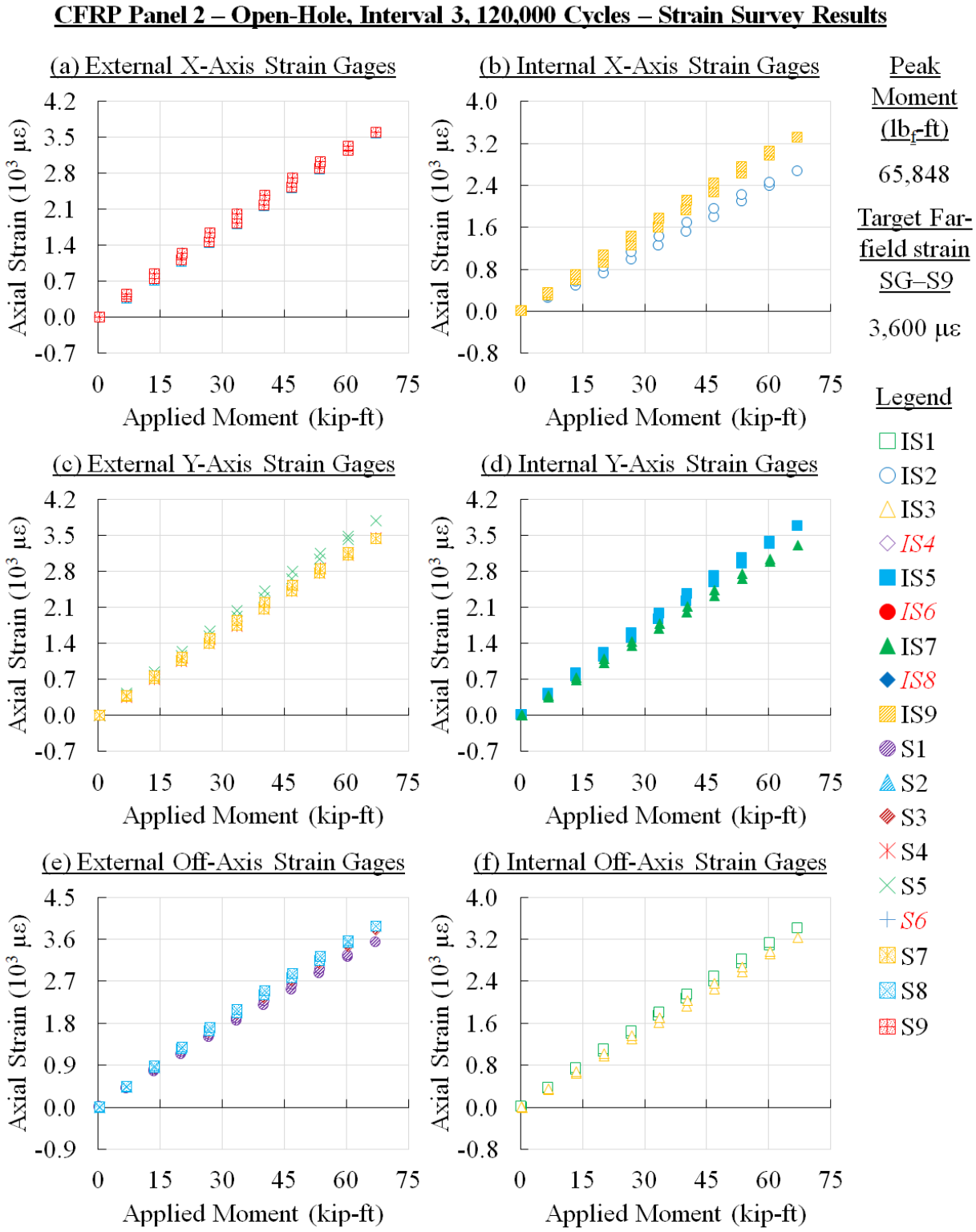

Figure 86. Panel 2 strain survey results at 120,000 cycles (interval 3)

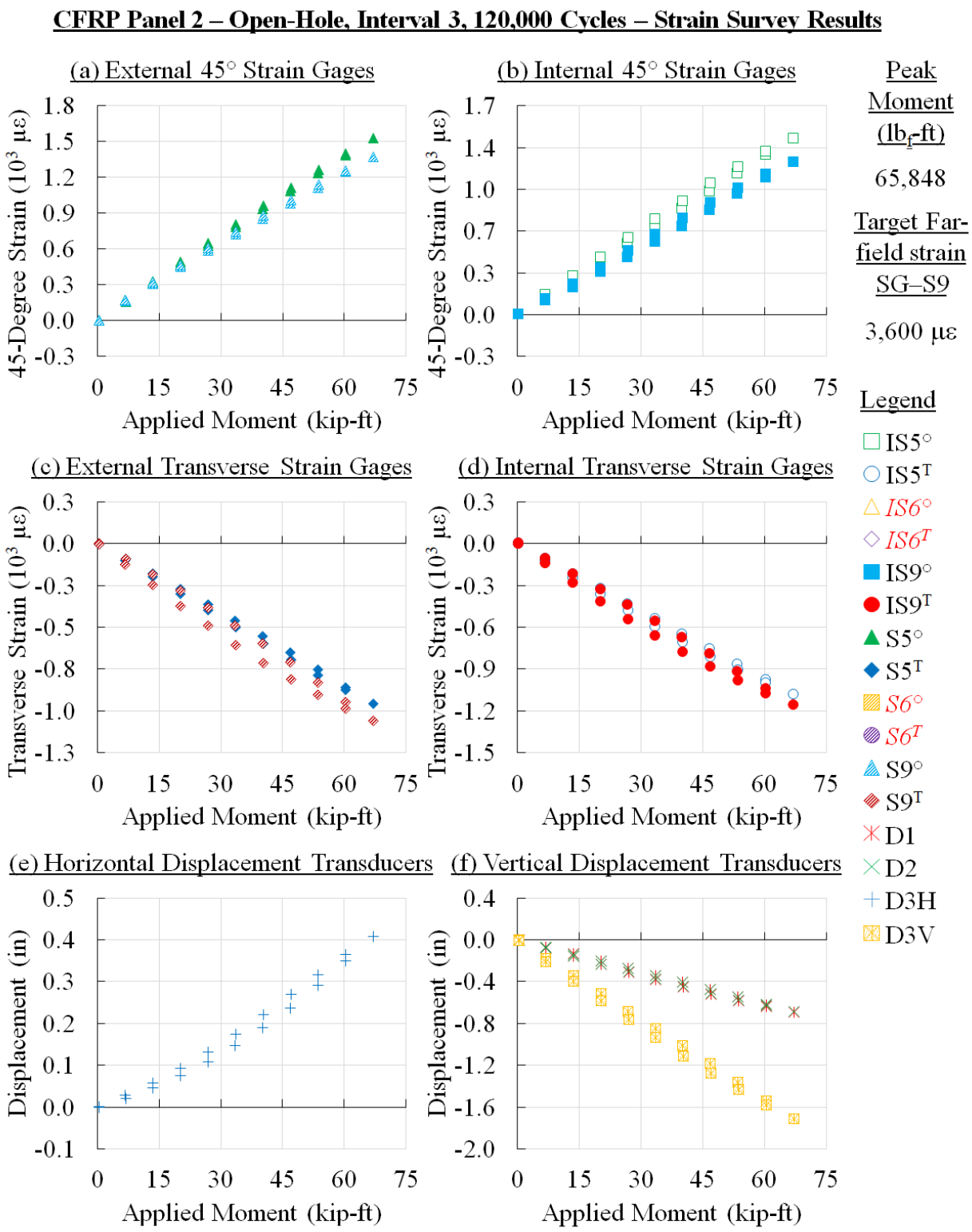

Figure 87. Panel 2 strain survey results at 120,000 cycles (interval 3)

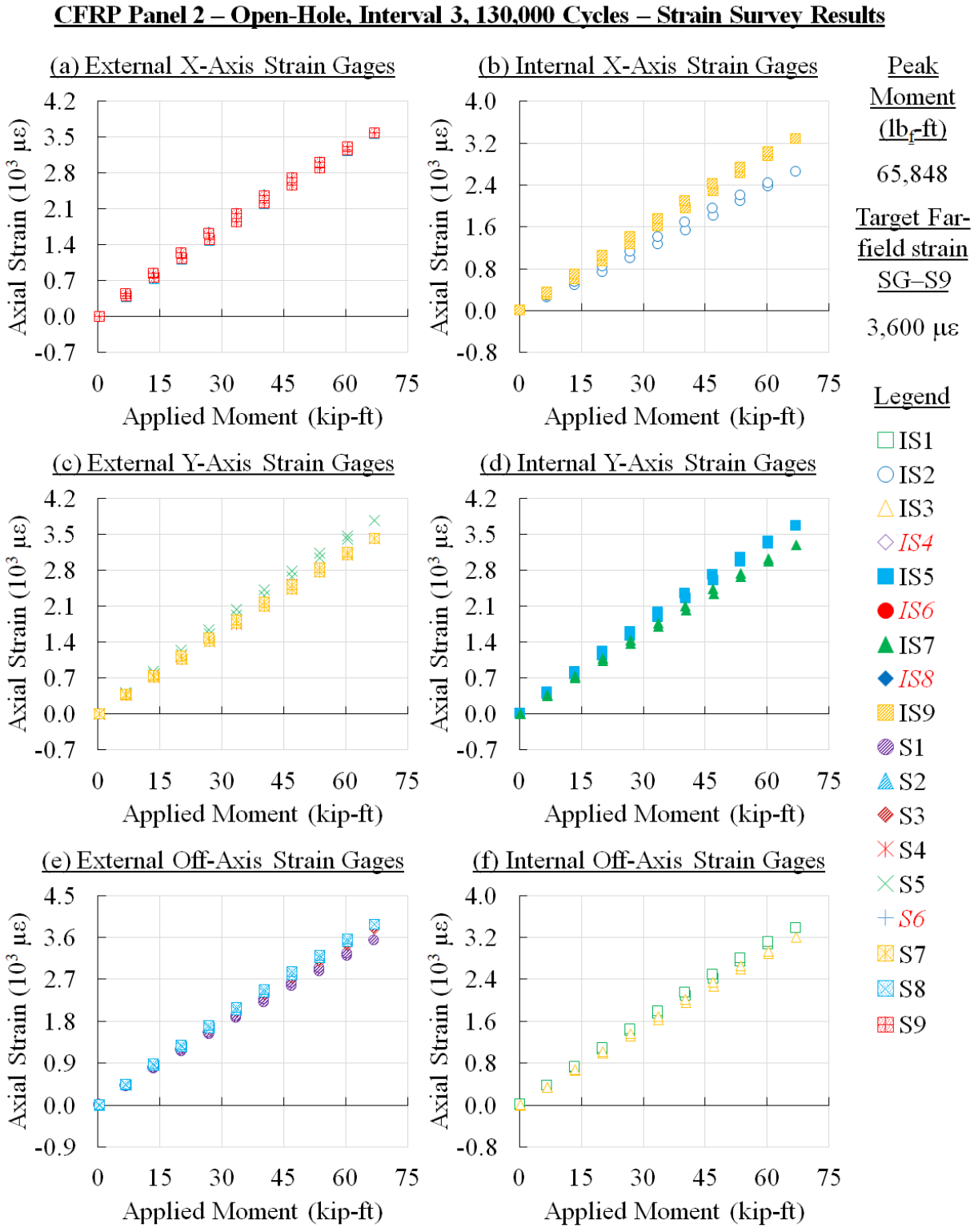

Figure 88. Panel 2 strain survey results at 130,000 cycles (interval 3)

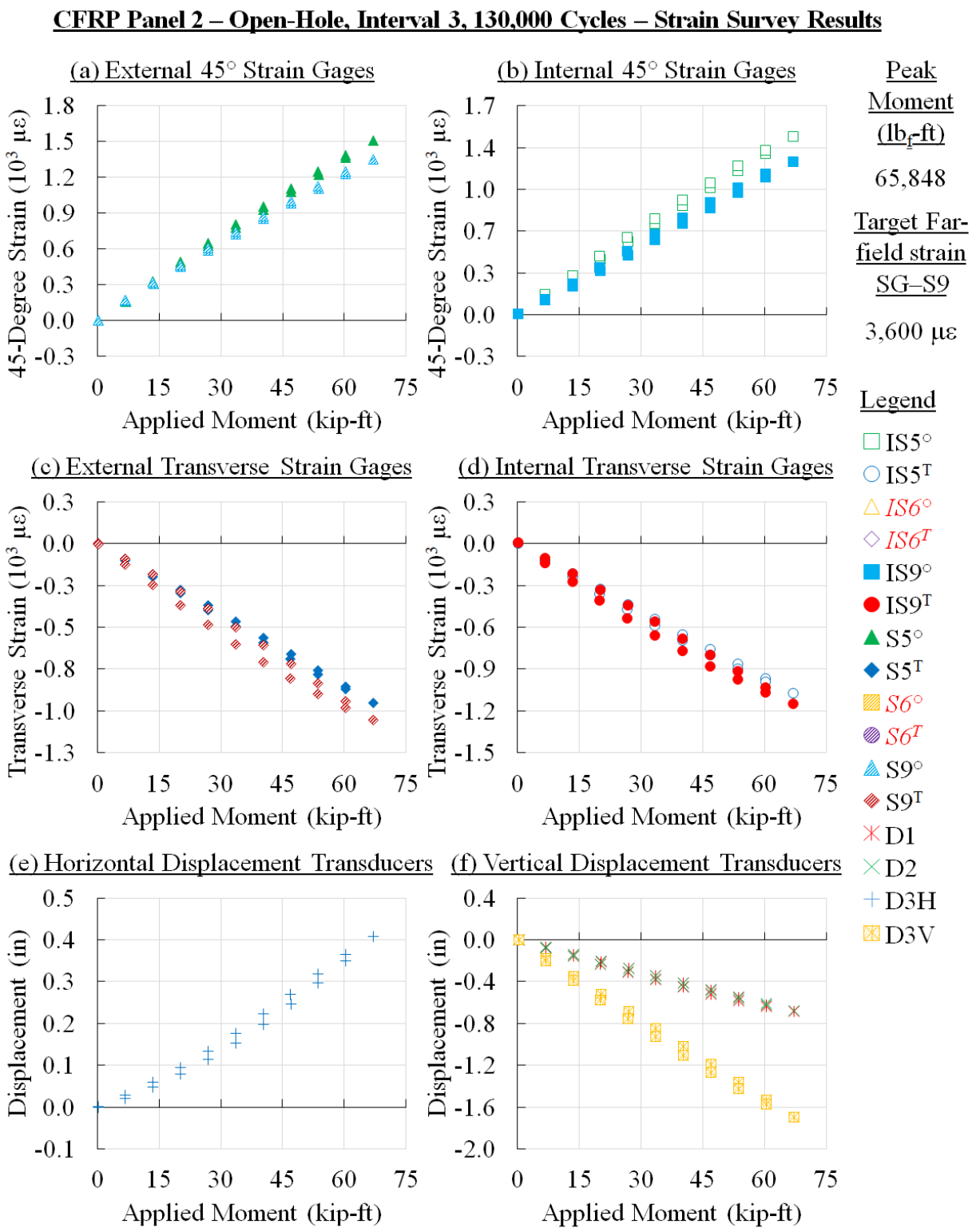

Figure 89. Panel 2 strain survey results at 130,000 cycles (interval 3)

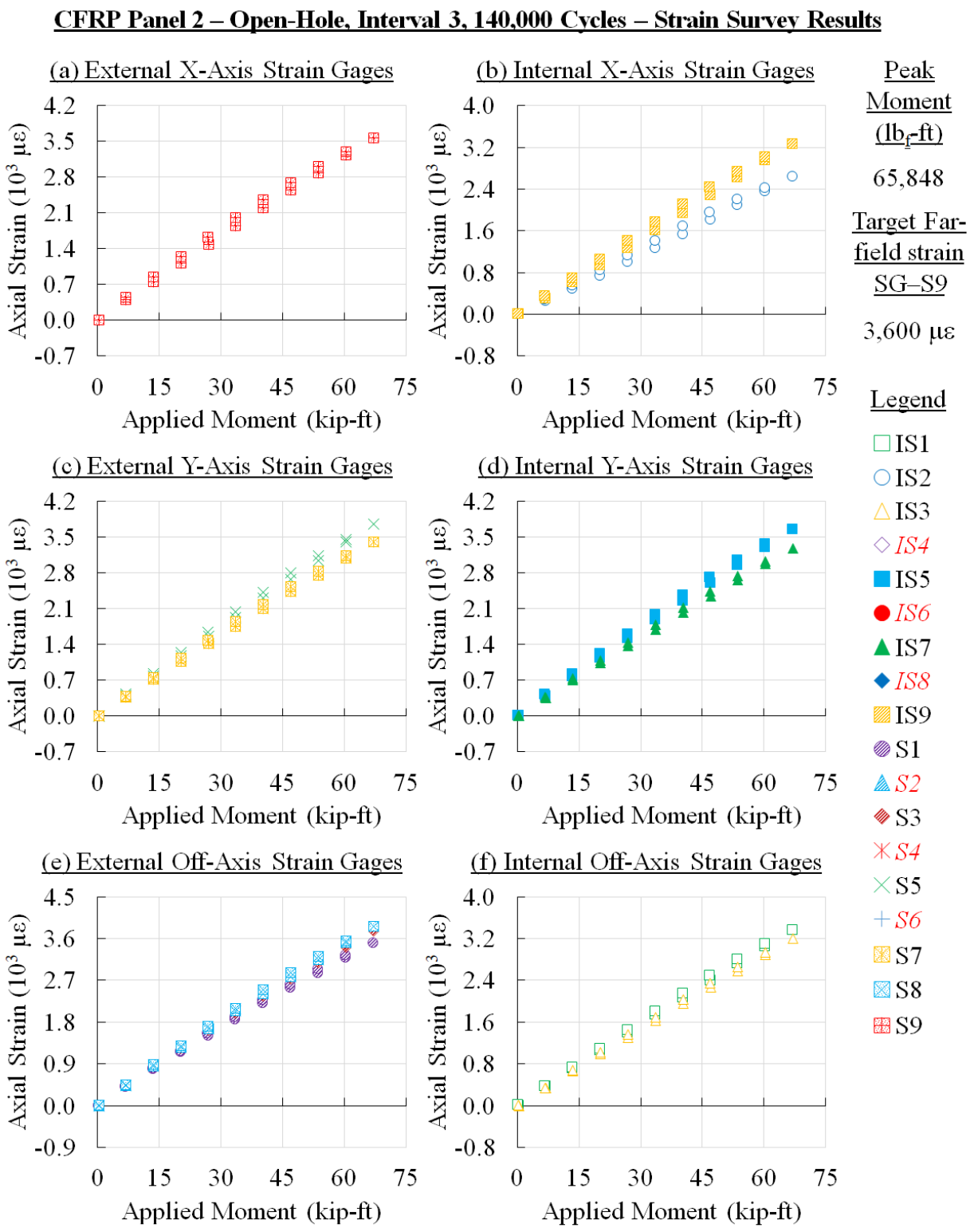

Figure 90. Panel 2 strain survey results at 140,000 cycles (interval 3)

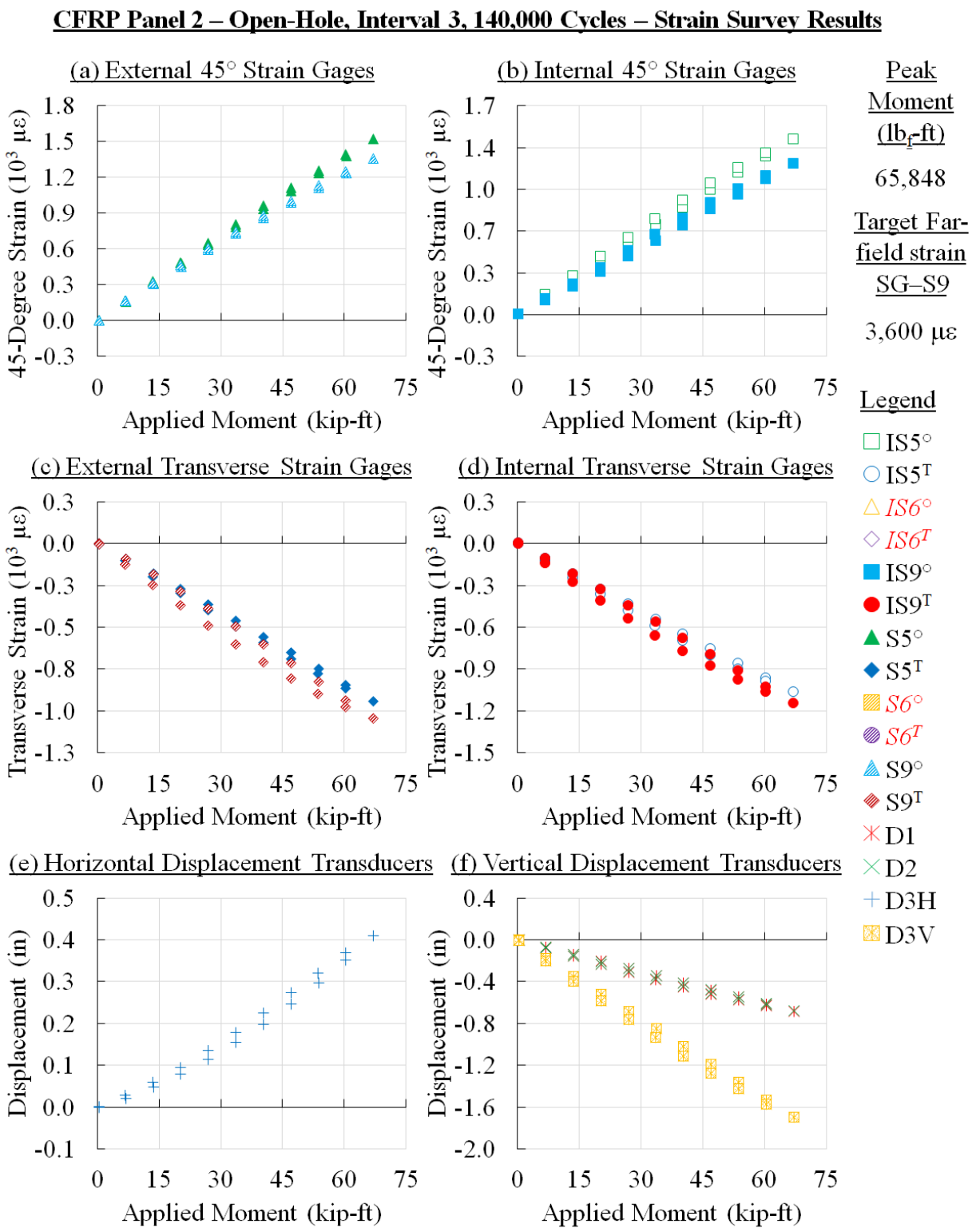

Figure 91. Panel 2 strain survey results at 140,000 cycles (interval 3)

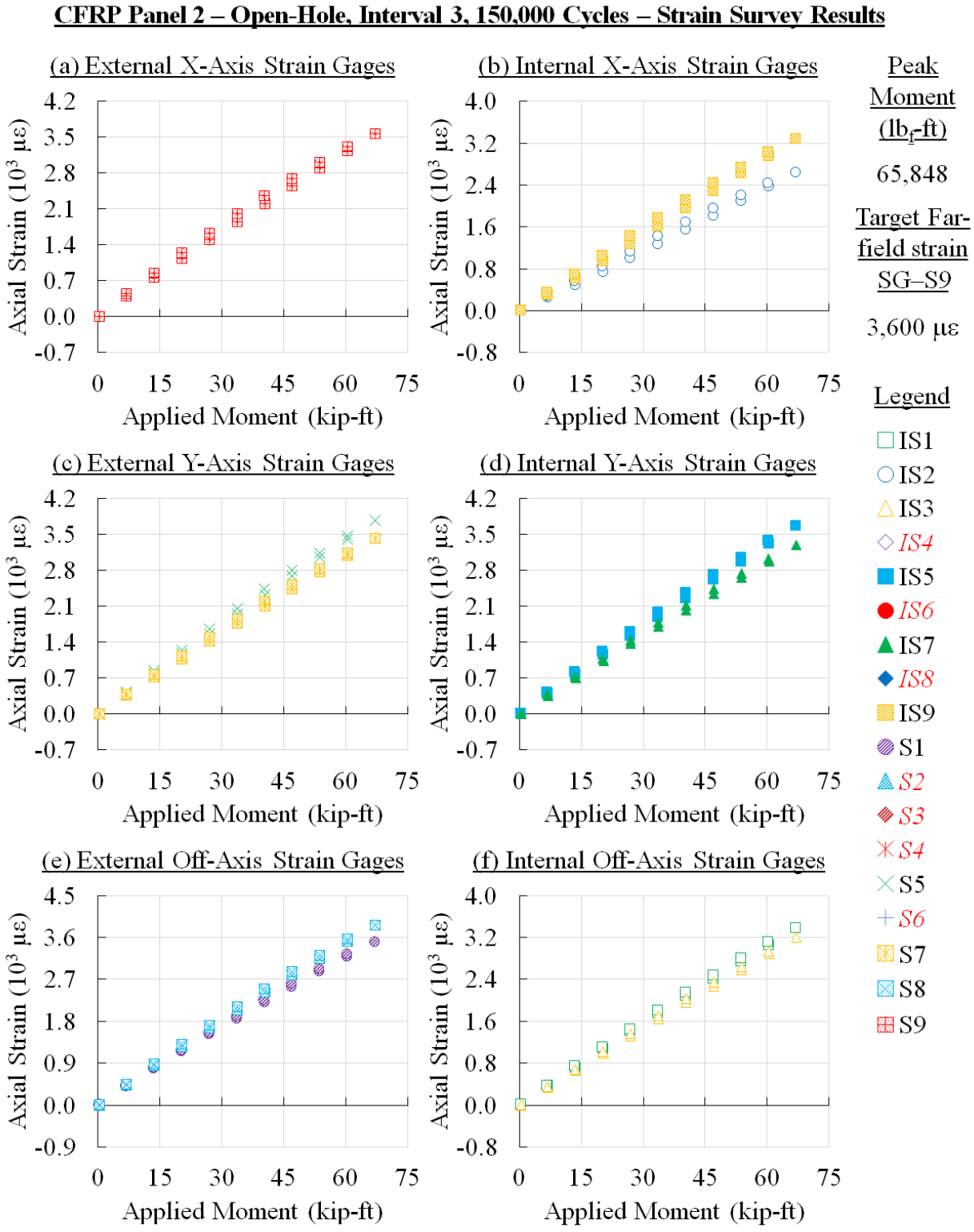

Figure 92. Panel 2 strain survey results at 150,000 cycles (interval 3)

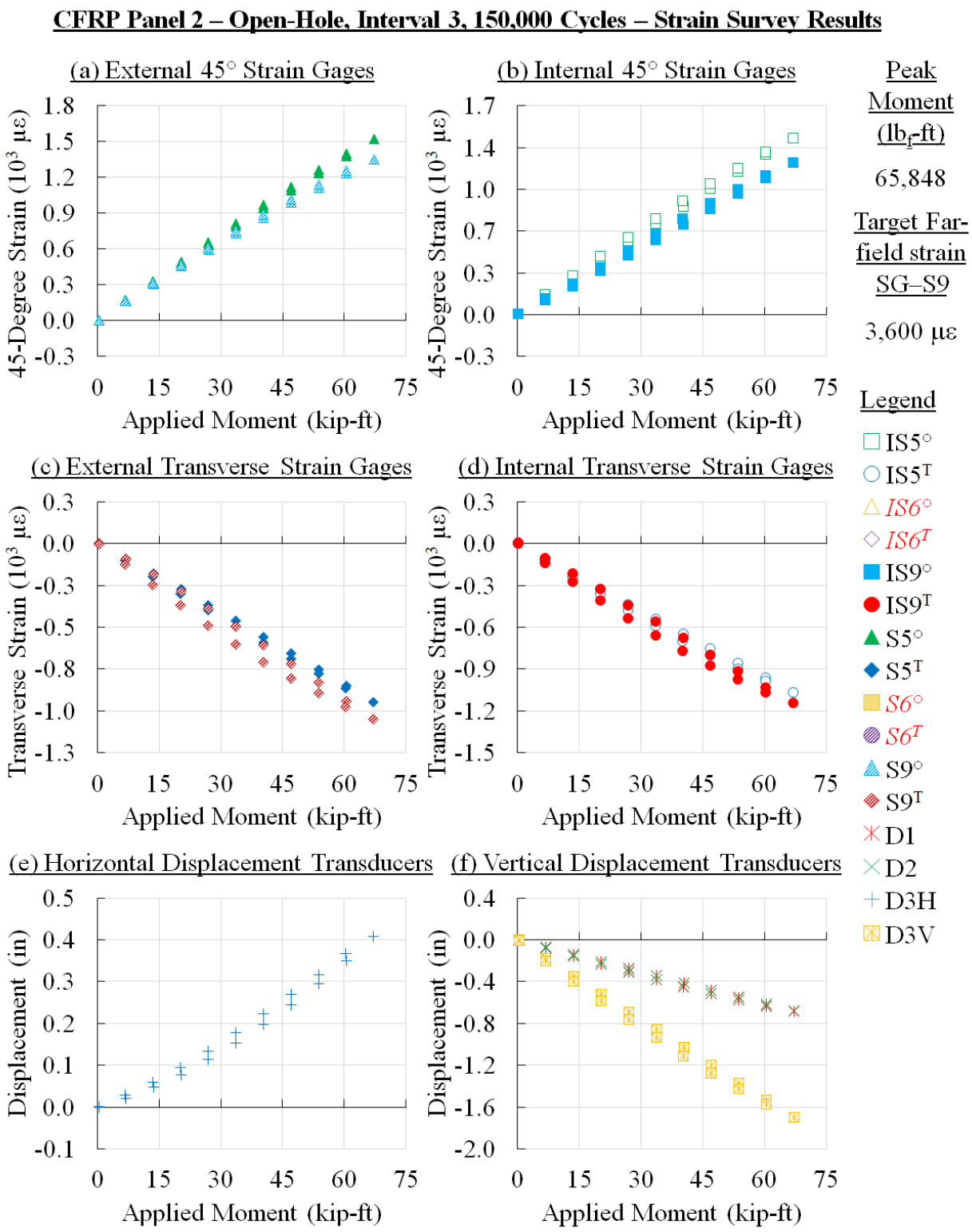

Figure 93. Panel 2 strain survey results at 150,000 cycles (interval 3)

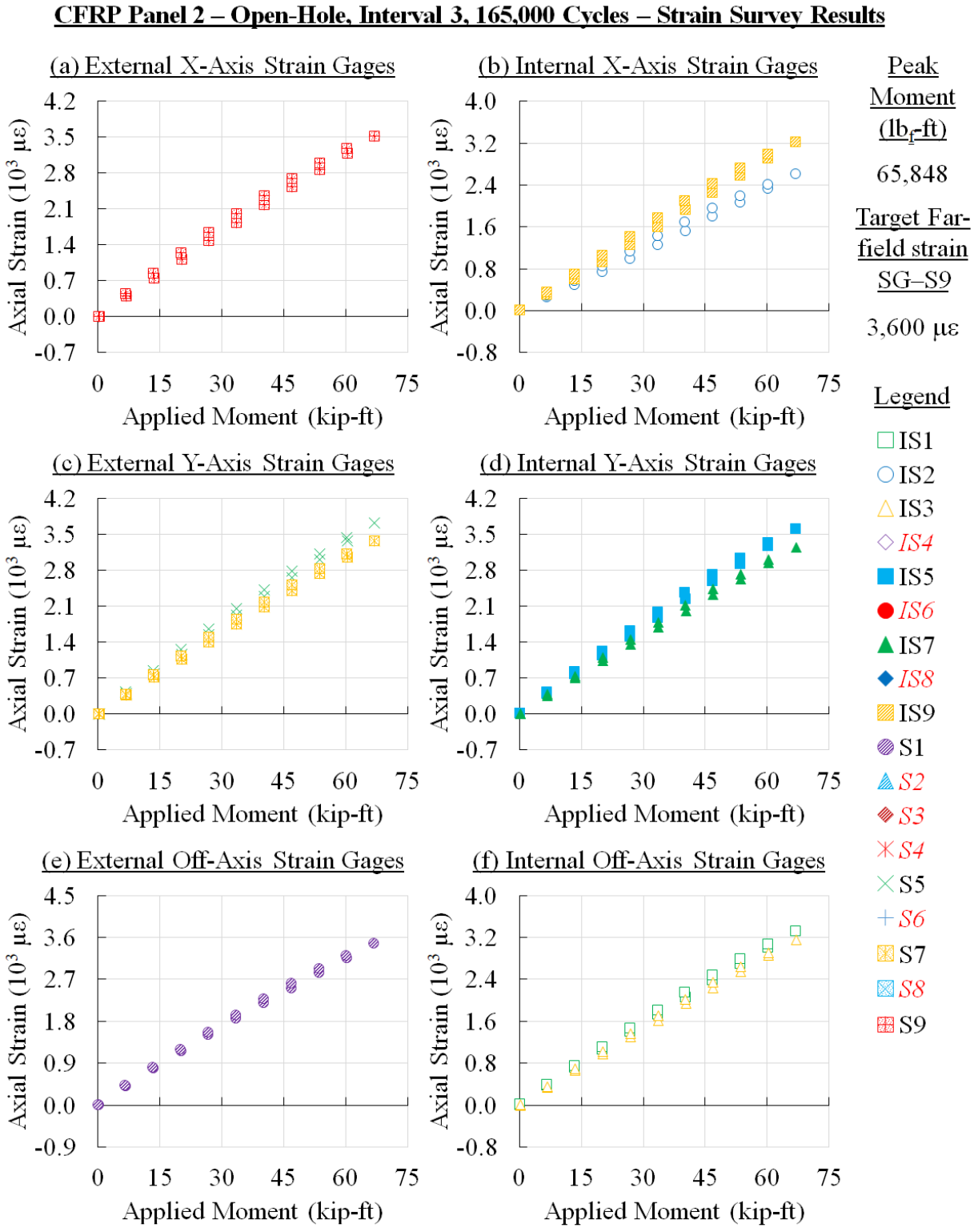

Figure 94. Panel 2 strain survey results at 165,000 cycles (interval 3)

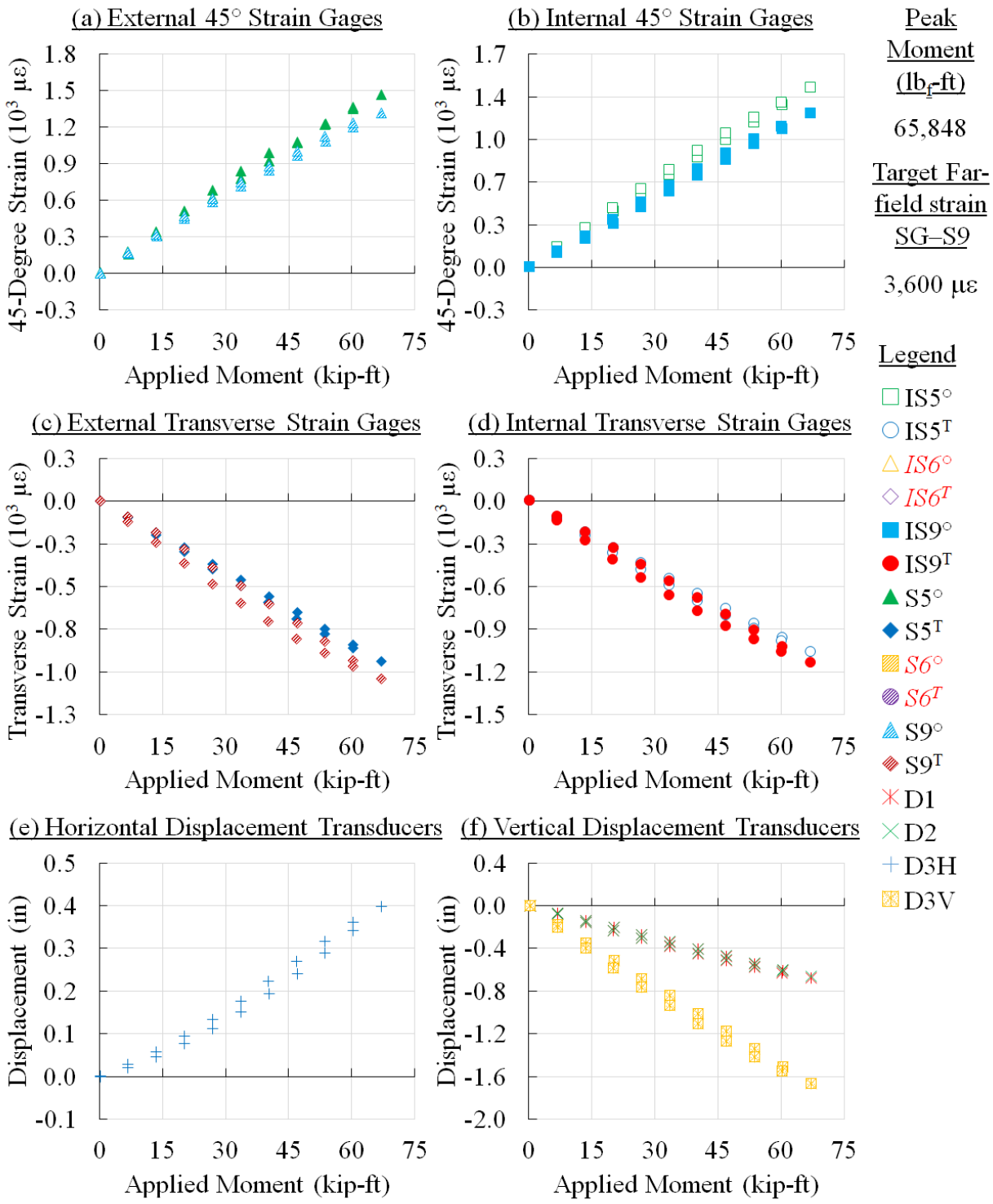

Figure 95. Panel 2 strain survey results at 165,000 cycles (interval 3)

C Strain and displacement during residual strength test

This appendix provides strain gages results captured during residual strength loading of the open-hole panel specimen. The open-hole panel was subjected to five successive quasi-static loading increments, the last of which was to load the panel up to failure, see Figure 96. These load increments were defined based on the predicted critical load (PCL) level, which was considered as 100% load level. Load increments 1 to 5 were 70%, 80%, 90%, 100% of PCL and final failure. Figure 96 – Figure 132 shows the applied loads, displacement, and strain results at each load increment of the residual strength test of panel 2. Load increment 2 was repeated as in the first attempt, the loads were not able to reach the target level of 80% due to the set system load limits and thus the test was terminated, see Figure 103 – Figure 108. The limits were reset and the second load increment (80%) was repeated. In addition, some data points during unloading are missing in load increment 1 (70%) because the hydraulic system stopped due to high gains setting, see Figure 97 – Figure 102. In all the figures in this appendix, *BM* stands for bending moment and the nomenclature used for strain gages and displacement sensors are the same as provided in Figure 34 and Figure 35 of appendix B, respectively.

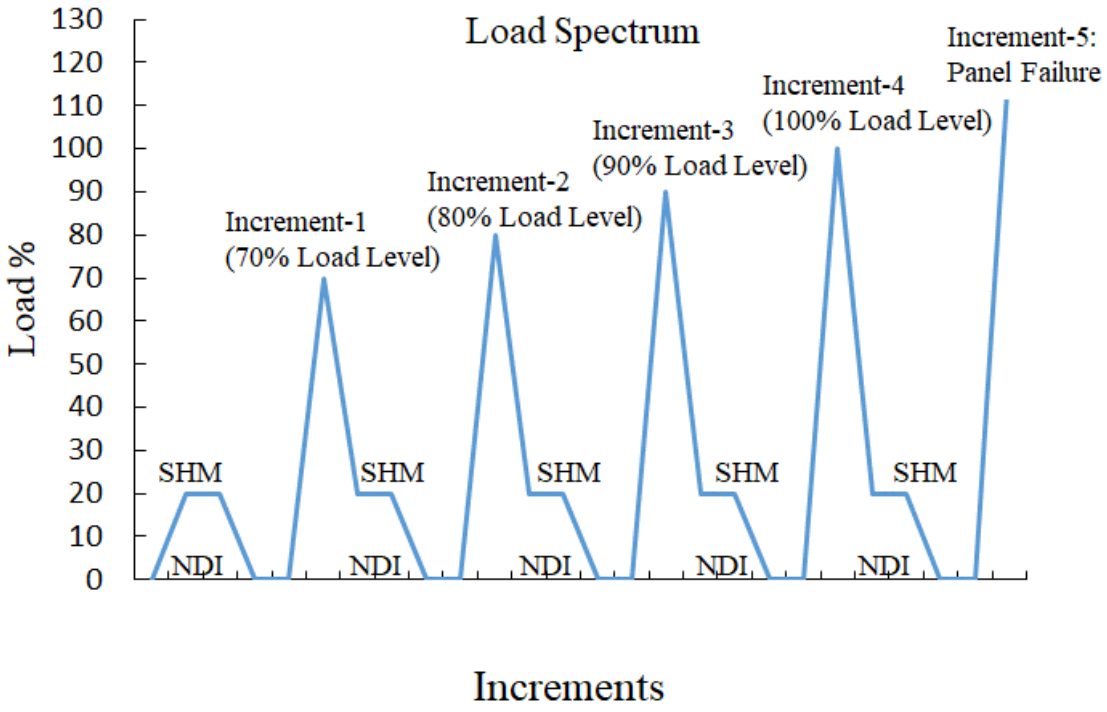

Figure 96. Residual strength load schematic for panel 2

CFRP Panel 2 – Open-Hole – Results of Residual Strength Loading Increment # 1

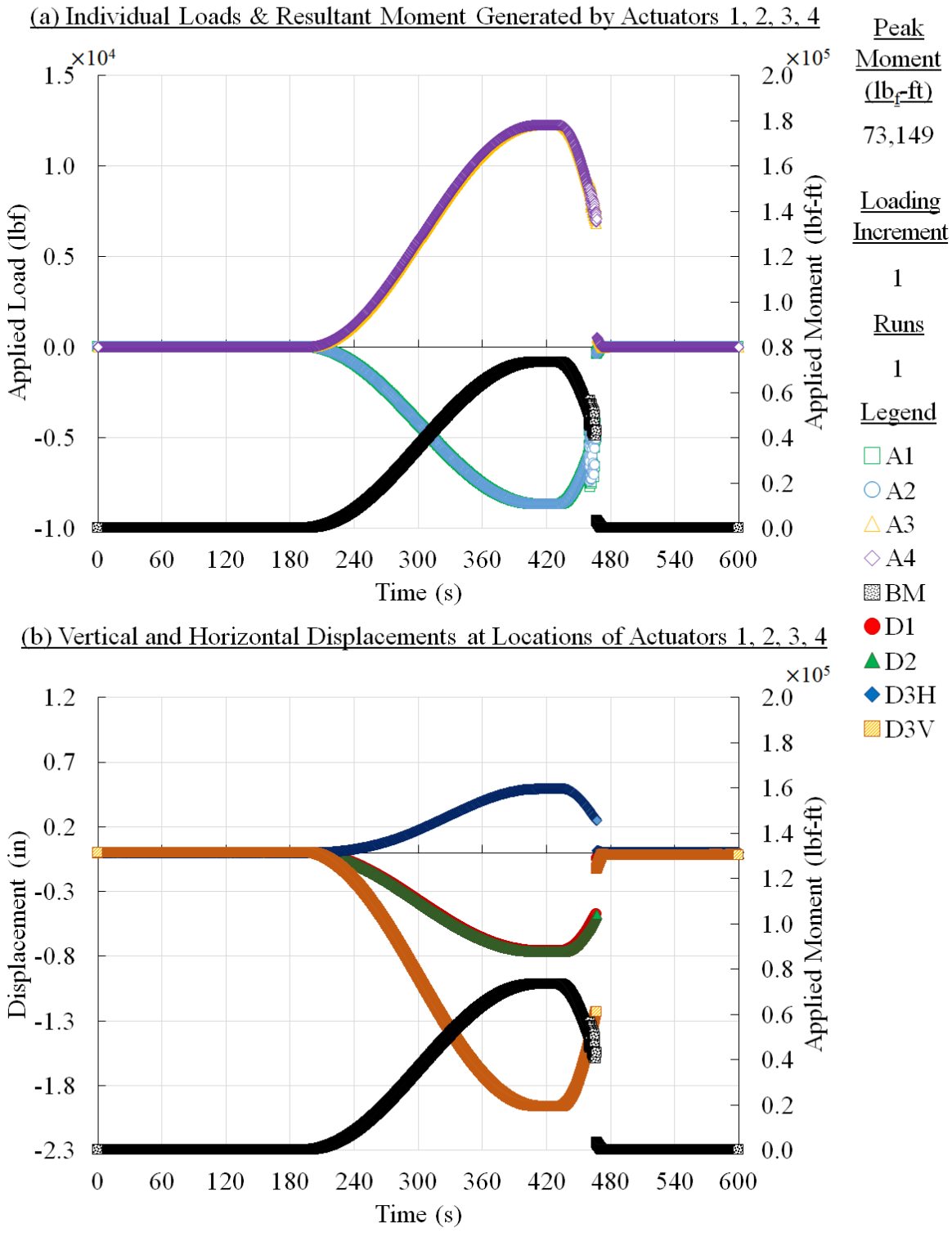

Figure 97. Panel 2 residual strength test results, loading increment 1 (70% load level)

CFRP Panel 2 – Open-Hole – Results of Residual Strength Loading Increment # 1

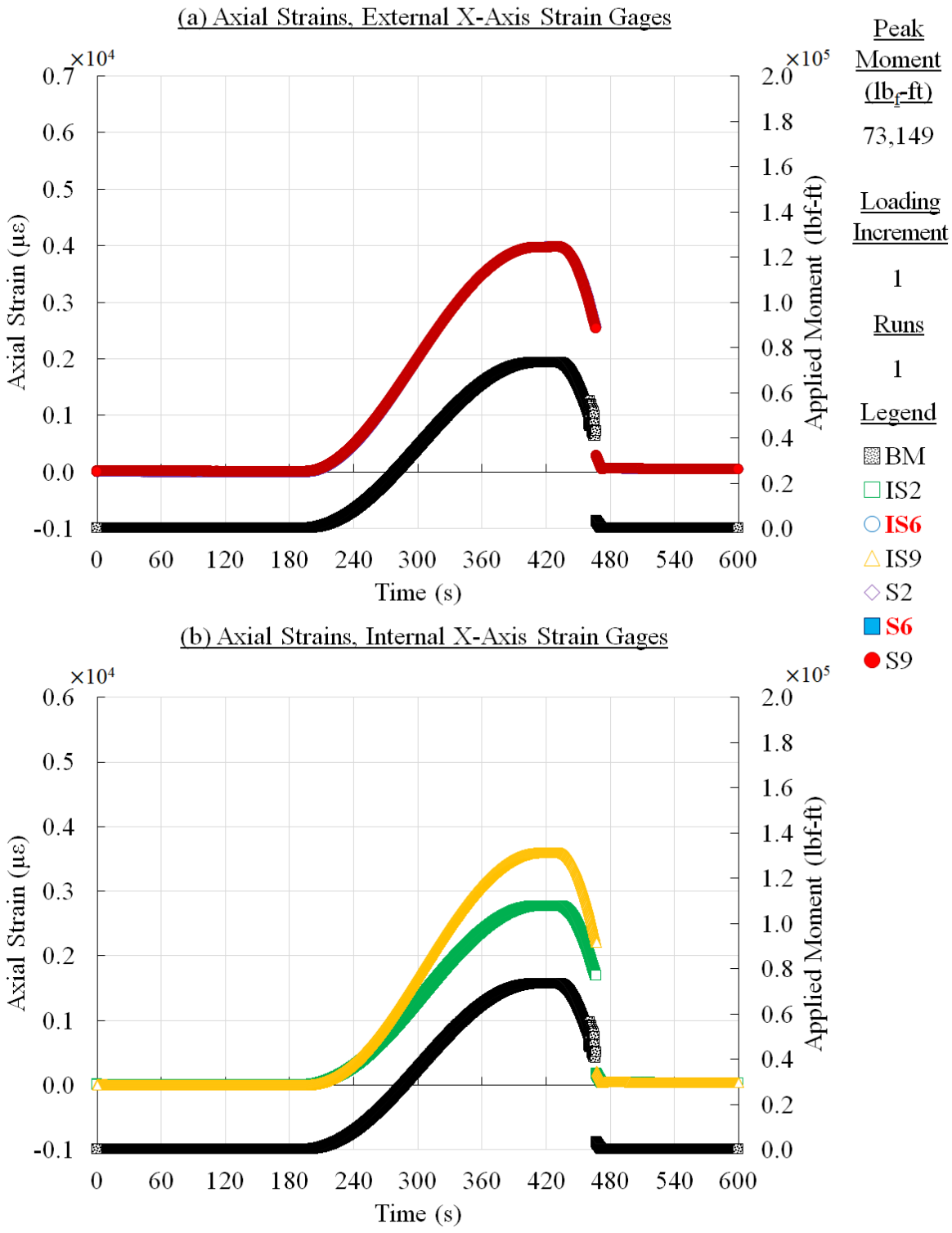

Figure 98. Panel 2 residual strength test results, loading increment 1 (70% load level)

CFRP Panel 2 – Open-Hole – Results of Residual Strength Loading Increment # 1

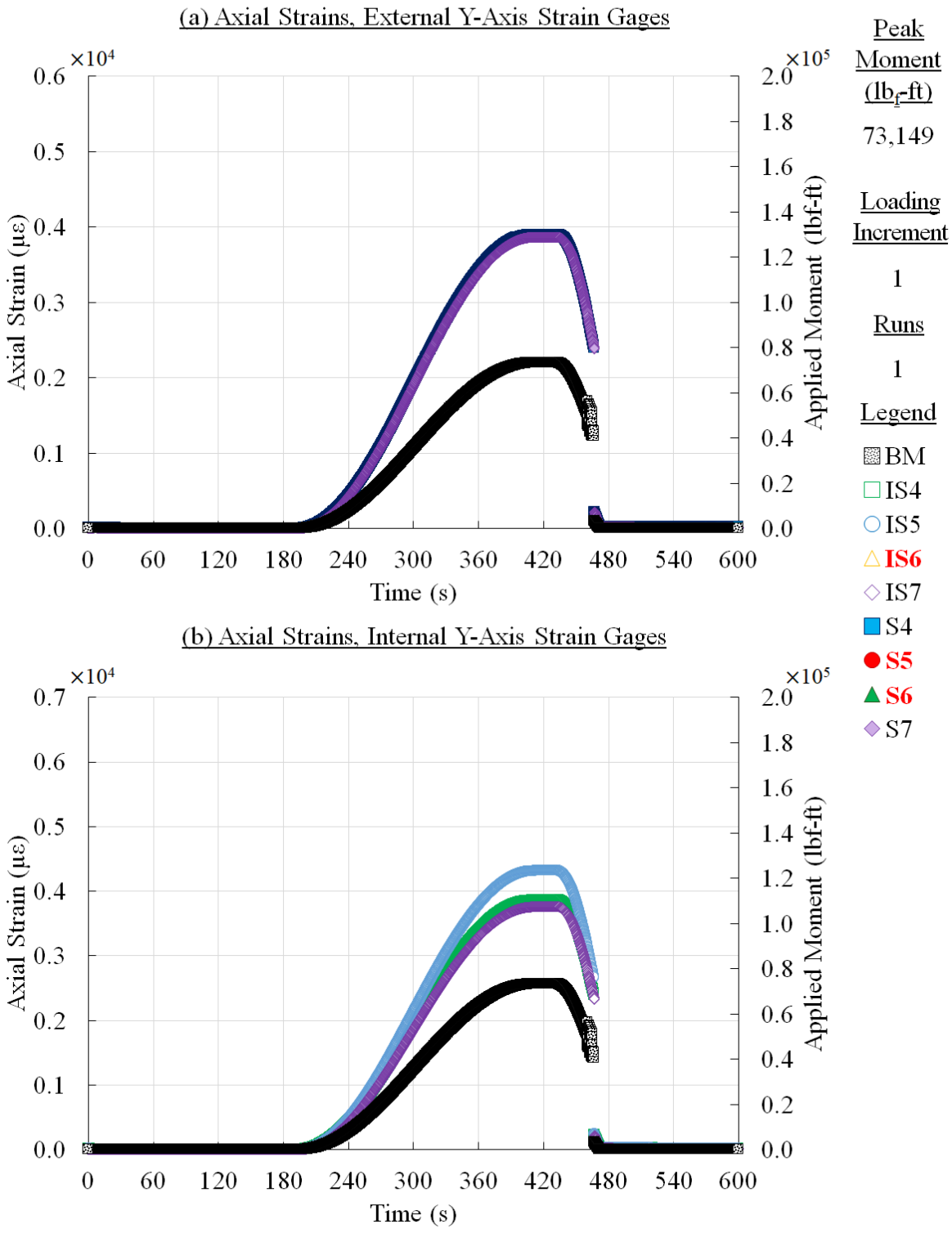

Figure 99. Panel 2 residual strength test results, loading increment 1 (70% load level)

CFRP Panel 2 – Open-Hole – Results of Residual Strength Loading Increment # 1

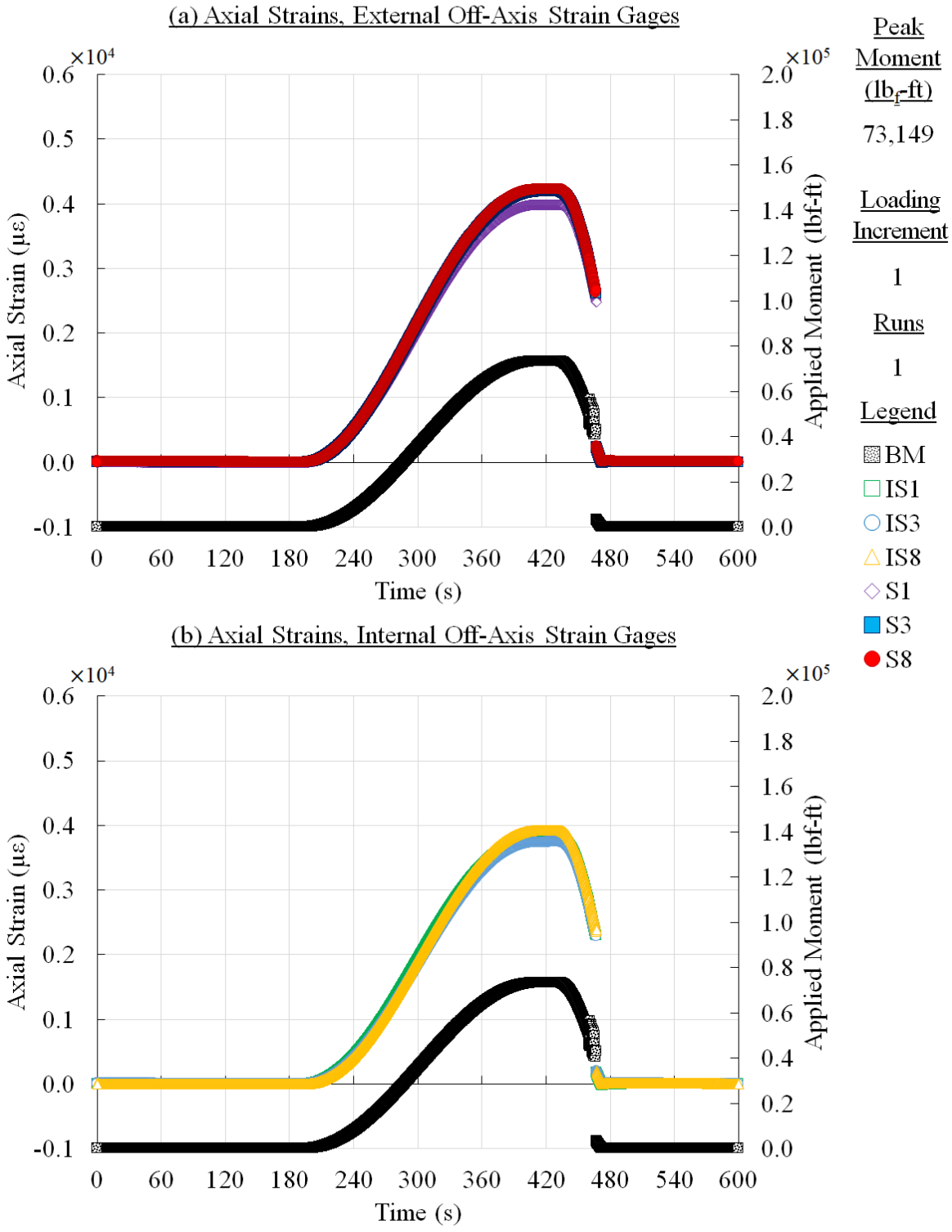

Figure 100. Panel 2 residual strength test results, loading increment 1 (70% load level)

CFRP Panel 2 – Open-Hole – Results of Residual Strength Loading Increment # 1

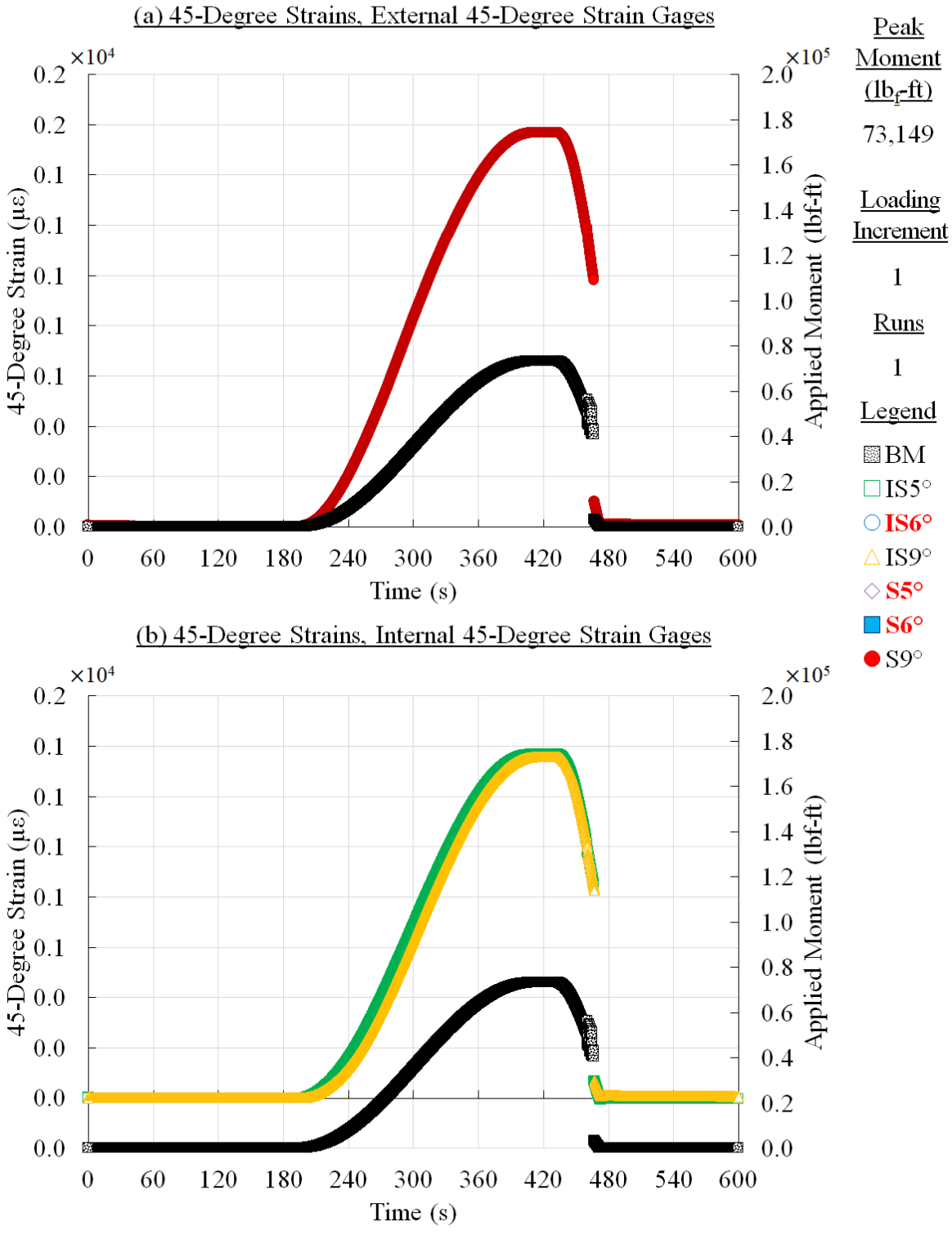

Figure 101. Panel 2 residual strength test results, loading increment 1 (70% load level)

CFRP Panel 2 – Open-Hole – Results of Residual Strength Loading Increment # 1

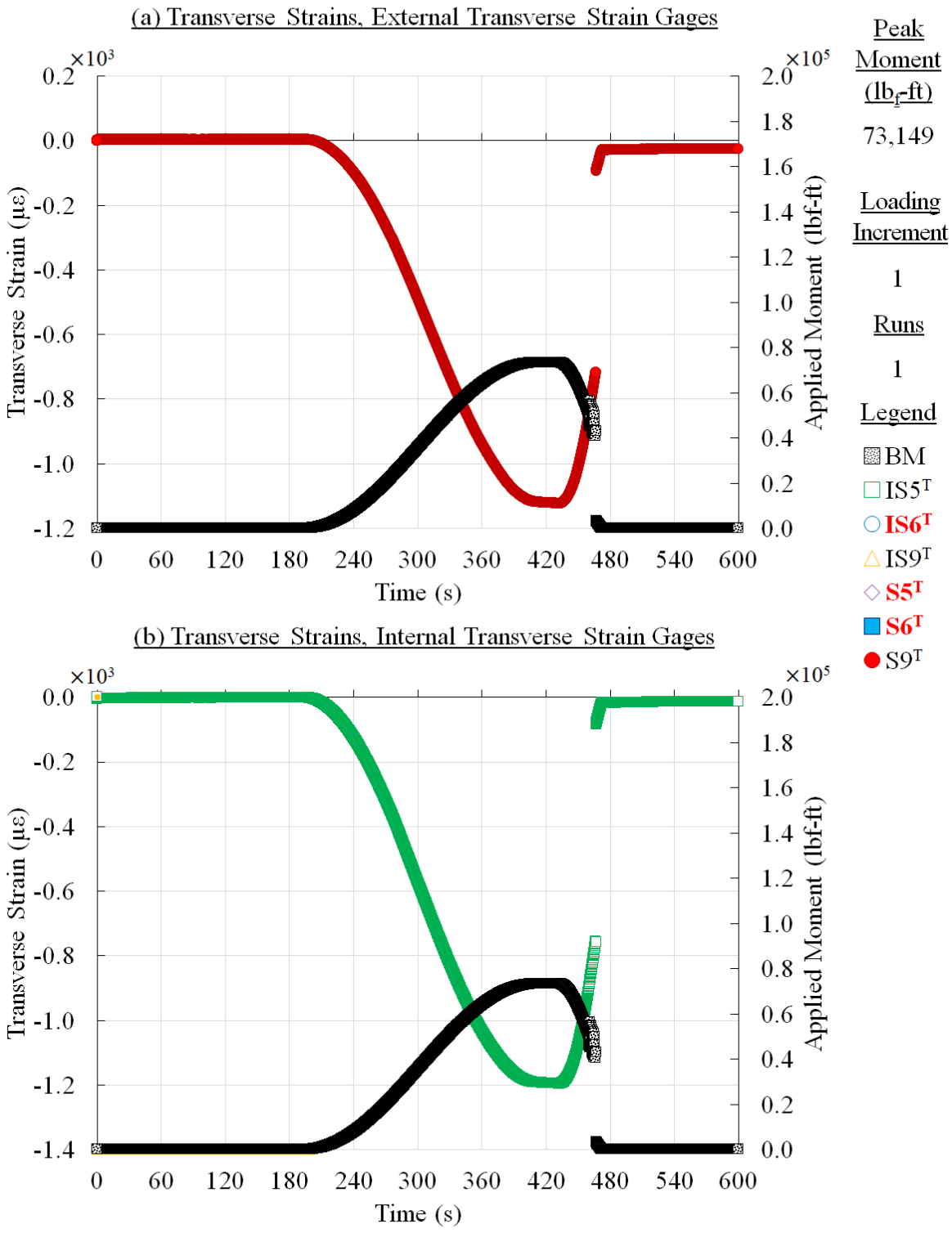

Figure 102. Panel 2 residual strength test results, loading increment 1 (70% load level)

CFRP Panel 2 – Open-Hole – Results of Residual Strength Loading Increment # 2

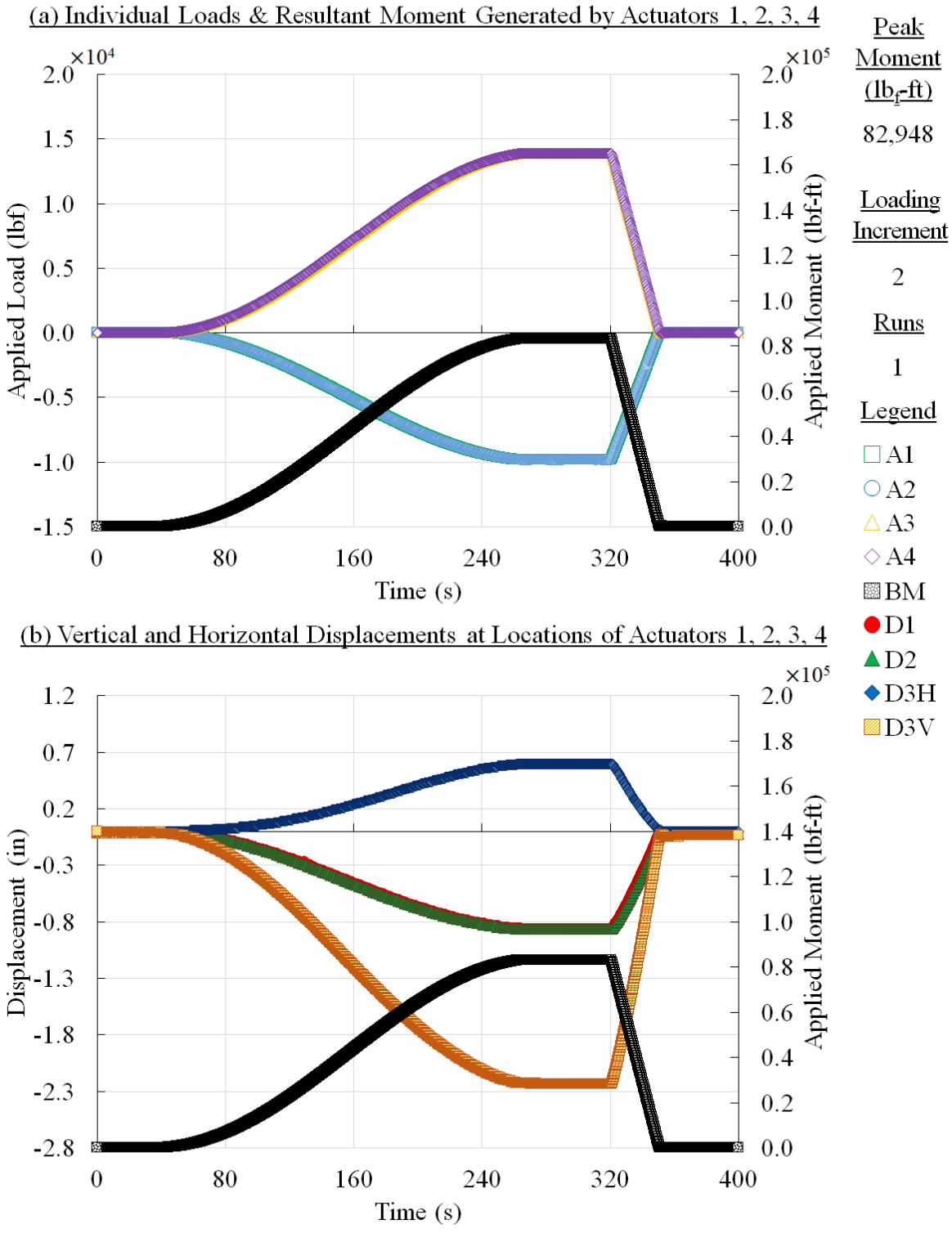

Figure 103. Panel 2 residual strength test results, loading increment 2 (80% load level, run 1)

CFRP Panel 2 – Open-Hole – Results of Residual Strength Loading Increment # 2

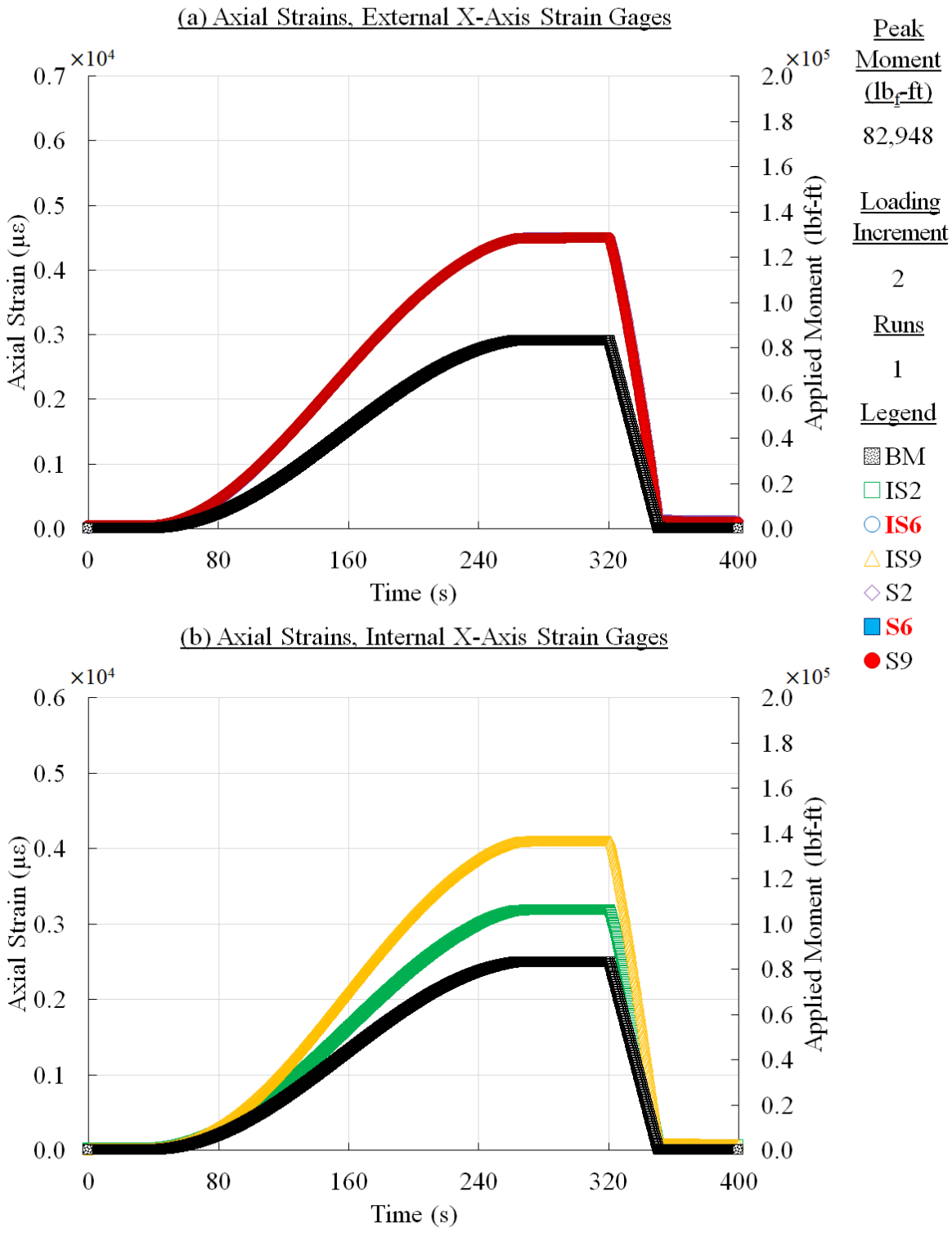

Figure 104. Panel 2 residual strength test results, loading increment 2 (80% load level, run 1)

CFRP Panel 2 – Open-Hole – Results of Residual Strength Loading Increment # 2

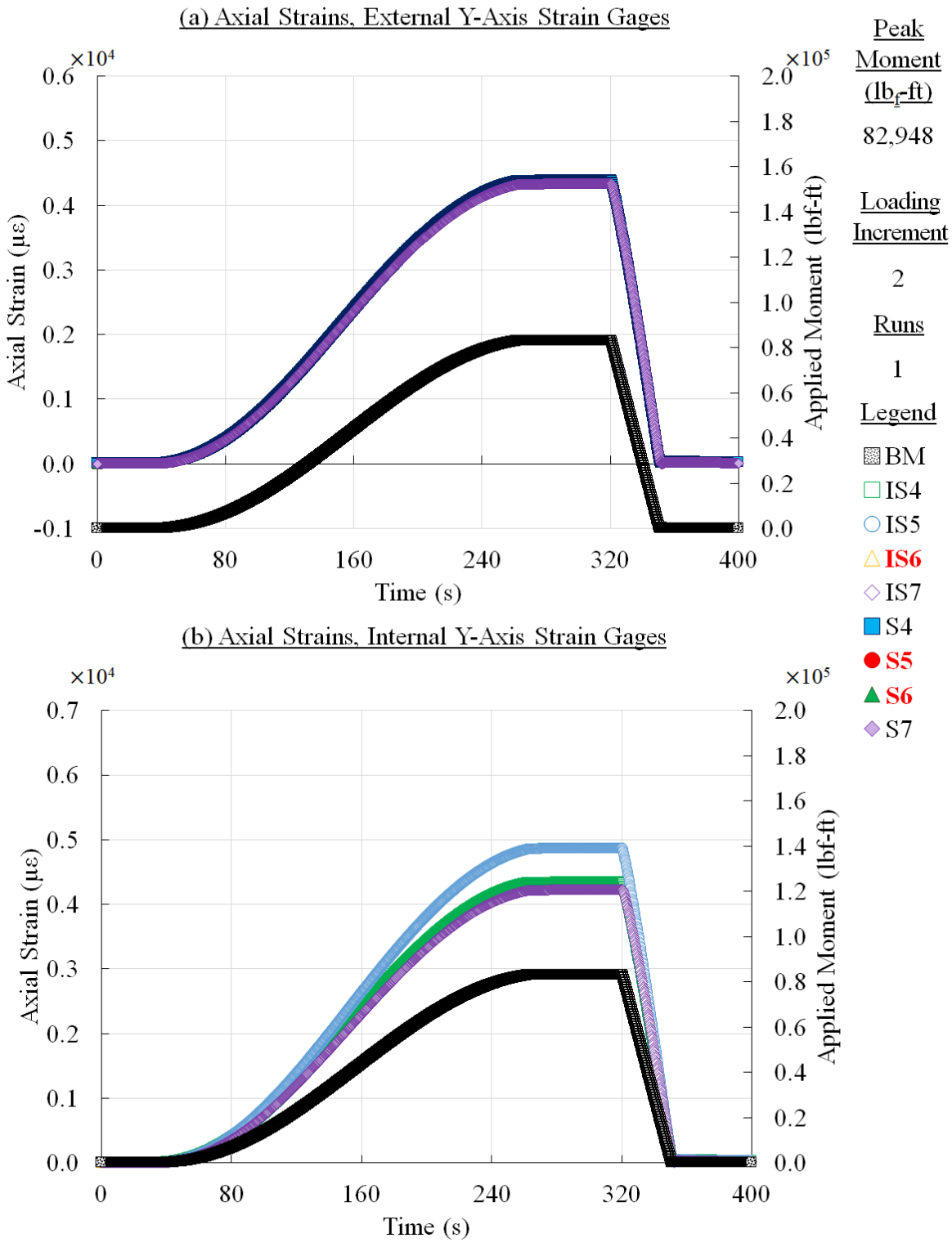

Figure 105. Panel 2 residual strength test results, loading increment 2 (80% load, run 1)

CFRP Panel 2 – Open-Hole – Results of Residual Strength Loading Increment # 2

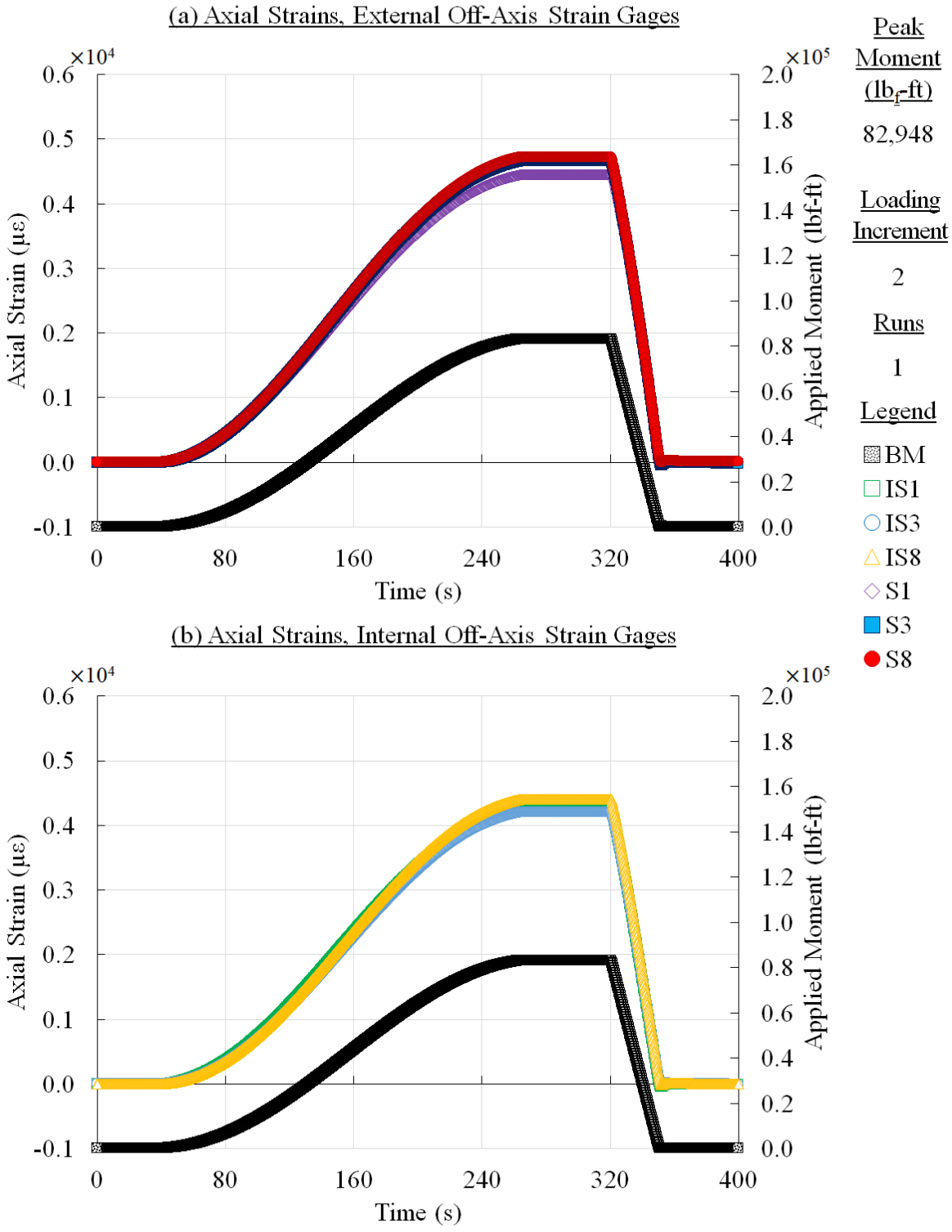

Figure 106. Panel 2 residual strength test results, loading increment 2 (80% load, run 1)

CFRP Panel 2 – Open-Hole – Results of Residual Strength Loading Increment # 2

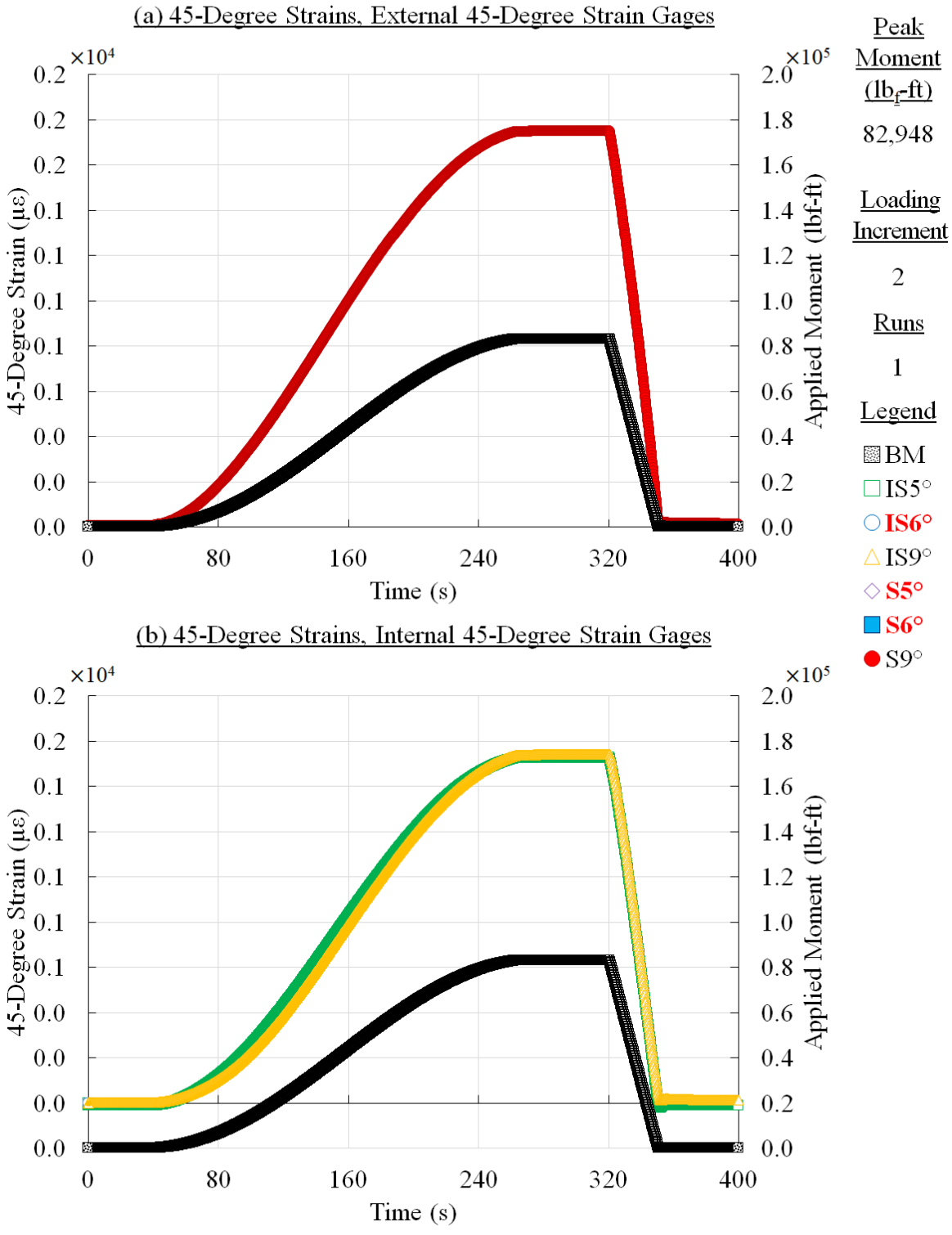

Figure 107. Panel 2 residual strength test results, loading increment 2 (80% load, run 1)

CFRP Panel 2 – Open-Hole – Results of Residual Strength Loading Increment # 2

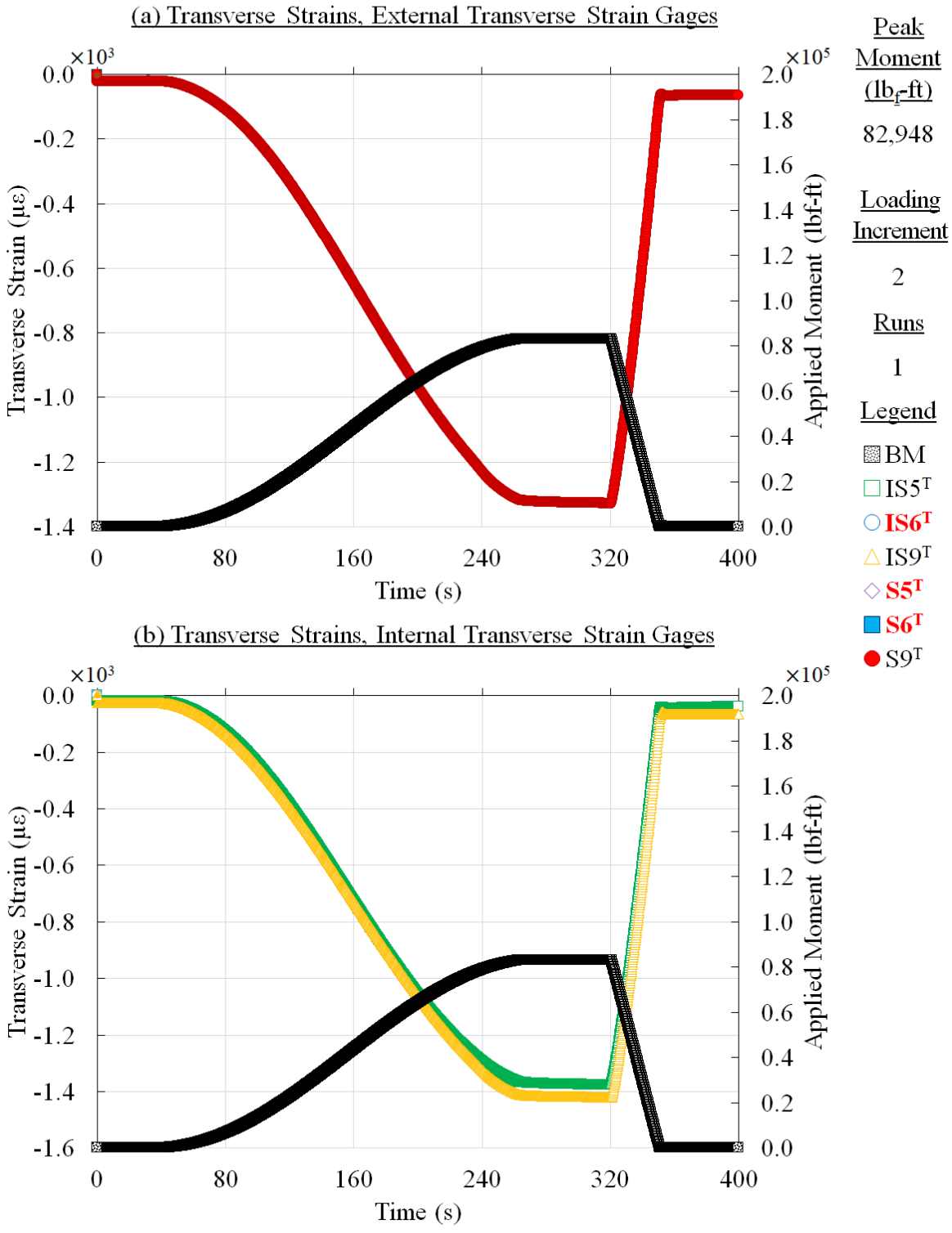

Figure 108. Panel 2 residual strength test results, loading increment 2 (80% load, run 1)

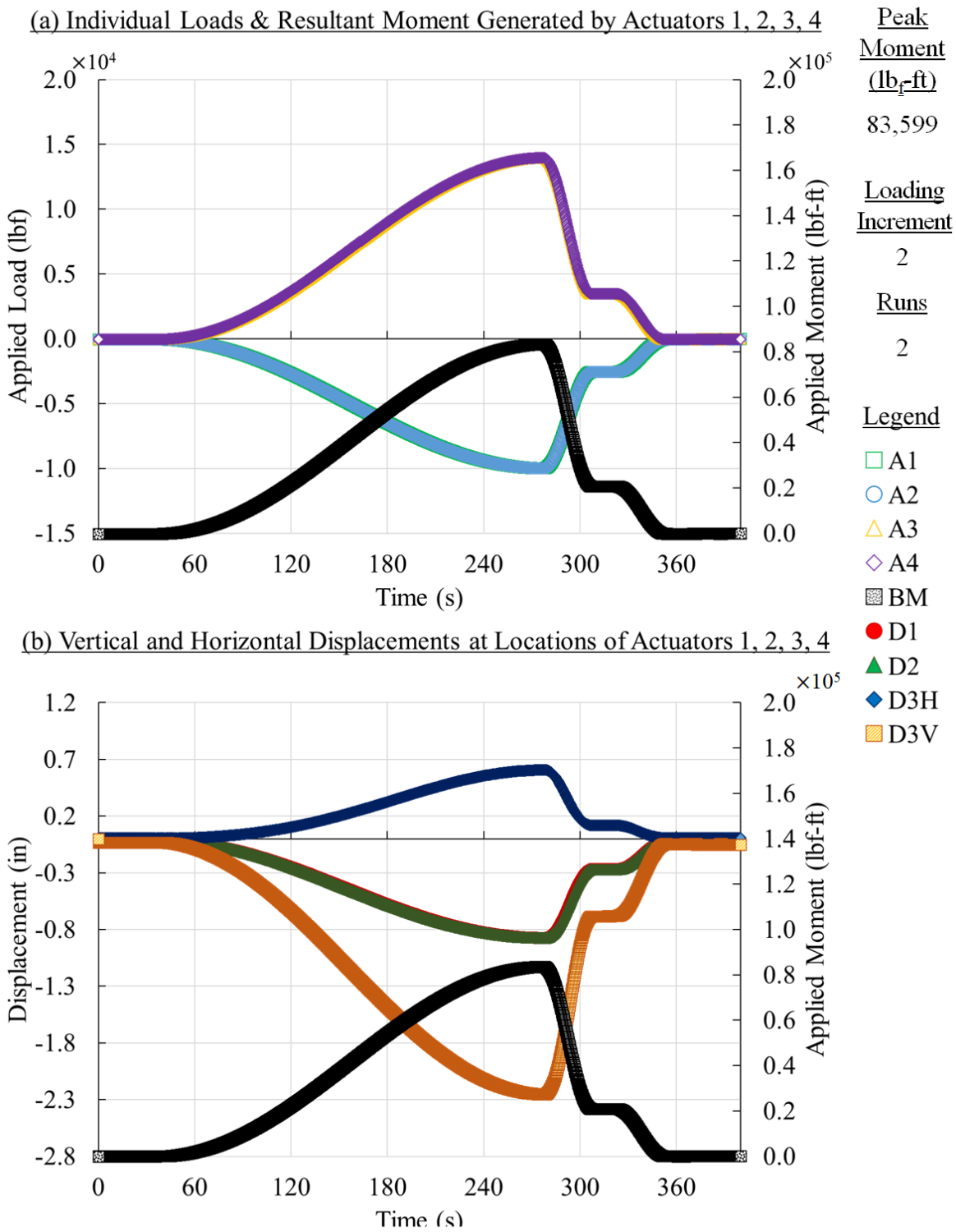

Figure 109. Panel 2 residual strength test results, loading increment 2 (80% load, run 2)

CFRP Panel 2 – Open-Hole – Results of Residual Strength Loading Increment # 2

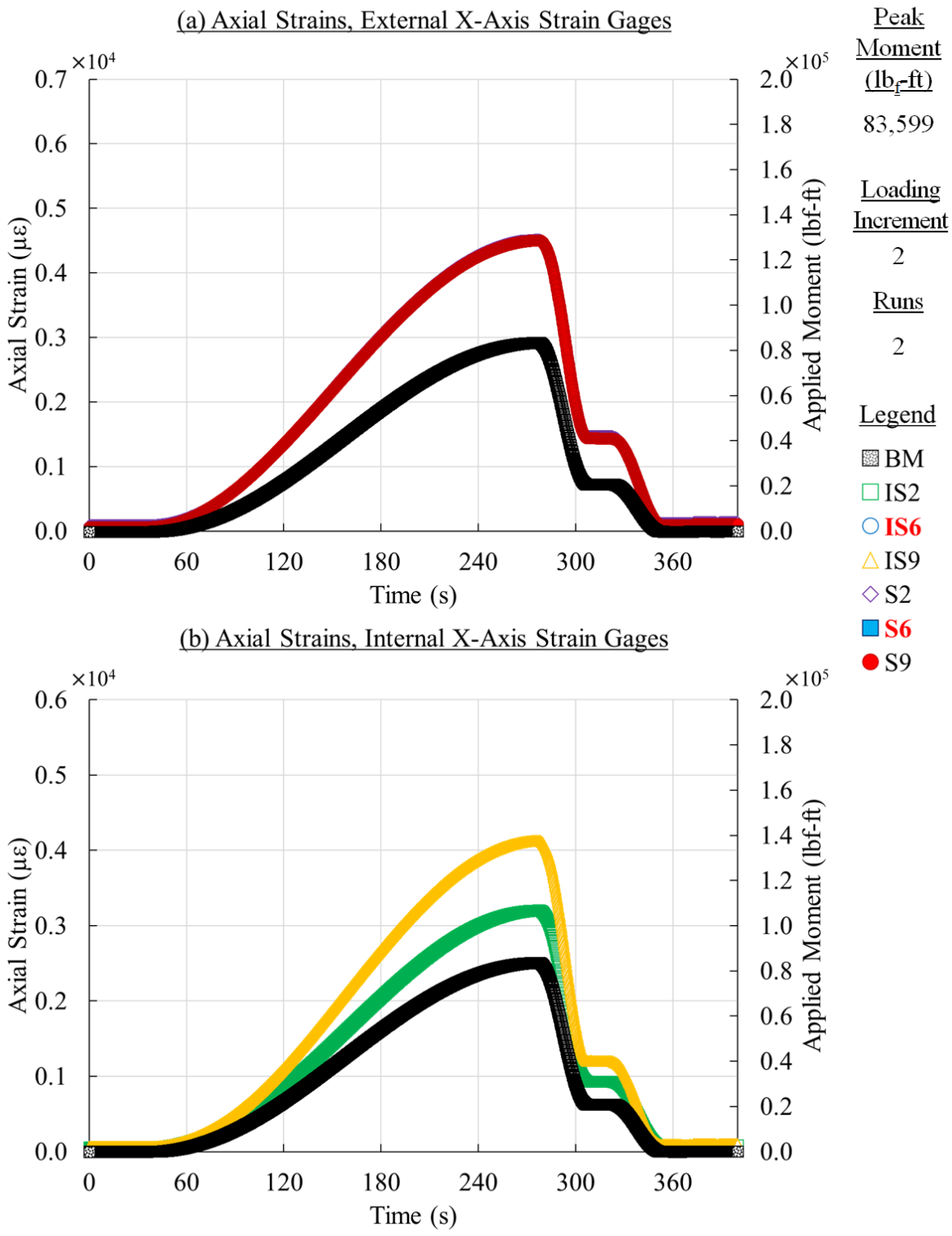

Figure 110. Panel 2 residual strength test results, loading increment 2 (80% load, run 2)

CFRP Panel 2 – Open-Hole – Results of Residual Strength Loading Increment # 2

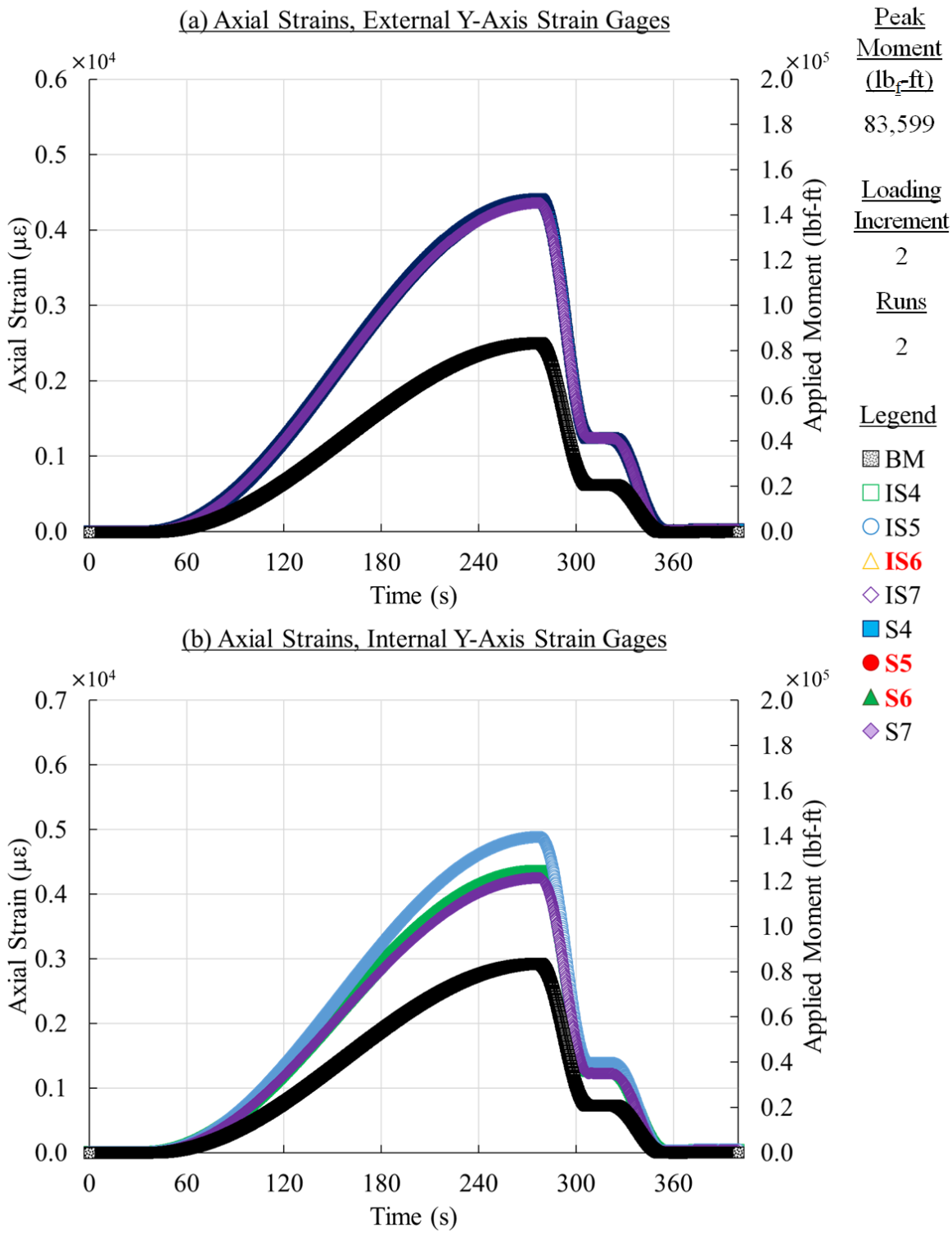

Figure 111. Panel 2 residual strength test results, loading increment 2 (80% load, run 2)

CFRP Panel 2 – Open-Hole – Results of Residual Strength Loading Increment # 2

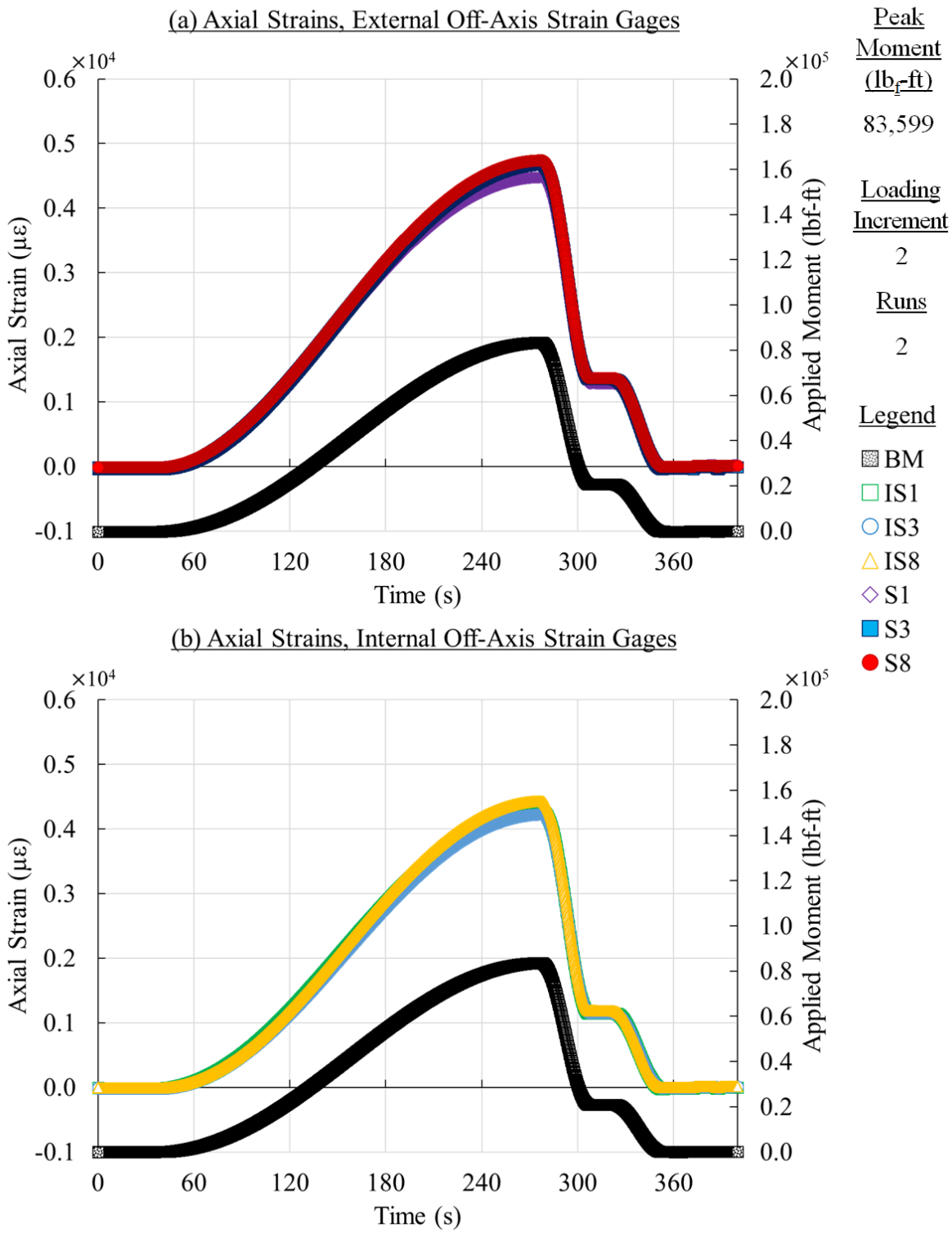

Figure 112. Panel 2 residual strength test results, loading increment 2 (80% load, run 2)

CFRP Panel 2 – Open-Hole – Results of Residual Strength Loading Increment # 2

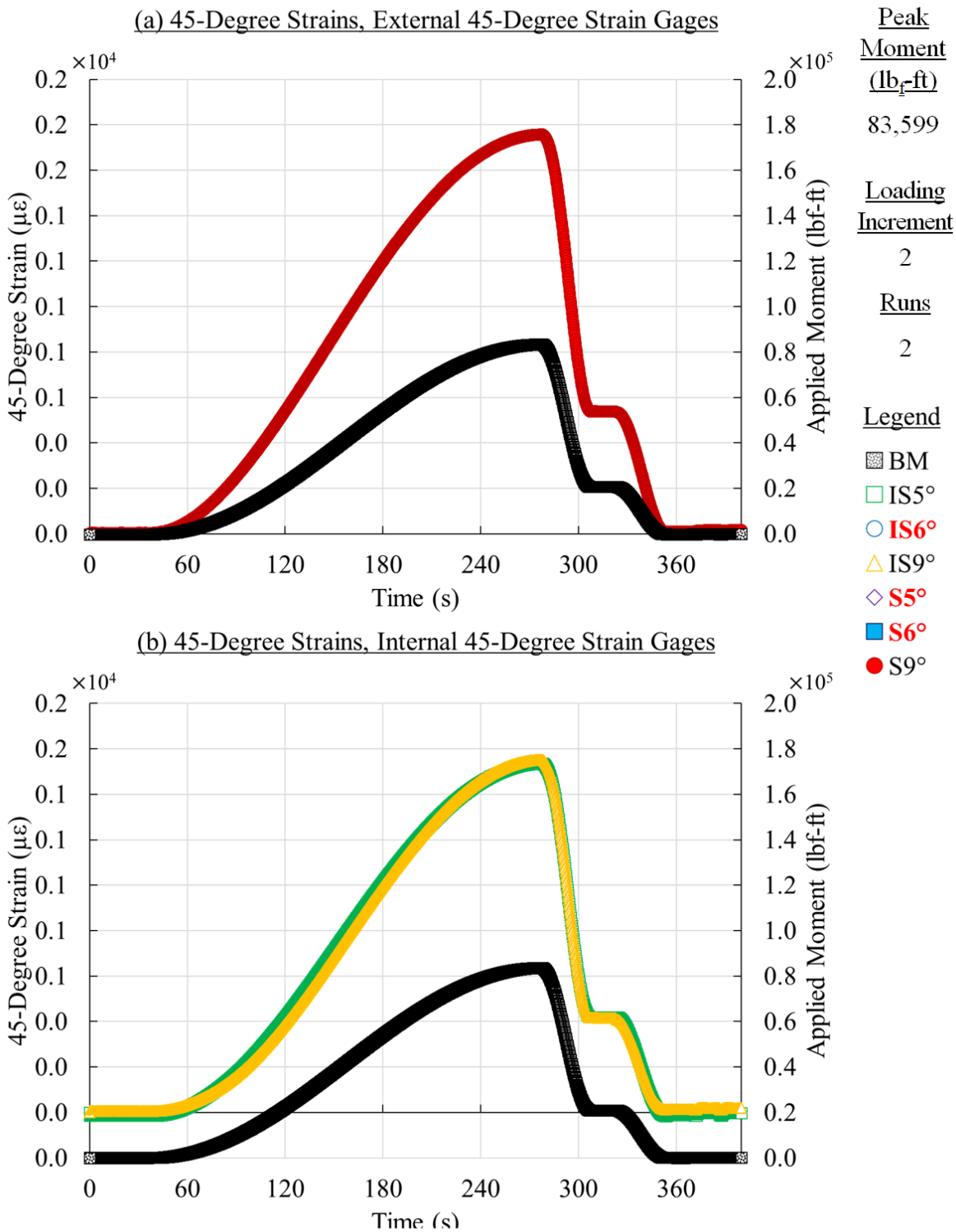

Figure 113. Panel 2 residual strength test results, loading increment 2 (80% load, run 2)

CFRP Panel 2 – Open-Hole – Results of Residual Strength Loading Increment # 2

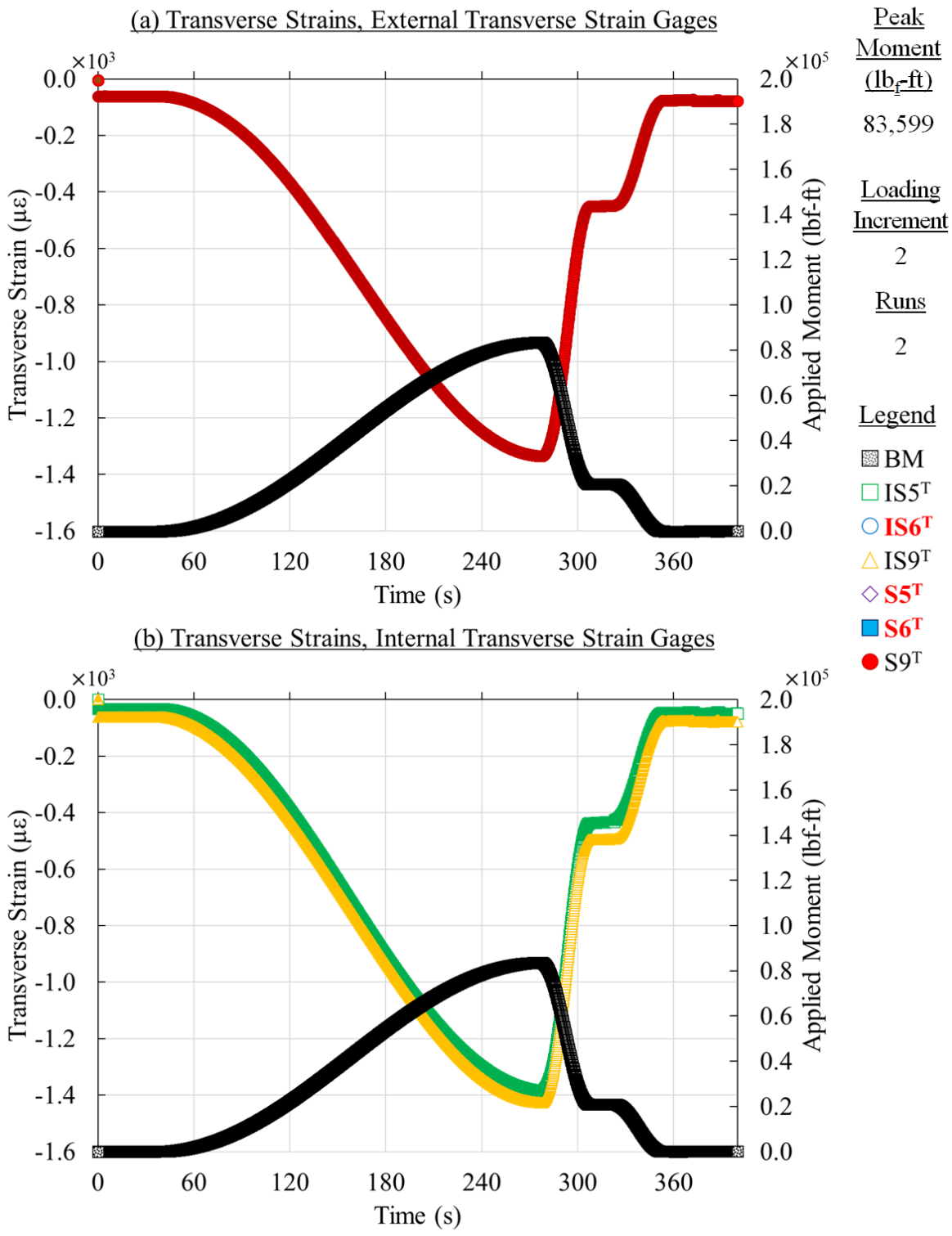

Figure 114. Panel 2 residual strength test results, loading increment 2 (80% load, run 2)

CFRP Panel 2 – Open-Hole – Results of Residual Strength Loading Increment # 3

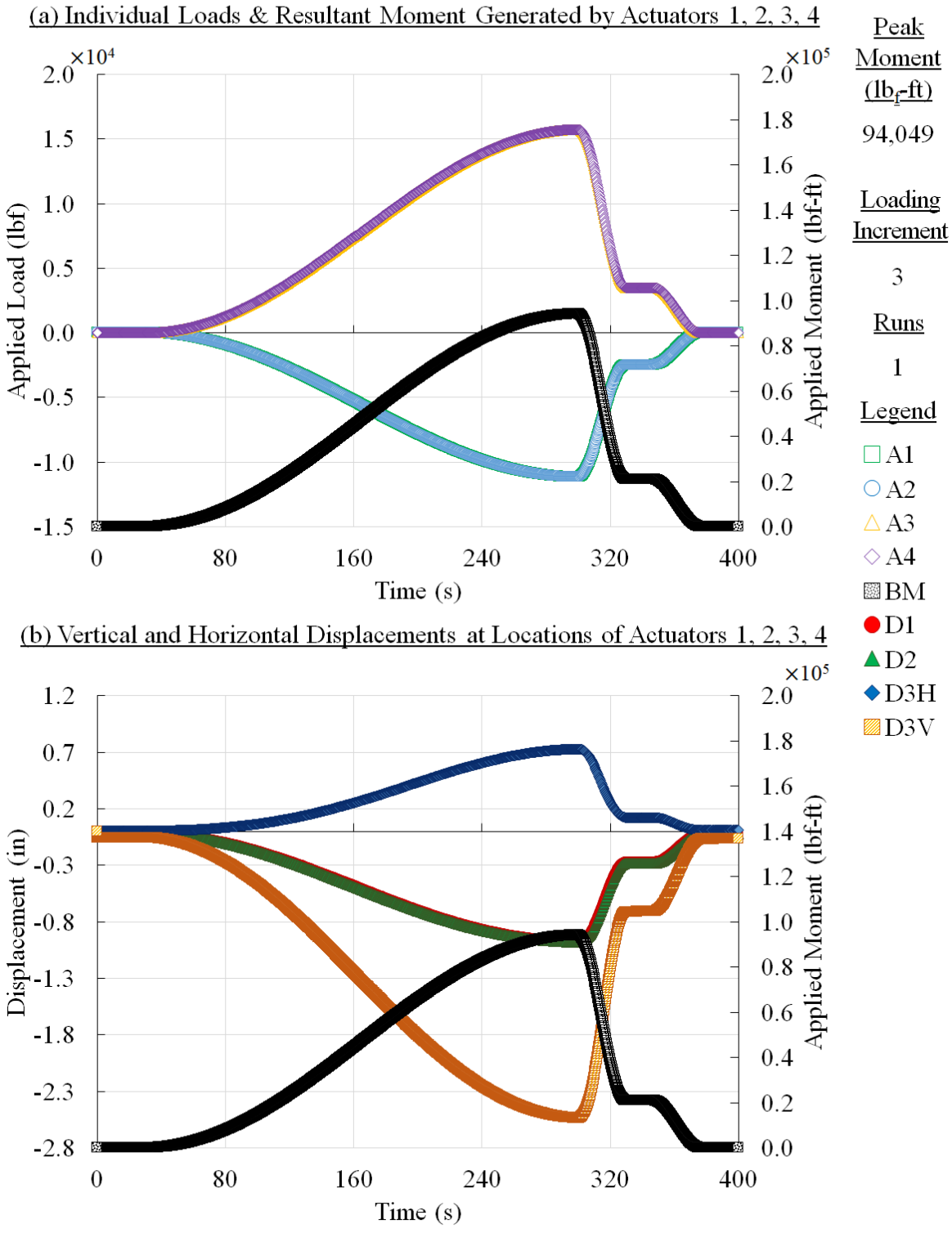

Figure 115. Panel 2 residual strength test results, loading increment 3 (90% load level)

CFRP Panel 2 – Open-Hole – Results of Residual Strength Loading Increment # 3

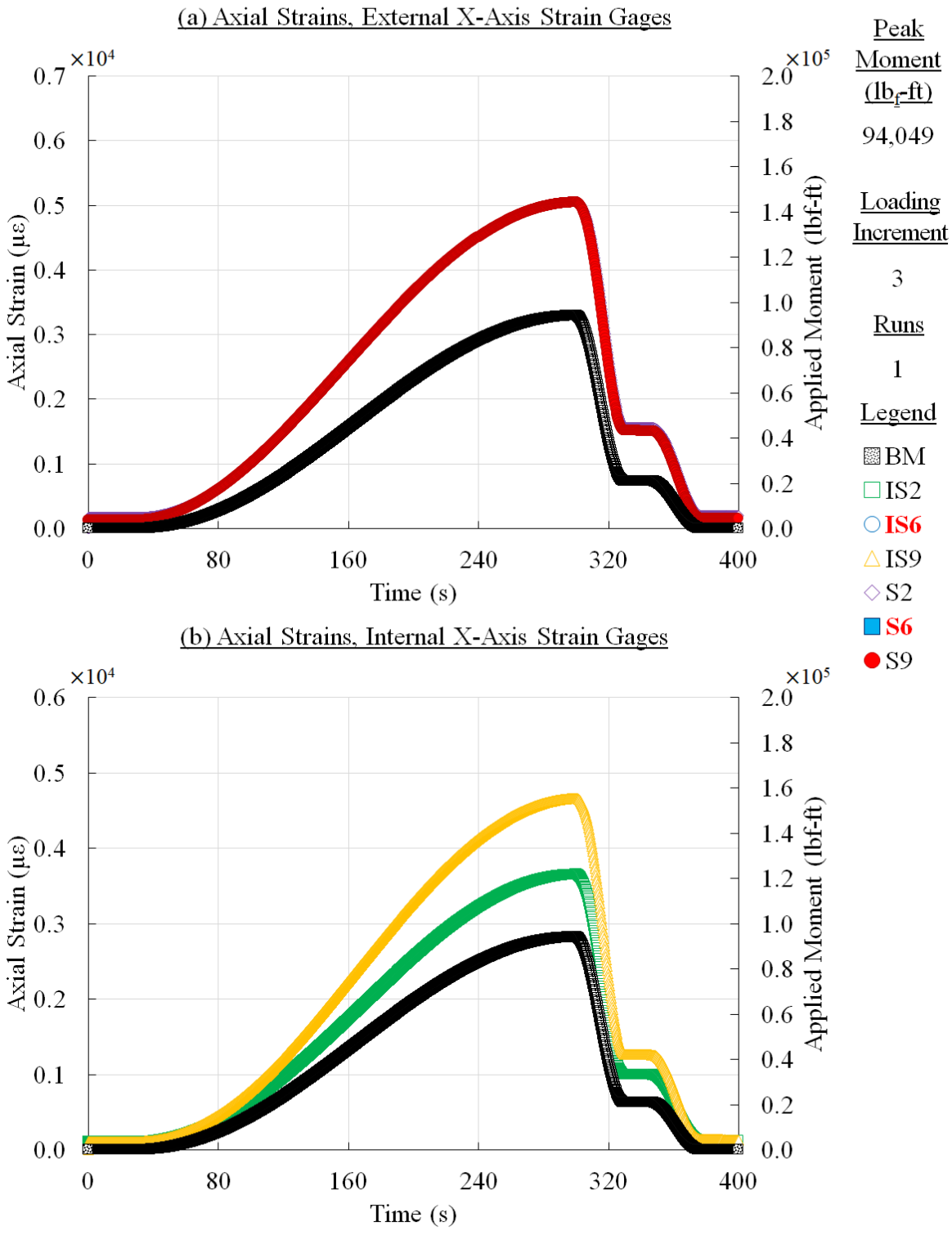

Figure 116. Panel 2 residual strength test results, loading increment 3 (90% load level)

CFRP Panel 2 – Open-Hole – Results of Residual Strength Loading Increment # 3

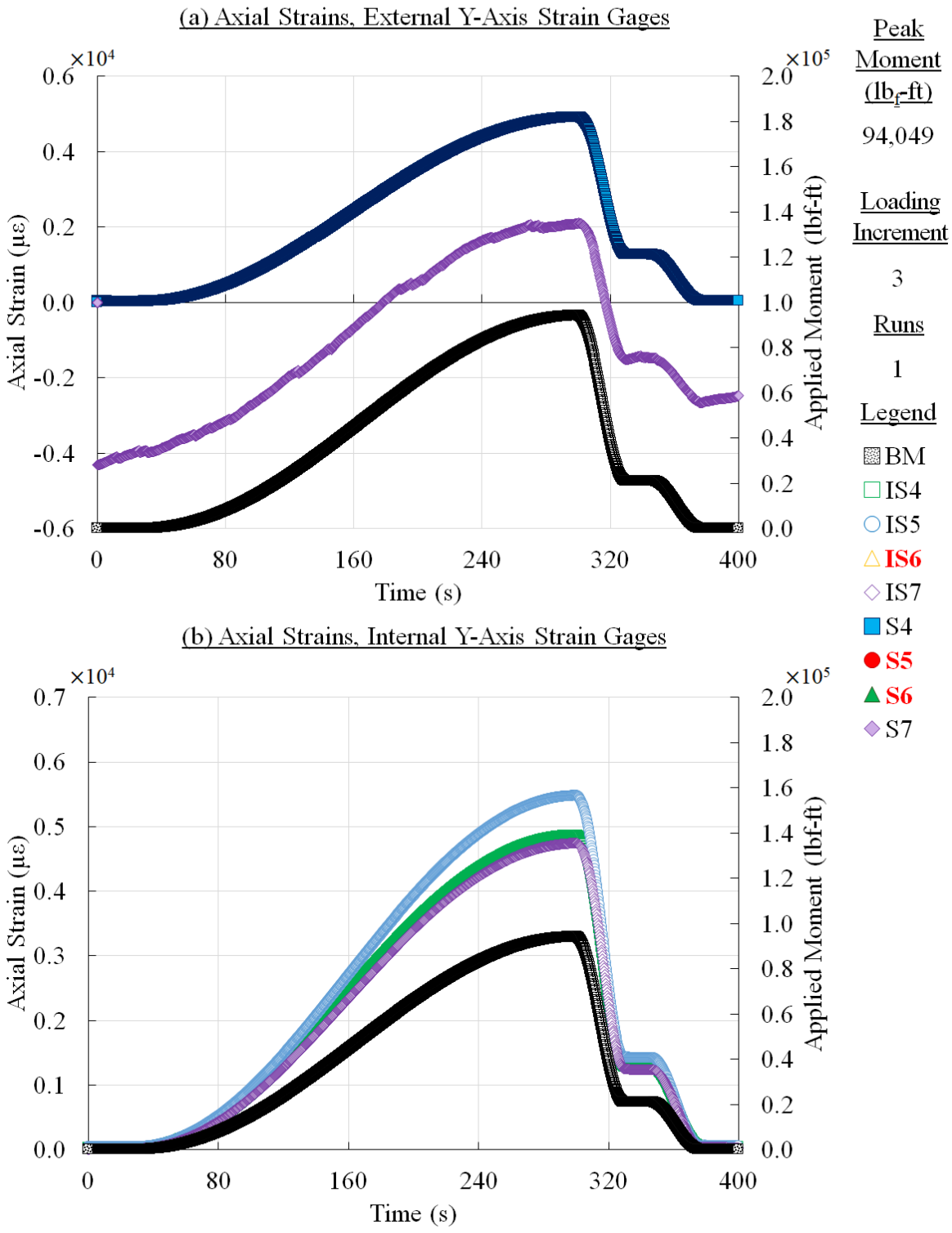

Figure 117. Panel 2 residual strength test results, loading increment 3 (90% load level)

CFRP Panel 2 – Open-Hole – Results of Residual Strength Loading Increment # 3

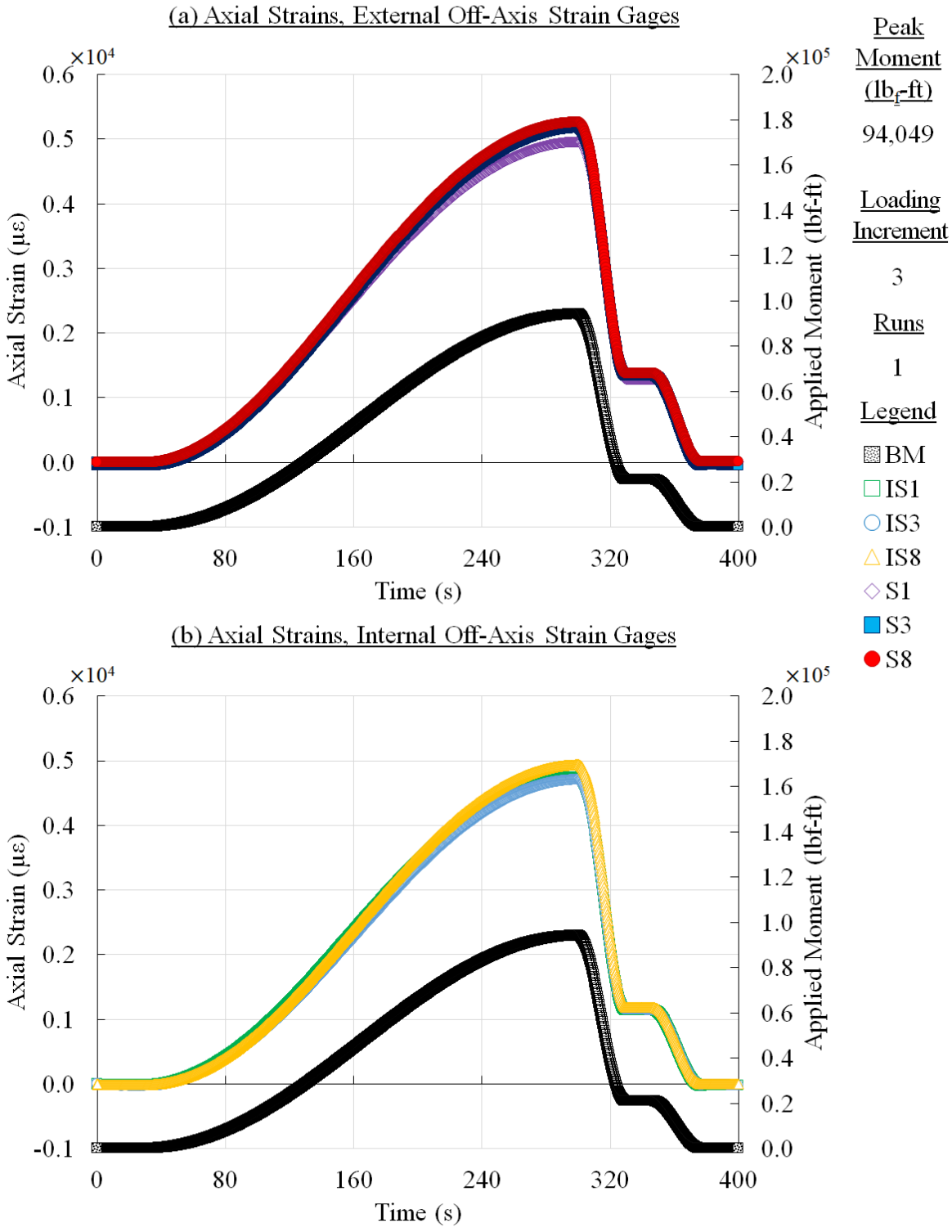

Figure 118. Panel 2 residual strength test results, loading increment 3 (90% load level)

CFRP Panel 2 – Open-Hole – Results of Residual Strength Loading Increment # 3

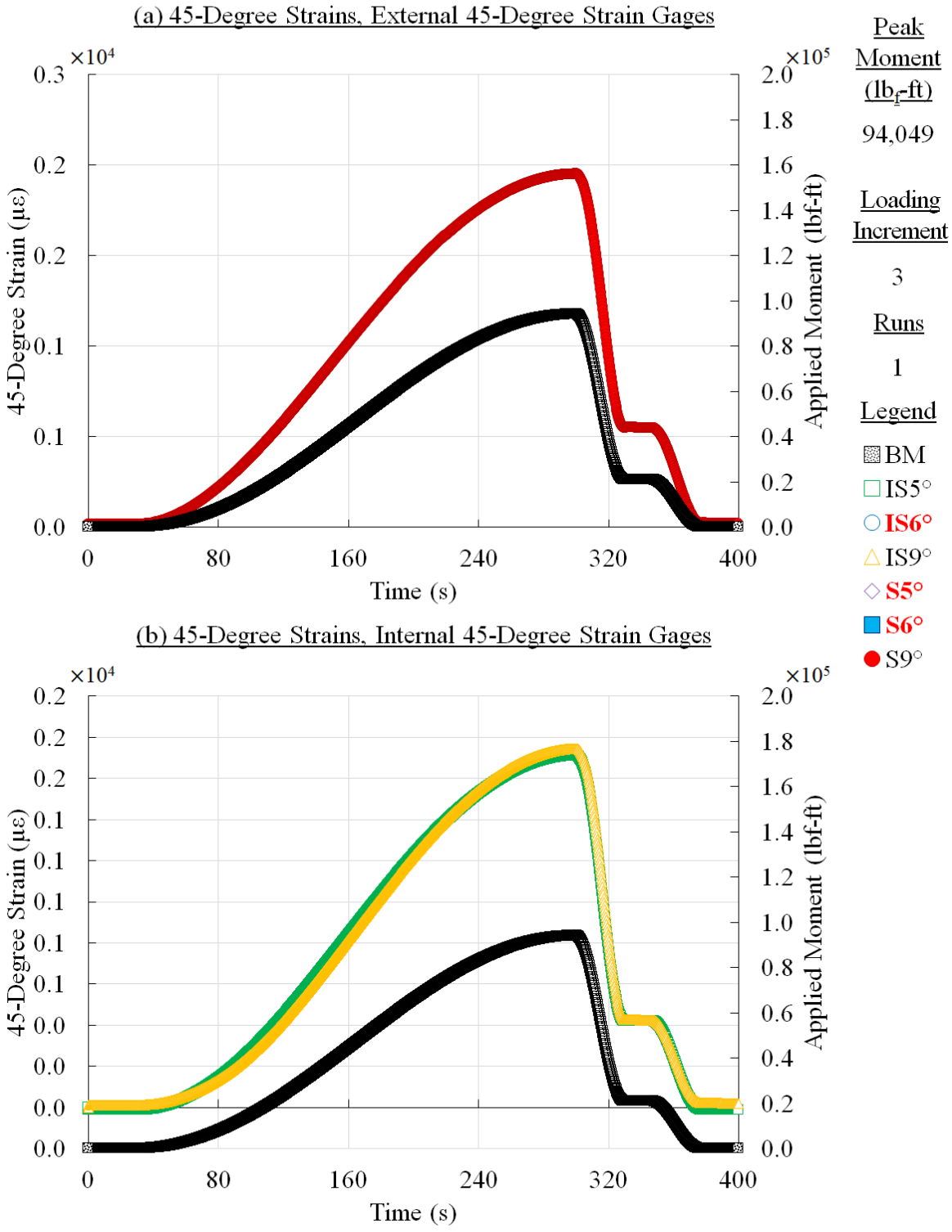

Figure 119. Panel 2 residual strength test results, loading increment 3 (90% load level)

CFRP Panel 2 – Open-Hole – Results of Residual Strength Loading Increment # 3

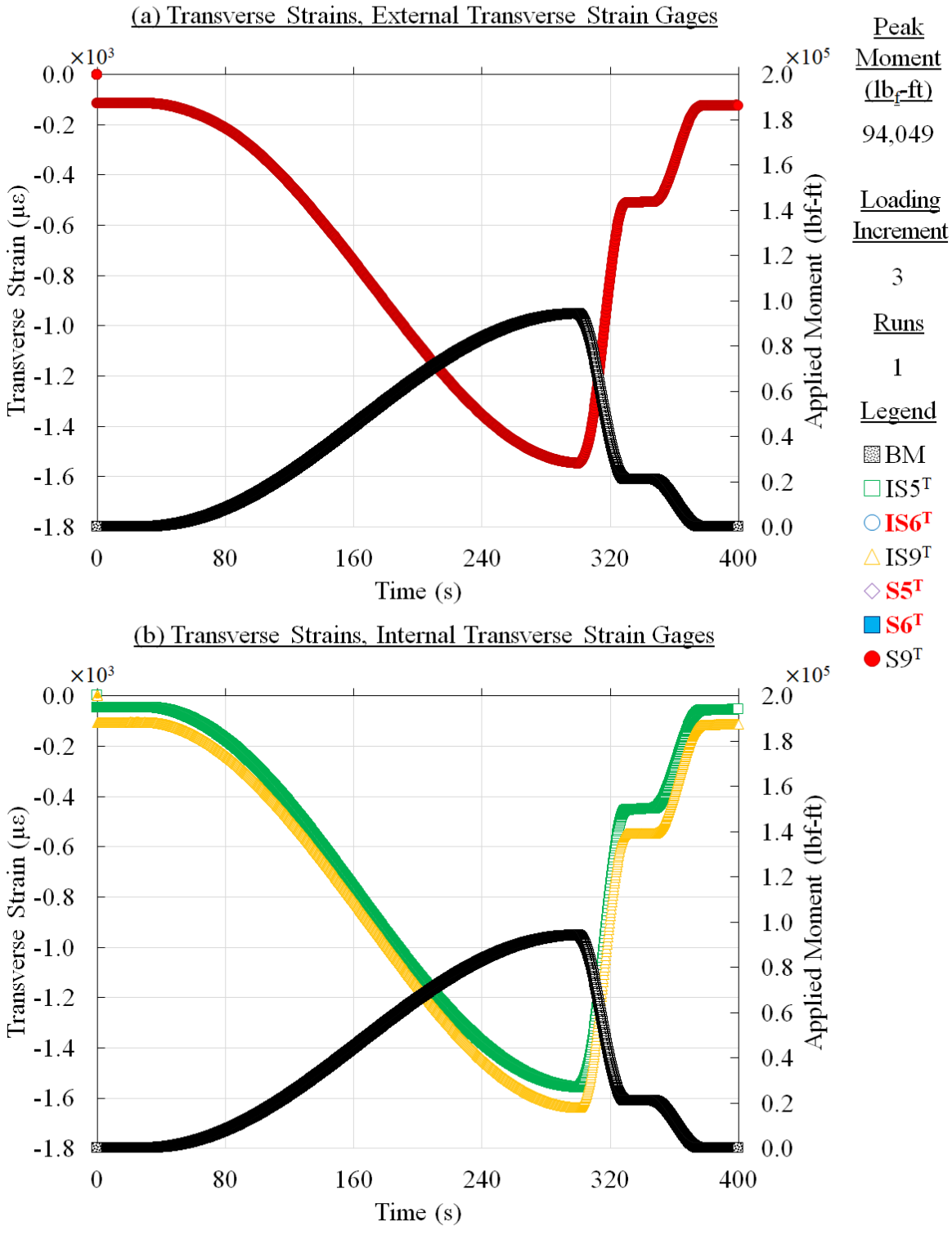

Figure 120. Panel 2 residual strength test results, loading increment 3 (90% load level)

CFRP Panel 2 – Open-Hole – Results of Residual Strength Loading Increment # 4

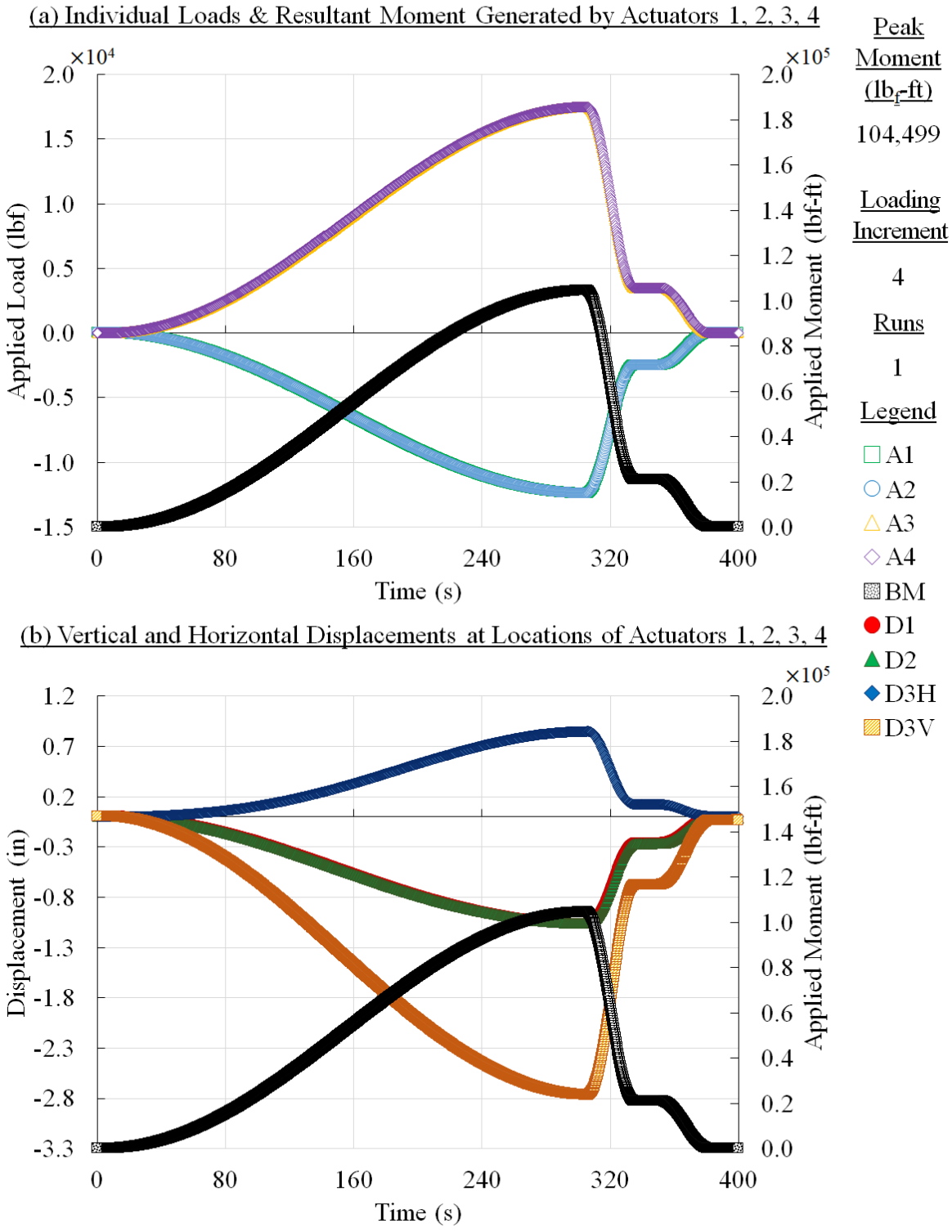

Figure 121. Panel 2 residual strength test results, loading increment 4 (100% load level)

CFRP Panel 2 – Open-Hole – Results of Residual Strength Loading Increment # 4

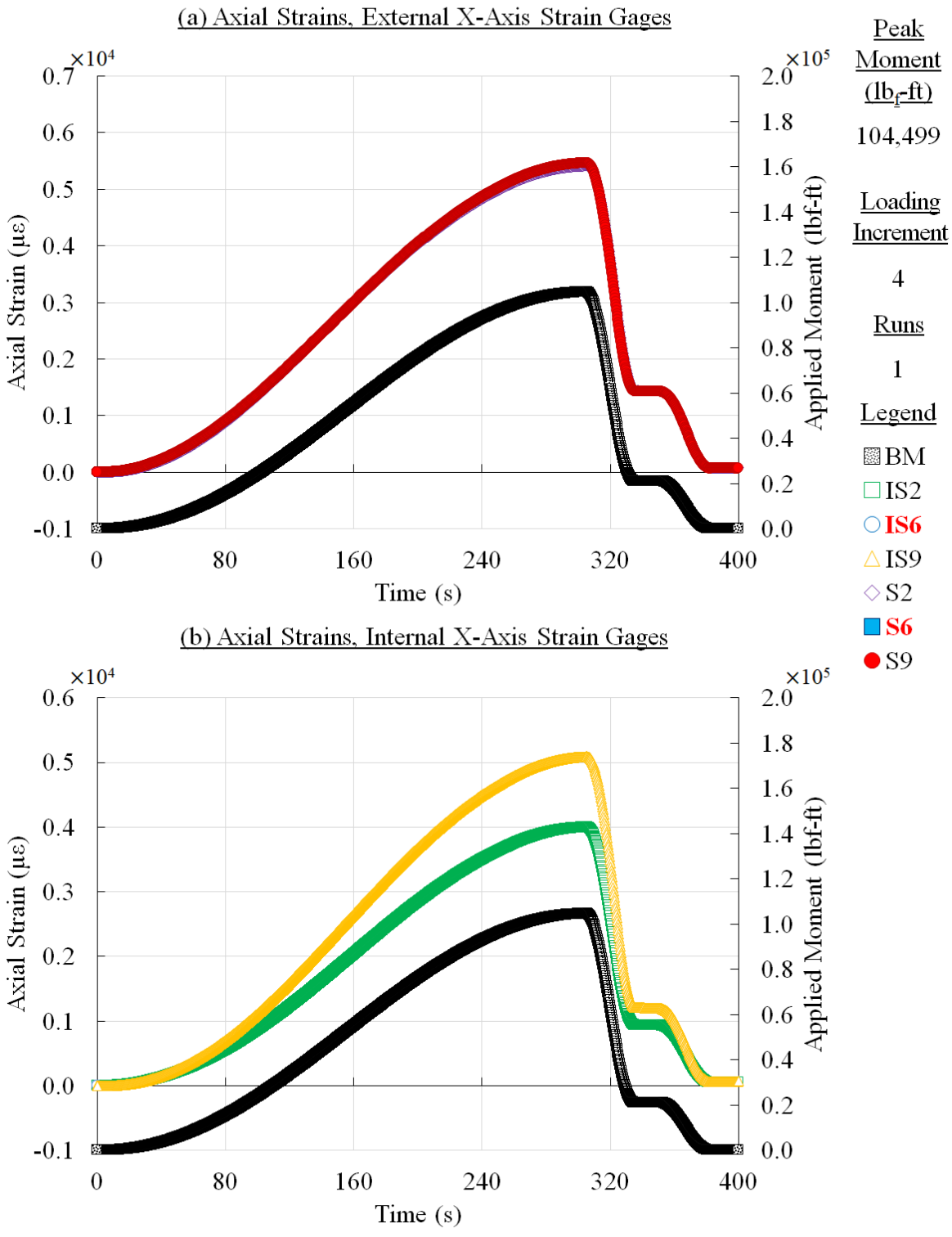

Figure 122. Panel 2 residual strength test results, loading increment 4 (100% load level)

CFRP Panel 2 – Open-Hole – Results of Residual Strength Loading Increment # 4

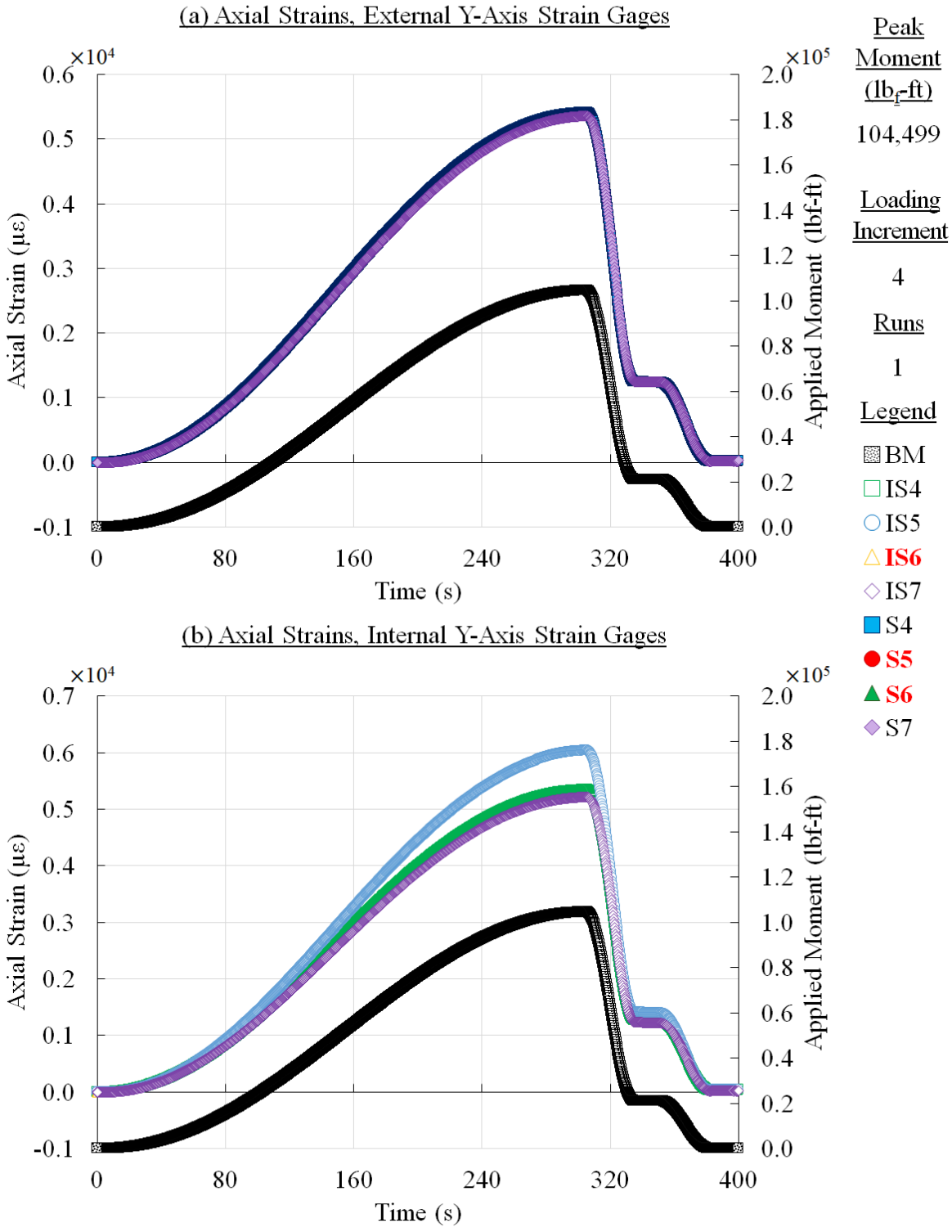

Figure 123. Panel 2 residual strength test results, loading increment 4 (100% load level)

CFRP Panel 2 – Open-Hole – Results of Residual Strength Loading Increment # 4

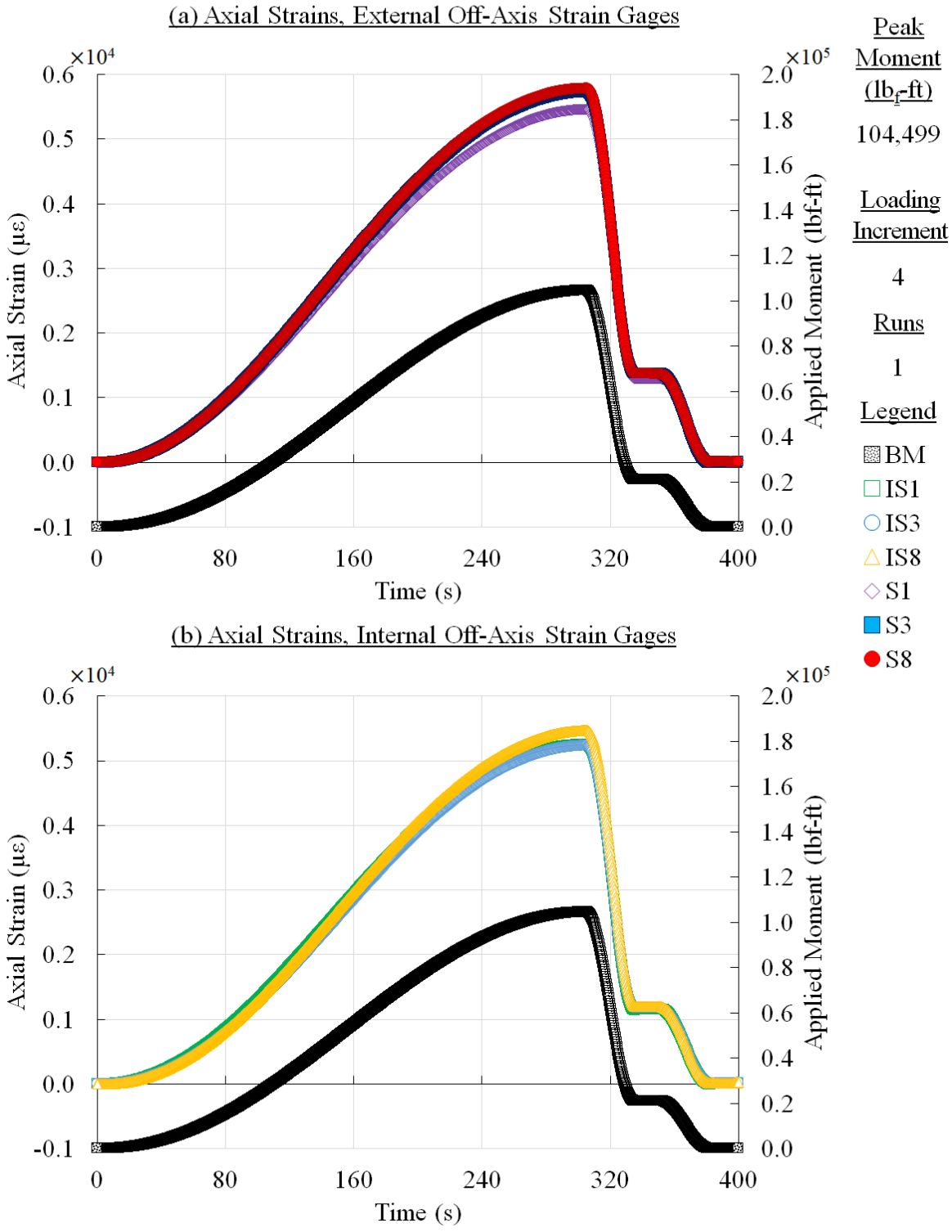

Figure 124. Panel 2 residual strength test results, loading increment 4 (100% load level)

CFRP Panel 2 – Open-Hole – Results of Residual Strength Loading Increment # 4

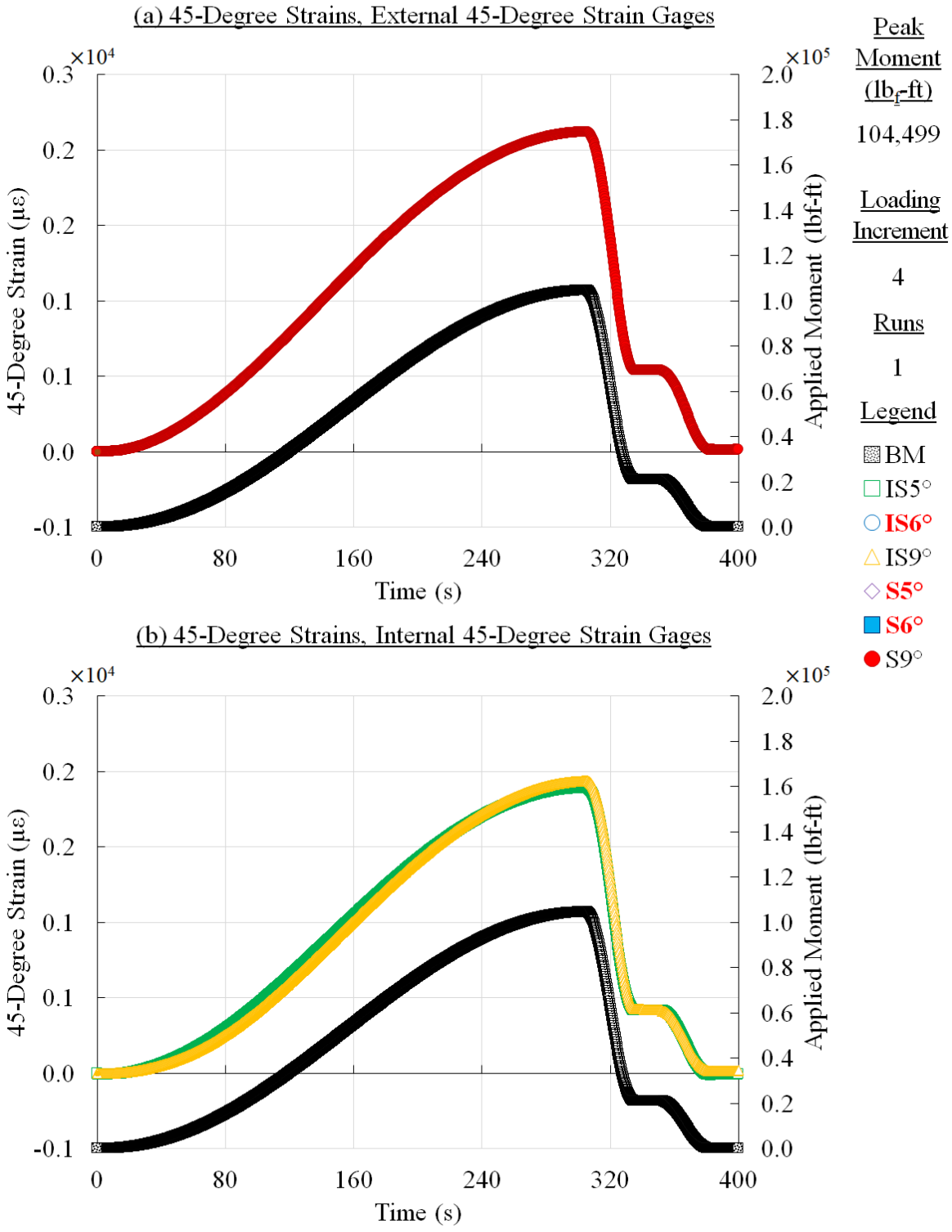

Figure 125. Panel 2 residual strength test results, loading increment 4 (100% load level)

CFRP Panel 2 – Open-Hole – Results of Residual Strength Loading Increment # 4

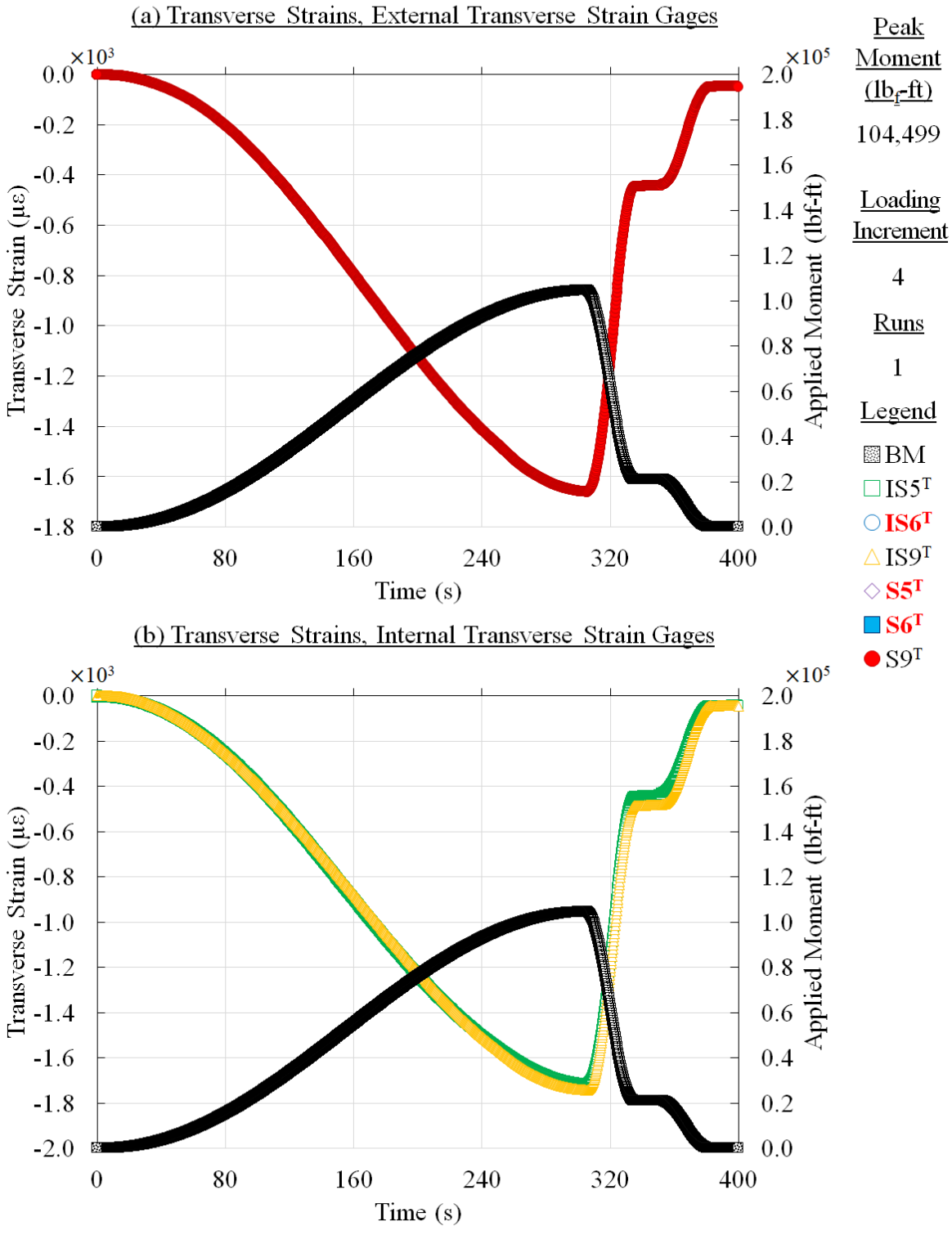

Figure 126. Panel 2 residual strength test results, loading increment 4 (100% load level)

CFRP Panel 2 – Open-Hole – Results of Residual Strength Loading Increment # 5

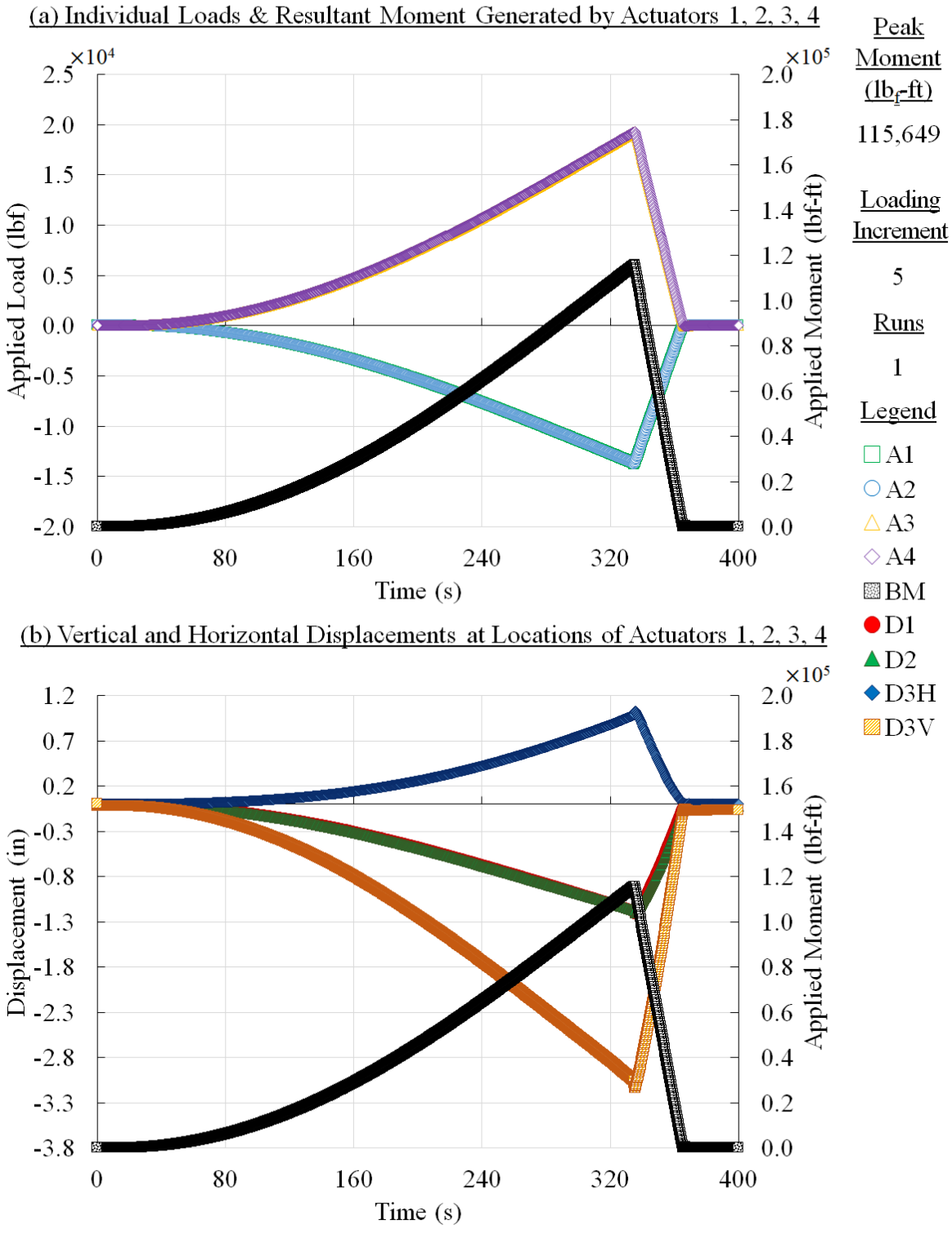

Figure 127. Panel 2 residual strength test results, loading increment 5 (final failure)

CFRP Panel 2 – Open-Hole – Results of Residual Strength Loading Increment # 5

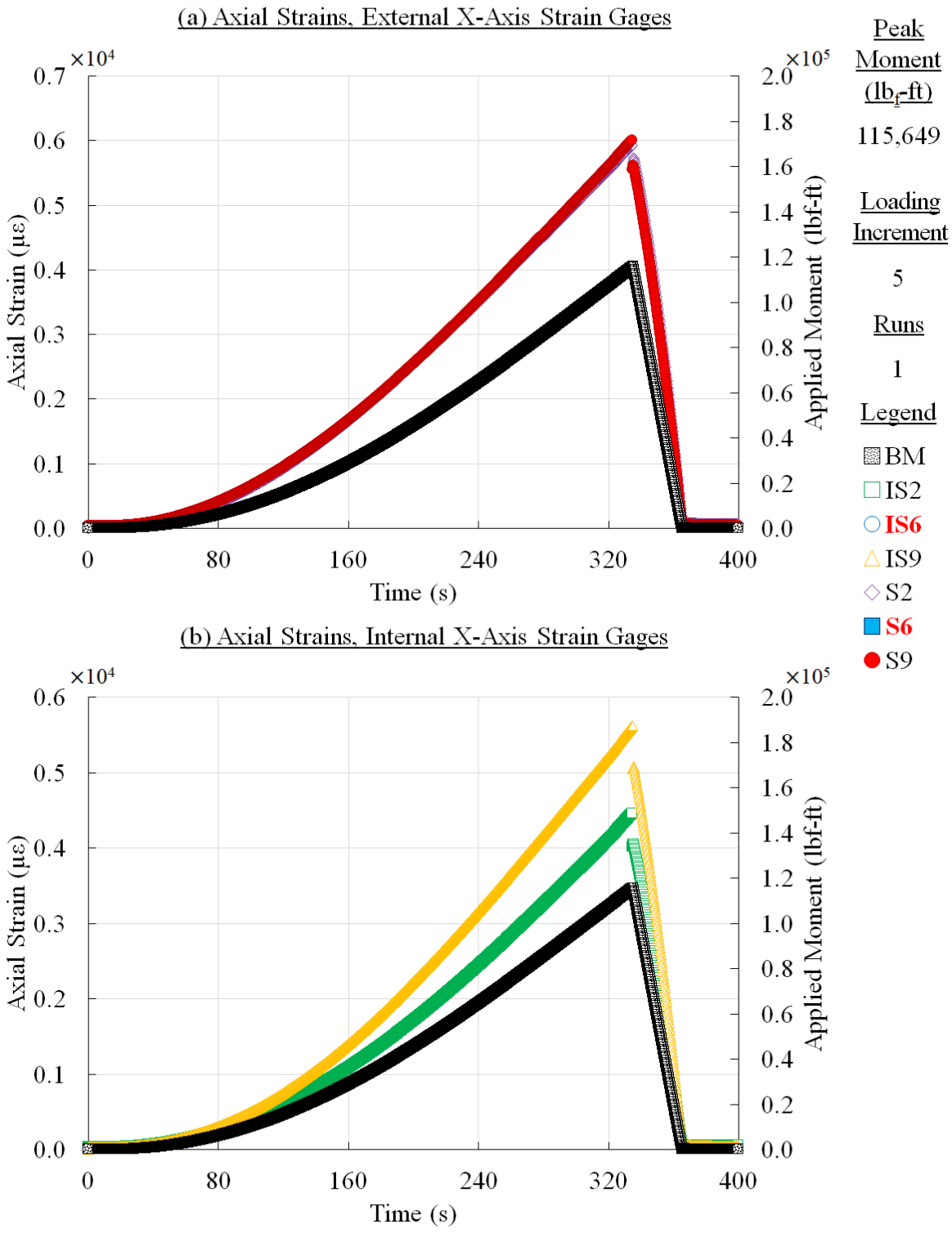

Figure 128. Panel 2 residual strength test results, loading increment 5 (final failure)

CFRP Panel 2 – Open-Hole – Results of Residual Strength Loading Increment # 5

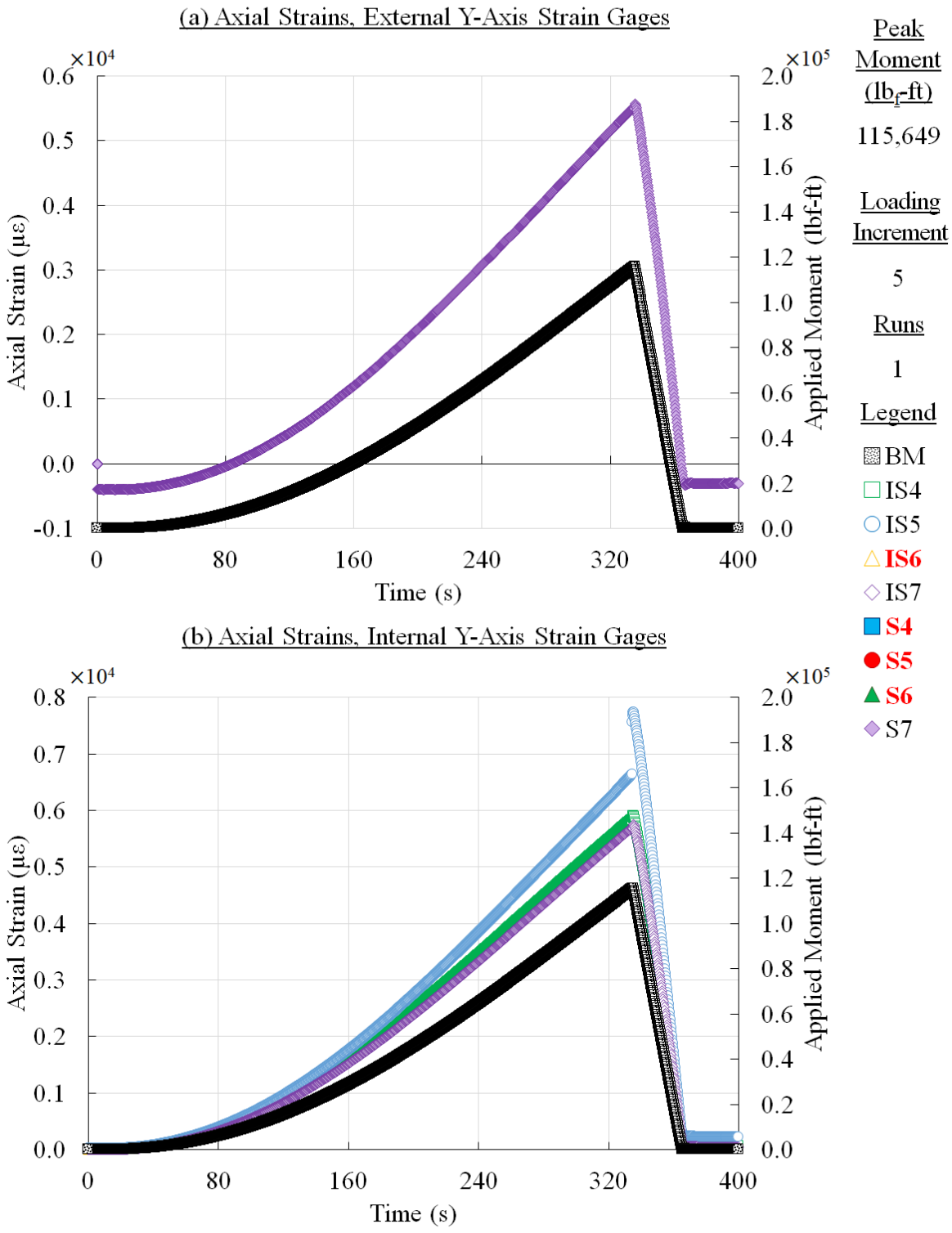

Figure 129. Panel 2 residual strength test results, loading increment 5 (final failure)

CFRP Panel 2 – Open-Hole – Results of Residual Strength Loading Increment # 5

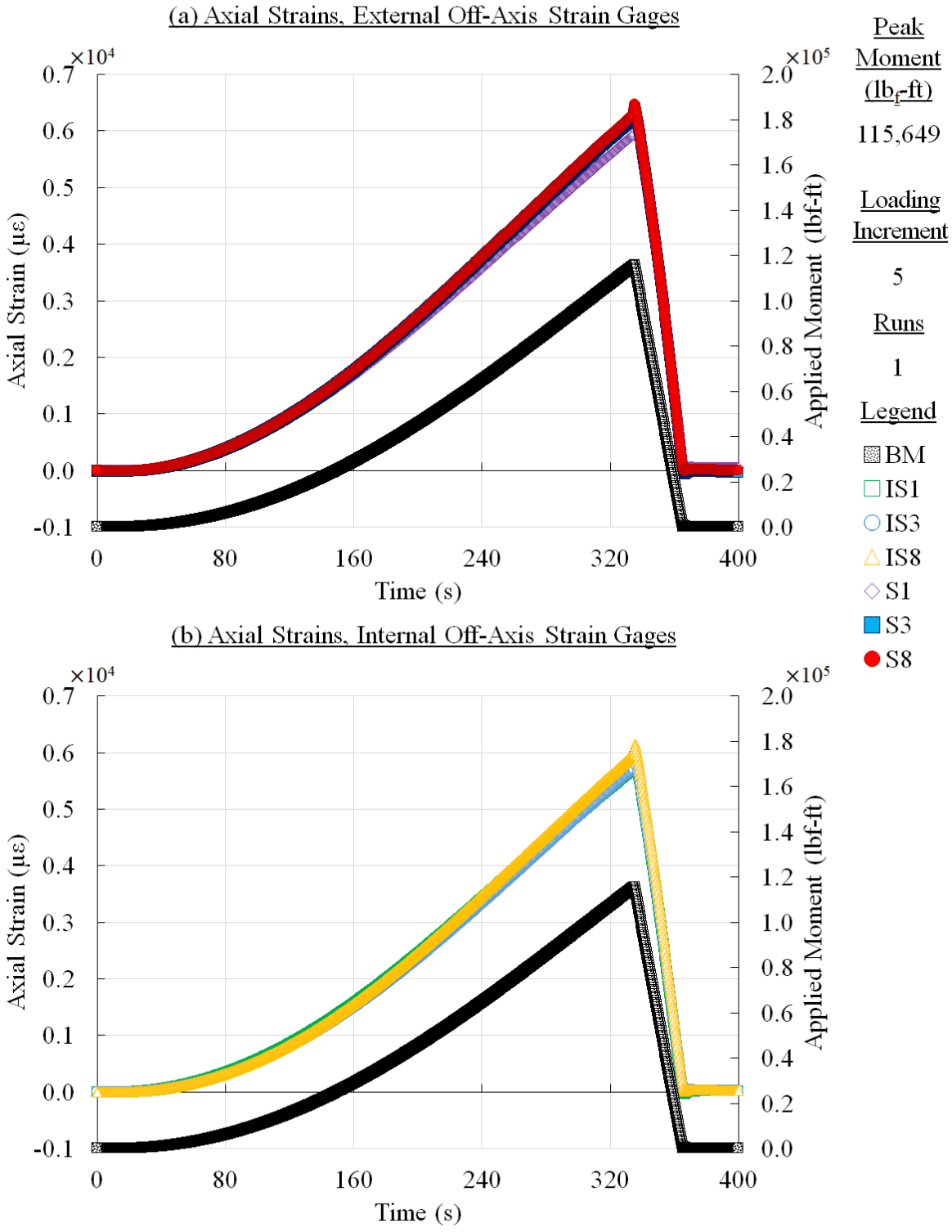

Figure 130. Panel 2 residual strength test results, loading increment 5 (final failure)

CFRP Panel 2 – Open-Hole – Results of Residual Strength Loading Increment # 5

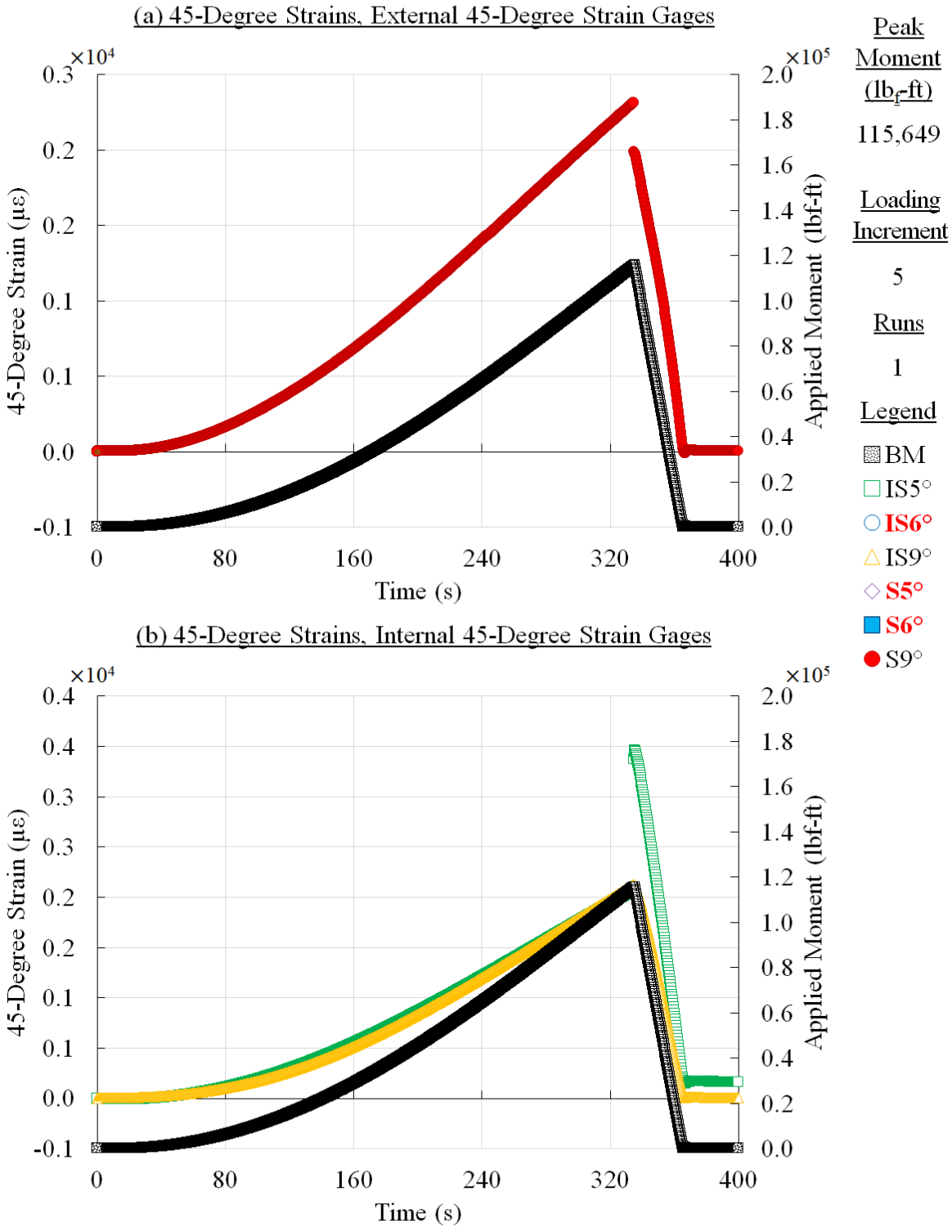

Figure 131. Panel 2 residual strength test results, loading increment 5 (final failure)

CFRP Panel 2 – Open-Hole – Results of Residual Strength Loading Increment # 5

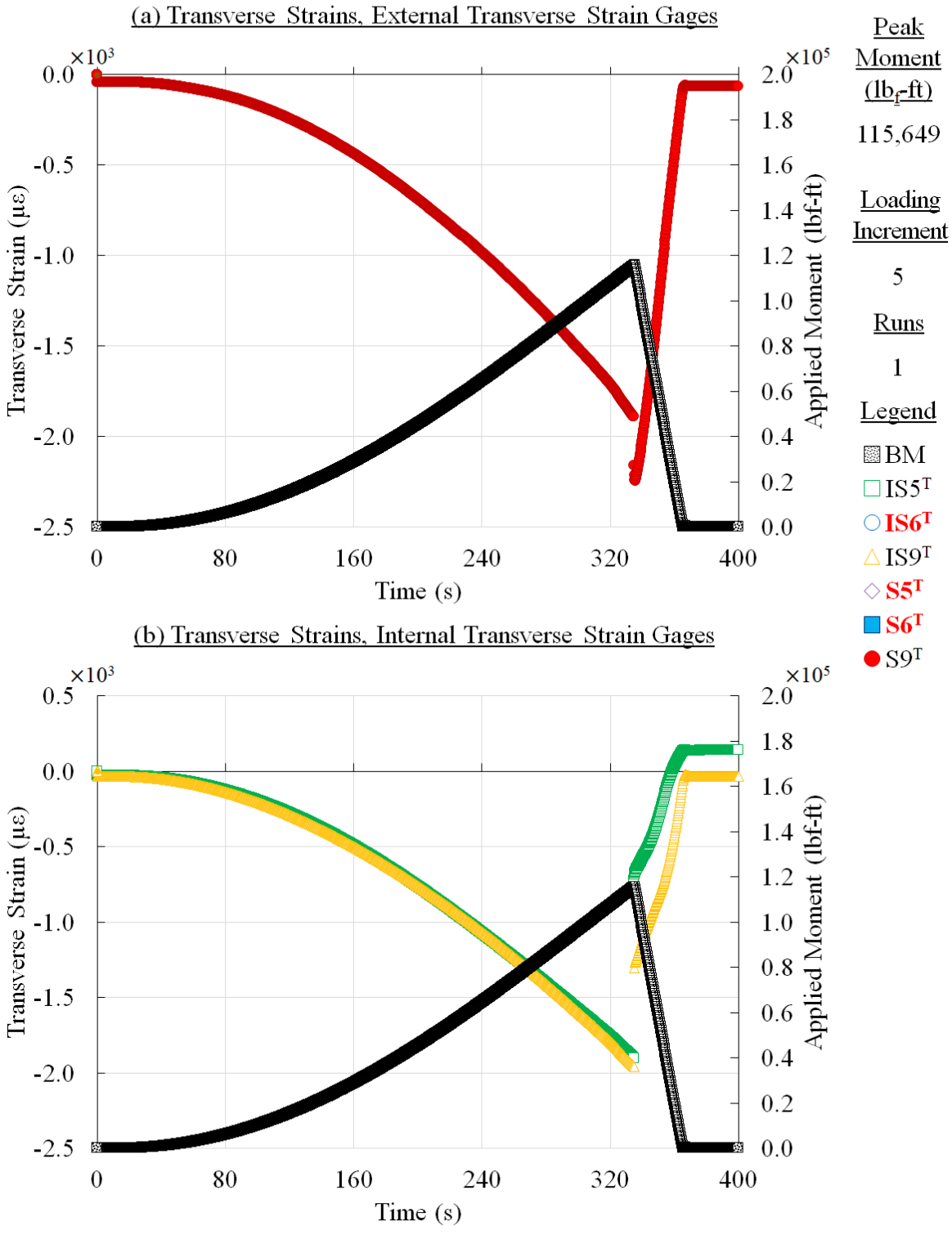

Figure 132. Panel 2 residual strength test results, loading increment 5 (final failure)

D Digital image correlation results

3D DIC is a non-contact, material-independent NDI method capable of utilizing sequential digital images of a specimen subjected to mechanical loading to measure in-plane deformation and strain, and in and out-of-plane displacements. Throughout the duration of the tests described herein, 5M ARAMIS 3D DIC systems were used to monitor strains exhibited in the central test sections of the panels during quasi-static strain surveys. Each 5M ARAMIS 3D DIC system consisted of a sensor unit, a sensor controller, a high-performance PC system, and ARAMIS 3D DIC analysis software. The sensor unit featured two 5-megapixel cameras with 12-mm (wide field of view) and 50-mm (narrow field of view) focal length lenses, a laser pointer, and two adjustable LED spotlights mounted on a circular support bar.

Panel 1 axial strain distributions are shown in Figure 133. Figure 134, Figure 135 and Figure 136 show the axial strain distribution during intervals 1, 2 and 3, respectively, for panel 2. Similarly, von-mises strains for panel 2 are shown in Figure 137 to Figure 139. Axial strains and von-mises strains during the residual strength loading for panel 2 focused on a wide field of view are shown in Figure 140 and Figure 141, respectively. Similarly, Figure 142 and Figure 143 shows axial strains and von-mises strains for panel 2 focused on a narrow field of view.

Pristine Panel DIC Results, Axial Strain

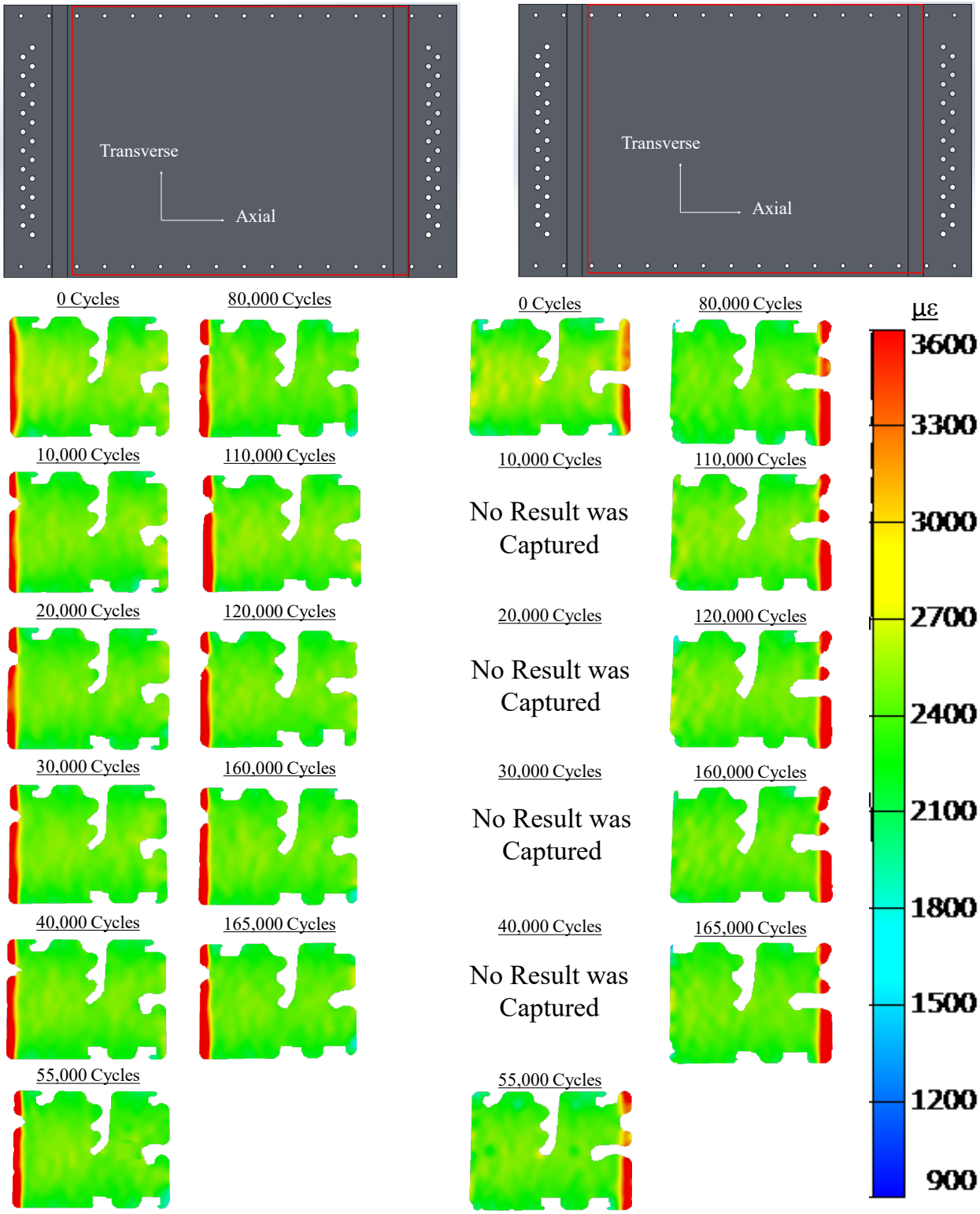

Figure 133. Panel 1 fatigue test results, axial strain

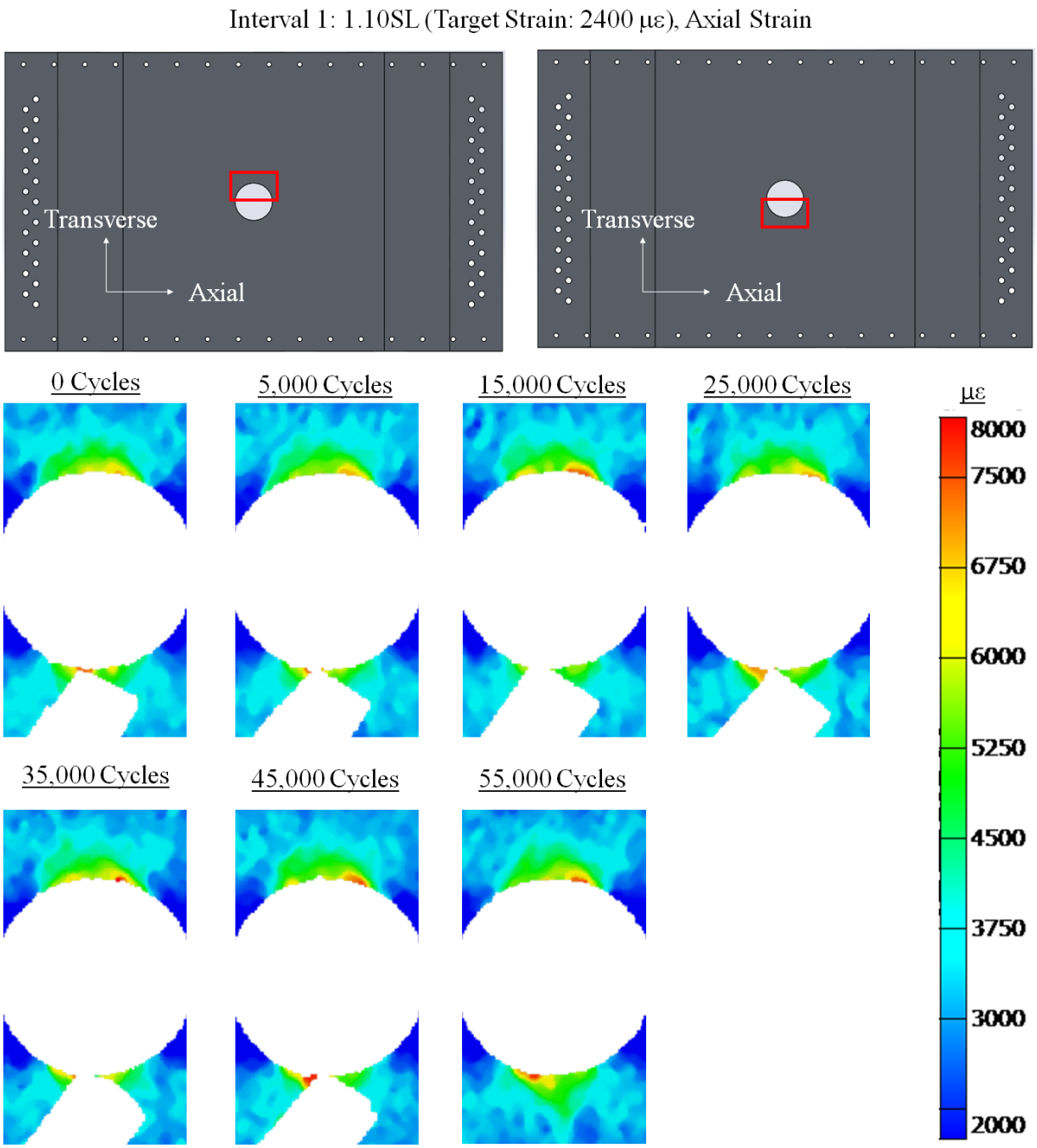

Figure 134. Panel 2 fatigue test results, axial strain (interval 1)

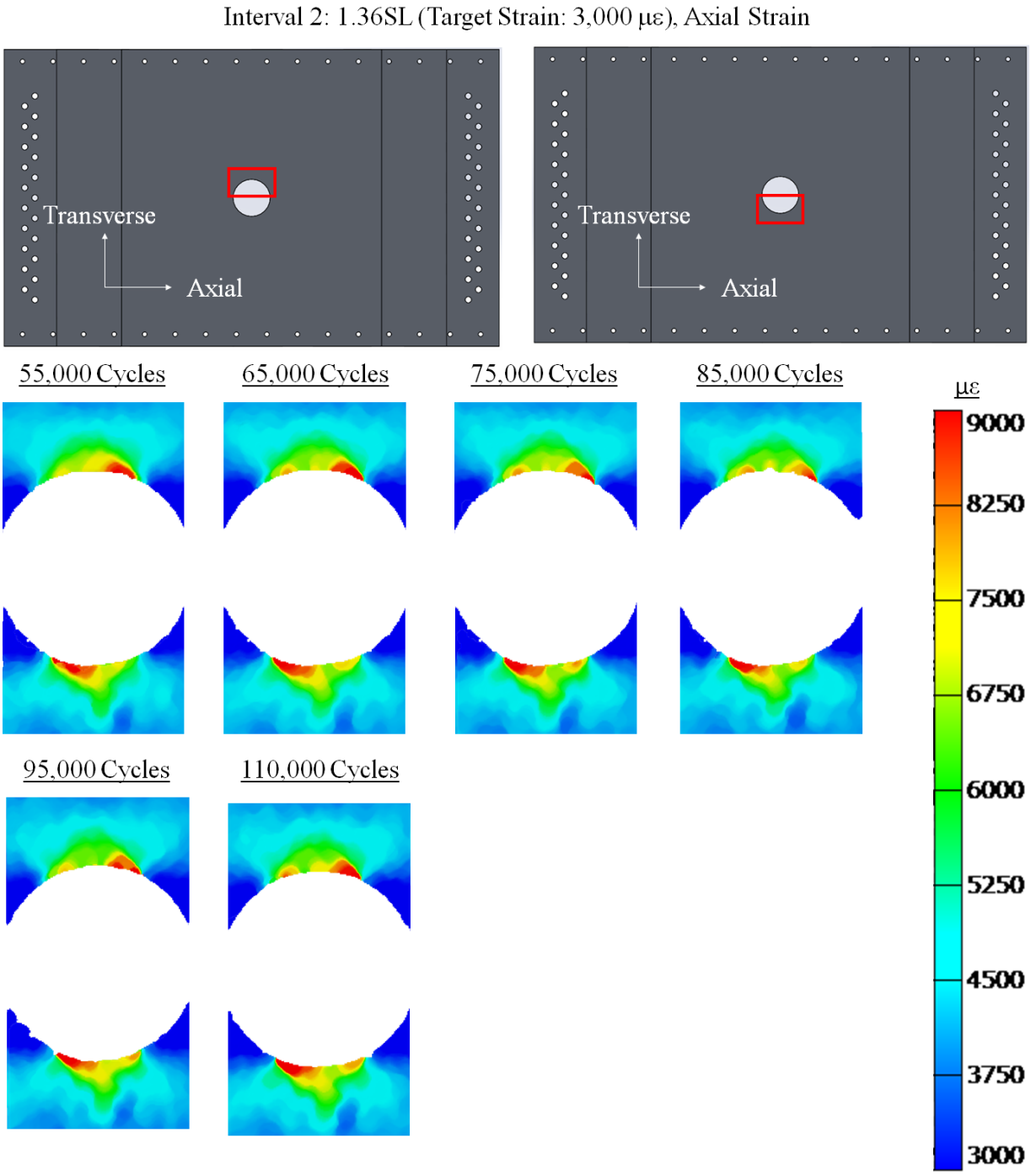

Figure 135. Panel 2 fatigue test results, axial strain (interval 2)

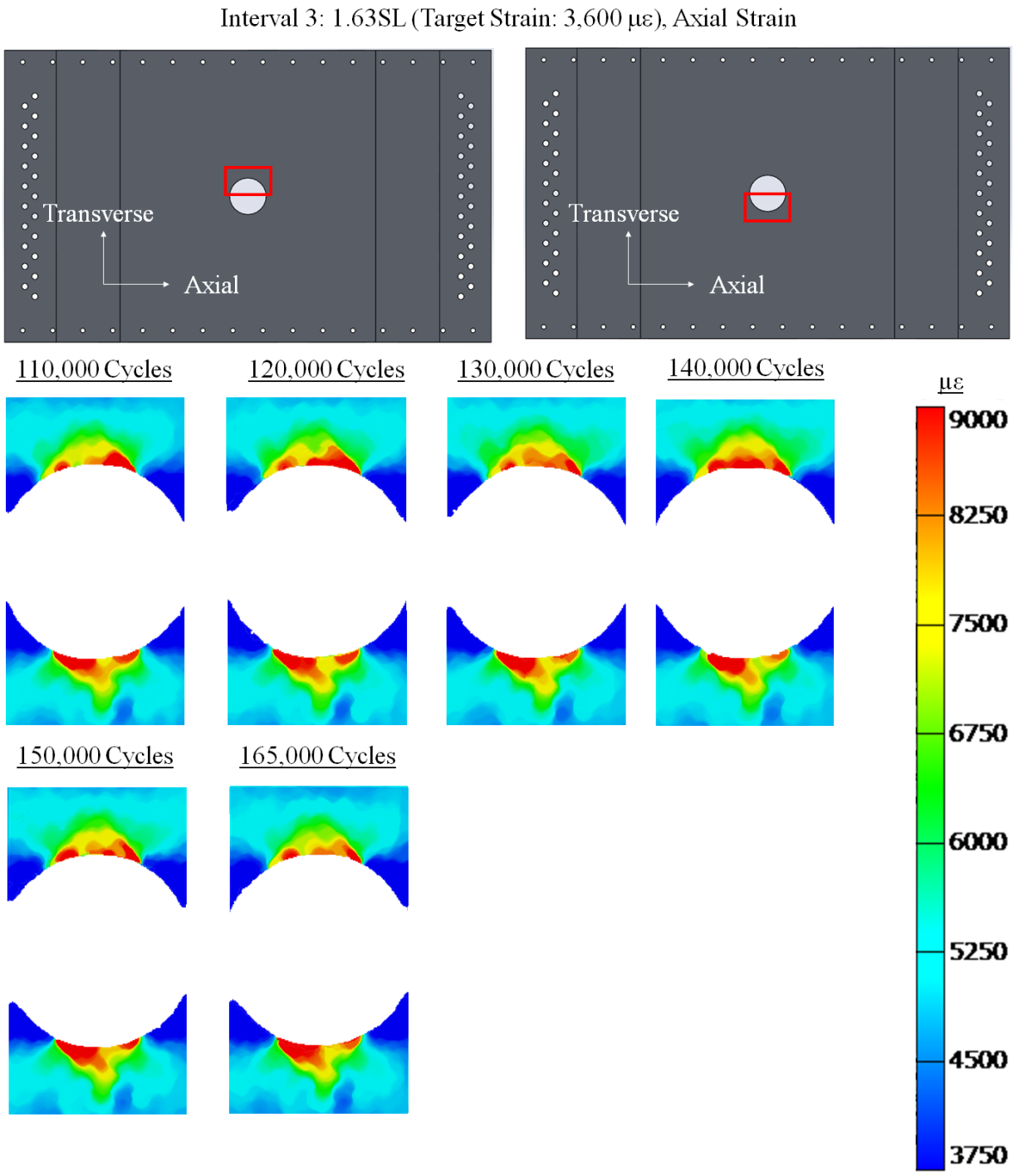

Figure 136. Panel 2 fatigue test results, axial strain (interval 3)

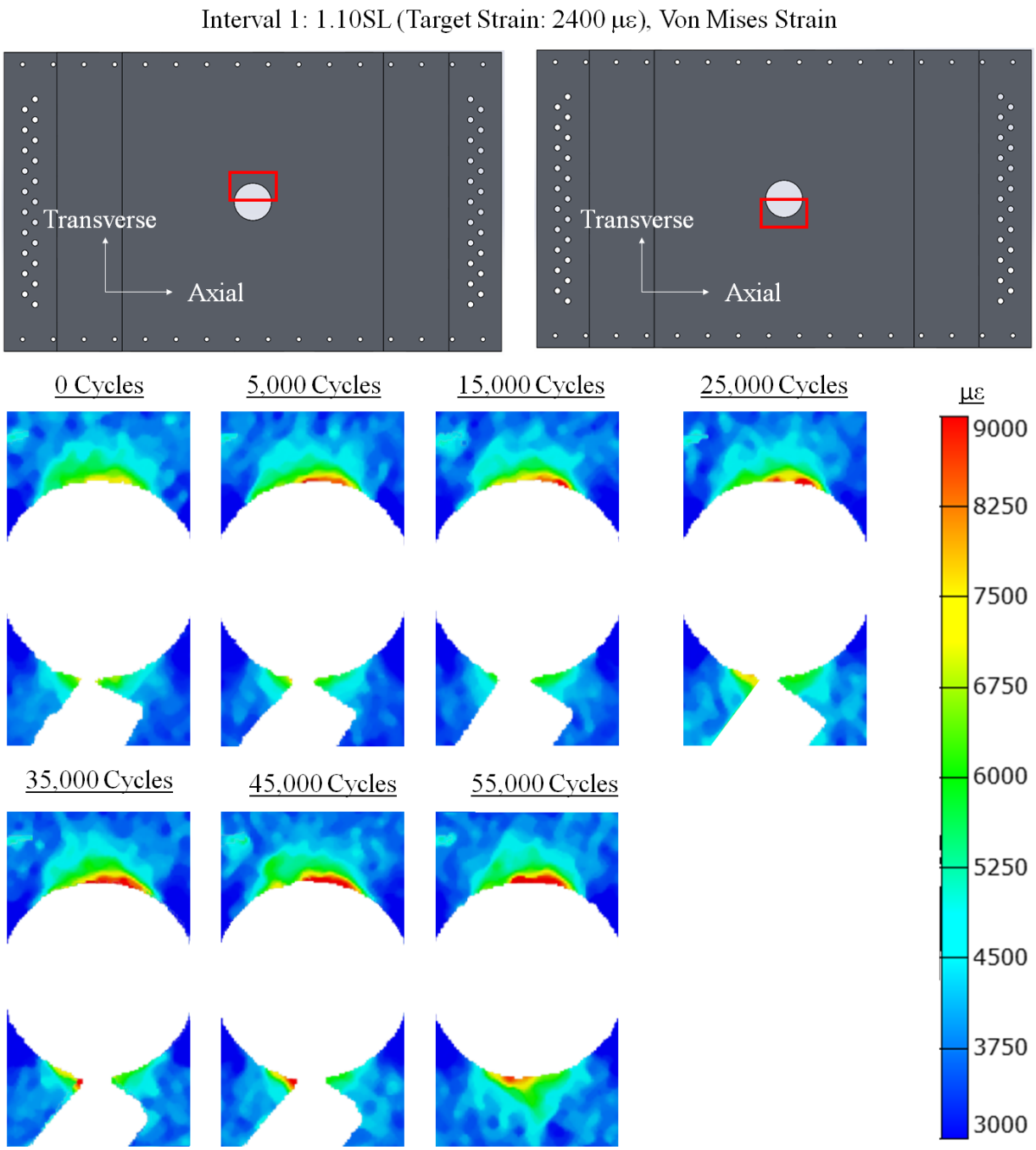

Figure 137. Panel 2 fatigue test results, von-mises strain (interval 1)

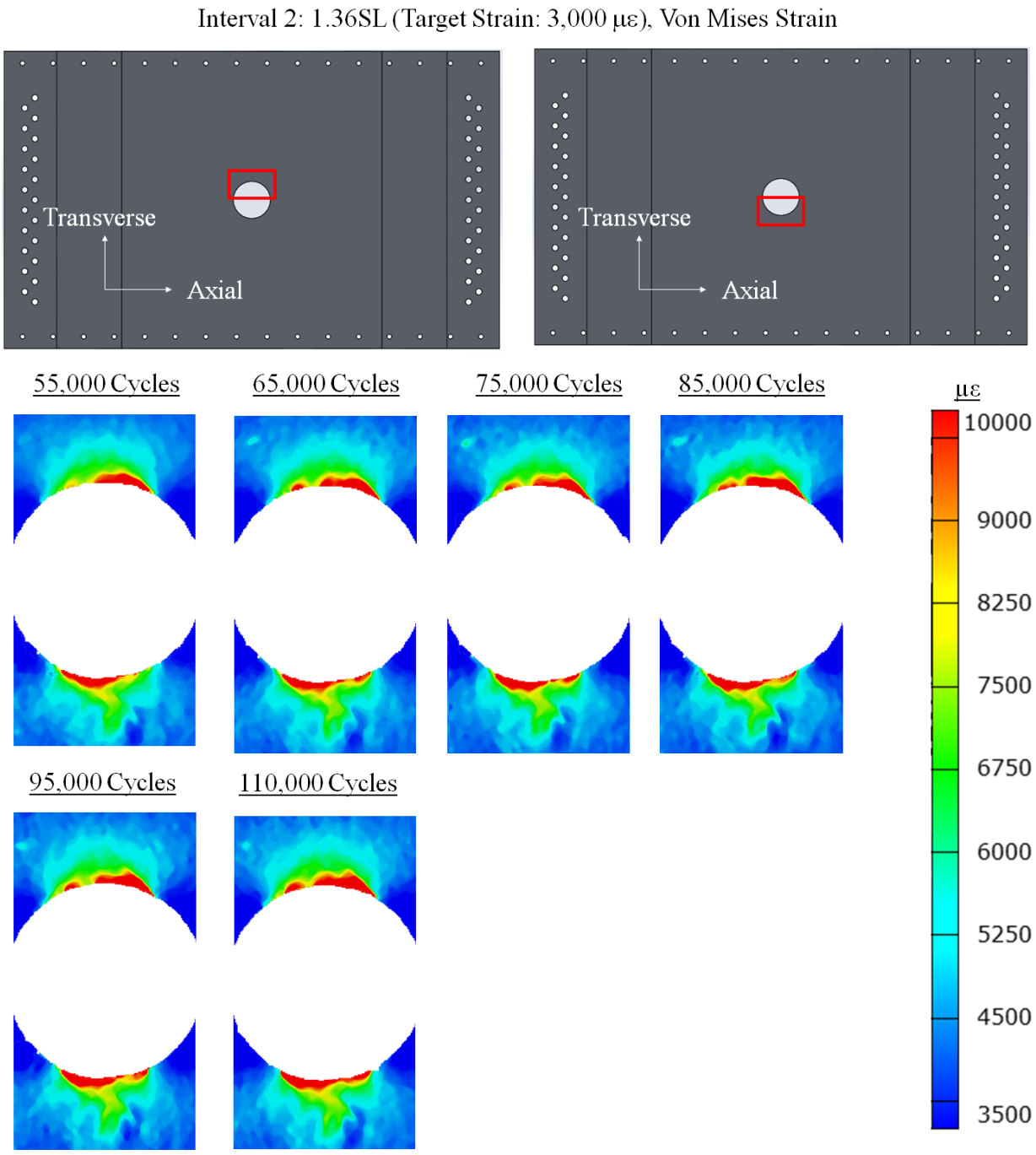

Figure 138. Panel 2 fatigue test results, von-mises strain (interval 2)

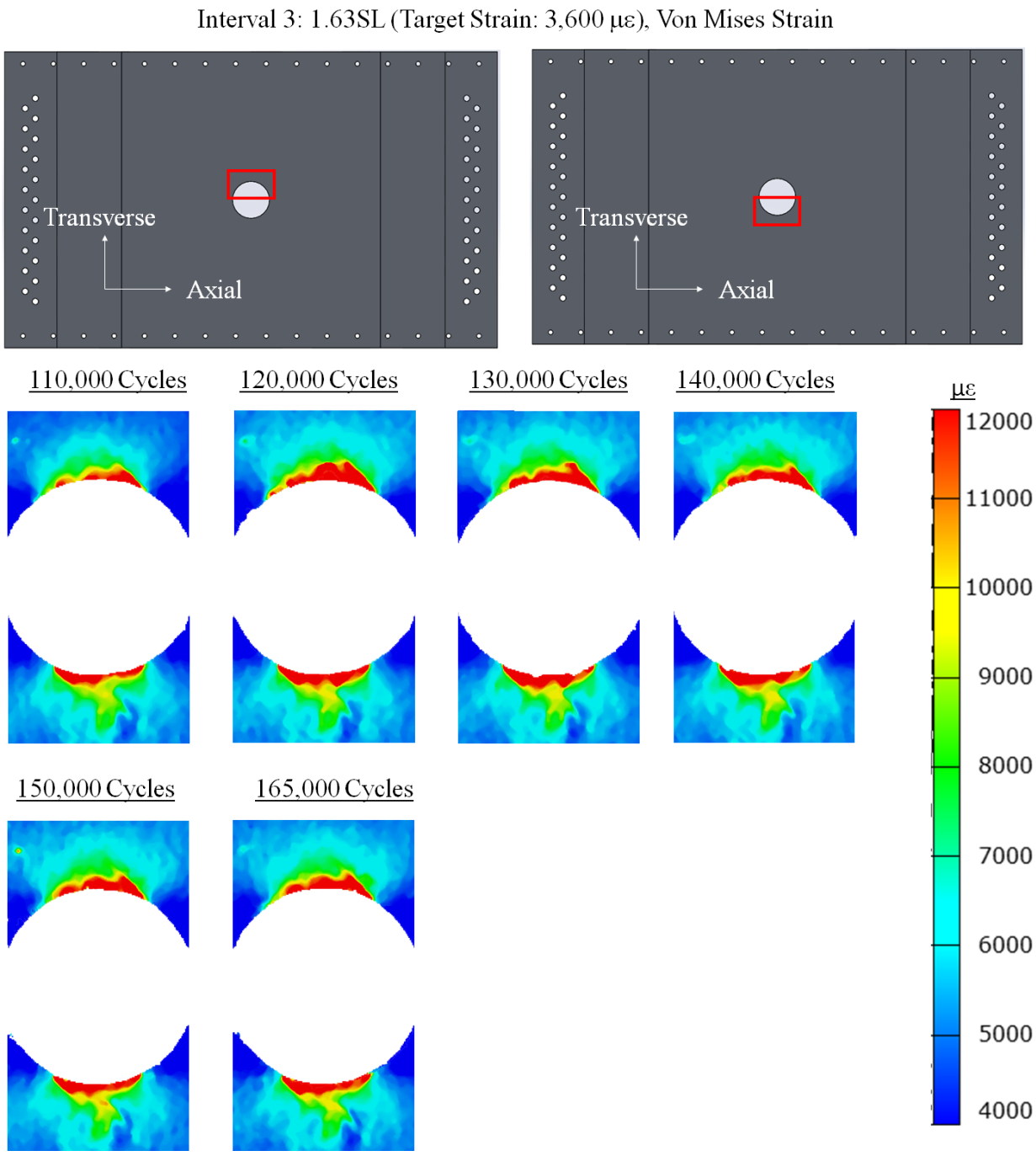

Figure 139. Panel 2 fatigue test results, von-mises strain (interval 3)

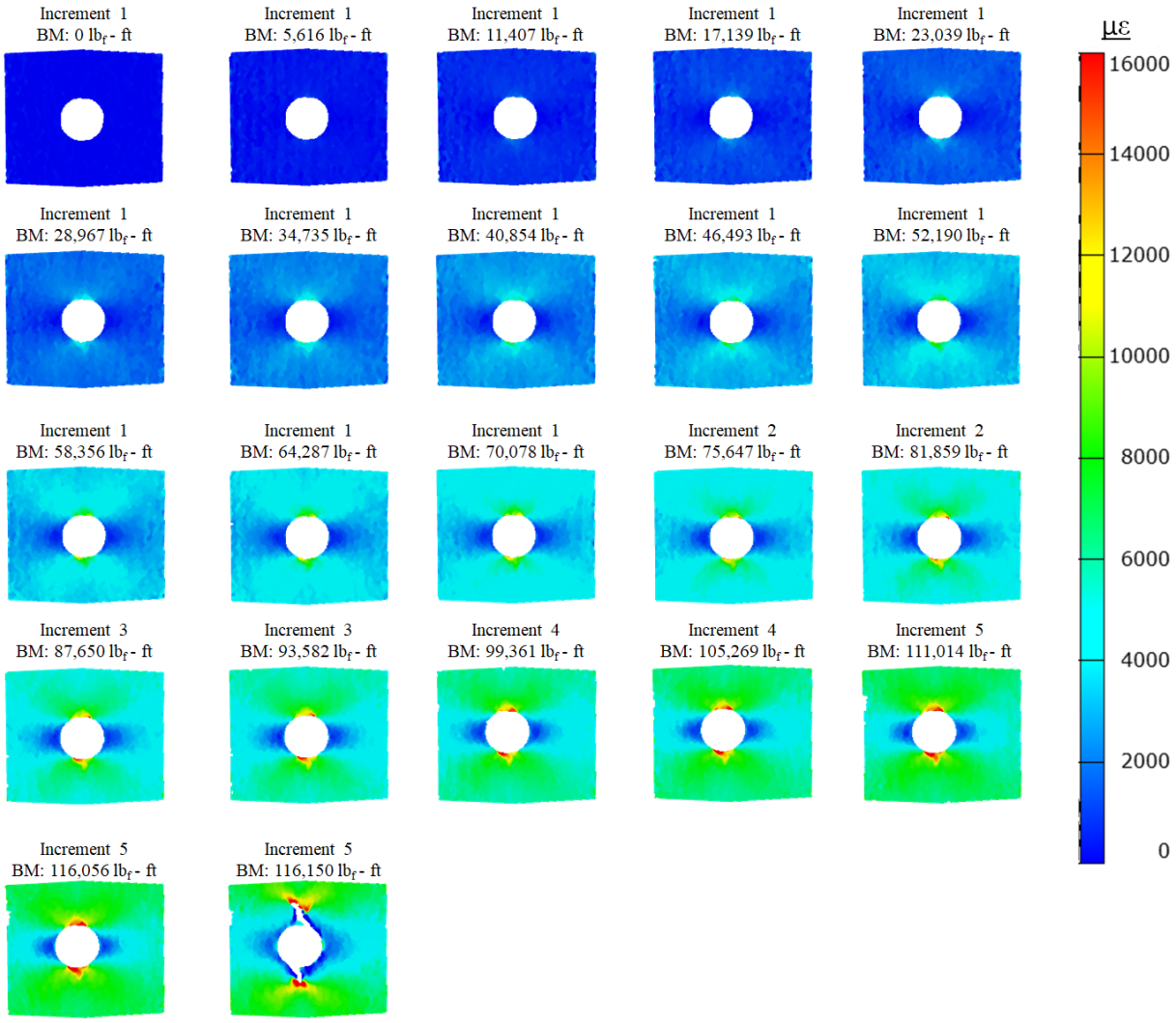

Figure 140. Panel 2 residual strength test results, wide field of view axial strain

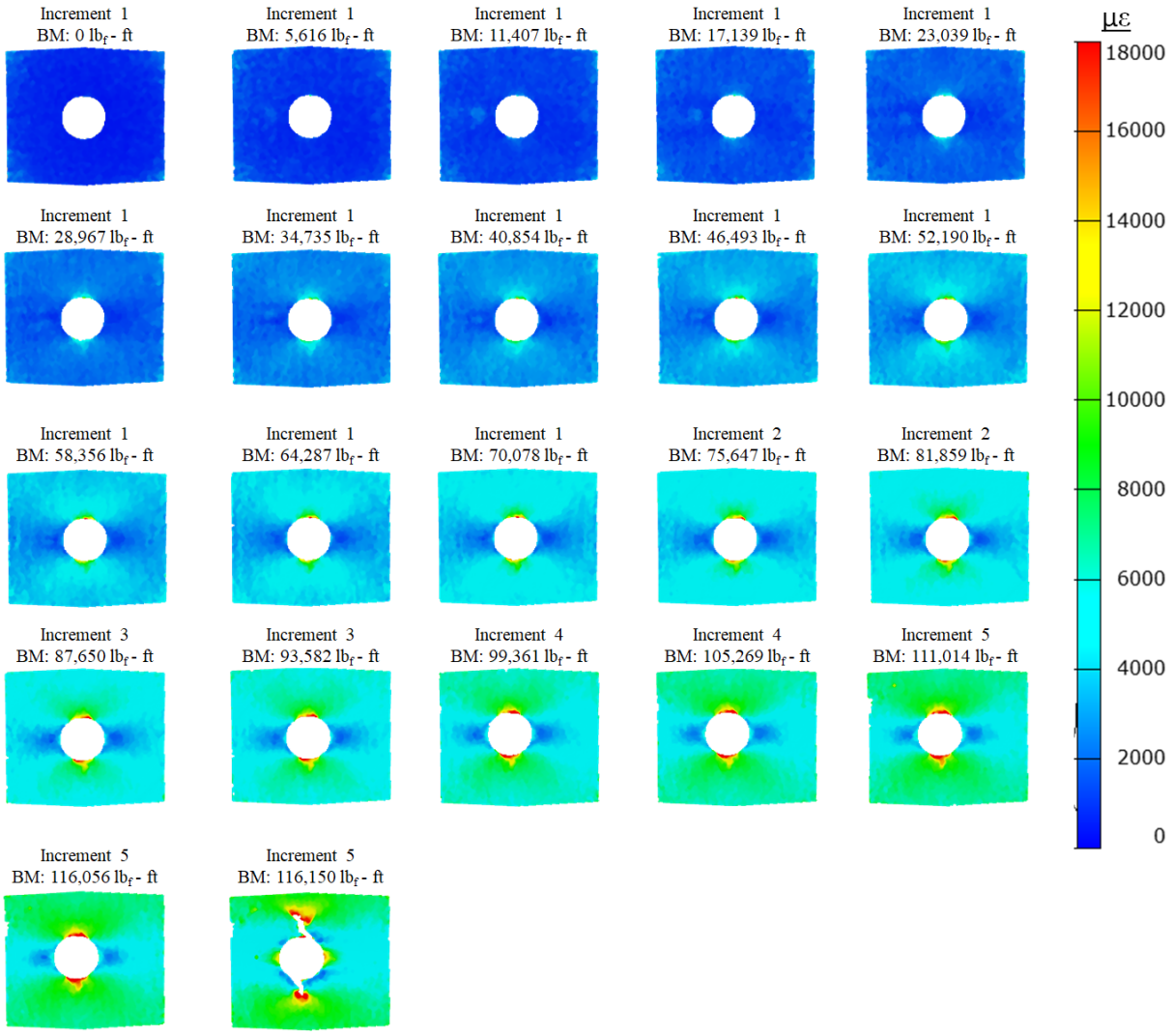

Figure 141. Panel 2 residual strength test results, wide field of view von mises strain

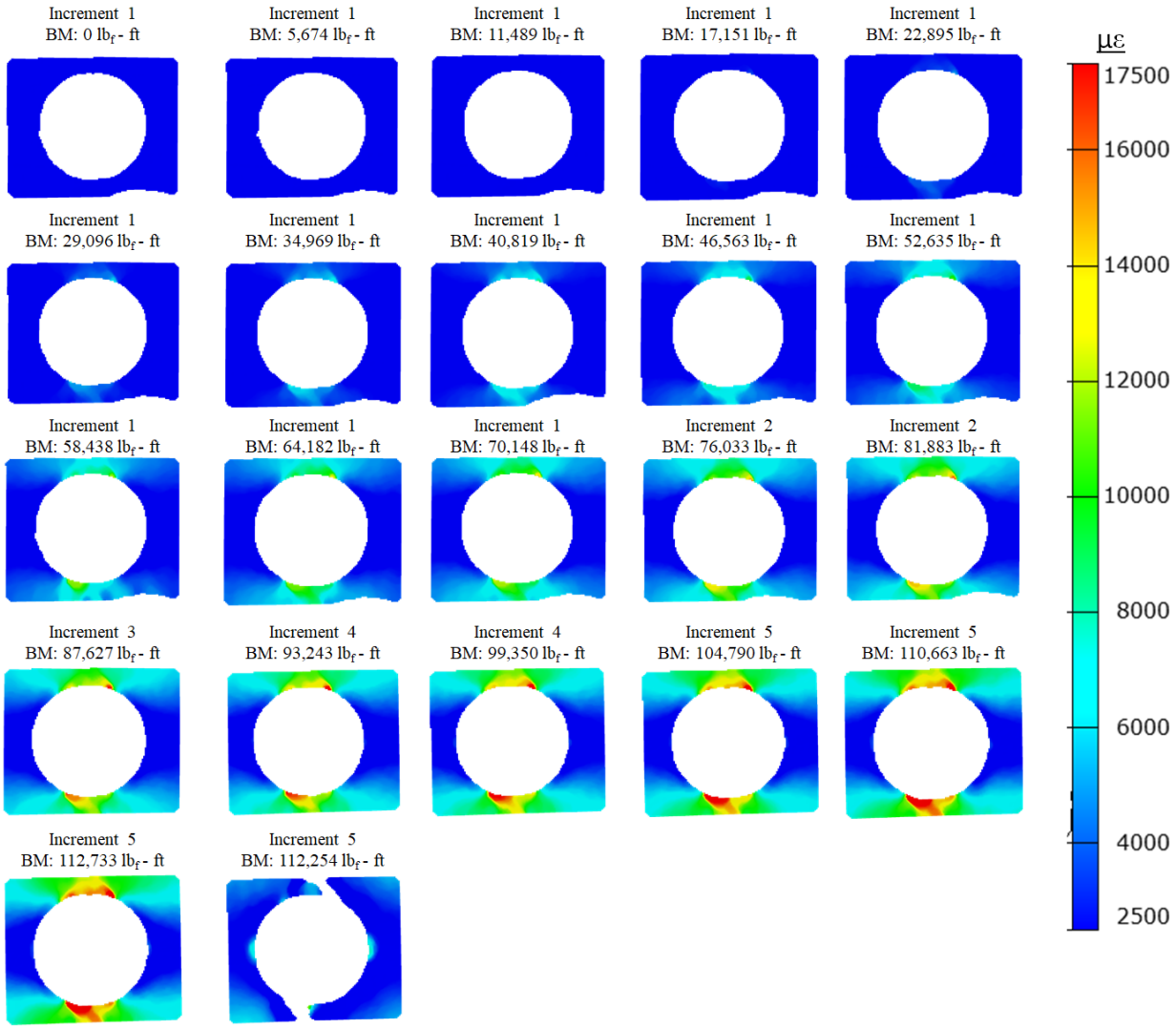

Figure 142. Panel 2 residual strength test results, narrow field of view axial strain

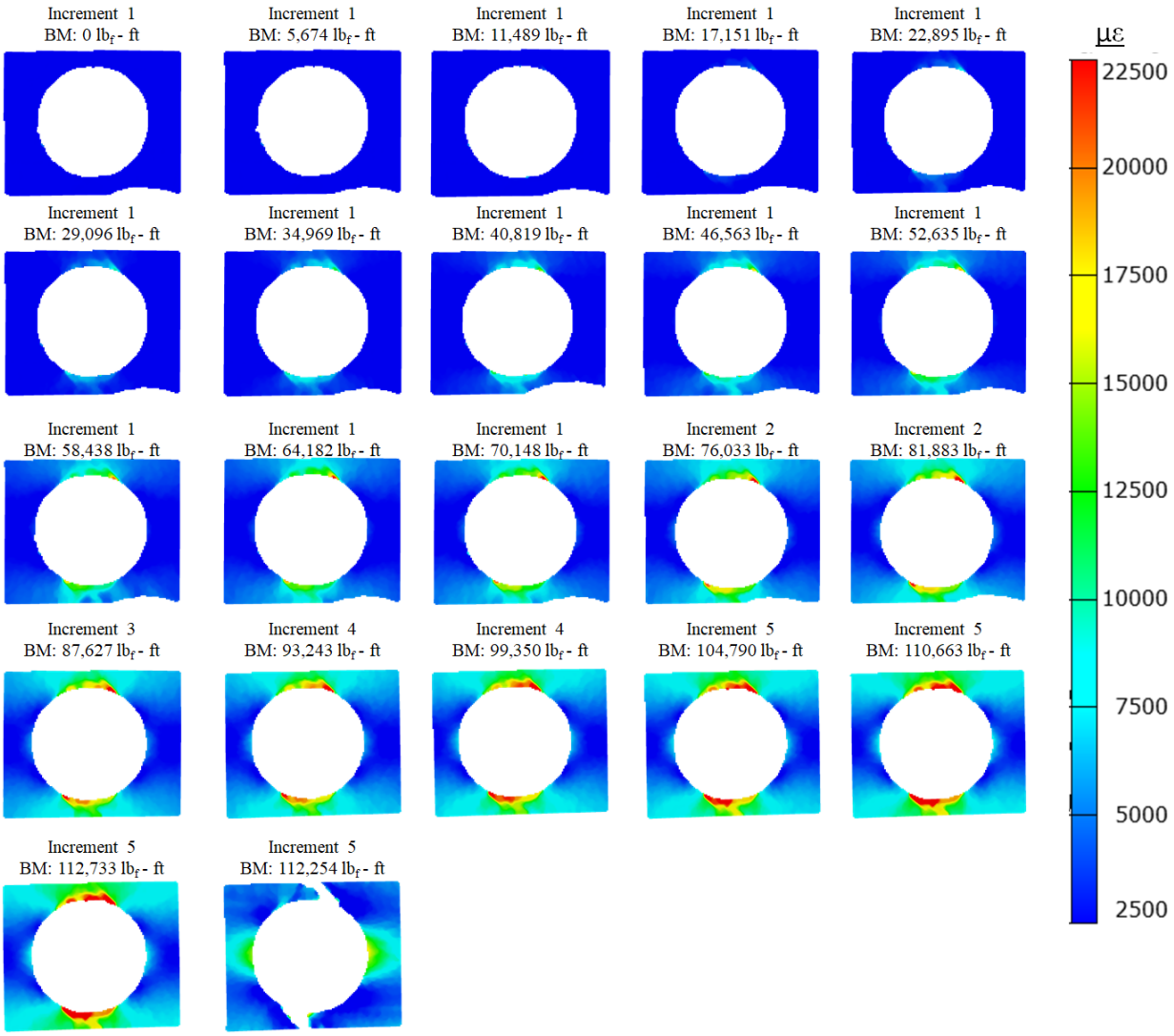

Figure 143. Panel 2 residual strength test results, narrow field of view von mises strain

E Visual results

This appendix provides visual results captured throughout fatigue and residual strength loading of the open-hole panel.

Close up images of the positive transverse edge of panel 2 hole for intervals 2 and 3 are shown in Figure 144 and Figure 145 and for the negative transverse edge in Figure 146 and Figure 147. Figure 148 shows the top view images of the hole in panel 2. Wide field of view and narrow field of view images of the hole during residual strength test are shown in Figure 149 and Figure 150.

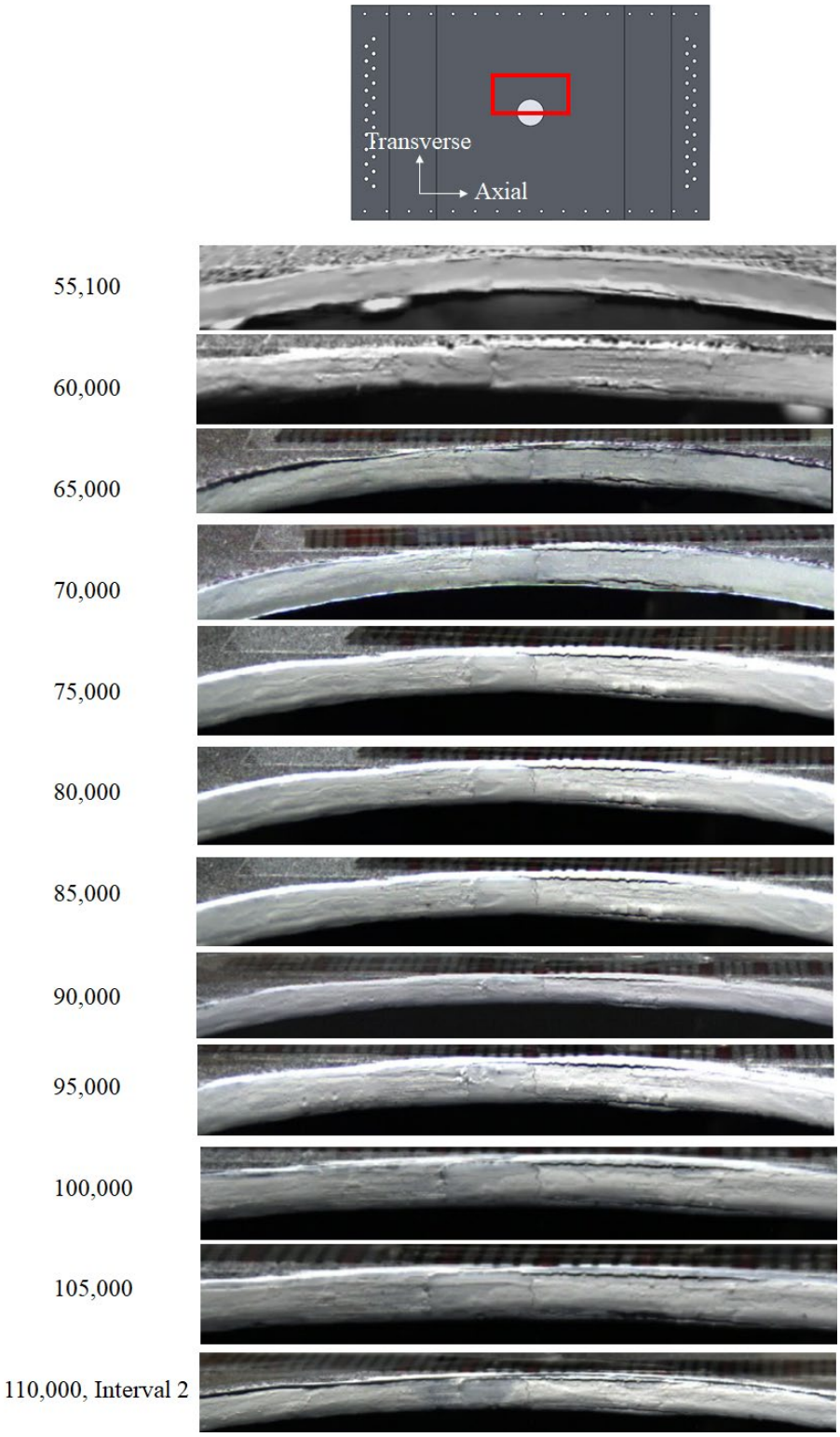

Figure 144. Panel 2 fatigue test, visual results for positive transverse hole edge (interval 2)

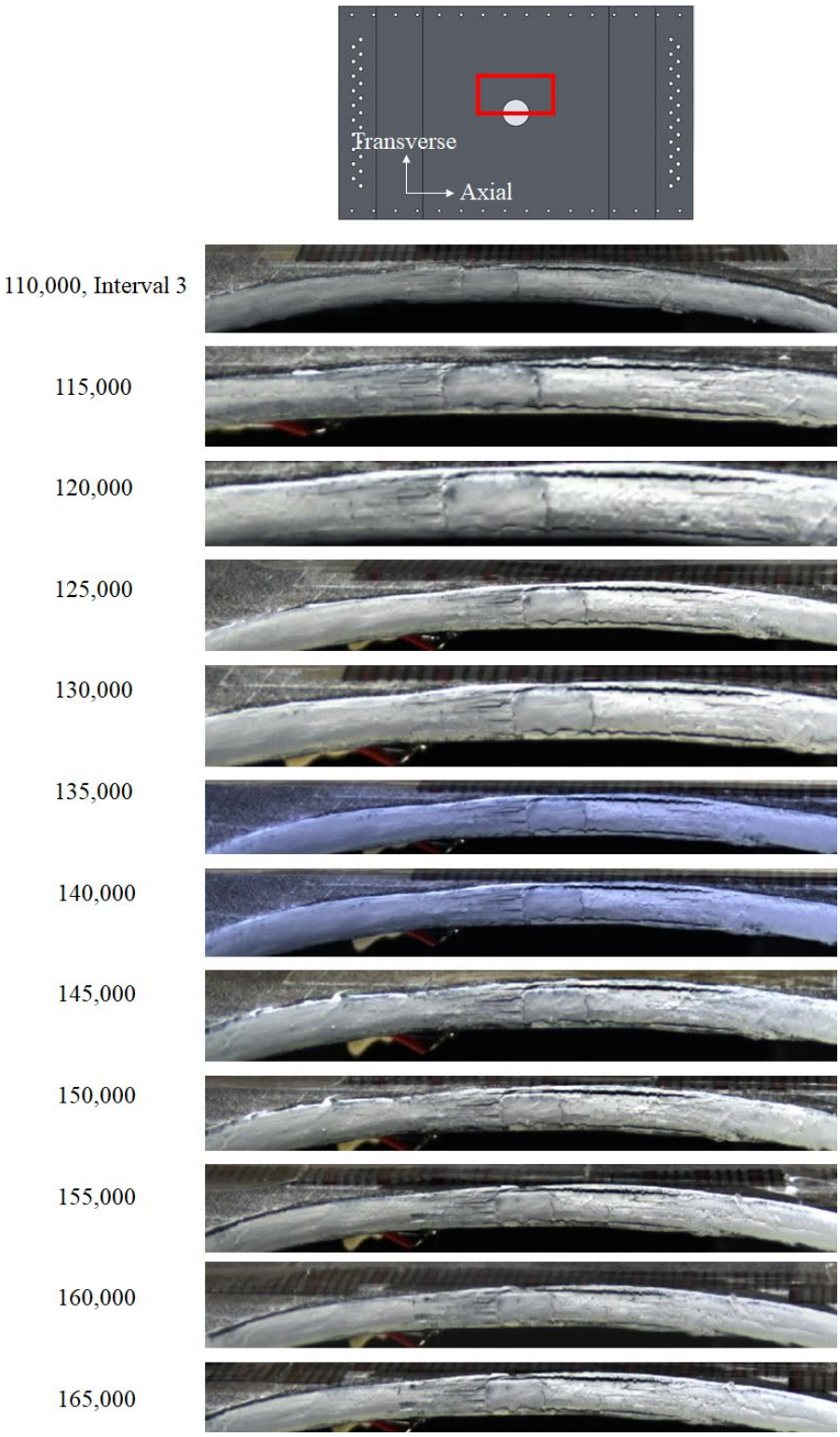

Figure 145. Panel 2 fatigue test, visual results for positive transverse hole edge (interval 3)

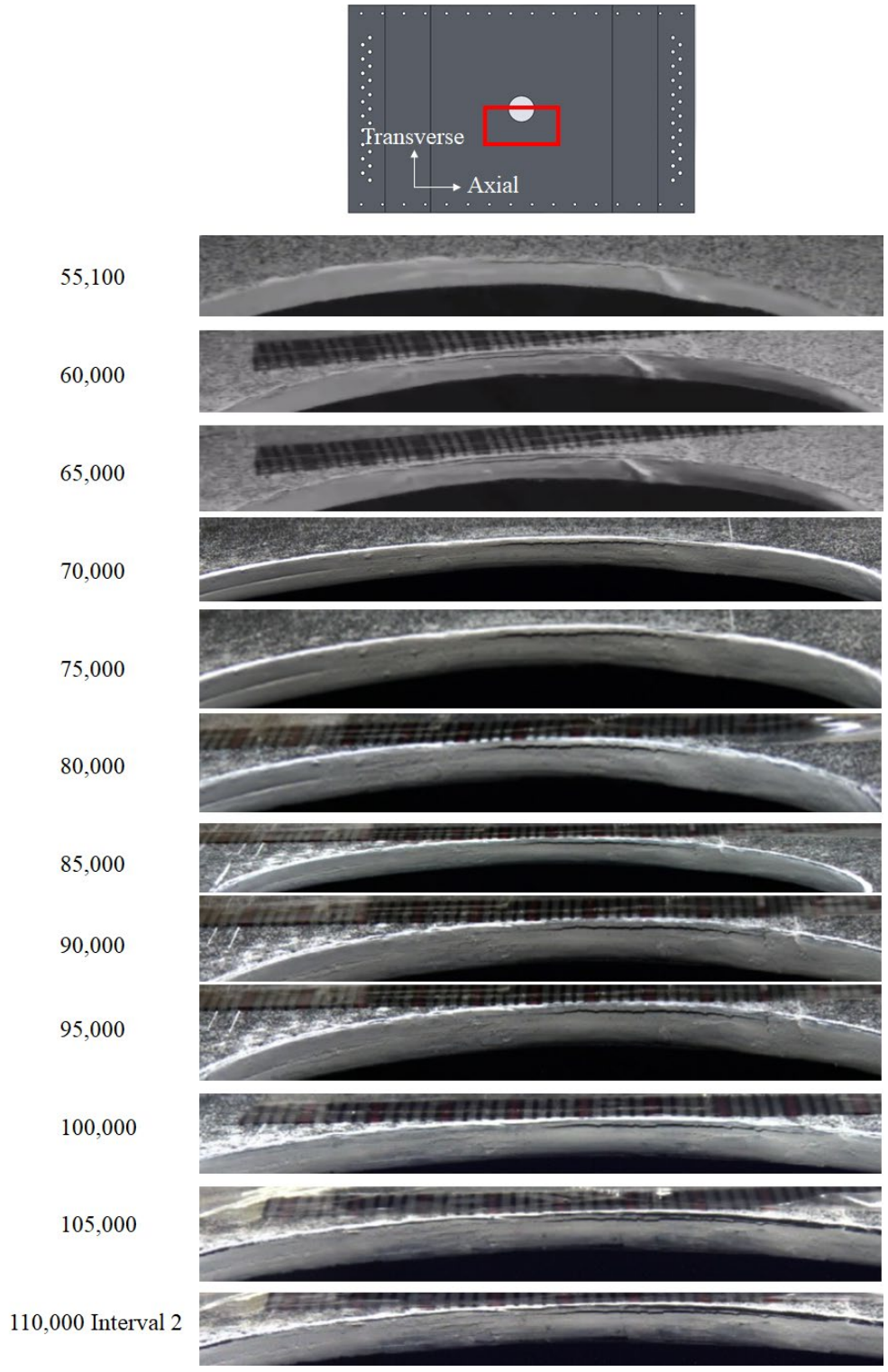

Figure 146. Panel 2 fatigue test, visual results for negative transverse hole edge (interval 2)

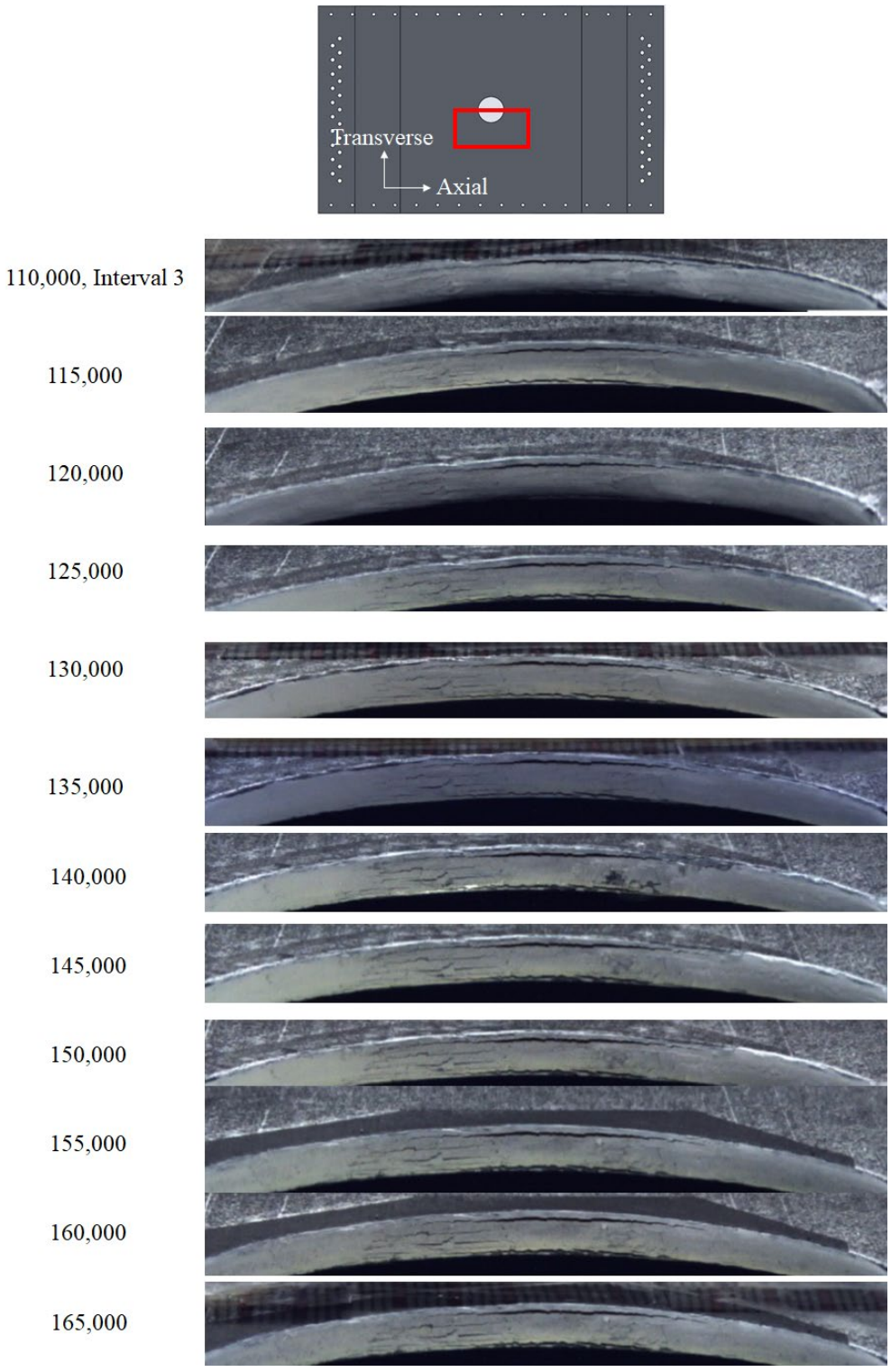

Figure 147. Panel 2 fatigue test, visual results for negative transverse hole (interval 3)

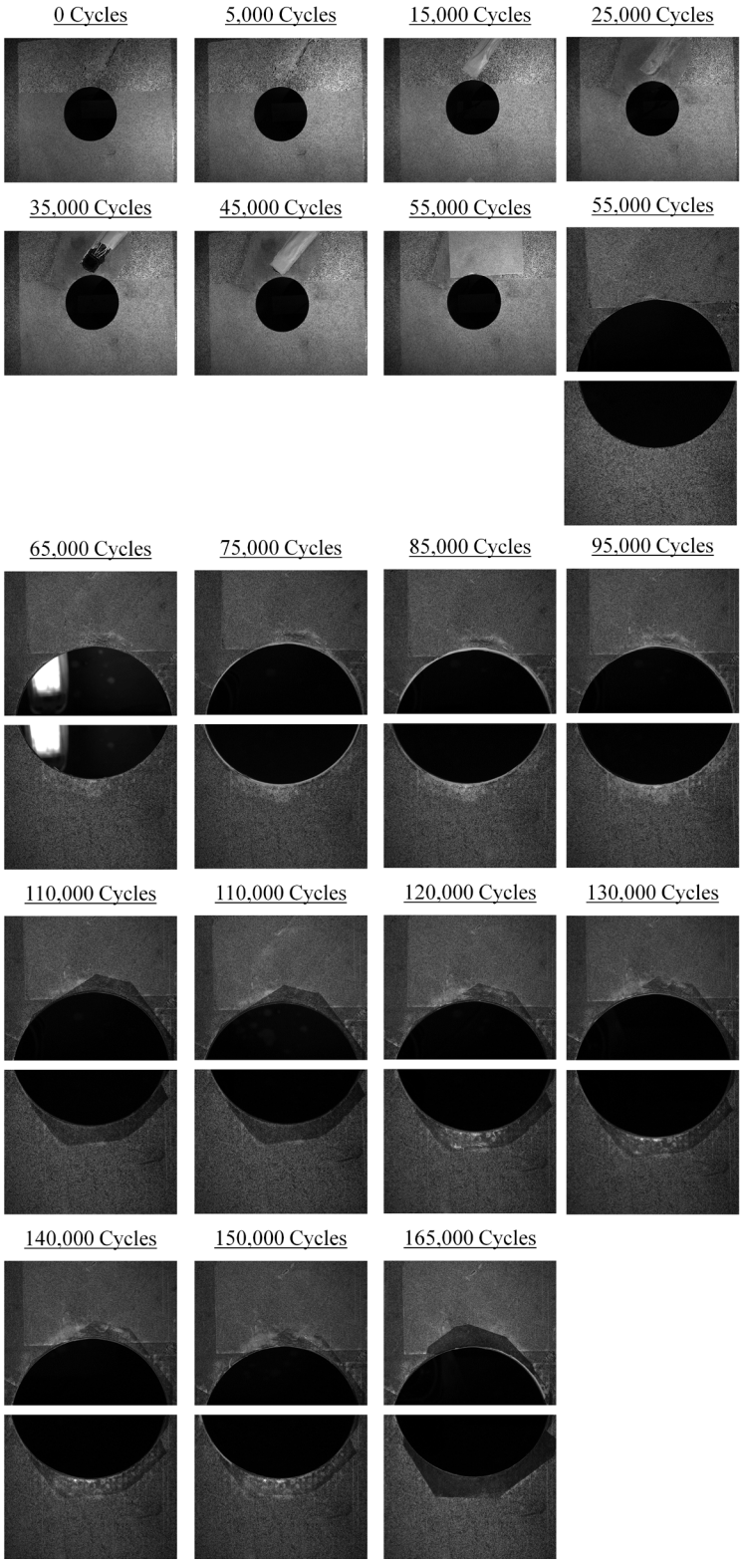

Figure 148. Panel 2 fatigue test, visual results

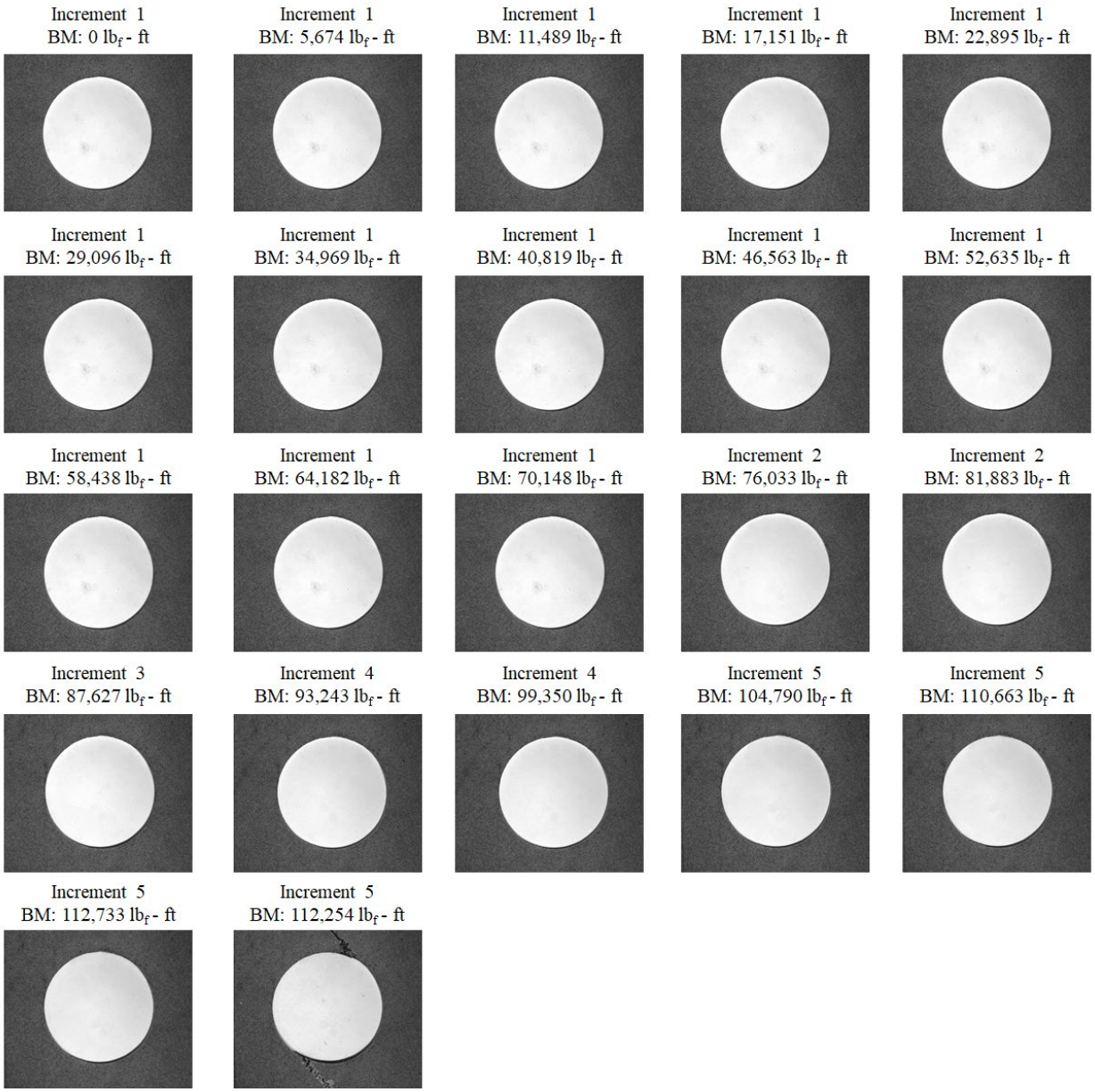

Figure 149. Panel 2 residual strength test, visual results by the left facing NFOV camera

Figure 150. Panel 2 residual strength test, visual results by the left facing WFOV camera

F Flash thermography results

This appendix provides flash thermography results captured throughout fatigue and residual strength loading of the open-hole panel.

Figure 151 shows the baseline thermography images of whole panel 2. The thermography images of the center hole captured during panel 2 fatigue test and residual strength test are shown in Figure 152 and Figure 153, respectively.

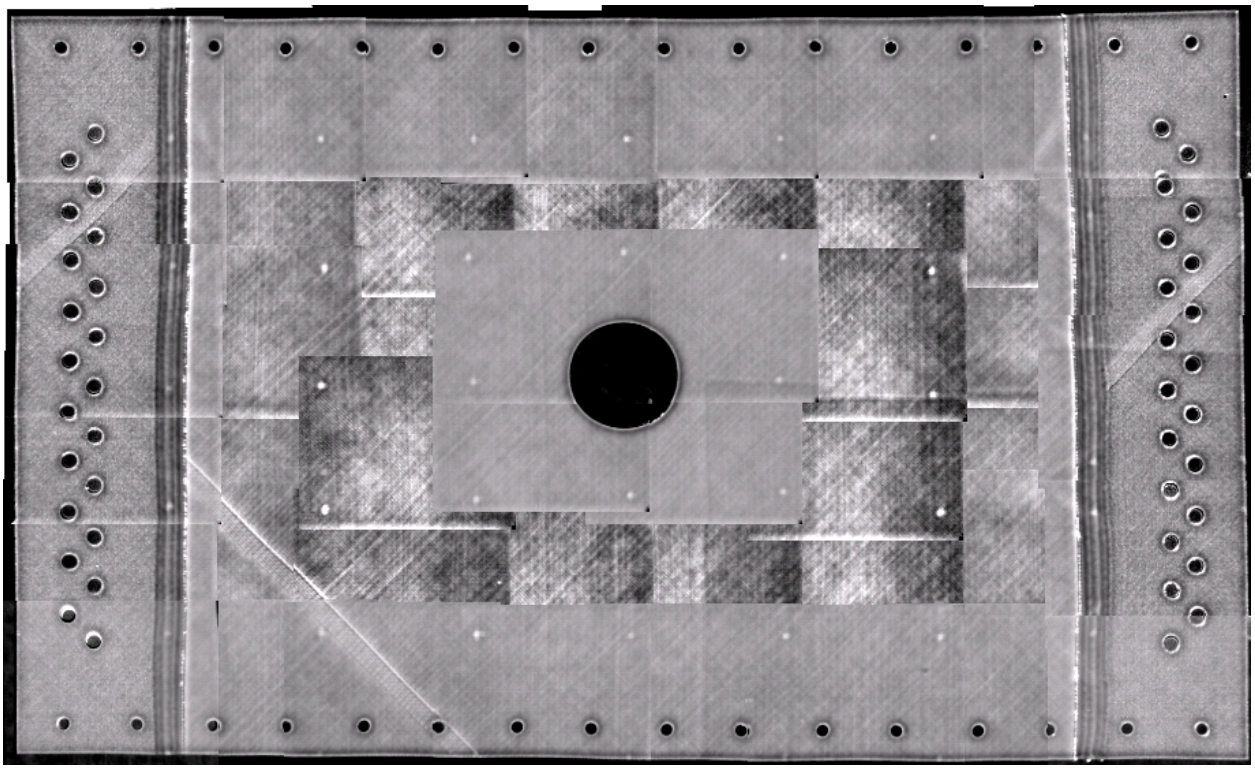

Figure 151. Flash thermography results captured for the open-hole panel before fatigue

Figure 152. Flash thermography results captured for panel 2 throughout fatigue

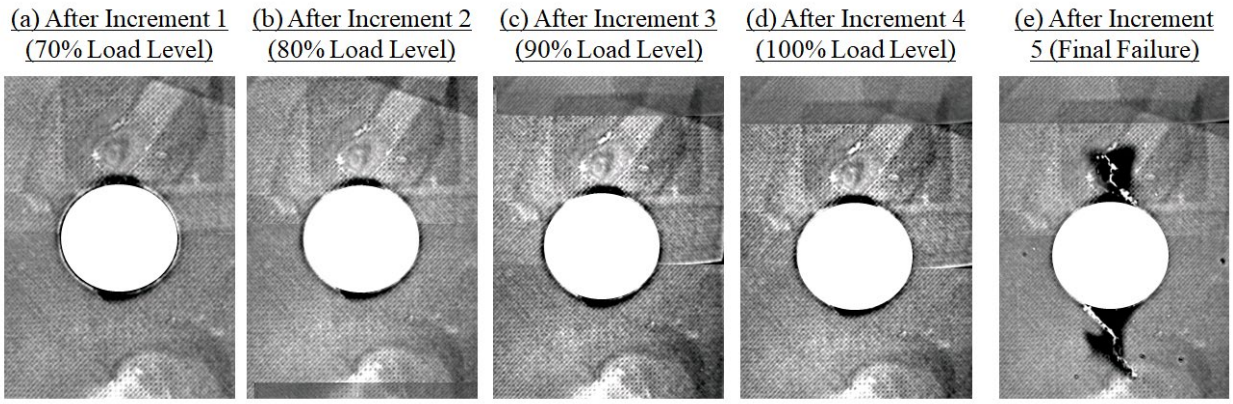

Figure 153. Flash thermography results captured for panel 2 throughout residual strength test

G Phased array ultrasonic results

This appendix provides phased array ultrasonic results captured throughout fatigue and residual strength loading of the open-hole panel.

Phased array results captured for the open-hole panel during fatigue are provided in Figure 154 and Figure 155, while phased array results captured during residual strength are provided in Figure 156 and Figure 157.

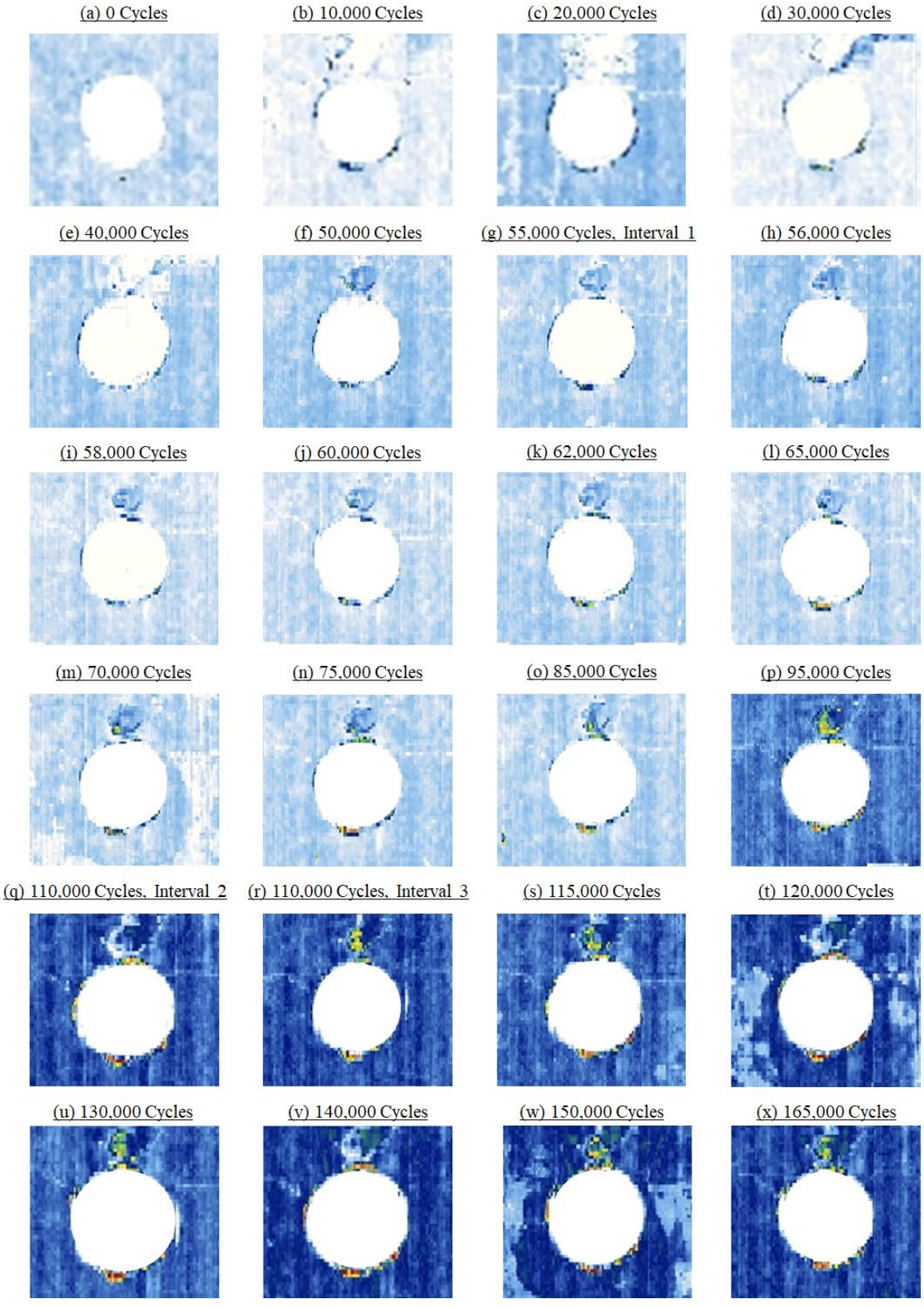

Figure 154. Phased array ultrasonic results (amplitude) for panel 2 throughout fatigue

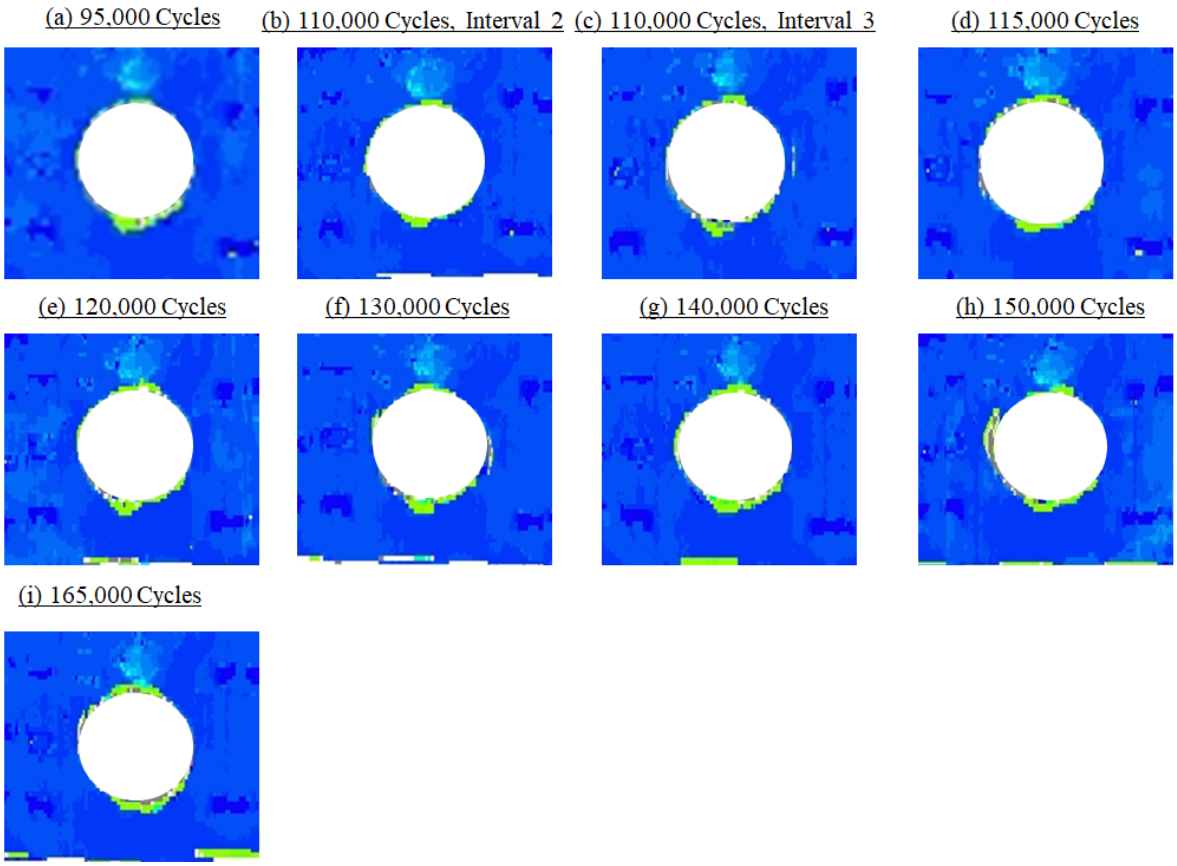

Figure 155. Phased array ultrasonic results (time of flight) for panel 2 during fatigue

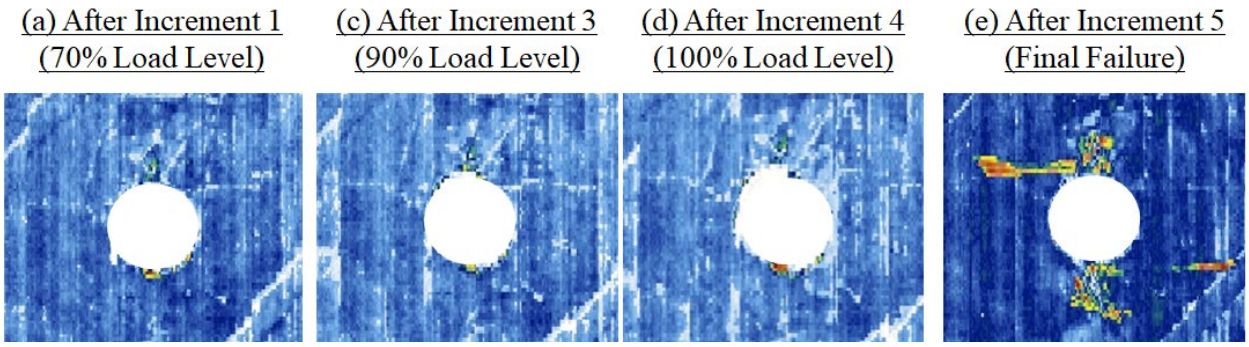

Figure 156. Phased array ultrasonic results (amplitude) for panel 2, residual strength test

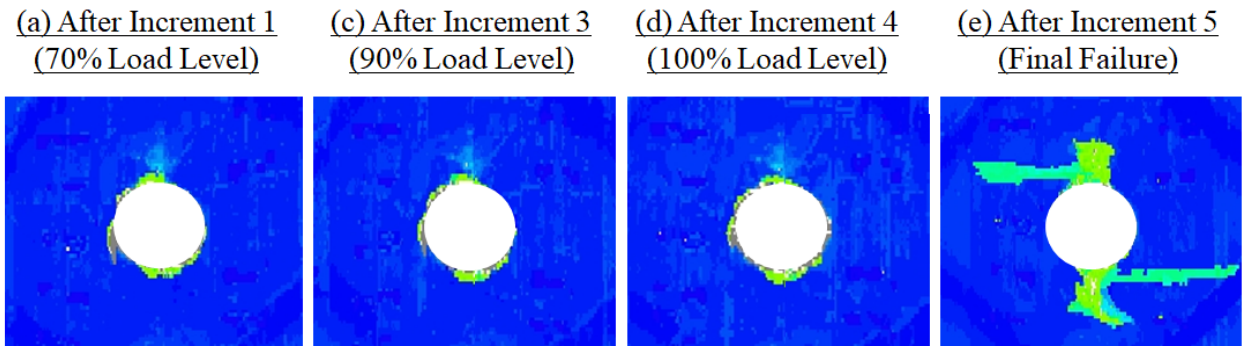

Figure 157. Phased array ultrasonic results (time of flight) for panel 2, residual strength test

H Pulse-echo ultrasonic results

This appendix provides pulse-echo ultrasonic results for the open-hole panel captured throughout fatigue loading, from 58,000 cycles to 165,000 cycles.

Figure 158 shows the schematic of delaminations at the hole edges outlined using pulse-echo inspection of panel 2.

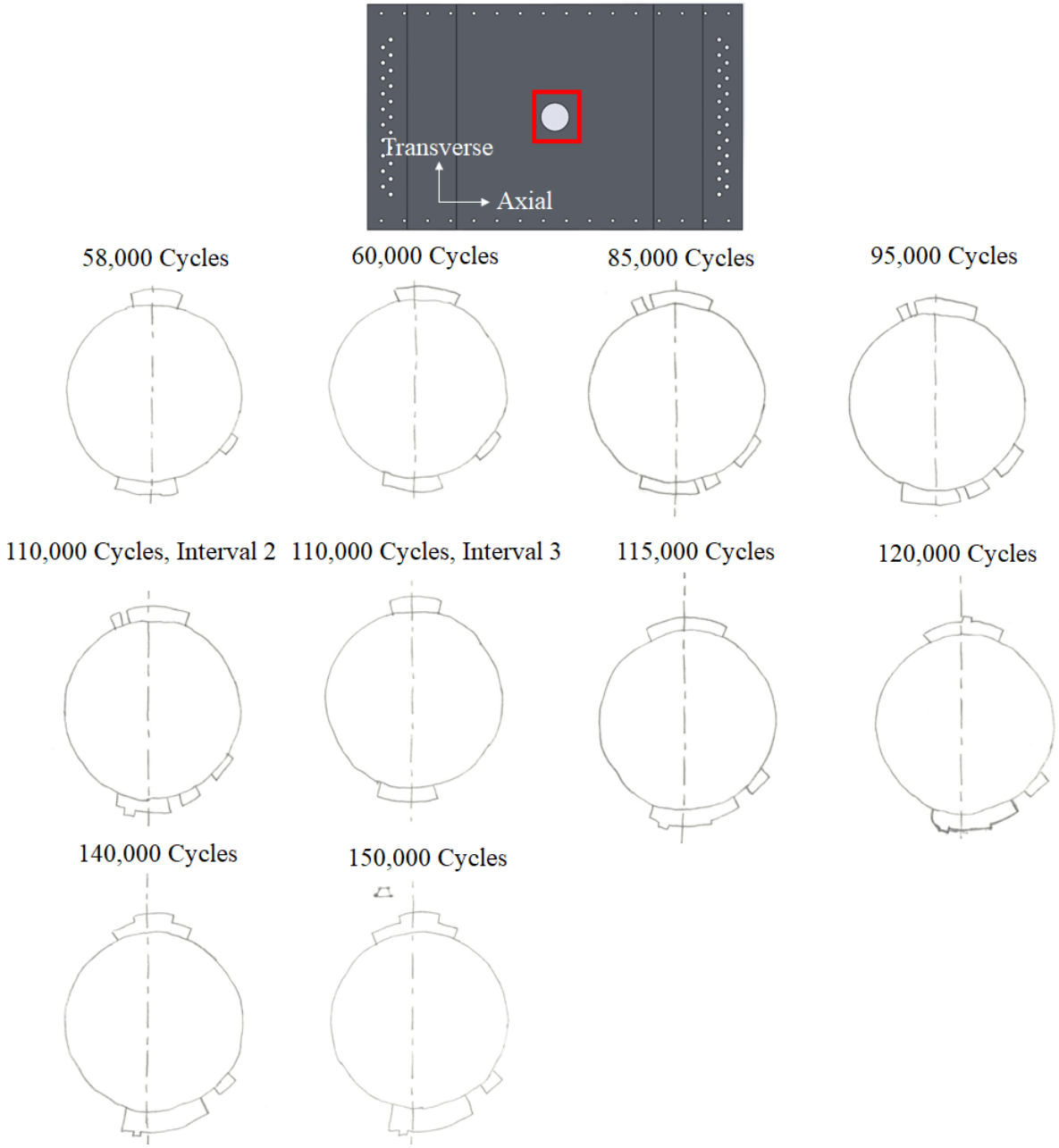

Figure 158. Pulse-Echo ultrasonic results captured for panel 2 throughout fatigue